



This work is protected by copyright and other intellectual property rights and duplication or sale of all or part is not permitted, except that material may be duplicated by you for research, private study, criticism/review or educational purposes. Electronic or print copies are for your own personal, non-commercial use and shall not be passed to any other individual. No quotation may be published without proper acknowledgement. For any other use, or to quote extensively from the work, permission must be obtained from the copyright holder/s.

WORK FUNCTION CHANGES OF CLEAN AND CONTAMINATED  
METAL FILMS IN VACUUM AND  
IN MERCURY VAPOUR

being

a thesis presented for the Degree of  
Doctor of Philosophy at the University  
of Keele.

by

D.L. Hampson, B.A.

Department of Physics,  
University of Keele,  
Keele,  
Staffordshire.

September, 1966

## ACKNOWLEDGEMENTS

I wish to express my gratitude to:

Dr. D. Elwyn Davies, for his guidance and helpful suggestions;

Professor D.J.E. Ingram, for the use of his laboratory and  
research facilities;

My friends in the Physics Department, in particular Dr. R.C. Maddison,

Dr. N.A. Surplice and Mr. P.C. Kimber, for their helpful discussion;

Messrs. W. Robinson and M. Cheney, for their assistance in

photographic work, and Messrs. G. Dudley and E. Greasley, for  
their help in constructional work;

Mr. F. Rowerth and his technical staff;

The Central Electricity Generating Board for the provision of a  
research grant;

Miss K.B. Davies, for the typing and presentation of this thesis.

Errors, like straws, upon the surface flow.

He who would search for pearls, must dive below.

Dryden

## SYNOPSIS

Considering the important industrial applications of mercury it is remarkable that so little work has been carried out on the characteristics of mercury surfaces. Prior to the present work, the last determination of the work function of mercury was determined over thirty years ago with somewhat unsophisticated apparatus.

In the present investigation contact potential difference techniques have been developed which enabled the work functions of solid and liquid mercury films to be measured.

The occurrence of impurity layers floating on top of liquid mercury surfaces is demonstrated, and their origin is traced to the contaminating action of the borosilicate glassware. Using liquid nitrogen techniques the impurity layers were frozen and subsequently submerged below clean condensed mercury films.

It has been demonstrated that the work function of mercury-free gold films is approximately 0.5eV higher than previous determinations made in conventional ultra-high vacuum systems employing mercury diffusion pumps.

In the course of this work a new measuring technique was developed which enables the work functions of volatile liquids and solids to be measured.

The clean surfaces were produced by condensing evaporated beams onto glass and metal substrates under residual gas pressures of less than  $10^{-9}$  torr. The measurements were carried out in both conventional glass ultra-high vacuum systems and demountable stainless steel systems.

## CONTENTS

<u>CHAPTER I</u>	<u>SURFACE PHYSICS</u>	
1.1	Introduction	1
1.2	Description of Solid Structure	2
1.3	Theory of Solid Structure	4
1.4	A Comparison of Internal and Surface Crystal Environments	12
1.5	Techniques used in the study of Surfaces	14
1.6	The Preparation of Clean Surfaces	18
1.7	The Factors which determine Surface Characteristics	23
1.8	Conclusion	26
<u>CHAPTER II</u>	<u>ELECTRON EMISSION AND WORK FUNCTION</u>	
	<u>MEASUREMENTS</u>	
2.1	Introduction	27
2.2	Types of Electron Emission	28
2.2.1	Thermionic Emission	28
2.2.2	Photoelectric Emission	32
2.2.3	Secondary Electron Emission	33
2.2.4	Field Emission	38
2.3	The Influence of Adsorbed Layers	42

2.4	The Influence of Temperature on Work Function Values	46
2.5	Experimental Methods used to measure Work Functions	47
2.5.1	The Thermionic Work Function	47
2.5.2	The Photoelectric Work Function	48
2.5.3	The Contact Potential Difference Work Function	49
2.6	Conclusion	51

**CHAPTER III A REVIEW OF PREVIOUS EXPERIMENTAL  
DETERMINATIONS**

3.1	Introduction	52
3.2	The Dependence of Work Function Values on the Method of Measurement	52
3.3	The Effect of Surface Structure	54
3.3.1	The Variation of Work Function as a Function of the Crystal Plane	54
3.3.2	The Influence of Surface Irregularities	56
3.3.3	The Variation of Work Function Values as a Function of Film Thickness	57
3.4	The Temperature Dependence of Work Function Values	59

3.5	The Influence of Adsorbed Films	61
3.5.1	Influence of Temperature on Adsorbed Layers	63
3.5.2	The Dependence of Work Function Values on Adsorbate Coverage	63
3.5.3	The Influence of Crystal Orientation on Adsorption	65
3.5.4	Reference Surfaces in Gases	66
3.6	Previous Determinations of the Work Function of Mercury	68
3.7	Conclusion and Statement of Problem	70

**CHAPTER IV**      **DESCRIPTION OF APPARATUS AND EXPERIMENTAL  
PROCEDURE**

4.1	Introduction	71
4.2	Method and Technique of Work Function Measurements	72
4.3	The Experimental Apparatus	73
4.4	The Glass Vacuum System	74
4.4.1	The Glass Ultra-High Vacuum System	75
4.4.2	Glass Vacuum Techniques	78
4.4.3	Construction of the Glass Experimental Tubes	80

4.5	The Stainless Steel Ultra-High Vacuum System	82
4.6	The Kelvin Electrode Vibrating System	85
4.7	Purification of Mercury	86
4.8	Summary	88

**CHAPTER V**      **CONTACT POTENTIAL DIFFERENCE MEASUREMENTS ON** 89  
**LIQUID AND SOLID MERCURY SURFACES: RESULTS**  
**AND DISCUSSION**

5.1	Introduction	89
5.2	Contact Potential Difference Measurements on Liquid Mercury Surfaces	90
	5.2.1 Tube 1	90
	5.2.2 Tube 2	94
5.3	Contact Potential Difference Measurements on Solid Mercury Surfaces	97
	5.3.1 Tube 3	97
	5.3.2 Tube 4	101
	5.3.3 Tube 5	106
5.4	Conclusions	109

DISCUSSION

6.1	Introduction	112
6.2	Preliminary Glass Partition Tube	113
6.3	Investigation of the Charge-Transfer Hypothesis; Using the Stainless Steel Equipment	116
6.4	The Influence of Glass Partitions on C.P.D. Determinations	120
6.4.1	C.P.D. Measurements between Gold Surfaces	120
6.4.2	C.P.D. Measurements between Gold and Tungsten Surfaces.	123
6.4.3	C.P.D. Measurements between Gold and Silver Surfaces	126
6.4.4	Summary of Results	127
6.5	The Stability of the Glass Partition	128
6.5.1	Effect of Increased Residual Gas Pressure	128
6.5.2	Change in the Surface Conditions of the Glass Partition as a Function of Distance	130
6.5.3	Conclusions	131
6.6	Determination of the Work Function of Liquid Mercury	132
6.7	Conclusions	135

CHAPTER VII      CONCLUSIONS AND SUGGESTIONS FOR FURTHER  
WORK

136

APPENDIX I      Penning Gauge Calibration Curve

APPENDIX II     Calibration of Crompton Voltmeter

APPENDIX III    Vapour Pressure of Mercury

Physical Constants of the metals investigated

LIST OF SYMBOLS

LIST OF FIGURES

REFERENCES

## CHAPTER I

### SURFACE PHYSICS

#### 1.1 Introduction

By their very nature all liquids, solids and gases have interfaces which determine an immense variety of physical and chemical properties. It is now known that many of the bulk properties of solids are influenced by the surface conditions of the material.

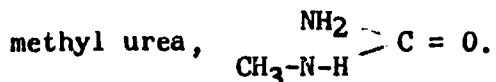
Using sophisticated techniques, it is now possible to prepare crystals which are free of dislocations (they are usually called whiskers). These dislocation-free materials are measured to be about 100 times stronger than ordinary crystals (1). Under ordinary conditions whiskers soon lose their high initial strengths. Minute imperfections on the surface (contamination spots such as local oxidation for example, or places where the surface is scratched by another object) are sources of dislocations that propagate through the crystal and thus weaken it.

In a similar manner the intrinsic strengths of non-crystalline materials, such as glass, have been shown to be critically dependent on the surface conditions of the sample (2).

It is difficult to imagine how industry and life could function without the catalytic action of surfaces. The amazing selectivity of certain catalysts can only be explained by correlating the surface and internal structure of the catalyst with the molecular structure of the reactants.

Enzymes are extremely specific in their catalytic action. Urease will catalyze the hydrolysis of urea  $\begin{array}{c} \text{NH}_2 \\ \diagdown \\ \text{C} = \text{O} \\ \diagup \\ \text{NH}_2 \end{array}$ , in dilutions as high as

one part of enzyme in 10 million of solution, yet it has no detectable effect on the hydrolysis rates of substituted ureas, for example,



It is now known that the three dimensional structure and topography of the enzymes are responsible for specific action. The reacting molecules "fit" into folds on the surface of the protein molecule, and only those that fit exactly undergo the required chemical change. This type of surface phenomena has been described as "hand and glove chemistry". Electronics is almost entirely based on the control of electrons emitted from surfaces in thermionic and solid state devices. Apart from its immense technological importance, electron emission is a valuable tool in the investigation of solid surfaces.

It can be seen that the importance of surfaces in technology is vast. This practical importance is equalled by their considerable scientific interest. Although the properties of surfaces have been used to considerable gain throughout modern civilization, their application has been based more on chance and intuition than on a basic understanding of surface phenomena.

The obvious relevance of the internal structure of materials to the discussion of surfaces has made necessary a review of the modern theories of solid state physics.

## 1.2 Description of Solid Structure

Solids can be usefully divided into two groups - crystalline and non crystalline. Most of the naturally-occurring and man-made solids are crystalline; this large group of solids can be usefully subdivided,

according to chemical, electrical, magnetic and thermal characteristics, into five types.

Briefly, the classification is as follows:-

- a) Metals
- b) Semiconductors
- c) Ionic crystals
- d) Valence crystals
- e) Molecular crystals

The main characteristics of metal single crystals are that they tend to be good reflectors of light and have good electrical conductivity, which decreases as the temperature is increased.

Semiconductors are distinguished by a feeble electronic conductivity, which increases with increasing temperature.

Ionic crystals (of which common salt, sodium chloride, is a good example) show good ionic conductivity at high temperatures, and cleave well along crystal faces. They are composed of ions produced from highly electro-positive and electro-negative elements.

Diamond is probably the best example of a valence crystal. It has a low electronic and ionic conductivity, great hardness and poor cleavage.

The fifth type of crystalline solid is the molecular crystal, which is usually composed of inactive atoms, such as the rare gases and saturated organic compounds such as benzene. They tend to have low melting and boiling points, and in the gas phase, are in the form of stable molecules.

Glass is an excellent example of a random non crystalline solid structure, being in many ways a compromise between crystalline and liquid properties. There is a considerable variation in the bond lengths and the energy required to break the bonds will therefore not be constant. Glasses on heating do not therefore have a sharp melting point, but soften gradually.

### 1.3 Theory of Solid Structure

There are two main theoretical approaches to the nature of solid structures.

In the first approach, which is usually called the tightly bound electron approximation, the treatment begins with the individual atoms of the final structure, which are initially considered to be an infinite distance away from their neighbours.

With a knowledge of the electronic structure of the separate atoms, it is possible to calculate how the individual atoms have their electronic energy levels altered as they are brought in from an infinite distance to their equilibrium positions in the final solid structure.

In the alternative approach, instead of starting with separate atoms, it is assumed that the nuclei of the atoms are in their final equilibrium positions in the solid structure. The treatment considers the effect of gradually feeding the electrons into the resulting field of force. Just as electrons in an atom obey the Pauli Principle, so the electrons in the final solid structure are limited in their choice of energy levels.

After calculating the final electronic field of force it is possible, using Pauli's Principle, to describe the solid structure of the material. This approach to the structure of solids is called the band model of solid state. The band theory of solids is usually employed to describe the structure of crystalline solids, and, since the great majority of the materials mentioned in this thesis are crystalline, the band theory will be described in greater detail.

### Band Theory of Solids

The band theory of solids was born out of the failure of the free electron theory of metals, and brief outline of this early theory is therefore relevant.

Sir J.J. Thomson's announcement in 1895 concerning the discovery of the electron inspired P. Drude (3) to propose in 1900 that the electrical and thermal properties of metals could be described by assuming that metals contain free electrons in thermal equilibrium with the lattice atoms. Insulators, on the other hand, were assumed to be built up from molecules that had their positions firmly fixed in the solid structure. Their electrons were also assumed to be firmly attached to the parent molecules.

Although the theory was successful in qualitatively explaining the difference between metals and insulators, it failed to explain why metals usually had a heat capacity in common with insulators, of about 6 cal/mol deg.

According to the classical free electron theory, all the valence electrons in a metal are free to move, and are thus called the conduction

electrons. They are assumed to be in thermal equilibrium with the lattice atoms. In fact, the conduction electrons are treated as an ideal gas of free electrons, and as a gas the electrons are assumed to have energies that have a Maxwell-Boltzman distribution.

This latter assumption produces a conclusion that is in contradiction to the observed facts. If the electrons obey the Maxwell-Boltzman energy distribution, their average energy will be directly proportional to their absolute temperature, and will therefore have a molar specific heat of  $\frac{3R}{2}$ .

The molar specific heats of metals are usually very near to  $3R$  - i.e.  $5.97$  kcal/kgm/mole  $C^{\circ}$ , in accordance with Dulong and Petit's law. This value of  $3R$  for the molar specific heats of metals can be deduced by neglecting the free electron gas in the calculations, and assuming that only the lattice atoms have average energies proportional to the absolute temperature.

Drude assumed, incorrectly, that the valence electrons have an energy distribution that is continuous, that is, there are no limitations on the energy values the electrons can have.

Wolfgang Pauli in 1925 postulated his now famous exclusion principle to explain the behaviour of electrons in atoms. It states that, in any one atom no two electrons have identical sets of quantum numbers. Although Pauli's exclusion principle was originally conceived to explain the behaviour of electrons in atoms, it is now appreciated to be of such a fundamental nature that it describes both matter and anti-matter. Atoms and nuclei cannot be explained without it. It is now

accepted as a cornerstone in all the theories that predict the behaviour of fundamental particles.

In 1926 E. Fermi and P. Dirac assumed that the energies of the free electrons are quantized, even though they are no longer restricted to their parent atomic orbitals. Starting with this assumption and the assumption that the electrons obey the exclusion principle, they calculated the energy distribution of the free electrons in a crystal at absolute zero, and how it changed as a function of temperature.

The energy distribution derived from these basic assumptions can be expressed in the form

$$\sum n_E = \frac{4\pi(2m)}{h^3} \frac{E^{\frac{1}{2}} \delta E}{e^{\left[\frac{E - E_F(0)}{kT}\right]} + 1}$$

where

$\sum n_E$  is the number of electrons per  $\text{cm}^3$  with an energy between  $E$  and  $E + \delta E$ .

$m$  is the mass of the electron =  $9.107 \times 10^{-28}$  gm.

$h$  is Planck's constant =  $6.624 \times 10^{-27}$  erg.sec.

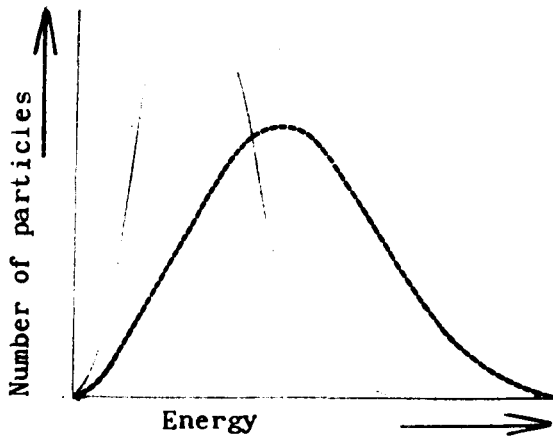
$k$  is Boltzman's constant =  $1.38 \times 10^{-16}$  erg/ $^{\circ}$ K

$T$  is the absolute temperature in  $^{\circ}$ K

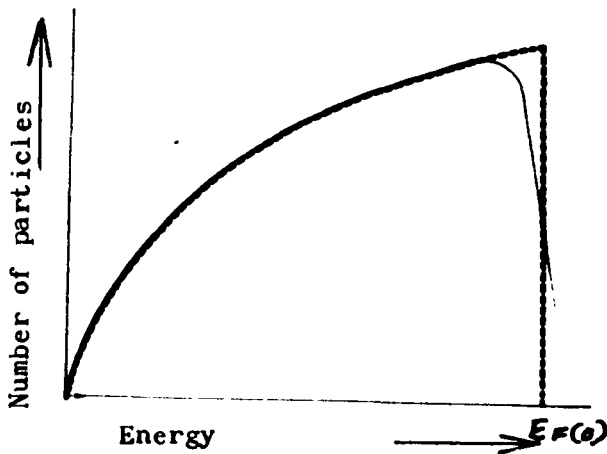
$E_F(0)$  is the Fermi level in ergs given by

$$E_F(0) \frac{h^2}{2m} \left(\frac{3N}{8\pi}\right)^{2/3}$$

where  $N$  is the number of electrons/ $\text{cm}^3$ .



Maxwell-Boltzmann Distribution of molecular energies in a classical gas varies with temperature. The energy distribution is narrower and the average energy lower at room temperature (continuous curve) than at some higher temperature (broken curve).



Fermi-Dirac Distribution of energies in an electron gas at absolute zero (broken curve) differs little from that at room temperature (continuous curve).

Figure 1.

The calculated distribution of the electron energies is very different from the Maxwell-Boltzman distribution. It can be seen (see Figure (1)) that at absolute zero the energy distribution ends abruptly and that at higher temperatures the energy distribution does not differ from the absolute zero distribution to any large extent. This extremely small change in the free electron energy distribution, as a function of temperature, explains why there is virtually no electron contribution to the specific heats of metals.

It can be seen from the Fermi Dirac distribution law that at absolute zero the valence free electrons are not all condensed into the lowest energy level, but progressively fill up the available energy levels from the ground state. The level which divides the filled from the vacant levels is known as the Fermi level at absolute zero and is denoted by  $E_F(0)$ .

The Fermi temperature of the valence electrons  $T_F$  is defined by:

$$T_F = \frac{E_F(0)}{k} \quad \text{where } k \text{ is Boltzman's constant.}$$

The electron velocity  $U_F$  at the Fermi level is defined by:

$$\frac{1}{2}mU_F^2 = E_F(0)$$

Values of the Fermi energies, temperatures and electron velocities are given in Figure (2).

It can be seen that the energy of the free electrons near the Fermi level greatly exceeds the mean energy of the lattice vibrations at normal temperatures.

A more informative model can be obtained by using a three dimensional coordinate system, with the radii of successive spheres being

	Li	Na	K	Rb
$E_F$ (ev)	4.72	3.12	2.14	1.82
$T_F$ (deg)	55,000	37,000	24,000	21,000
$u_F$ (cm/sec)	$1.31 \times 10^8$	$1.07 \times 10^8$	$0.85 \times 10^8$	$0.80 \times 10^8$
	Cs	Cu	Ag	Au
$E_F$ (ev)	1.53	7.04	5.51	5.51
$T_F$ (deg)	18,000	82,000	64,000	64,000
$u_F$ (cm/sec)	$0.75 \times 10^8$	$1.58 \times 10^8$	$1.40 \times 10^8$	$1.40 \times 10^8$

Figure 2.

directly proportional to the successive velocities of the electrons. As the electron energies increase, the surface areas of the spheres become larger and can therefore contain more electrons.

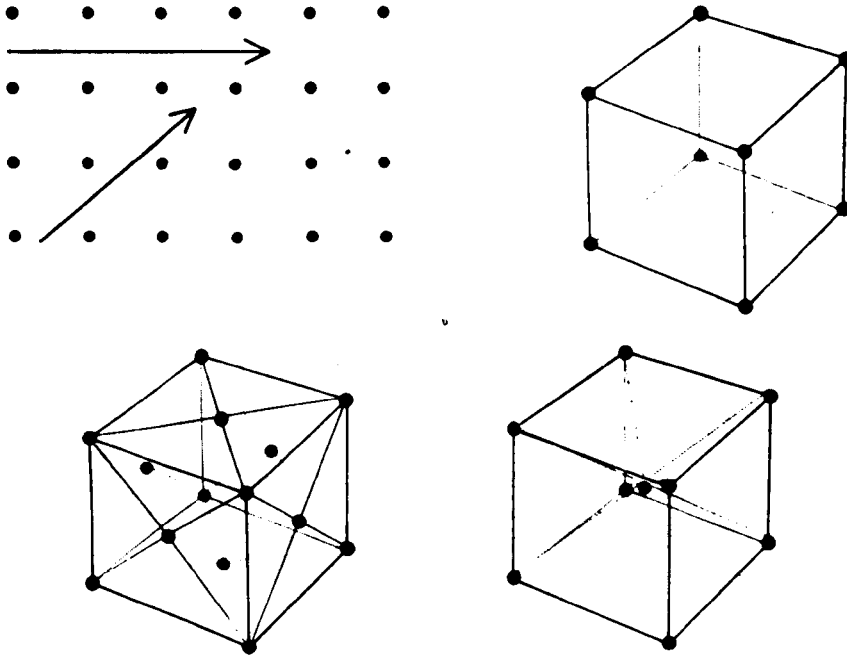
In the velocity space system, the Fermi level becomes the Fermi surface, that is, the sphere that separates the occupied from the unoccupied velocities; the velocity of the electrons at the Fermi surface is known as the Fermi velocity  $U_F$ .

So far, the only restriction applying to the free electron energies that has been discussed is the exclusion principle, from which was derived the Fermi Dirac energy distribution.

The electrons being charged are influenced by the other charged particles in the lattice system. In other words, the other electrons and positively charged lattice ions modify the free electrons' energy distribution.

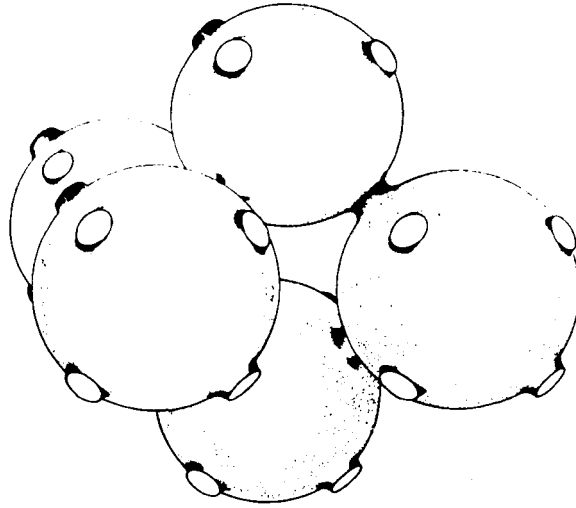
D. Bohm and D. Pines (4) in the early 1950s suggested that the free electrons do not influence each other to any marked extent because of two factors. Firstly, because of their negative charge the electrons repel each other and will therefore arrange themselves so that they are the greatest possible distance apart. The second factor is that of the positive lattice ions. The ions will tend to screen the electrons from each other, and so the electrostatic force of repulsion between the valence electrons will be further reduced.

Although the free electrons affect each others' behaviour only to a small extent, the effect the lattice has on the valence electrons' motion is considerable.

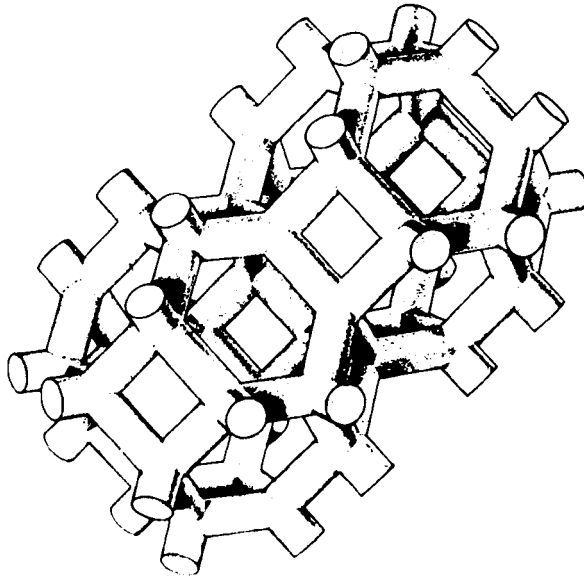


**EFFECT OF LATTICE STRUCTURE** on electron motion in a metal (and thus on the shape of its Fermi surface) is considerable. In a simple cubic lattice an electron (*horizontal arrow at top left*) moving along a row of positive ions (*dots*) interacts more often with the ions than one moving diagonally does. The effects are more complicated in face-centered cubes (*bottom left*) and body-centered cubes (*bottom right*) than in a simple cube (*top right*).

Figure 3.



Extended-zone scheme of copper



Extended-zone scheme of lead

Figure 4.

Consider a simple cubic lattice (see Figure 3); an electron moving parallel to the positive ions, i.e. towards a face experiences a different electrostatic field from an electron moving diagonally towards a corner.

Because the intensity of the electrostatic field depends on the direction of motion within the lattice, it follows that the electrons will have an energy distribution that is spatially dependent.

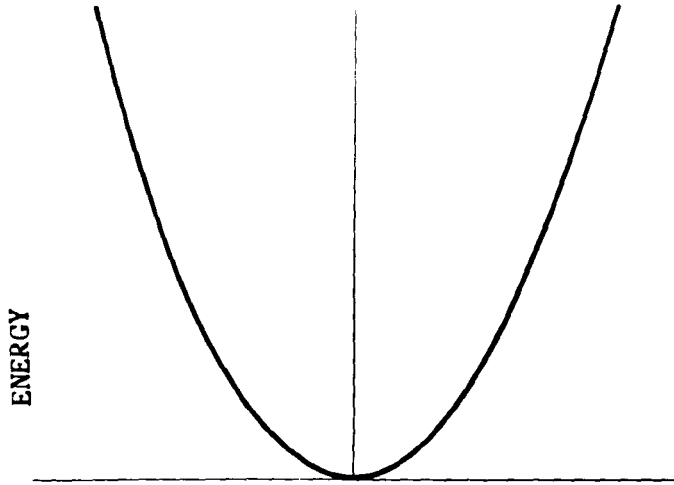
Because the positive lattice ions influence the free electrons' energy distribution, the Fermi surfaces are distorted, and instead of being spheres, they have bulges in particular directions (see Figure (4)).

The moving electrons, besides being affected by the electrostatic field of the lattice ions are diffracted by the regular lattice spacings. The most important consequence of this diffraction, is that it leads to the existence of energy gaps in the free electrons' energy distribution. L. Brillouin was the first man to calculate the values of these energy gaps and hence they have become known as "Brillouin zones".

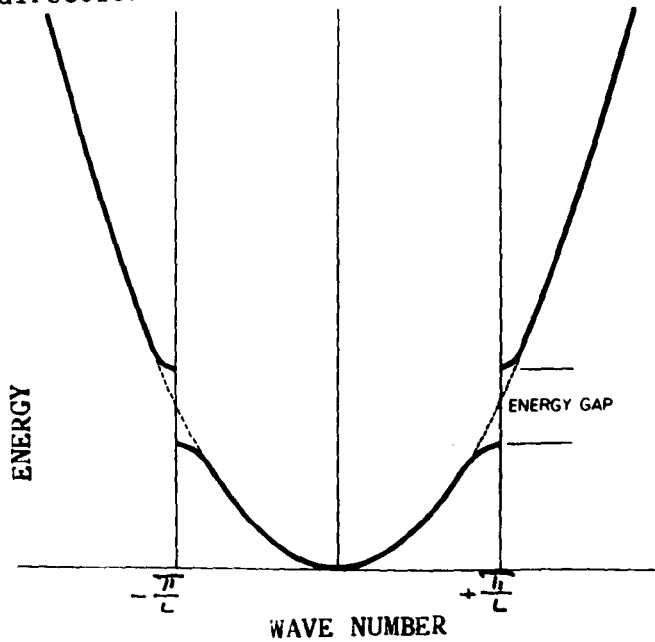
Brillouin used the "wavenumber" (the wavenumber is the number of wavelengths in a distance of  $2\pi$  cm., i.e.  $\frac{2\pi}{\lambda}$ ) in his calculations instead of wavelengths, for ease of calculation.

A plot of energy as a function of wave number illustrates the nature of these energy gaps (see Figure (5)).

In a crystal the lattice spacings are spatially dependent and thus the allowed and forbidden energy levels will depend on the direction of the free electrons' motion (see Figure (6)).

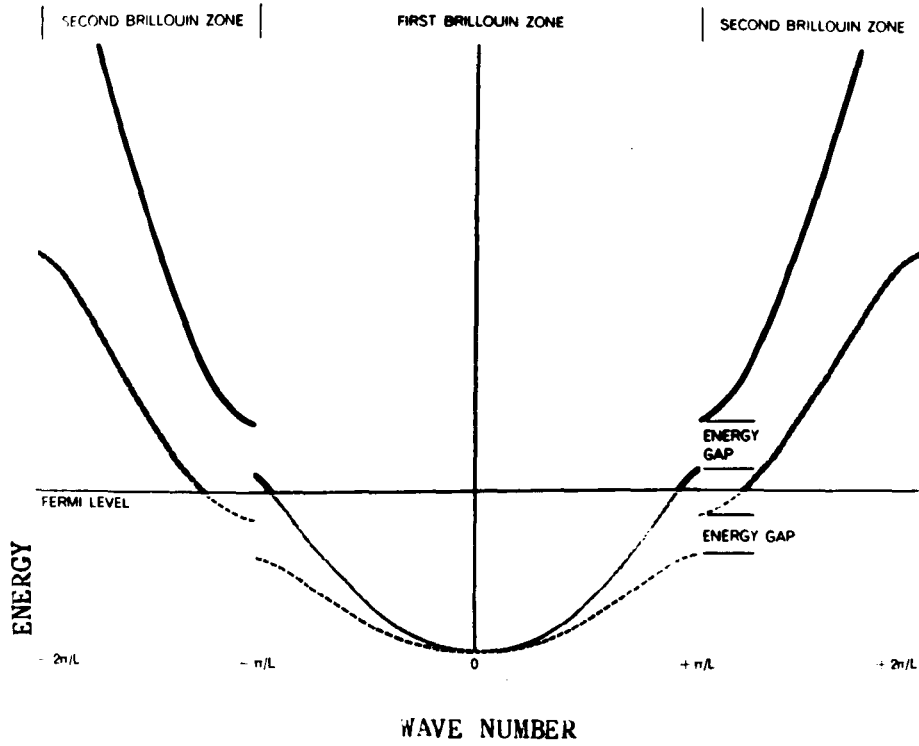


Plot of energy against wave number for an electron moving at different speeds in a particular direction in a metal is a parabola.



Plot of energy against wave number for an electron moving in a particular direction approximates a parabola with "energy gaps".  $L$  represents the distance between two positive ions in the lattice through which the electron travels.

Figure 5.



Wave-number spaces in which energy is plotted against wave number are plotted for electrons moving in two different directions. The Fermi level marks the highest energy state occupied by electrons; occupied states (grey curves) are below it and empty states above (black curves). The wave number at which the curves meet (at the Fermi level) gives the position of the Fermi surface in a particular direction in wave-number space.

Figure 6.

Without this concept of energy gaps it is difficult to explain the great difference in electrical conductivity between metals, semiconductors, and insulators. The resistivities range from  $10^{-8}$  ohm.cm for metals to  $10^{22}$  ohm.cm for good insulators. This difference of  $10^{30}$  in resistivity is one of the widest ranges in nature.

Metals, semiconductors and insulators are often represented by their energy gaps, or allowed bands. This useful treatment is known as the band theory of solids.

In the case of metals (see Figure (7)) the highest energy band is unfilled; the electrons in this band can easily be excited from their lower energy levels to higher vacant levels. The electrons can therefore be easily raised to the empty conduction bands by an electric field, so that the material acts as an electrical conductor.

At absolute zero semiconductors and insulators have completely filled valence bands (see Figure (7)) and, because the forbidden band is too wide for electrons to traverse, there is no mechanism for charge transfer. These materials are therefore poor conductors of electricity. The difference between semiconductors and insulators is in the width of the forbidden band, insulators having wider forbidden bands than semiconductors.

At room temperature a few of the electrons in the valence band of semiconductors have sufficient thermal energy to cross the forbidden band and enter the empty conduction band. The electrical conductivity increases as a function of temperature, because more electrons cross the forbidden band as their thermal energies are increased.

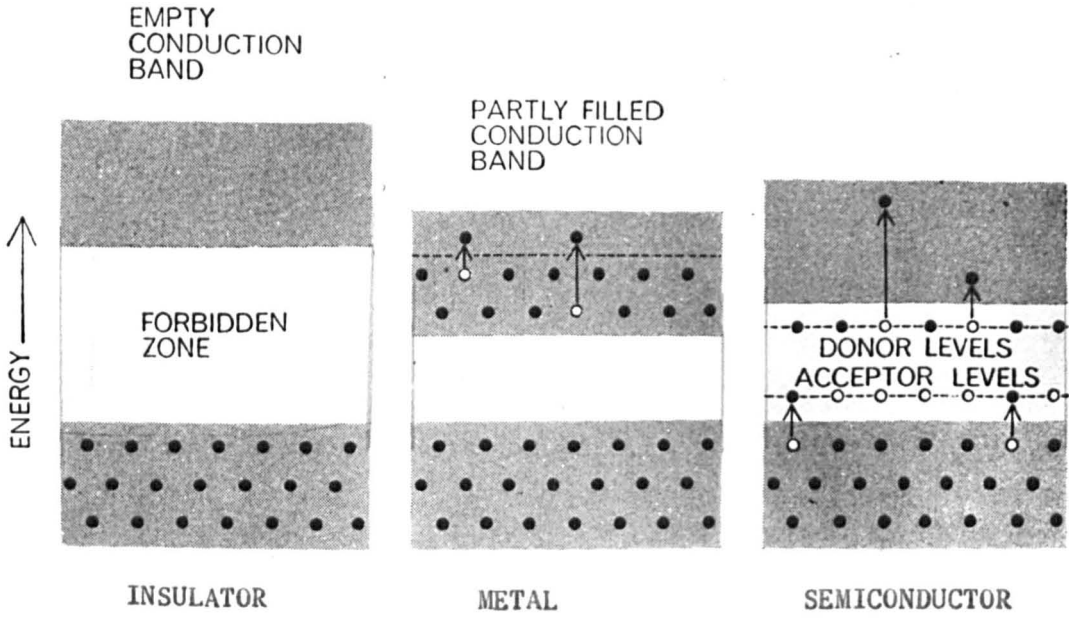
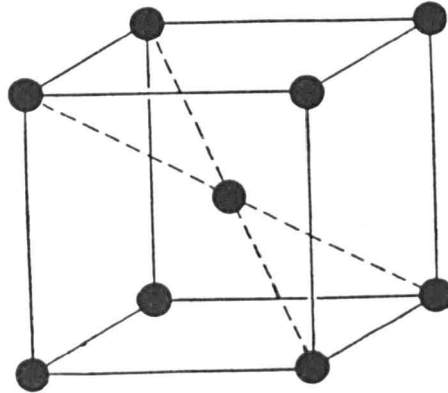


Figure 7.

(a)



One typical structure of metals - the body-centred cubic structure. The atoms inside the crystal are all surrounded by eight neighbouring atoms (top diagram), but atoms at the surface have varying numbers of nearest neighbours (bottom diagram); white atoms have four, dark grey five, light grey six and black seven.

The numbers refer to the crystal plane.

(b)

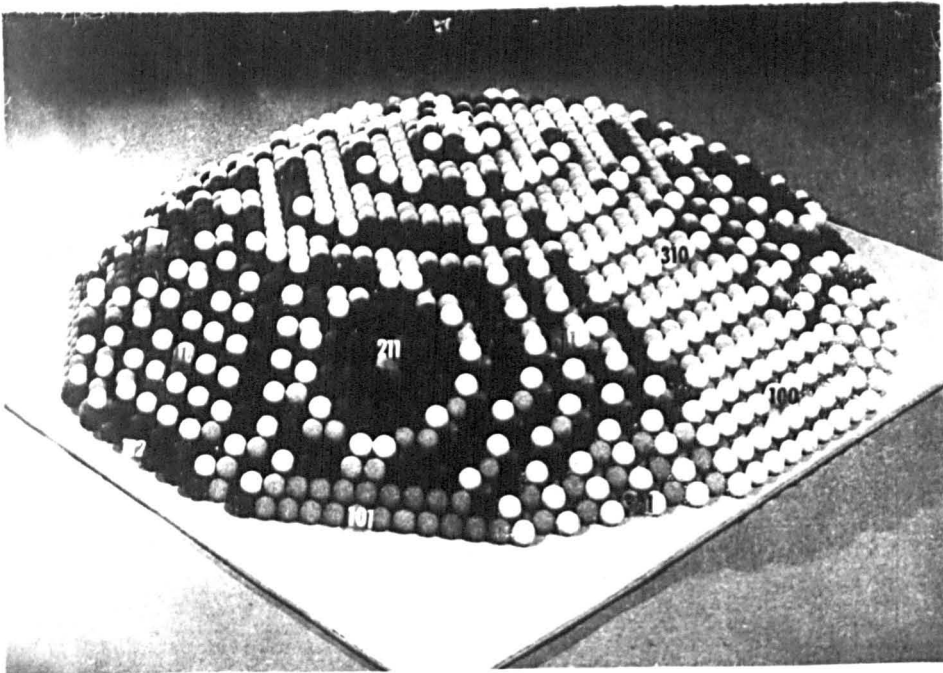


Figure 8.

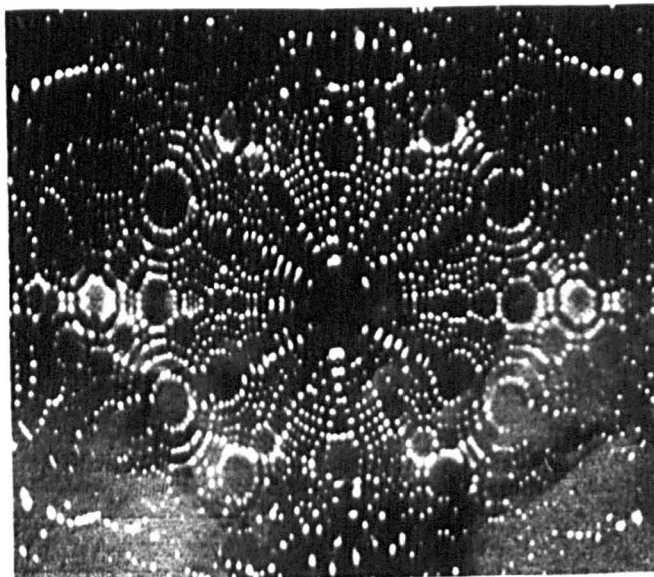
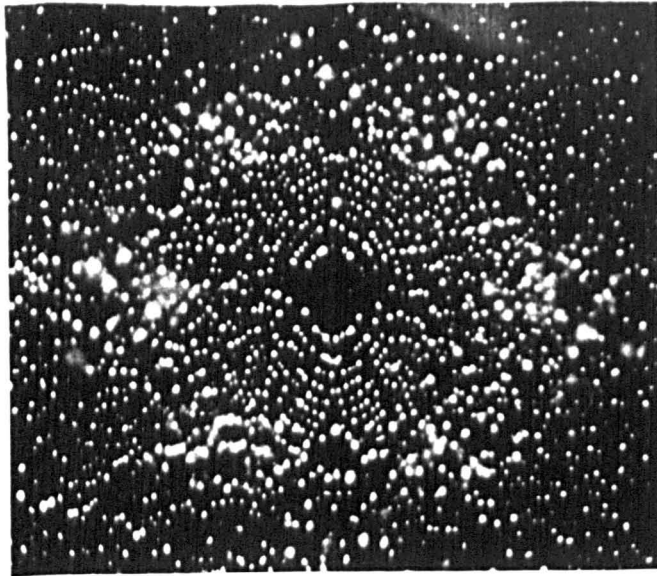
The characteristics of intrinsic semiconductors are changed by the addition of small amounts of impurities. For example, the electrical conductivity of a pure silicon crystal is increased by a factor of  $10^3$  by the addition of boron impurity atoms, in the proportion of 1 boron atom to  $10^3$  silicon atoms.

The addition of impurity atoms into the lattice of an intrinsic semiconductor lattice produce additional electronic energy levels called impurity levels. If these are located just below the conducting band they are known as donor levels, and if they are situated just above the valence band they are termed acceptor levels. The energy required to raise electrons from the donor levels to the conduction band, or from the valence band to the acceptor levels is small compared with the energy gap of the pure material. It is therefore possible for materials to behave as semiconductors, although the energy gap between the conduction and valence bands of the pure material is large.

#### 1.4 A Comparison of Internal and Surface Crystal Environments

In metals the energy distribution of free electrons is determined by the atomic energy levels and the influence of the crystal lattice; therefore any departure from the ideal bulk structure will change the free electron energy distribution. Hence, atoms that are on the surface of a crystal have an electronic environment different from that in the interior of the sample.

Consider a body-centred cubic structure:- the atoms inside the crystal are surrounded by eight neighbouring atoms (see Figure (8a)), but atoms on the surface vary in their number of nearest neighbours.



Chemical behaviour of different planes in a crystal may vary just as much as that of entirely different solids. The (110) plane of tungsten does not adsorb nitrogen at room temperature although all other planes do; this is shown by the photographs of a clean crystal (above) and the same crystal after exposure to nitrogen (below). The (110) plane in the centre remains uncontaminated.

Figure 9.

depending on the plane in which they are situated. This difference in environment as a function of position is illustrated in Figure (8b). It can be seen that the atoms on the more densely packed planes have the highest number of neighbouring atoms. Consequently, the properties of the atoms and the behaviour of the electrons will depend on position in the material.

In chemical reactions different crystal planes of a clean surface may act like entirely different substances. Molecular nitrogen is dissociated and then strongly adsorbed by a clean tungsten surface. The efficiency of this dissociation and adsorption varies considerably from one crystal plane to another (5,6). At room temperature, the tungsten [110] plane, which is the most densely packed does not cause the dissociation and adsorption of nitrogen; it remains uncontaminated while the other less densely packed planes are covered with a dense layer of adsorbed nitrogen (see Figure (9)).

In common with chemical properties the physical properties of a surface vary from one crystal plane to another. The dynamical properties of the surface atoms are different from the atoms in the bulk of the crystal. Conventional and low energy electron diffraction results (7,8) indicate that the mean square vibrational amplitude of atoms at the surface of silver, copper and nickel crystals is greater than that of atoms in the interior of the crystal. The mean square vibrational amplitude of the atoms will also depend on which crystal plane they are situated (e.g. the mean square vibrational amplitude of an atom will be

greater if it is on the [001] plane, than if it is on the [110] crystal plane).

Surface atoms differ from internal ones in another important respect; the amplitude of their component of vibration that is normal to the surface is not equal to the tangential component (9).

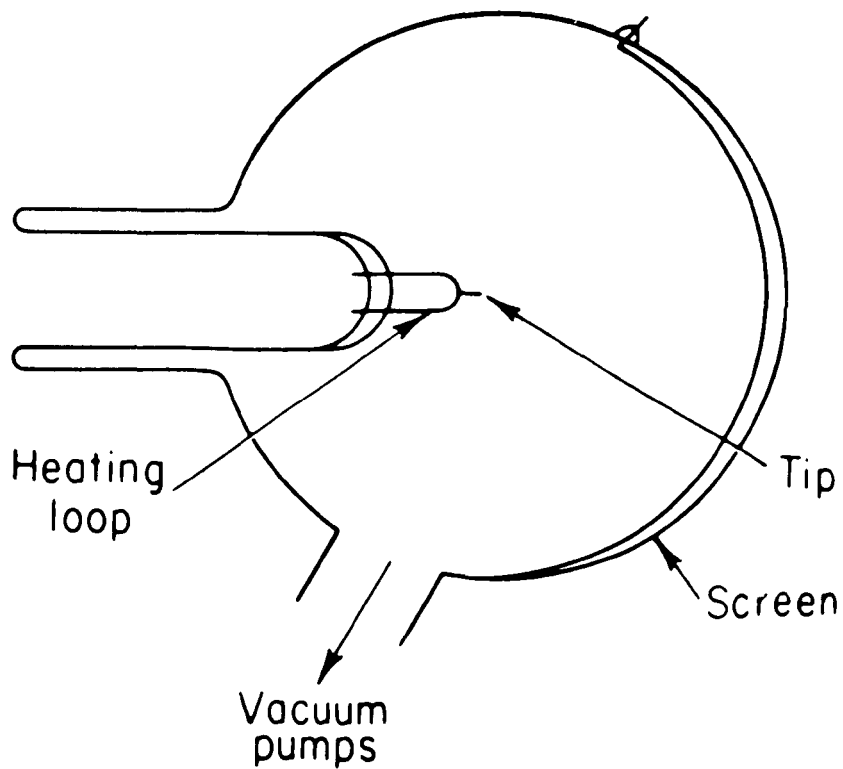
As the behaviour of the electrons in the interior of crystals is spatially dependent, it is not surprising that as the free electrons approach a surface their energy distribution will depend on which plane they are approaching. It therefore follows that the energy required to remove an electron from the metal (i.e. the work function) will depend on the crystal plane of the surface.

## 1.5 Techniques used in the Study of Surfaces

Most of the techniques used to investigate the nature of surfaces observe the particles and electromagnetic radiation emitted or reflected by the surfaces.

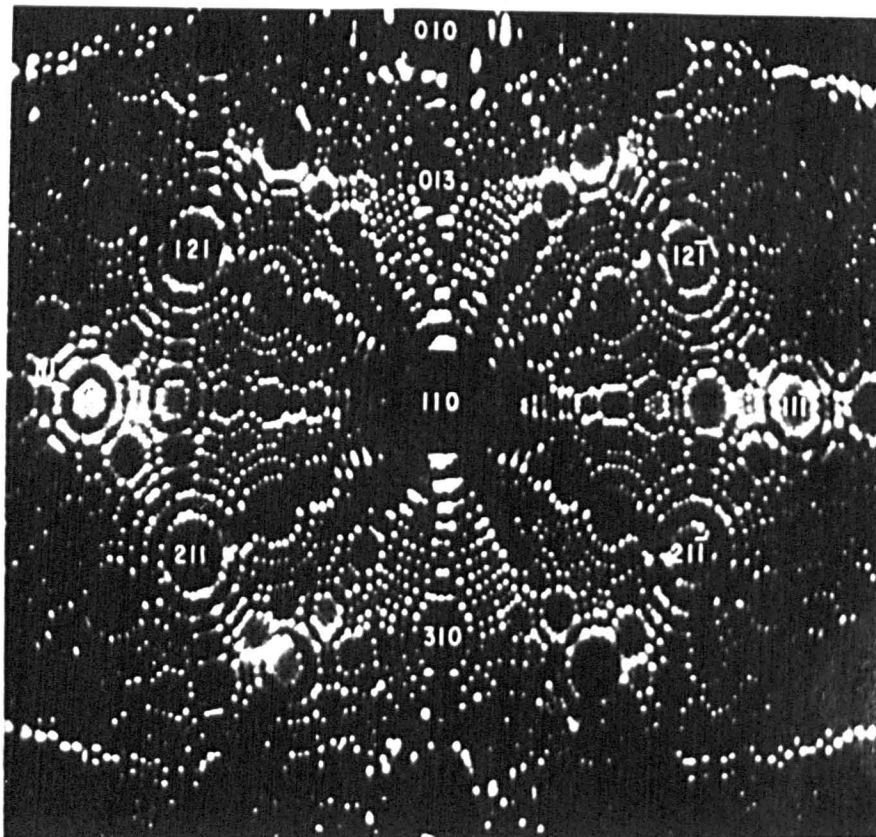
The influence of the optical microscope in surface science has been immense, and until about 1930 it was one of the most powerful instruments used in probing surface structures.

By the end of the nineteenth century, the optical microscope was capable of magnifications of about a thousand but because of the wave nature of light any further increase in magnification was impossible. Unfortunately, there are only a few limited techniques available which are capable of focussing electromagnetic radiation of shorter wavelengths than the visible section of the spectrum. This difficulty in focussing radiation of high frequencies led to the development of the electron



Schematic diagram of a field emission microscope.

Figure 10.



Surface of tungsten photographed  
in the field-emission microscope.

Figure 11.

microscope in the early 1930s.

The initial stimulus for an electron microscope came from Hans Busch, who argued that the electro-magnetic solenoid used in the cathode ray tube was equivalent to an optical lens. By 1933 Ruska, at the Technische Hochschule in Berlin, had produced a two-stage electron microscope with a maximum magnification of 10,000 and a resolving power of 500 Angströms. Modern electron microscopes have a resolving power that is limited to about four Angströms. With such a resolution it is possible to distinguish atomic lattices of large spacing, but not individual atoms or the lattices of metals.

With the development of the field emission microscope it is now possible to resolve individual atoms of a limited range of materials (10). In the field emission microscope the particles which produce the image are not focussed by a lens system, and therefore, technically the instrument is not a microscope in the conventional sense.

The sample is in the form of a fine electropolished point and is placed in an evacuated chamber (see Figure (10)). When a high potential (usually a few kilovolts) is applied between the tip and a conducting spherical phosphor screen, electrons are emitted from the point.

The amount of field emission current is dependent on the work function of the surface, and since the emitted electrons follow the radial lines of force, it therefore follows that a highly magnified image of the point is produced on the fluorescent screen.

A typical photograph obtained from the field emission microscope is shown in Figure (11). The bright patches in the photograph correspond

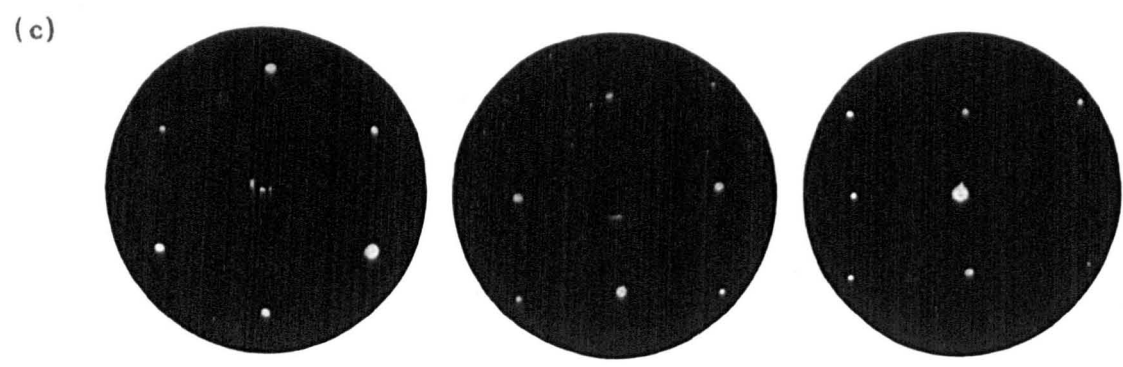
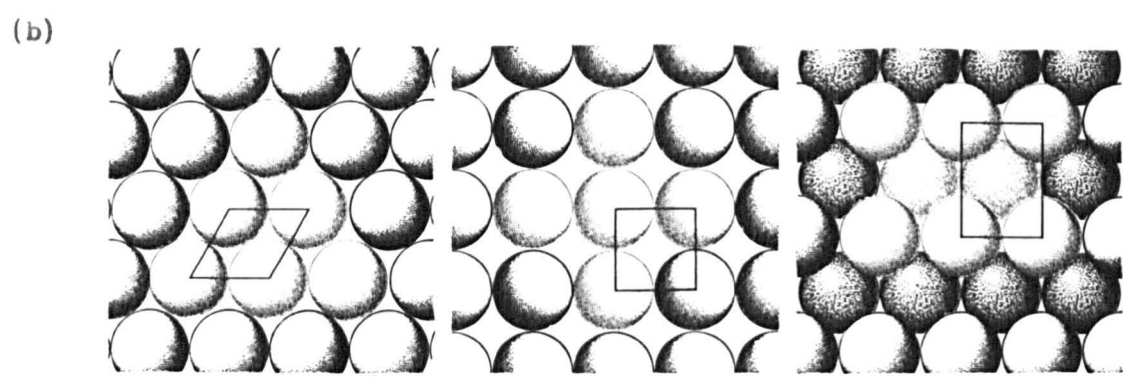
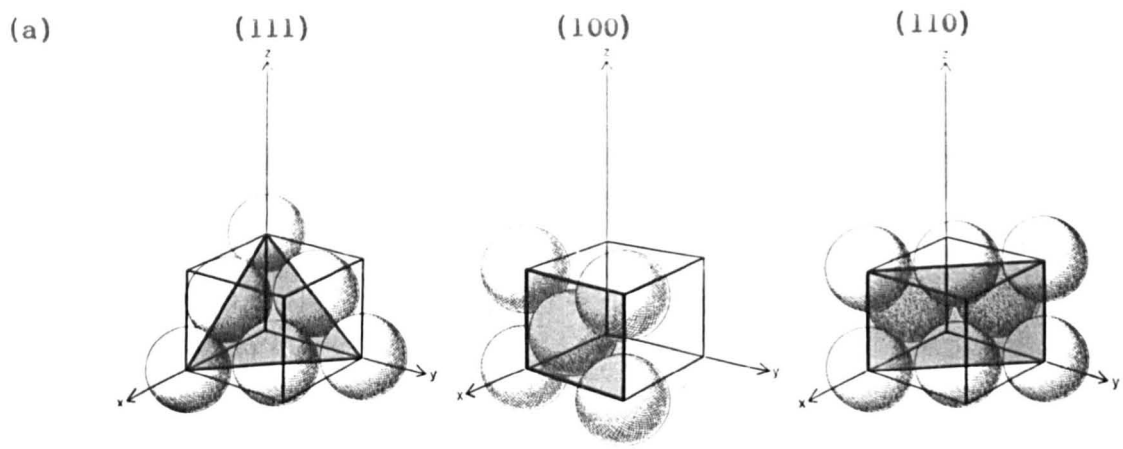


Figure 12.

to the individual atoms of an atomically clean tungsten surface. The different lattice planes are given by the numbers. In the (111) plane the atoms are only  $4.5\text{\AA}$  apart, and the diameter of the surface shown is about  $1,000\text{\AA}$ , which illustrates the instrument's excellent magnification and resolution.

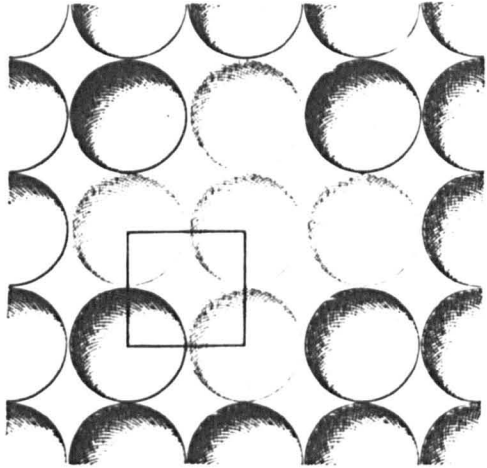
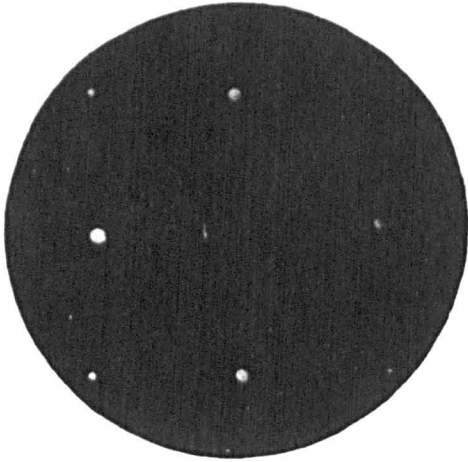
Beams of electrons have been used as a powerful tool for examining the surface structure of a variety of crystals. To obtain an atomic diffraction pattern the incident waves must be of shorter wavelength than the inter-atomic spacings on the crystal surface.

Electrons with an energy of about 100 volts have a de Broglie wavelength of approximately  $1\text{\AA}$ , and as their penetration is limited to the outer atomic layers of the surface, the diffraction pattern produced by the reflected electrons discloses the surface structure.

Consider a face-centred cubic structure (see Figure (12)). The three diagrams in Figure (12a) show the three simplest surfaces that are produced by cutting sections through it. The three diagrams in Figure (12b) illustrate the structure of the different surfaces. It can be seen that the surface atoms on the three faces have different environments. The diffraction patterns produced by the (111), (100) and (110) faces of a face-centred cubic structure are shown in Figure (12c). It is possible to calculate the arrangement of the surface atoms from such diffraction patterns.

Low energy electron diffraction techniques are also used to investigate the configuration of adsorbed atoms on clean surfaces.

(a)



(b)

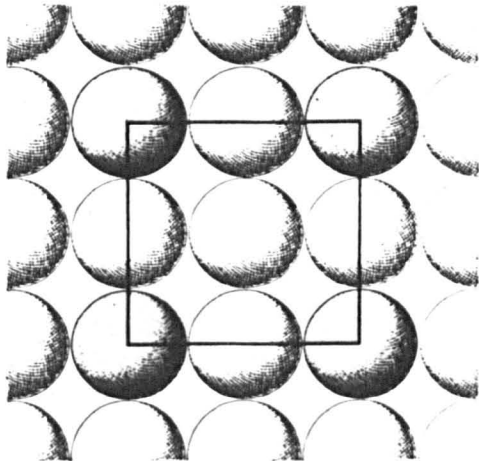
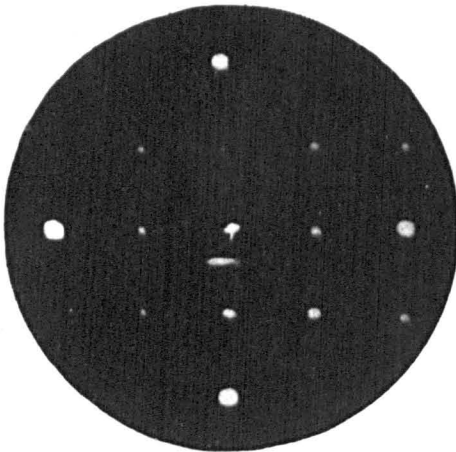


Figure 13.

A clean nickel (100) face produces a diffraction pattern as shown in Figure (13b). When oxygen is admitted into the vacuum system containing the exposed nickel (100) face, the diffraction pattern changes from the one illustrated in Figure (13b), and gradually a number of diffuse streaks appear. As more oxygen is adsorbed these streaks coalesce into new sharp spots. The new diffraction pattern is a square array half the size of the original (i.e. Figure (13a)).

The new surface arrangement contains atoms of both nickel and oxygen. These diffraction patterns indicate that oxygen adsorption causes complete rearrangement of the nickel atoms on the crystal surface, and the rearrangement begins when only a partial layer of oxygen atoms has been adsorbed.

Electrical resistance measurements of thin conducting layers deposited on non-conducting substrates provide a means of investigating the surface characteristics of thin films.

If the film under investigation is thin (i.e. less than 100 atomic layers) its electrical conductivity will be influenced to a considerable extent by the nature of the surface.

From electrical conductivity measurements as a function of film thickness and temperature, it is possible to determine how the behaviour of the conduction electrons is influenced by lattice defects and scattering at the surface.

There is always a change (usually an increase) in the electrical resistance of thin films when they adsorb gases (11). At room temperature the changes are small, usually less than 5% for most gases. Hence,

electrical conductivity measurements are a useful probe in the investigation of surfaces. The technique has the added advantage of not changing the surface under investigation, and so can be used to monitor surface reactions.

The work required to remove an electron from a metal is known as the work function. This quantity depends upon the properties of the bulk material and the nature of the surface. It is therefore possible to determine from work function measurements the characteristics of surfaces, and how they change as a function of:

- a) temperature;
- b) adsorption;
- c) crystal orientation;
- d) the internal structure of the material.

As the subject of this thesis is work function measurements and their interpretation, this topic will be discussed in detail in the next chapter.

## 1.6 The Preparation of Clean Surfaces

A clean surface exposed to a gas at atmospheric pressure is subjected to  $3 \times 10^{23}$  molecular impacts per square centimeter per second. Many of the gas molecules do not rebound elastically, but are adsorbed onto the clean surface. This process of adsorption continues until the surface is covered by many layers of molecules. The time taken for a monolayer to form is inversely proportional to the pressure. For air at a pressure of 1 torr the time taken is approximately  $10^{-6}$ secs, at a pressure of  $10^{-10}$  torr it is more than five hours.

For this reason, ultra-high vacuum conditions are essential for the preparation of clean surfaces.

Clean surfaces may be prepared on metallic and non-metallic substrates by several different techniques, the principle methods of producing clean metal films being:

- a) Vacuum evaporation
- b) Crystal cleavage
- c) Elimination of impurities by heat treatment
- d) Desorption of surface residues by electron bombardment
- e) Cathodic sputtering
- f) Field evaporation

Vacuum evaporation has the advantage that many types of substrate can be used. One of the main criteria for the choice of substrate is that it should have a low vapour pressure (i.e., below about  $10^{-12}$  torr)

The material to be evaporated is initially heated to a temperature just below the temperature at which it has an appreciable vapour pressure. The impurities which are more volatile than the material are therefore eliminated by evaporation. A further temperature rise vaporizes the purified material - leaving behind the less volatile contaminants.

The thickness of condensed films can be controlled to finer limits than is possible with other methods of film production. This precise control of film thickness, coupled with monitoring techniques (e.g. quartz crystal measuring methods) has enabled the properties of surfaces to be investigated as a function of thickness.

The structure of evaporated films is found to be highly dependent on the condition of the substrate surface, the initial temperature of the substrate, any subsequent heat treatment, and the evaporation rate. It can be seen that vacuum evaporation is an extremely versatile process.

Clean surfaces can be produced by breaking or cleaving single crystals in high vacua. The availability of almost perfect large single crystals limits the general application of the technique, but the greatest limitation is the small number of materials with suitable cleavage planes.

The great advantage of this method is that definite clean crystal planes can be produced at low temperatures (i.e. ambient), thus reducing the possibility of lattice defect formation, which often occur if other techniques are used.

Under favourable conditions clean surfaces can be produced by maintaining the material at a high temperature for prolonged periods of time. The adsorbed residues are desorbed provided they are less firmly bonded to the surface than the atoms of the material itself.

This method is rather limited in its application, since the surface to be cleaned has to be stable at high temperatures, usually in the order of  $1500^{\circ}\text{C}$ . Hence, only the more refractory materials (such as tungsten, molybdenum, tantalum and silicon) respond to this treatment.

Unfortunately, at the high temperatures needed to desorb the surface residues, impurities dissolved in the bulk material will tend

to diffuse towards the surface. G.E. Moore (12,13) investigated the production of further surface residues from dissolved impurities. He concluded that the carbon monoxide evolved from hot refracting metals was produced from dissolved carbon and oxygen atoms, which had diffused to the surface of the metal, where they combined to produce the carbon monoxide molecules.

Clean surfaces can be produced by bombarding contaminated materials with low-power density beams of electrons (i.e.  $5 \times 10^{-5}$  amp/cm<sup>2</sup> at 100 volts). The adsorbed impurities are desorbed in the form of an ion current.

D. Lichtman (14) has investigated the mechanism of electron beam induced desorption by comparing thermal and electron induced desorption data. He concluded that under favourable conditions surfaces can be cleaned by electron bombardment.

If the power of the bombarding beam is sufficiently small the temperature rise of the surface will be negligible, therefore impurities dissolved in the bulk of the material will not diffuse to the surface easily.

Low energy electron diffraction techniques have been employed by R.M. Bruger and co-workers (15) to demonstrate that clean surfaces can be produced by cathodic sputtering techniques, in conjunction with heat treatment.

The surface to be cleaned by sputtering is placed in a pure inert atmosphere of argon, at a pressure of about  $10^{-3}$  torr. The bombarding positive ions are produced in a discharge maintained by an applied

voltage of about 500 volts. The positive ion current density is kept at a low value (i.e.  $100\mu\text{amps}/\text{cm}^2$ ) to prevent surface pitting. Atomically clean surfaces of the refractory metals such as titanium and nickel have successfully been produced by this technique. Their final surface structures were found to be parallel to the atomic planes of the bulk material.

In conclusion, this method is limited in its application, since, it is unlikely that gas molecules will be completely prevented from entering the structure of the surface in the case of the more reactive metals.

Under favourable conditions clean surfaces can be prepared by using high electrostatic field techniques. Field evaporated surfaces are usually produced in field ion microscopes by increasing the potential of the tip so that the field is about  $10^9$  volts/cm near the surface of the tip (16). Weakly held surface contamination and irregularities are removed from the surface of the metal sample by the high field. Repeated field evaporation removes successive atomic layers and it is thus possible to observe defects present in the bulk of the material as they emerge at the surface (17).

This technique has the advantage that it can be applied to a wide range of materials, but unfortunately, it can only prepare clean surfaces with an area of approximately  $10^{-10}$   $\text{cm}^2$ .

## 1.7 The Factors which determine Surface Characteristics

Many investigators have studied the physical and chemical properties of surfaces under what were considered to be identical conditions. Until recently, the reproducibility of the experiments has been extremely poor. The lack of agreement was due mainly to the residual gases (which were of unknown composition) adsorbed by the surfaces and incorporated in the film material during condensation.

In any investigation of the physical and chemical properties of thin films it is essential to measure the characteristics of the bulk material, the surface, and the gas phase residues. It is therefore considered appropriate to summarize the factors which influence the properties of surfaces. Modern ultra-high vacuum techniques are incapable of attaining absolute vacuum conditions; and hence all surfaces are in gaseous environments and are thus liable to contamination.

The residual gases can affect the nature of surfaces in two ways.

Firstly, the presence of a gas atmosphere during the growth of a thin film can influence the internal structure of the material. Reactive gases such as oxygen will be incorporated in the bulk structure of the thin film, during condensation. The resulting surfaces will tend to have irreproducible physical and chemical properties.

Secondly, there is the effect of surface contamination. An adsorbed layer of gas can change the properties of surfaces to a marked extent.

Many investigators (18,19) have observed the change in electrical conductance of thin metal films (i.e. less than 100 atomic layers) when a gas is adsorbed. These conductance changes, which are of the order of a few per cent, are usually interpreted as being due to the adsorbed gas layers influencing the behaviour of the conductance electrons.

Most of the chemical and physical properties of clean surfaces are influenced by the addition of adsorbed layers. It is therefore essential to monitor total and partial pressures at every stage of an experiment.

In any investigation of surface properties it is essential to have information concerning the nature of the bulk structure of the material. The characteristics of surfaces can be affected by the nature of the underlying layers in three main ways:-

- a) The structure of the pure material.
- b) The influence of lower layers having a different structure from the surface material.
- c) The thickness of the film.

The properties of an idealized perfectly clean surface would be determined solely by the structure of the underlying bulk material - if it were possible to produce an absolute vacuum and materials of perfect purity. Hence, the properties of real surfaces are not determined only by the characteristics of the pure bulk material.

Since, the properties of surfaces are dependant on their microscopic geometry, rough and smooth surfaces of the same material will have different chemical and physical properties.

It has been shown that the microscopic structure of a surface depends on its method of production, and hence a clean film prepared by evaporation will have different properties from a surface produced by cleaving. As the roughness of surfaces is difficult to measure in absolute terms it has been found useful to introduce the "surface roughness factor", which is defined as the ratio of the actual to the geometric areas. For example, the typical roughness factor of an evaporated aluminium film is about 2.5, and that of an evaporated rhodium surface can be as high as 10 (106).

It is therefore imperative in any investigation of surfaces to have as complete an understanding as possible of the internal and surface structures.

The thickness and nature of the underlying layers can influence the behaviour of a surface.

Investigations (20) have demonstrated that the electrical conductivity of films varies as a function of thickness. The crystalline properties of films also vary as a function of film thickness. A series of experiments has recently been performed (21) to investigate recrystallization in copper and gold films. The time of recrystallization was found to increase with decreasing thickness.

The surface micro-structure of a substrate can influence the structure of a deposited film. This phenomenon of oriented intergrowth between two crystalline materials is called epitaxy. Hence, in considering the properties of any given surface it is imperative to measure the film thickness, and state the substrate surface structure.

When a material is heated, the kinetic energy of its atoms and their interatomic distances increase, and therefore it is not surprising that the chemical and physical properties of surfaces vary as a function of temperature.

Research into the adsorption rates of gases on clean surfaces as a function of temperature, has been performed by a number of workers (22). From those and similar experiments it is apparent that most surface phenomena are temperature dependant.

## 1.8 Conclusion

In this chapter the theoretical and practical importance of surfaces, and in particular solid surfaces, has been stressed.

Much of the previous work in this field has been complicated by ill-defined conditions produced by exposure to gas phase residues. Therefore, to obtain meaningful measurements of surface properties it is necessary to initially prepare clean surfaces, and any subsequent contamination must be clearly defined.

One of the most informative tools used to investigate surface phenomena is the study of work function measurements.

The following chapter is concerned with the measurement and interpretation of work function values.

## CHAPTER II

### ELECTRON EMISSION AND WORK FUNCTION MEASUREMENTS

#### 2.1 Introduction

The technology of electronics began in 1883 when T.A. Edison patented what became known as the "Edison" effect and what is now known as thermionic emission. This effect was applied by Fleming in 1904 to rectification and by L. de Frost in 1906 to amplification.

A considerable part of modern electronics is based on the emission of electrons from surfaces, and the control of these electrons to perform various tasks.

Electrons can be induced to leave a surface by two methods:-

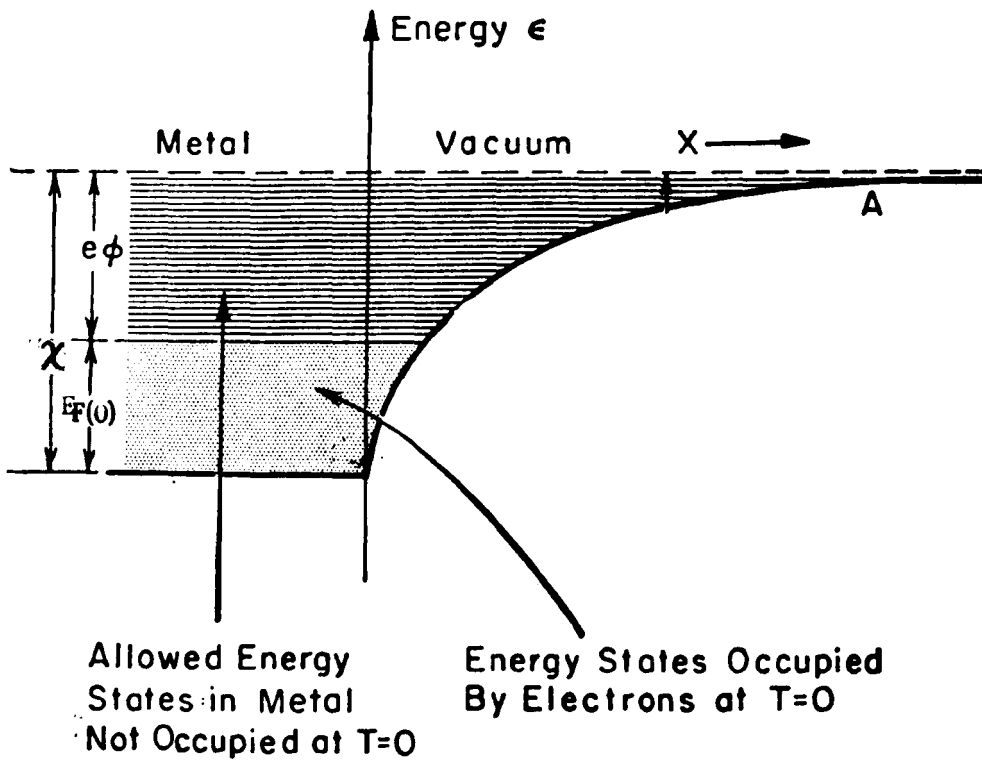
(A) By giving the electrons sufficient energy to overcome the surface barrier.

(B) By thinning and reducing the height of the surface barrier by the presence of a strong applied electrostatic field.

The theoretical treatment of these two methods will be discussed separately.

The band theory of solids, which was outlined in the previous chapter, serves as a useful model in the explanation of electron emission. The electrons have energies which are distributed up to the Fermi level  $E_F(0)$  (Figure (1)).

If the potential energy of an electron in the partly filled conduction band is lower by a factor of  $\chi$  than one which is an infinite distance above the surface, then the work required to remove an electron



Energy levels in a metal and the potential energy of an electron near the metal surface.

Figure 14.

from the metal (usually known as the work function) will be the difference  $(\chi - E_F(0))$  see Figure (14).

The work function  $\phi$  arises from two effects. The first is the electrostatic or image force, between the emitted electron and its induced "mirror image" in the metal. The second component arises from the difference in chemical potential between an electron in the metal and one an infinite distance above the surface.

The potential energy of an electron due to the action of these two forms is shown as a function of its distance above the surface in Figure 14.

It is assumed that the surface is a structureless equipotential plane and that there are no fields due to space charge effects nor an applied electrostatic field, (23).

## 2.2 Types of Electron Emission

### 2.2.1 Thermionic Emission

The idealized example of thermionic emission from a clean metal surface will be considered.

The number of electrons per second approaching the surface with sufficient energy in a direction normal to the surface to escape over the potential barrier will be calculated.

It is convenient to express the Fermi-Dirac distribution in terms of momentum  $P$ .

$$\int n_p = \frac{8\pi}{h^3} \frac{p^2 \int p}{\exp \left[ \left( \frac{E - E_F(0)}{kT} \right) \right] + 1} \quad (2-1)$$

where  $\delta n_p$  is the number of electrons per  $\text{cm}^3$  with momentum between  $P$  and  $P + \delta P$ .

The momentum  $P$  is the vector sum of  $P_x, P_y$  and  $P_z$ , and if the  $yz$  plane is considered to be the emitting surface, only the  $P_x$  component, which is normal to this plane need be considered.

Hence equation (2-1) can be transformed as

$$\delta n_x = \frac{2 \delta P_x}{h^3} \int_0^{\infty} \frac{2\pi r dr}{\exp \left[ \frac{(E - E_{F(0)})}{kT} \right] + 1} \quad (2-2)$$

where  $\delta n_x$  is the number of electrons per  $\text{cm}^3$  with momentum in the  $x$  direction between  $P_x$  and  $P_x + \delta P_x$ ;  $r$  is the resultant momentum in the  $yz$  plane, given by:  $r^2 = P_y^2 + P_z^2$

Because the electrons obey a Fermi-Dirac distribution of energy  $E - E_{F(0)}$  is large compared with  $kT$  and so the unity in the denominator of (2-2) can be neglected.

The electron energy  $E$  in (2-2) is given by

$$E = \frac{(P_x^2 + P_y^2 + P_z^2)}{2m} = \frac{(P_x^2 + r^2)}{2m}$$

Substituting this value of  $E$  into (2-2) and integrating

$$\delta n_x = \frac{4\pi m k T}{h^3} \exp\left(\frac{E_{F(0)}}{kT} - \frac{P_x^2}{2m k T}\right) \delta P_x \quad (2-3)$$

The electrons which have a momentum which is greater than  $P_x$  can pass through the potential barrier of total height  $\chi$ .

where

$$\frac{P_x^2}{2m} = \chi = E_{F(0)} + \phi$$

The current carried by each electron will be the product of its charge and velocity, which is  $\frac{eP_x}{m}$ .

The total emitted current per unit area is given by:

$$I = \frac{4\pi emkT}{h^3} \exp \frac{E_F(0)}{kT} \int_{P_x}^{\infty} \frac{P_x}{m} \exp \left( - \frac{P_x^2}{2mkT} \right) . dP_x$$

$$= \frac{4\pi emk^2 T^2}{h^3} \exp \left( \frac{E_F(0)}{kT} - \frac{P_x^2}{2mkT} \right) \quad (2-4)$$

But  $\frac{P_x^2}{2m} = E_F(0) + \phi$  therefore (2-4) reduces to

$$I = \frac{4\pi emk^2}{h^3} . T^2 \exp \left( - \frac{\phi}{kT} \right) \quad (2-5)$$

$$= A_0 T^2 \exp \left( - \frac{\phi}{kT} \right) \quad (2-6)$$

Equation (2-6) is usually called the Richardson-Dushman equation (24).

The proportionality constant (usually known as the Richardson constant) has the numerical value of  $3.6 \times 10^{11}$  when measured in e.s.u., and 120 when the current is measured in amperes.

Equation (2-6) suggests that it is possible to obtain a value for  $\phi$  from the gradient of the straight line obtained when  $\log \frac{I}{T^2}$  is plotted as a function of  $\frac{1}{T}$ . Thermionic emission from real surfaces is complicated by a number of factors:-

- (i) The actual area of the electron emitter is never equal to the macroscopic geometric area.
- (ii)  $\phi$  changes as a function of temperature. (The change in work function as a function of temperature  $\frac{d\phi}{dt}$  is usually  $10^{-4}$  ev/ $^{\circ}$ C for metals.)

(iii) In the derivation of equation (2-6) it was assumed that  $\phi$  is constant for all positions on the surface. This assumption is only valid for uncontaminated planes of a single crystal.

(iv) A fraction of the electrons with sufficient energy to pass through the surface barrier are reflected (25); this, however, for clean metals, is likely to involve only a small correction.

### The Energy Distribution of the Emitted Electrons

The energy distribution of the emitted electrons can be derived from the Richardson-Dushman equation.

The total number of electrons emitted per  $\text{cm}^2$  per second is given by

$$N = \frac{4\pi mk^2}{h^3} T^2 \exp\left(-\frac{\phi}{kT}\right) \quad (2-7)$$

The number of electrons arriving at the surface per  $\text{cm}^2$  per second with velocities normal to the surface in the range  $dV_x$  and  $P_x \geq P_{x_0}$  is obtained from equation (2-3).

$$n(V_x) V_x dV_x = \frac{4\pi m^2 kT}{h^3} \exp\left(\frac{E_F(0)}{kT} - \frac{mV_x^2}{2kT}\right) V_x dV_x \quad (2-8)$$

If  $V_{ex}$  represents the velocity of an electron after emission on the x- direction, then

$$\frac{1}{2}mV_{ex}^2 = \frac{1}{2}mV_x^2 - E_F(0) - \phi$$

$$V_{ex} dV_{ex} = V_x dV_x \quad (2-9)$$

The velocity distribution  $F(V_{ex})dV_{ex}$  of the emitted electrons can be obtained by dividing (2-8) by (2-7) and then substituting (2-9);

one obtains

$$\frac{F(v_{ex})dv_{ex}}{N} = \frac{mv_{ex}}{kT} \exp\left(-\frac{mv_{ex}^2}{2kT}\right) dv_{ex} \quad (2-10)$$

Hence, the velocity distribution normal to the surface exhibits a Maxwellian form.

The Richardson-Dushman equation and the energy distribution of the emitted electrons have been derived by Nordheim (26, 27) using statistical mechanics.

### 2.2.2 Photoelectric Emission of Electrons

In the phenomenon of photoelectric emission, which was discovered by Hertz in 1887 (28) the electrons gain sufficient energy to overcome the surface barrier by absorbing a photon.

The maximum kinetic energy  $E$  of a photo electron on emission at a temperature of  $0^\circ\text{K}$ , is given by the Einstein relationship

$$E = h\nu - \phi$$

where  $\nu$  is the frequency of the incident electro-magnetic radiation, and  $\phi$  is the difference between the Fermi energy of the emitted electron in the metal and the vacuum level.

It was shown in Chapter I that at absolute zero the Fermi-Dirac distribution of electron energies ends abruptly at  $E_F(0)$ . However, at higher temperatures the energy distribution does not end abruptly at  $E_F(0)$  but tails off, and a fraction of the electrons have energies that are greater than  $E_F(0)$ . Consequently, at temperatures above  $0^\circ\text{K}$  the photo electric threshold frequency is not sharply defined.

### 2.2.3 Secondary Electron Emission

Austin and Starke (29) discovered the phenomenon of secondary electron emission in 1903, while investigating the reflection of electrons by metals.

When a solid is bombarded with a beam of electrons, several processes can occur, the nature of which will depend on the characteristics of the material and on the energy distribution of the incident electron beam:

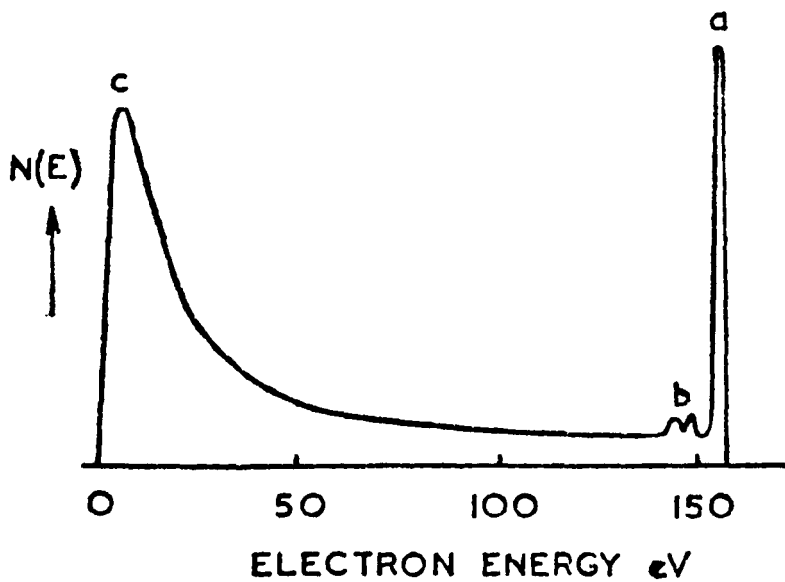
- (1) A fraction of the incident electrons, or primaries, will be elastically reflected.
- (2) The remainder of the electron beam will penetrate the solid and lose energy by exciting the lattice electrons. Some of these primary electrons which have lost a fraction of their original energy return to and escape from the surface. These electrons are known as inelastically reflected primaries.

The lattice electrons which have been excited by the primaries lose their energy in a number of ways:-

- (a) Emission of a photon.
- (b) Dissipation of the energy into heat.
- (c) Escaping from the lattice.

It is therefore possible to distinguish between three categories of electrons emitted from the surface:-

- (i) Elastically reflected primaries.
- (ii) Inelastically reflected primaries.
- (iii) Excited lattice electrons, usually called the true secondaries.



Energy distribution of secondary electrons

Figure 15.

A typical energy distribution, obtained by Rudberg (30,31), illustrates the three categories of electron emission (Figure (15)). It can be seen that there are three peaks in the distribution curve, denoted by a, b and c.

The sharp peak (a) is produced by the primary electrons which have been reflected without loss of energy.

The small fluctuations in the curve at (b) correspond to the inelastically reflected primaries.

The broad low energy peak (c) is due to the true secondary electrons produced in the material by the primary beam.

#### Theory of Secondary Emission

To date, no theory has satisfactorily explained the mechanisms of secondary electron emission. The lack of agreement between experimental observations and existing theories is due, mainly to incomplete understanding of the interaction of the primary electrons with the lattice electrons in the solid. There is also insufficient information concerning the electron energy distribution in many of the materials investigated.

The general shape of the secondary electron yield curves will be derived from a classical approach rather than a wave-mechanical one.

The calculation of the secondary electron yield is simplified if the phenomenon is considered to be split up into two separate stages:-

(A) The production of the secondaries by the primary electron beams

(B) the probability of the secondaries reaching the surface and escaping from it.

To calculate the secondary emission coefficient  $\delta$  a number of assumptions are made:

- (a) The incident primary electrons are normal to the surface.
- (b) The primaries after they have entered the material continue to travel in straight lines that are perpendicular to the surface.
- (c) The primary electrons lose energy in accordance with Whiddington's Law:-

$$-\frac{dE_p(x)}{dx} = \frac{A}{E_p(x)} \quad (2-11)$$

where  $E_p(x)$  is the energy at a depth  $x$  and  $A$  is a constant that is characteristic of the material.

- (d) The number of secondaries produced by a single primary electron in a layer  $dx$  is proportional to  $\frac{dE_p}{dx}$  divided by the average excitation energy required to produce a secondary,  $\epsilon_e$ . Hence,

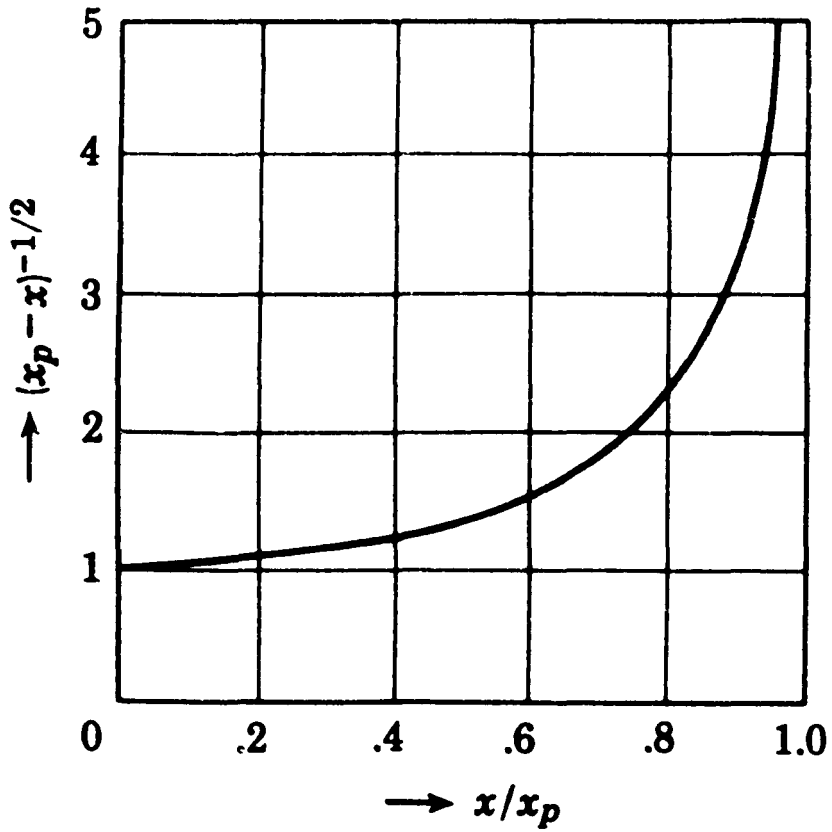
$$n(x) = -\frac{1}{\epsilon_e} \cdot \frac{dE_p}{dx} \quad (2-i2)$$

- (e) The probability of a secondary electron produced at a depth  $x$  reaching and escaping from the surface is:

$$f(x) = f(0) e^{-\alpha x} = f(0) e^{-x/x_s} \quad (2-13)$$

where  $f(0)$  is the probability of escape of a secondary produced near to the surface.

$$x_s = \frac{1}{\alpha} \text{ is considered to be the range of the secondaries.}$$



The second electron yield along the primary path.

Figure 16.

Neglecting the velocity distribution of secondary electrons, the secondary emission coefficient  $\delta$  may be written in the form

$$\delta = \int n(x) f(x) dx \quad (2-14)$$

where  $n(x)dx$  represents the number of secondaries produced in a layer of thickness  $dx$  at a depth of  $x$ , by one primary electron.  $f(x)$  is the probability of a secondary electron reaching and escaping from the surface.

Although the integral extends over the whole thickness of the material, in practice the primary electrons lose most of their energy within a distance of a few hundred Angstroms from the surface.

It follows from (2-11) that if  $E_{p_0}$  is the energy of the primary electrons as they hit the surface, the energy of the primary electrons as a function of distance is given by

$$E_{p(x)}^2 = E_{p_0}^2 - 2Ax \quad (2-15)$$

It can be seen that the approximate maximum distance of penetration of the primary electrons  $x_p$  is obtained by letting  $E_p = 0$ . It thus follows that:

$$x_p = \frac{E_{p_0}^2}{2A} \quad (2-16)$$

The range of the primary electrons is therefore proportional to the square of their energy.

From (2-12), (2-15) and (2-16)

$$n(x) = \left(\frac{A}{2}\right)^{\frac{1}{2}} \cdot \frac{1}{\epsilon_e(x_p-x)^{\frac{1}{2}}} \quad (2-17)$$

$\frac{x}{x_p}$  as a function of  $(x_p - x)^{-\frac{1}{2}}$  is illustrated in Figure (16).

It can be seen that most of the secondary electrons are produced

Neglecting the velocity distribution of secondary electrons, the secondary emission coefficient  $\delta$  may be written in the form

$$\delta = \int n(x) f(x) dx \quad (2-14)$$

where  $n(x)dx$  represents the number of secondaries produced in a layer of thickness  $dx$  at a depth of  $x$ , by one primary electron.  $f(x)$  is the probability of a secondary electron reaching and escaping from the surface.

Although the integral extends over the whole thickness of the material, in practice the primary electrons lose most of their energy within a distance of a few hundred Angstroms from the surface.

It follows from (2-11) that if  $E_{p_0}$  is the energy of the primary electrons as they hit the surface, the energy of the primary electrons as a function of distance is given by

$$E_{p(x)}^2 = E_{p_0}^2 - 2Ax \quad (2-15)$$

It can be seen that the approximate maximum distance of penetration of the primary electrons  $x_p$  is obtained by letting  $E_p = 0$ . It thus follows that:

$$x_p = \frac{E_{p_0}^2}{2A} \quad (2-16)$$

The range of the primary electrons is therefore proportional to the square of their energy.

From (2-12), (2-15) and (2-16)

$$n(x) = \left(\frac{A}{2}\right)^{\frac{1}{2}} \cdot \frac{1}{\epsilon_e (x_p - x)^{\frac{1}{2}}} \quad (2-17)$$

$\frac{x}{x_p}$  as a function of  $(x_p - x)^{-\frac{1}{2}}$  is illustrated in Figure (16).

It can be seen that most of the secondary electrons are produced

near the end of the path of the primary electrons.

The general shape of the secondary emission yield curves can be obtained by considering primary electrons with very low and very high energies.

At very low primary energies  $x_p \ll x_s$ , and therefore the probability of a secondary escaping from the surface may be taken as  $f(0)$ . Hence, from (2-14) and (2-12),

$$\delta = f(0) \int n(x) dx = f(0) \frac{E_{P0}}{\epsilon_e} \quad \text{when } x_p \ll x_s.$$

It can be seen that for low primary energies the secondary electron yield  $\delta$  should rise proportionally to the primary energy  $E_{P0}$ .

At very high primary energies  $x_p \gg x_s$  only the secondary electrons produced in the range  $0 \leq x \leq x_s$  need be considered, because  $f(x)$ , being an exponential function of  $x$ , decreases rapidly with increasing  $x$ . It is apparent from Figure (16) that the production of secondary electrons as a function of depth can be considered to be nearly constant when  $\frac{x}{x_p}$  is small.

Hence, from (2-16) and (2-17)

$$n(x) = n(0) = \frac{A}{\epsilon_e E_{P0}}$$

Therefore, from (2-14) it follows that

$$\begin{aligned} \delta &= \frac{A}{\epsilon_e E_{P0}} \int_0^{\infty} f(x) dx \\ &= \frac{A}{\epsilon_e E_{P0}} \cdot \frac{f(0)}{\alpha} \quad \text{when } x_p \gg x_s \end{aligned}$$

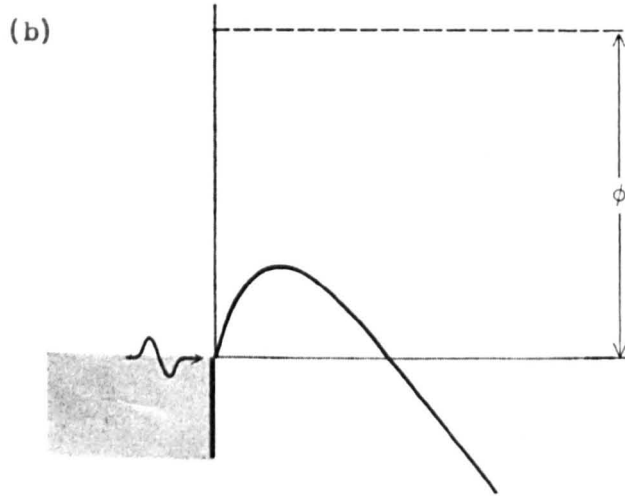
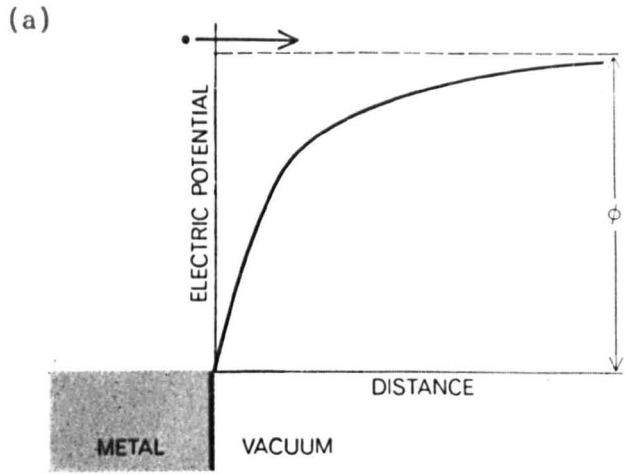


Figure 17.

It can thus be seen that for high primary energies the secondary electron yield  $\delta$  is inversely proportional to the primary energy.

Considering the nature of secondary electron yield at high and low primary electron energies, it is clear that  $\delta$  will have a maximum value at a primary energy corresponding to  $x_p \approx x_s$ .

It is also possible to produce secondary electron emission by bombarding materials with ion beams (32). However, the mechanism of secondary emission produced by ion bombardment is quite different from that of electron bombardment. Electron induced emission is basically a bulk effect while ion bombardment is essentially a surface one. Hence, the theoretical treatment is completely different.

#### 2.2.4 Field Emission of Electrons

Field emission was discovered in 1897 by R.W. Wood, who observed that electrons could be emitted from surfaces without any input of energy. Field emission may be defined as the emission of electrons from a surface under the action of an applied electrostatic field. In photo emission and thermionic emission the electrons leave the material by gaining sufficient energy to overcome the potential barrier. In field emission the mechanism is quite different; the barrier is thinned and lowered by the applied field so that some of the unexcited electrons can "tunnel" through and escape. The process is illustrated in Figure (17). It can be seen that without an applied field (a) an electron can escape from the surface only if it is given sufficient energy to surmount the work function of  $\phi$ . The presence of a strong

electrostatic field (b) (typically about  $10^6$  volts/cm) thins and lowers the barrier so that electrons can leak away through it.

This electron tunneling which is a quantum-mechanical phenomenon, can be more easily comprehended by considering the Heisenburg uncertainty principle, which states that the product of the uncertainty of momentum  $\Delta P$  and the uncertainty of position  $\Delta x$  is roughly equal to Planck's constant; that is

$$\Delta P \cdot \Delta x \approx \frac{\hbar}{2}$$

where  $\hbar = \frac{h}{2\pi}$ ,  $h$  being Planck's constant.

If electrons near the Fermi level are considered, their uncertainty in energy is equal to the height of the barrier  $\phi$ , therefore the uncertainty in momentum is  $(2m\phi)^{\frac{1}{2}}$ . From Heisenburg's principle this gives the uncertainty in position to be

$$\frac{\hbar}{2(2m\phi)^{\frac{1}{2}}}$$

This lack of uncertainty in position will be of the same order as the barrier width  $\frac{\phi}{F_e}$ , where  $F$  represents the applied field.

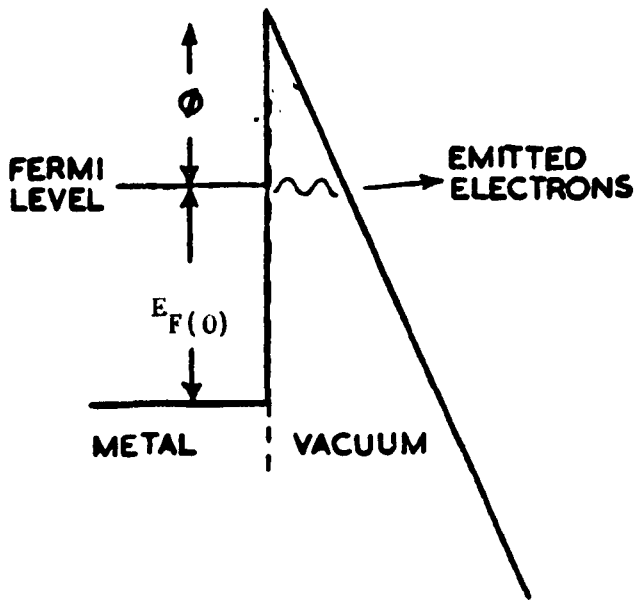
Therefore

$$\frac{\phi}{F_e} = \frac{\hbar}{2(2m\phi)^{\frac{1}{2}}}$$

or that

$$2\left(\frac{2m}{\hbar^2}\right)^{\frac{1}{2}} \frac{\phi^{\frac{3}{2}}}{F_e} \approx 1$$

The above relationship is found to agree fairly well with the conditions for field emission.



Simplified triangular model of the surface barrier when subjected to a strong field.

Figure 18.

### Fowler-Nordheim Theory of Field Emission

The wave-mechanical approach to field emission will be considered, using the concept  $|\psi|^2$  as the probability of an electron being in any particular position. The potential barrier will be assumed to be triangular. This, of course, is not the case, but calculations and observations show that the derived results agree to within 20% with actual field emission conditions.

It will be seen from Figure (18) that for an applied field of  $4 \times 10^7$  volts/cm and a work function of 4 volts, electrons near the top of the Fermi level  $E_F(0)$  will have to tunnel through a barrier of thickness  $10^{-7}$  cm.

The Schrodinger wave equation will be used to consider the one-dimensional case in the x direction, which is normal to the surface. Inside the material the behaviour of the electrons is described by

$$\frac{d^2 \psi}{dx^2} + \frac{8\pi^2 m}{h^2} E \psi = 0$$

where E is the kinetic energy of the electron.

Outside the metal and inside the triangular potential barrier the behaviour of the electrons is described by

$$\frac{d^2 \psi}{dx^2} + \frac{8\pi m}{h^2} [ E - (\phi + E_F(0)) + Fe_d ] \psi = 0$$

where F is the field strength.

It is possible to solve these two equations using the surface boundary conditions, namely, that  $\psi$  and  $\frac{d\psi}{dx}$  are continuous when  $x = 0$ .

Inside the potential barrier the solution to the wave equations is given by

$$D(E) = \frac{4E(\phi + E_{F(0)} - E)^{\frac{1}{2}}}{(\phi + E_{F(0)})} \cdot \exp \left[ -\frac{4}{3} \left( \frac{8\pi^2 m}{h^2} \right)^{\frac{1}{2}} \frac{(\phi + E_{F(0)} - E)^{3/2}}{eF} \right] \quad (2-18)$$

where  $D(E)$  is the fraction of electrons of energy  $E$  which can tunnel through the potential barrier.

The total number of electrons tunnelling through the barrier and hence the current leaving the surface, can be calculated by multiplying the number of electrons arriving at the surface (derived from the Fermi-Dirac distribution law) by equation (2-18). When this is integrated with respect to energy the result is the Fowler-Nordheim relationship (33).

$$I = \frac{e}{2\pi h} \frac{(E_{F(0)})^{\frac{1}{2}} F^2}{(\phi + E_{F(0)}) \phi^{\frac{1}{2}}} \exp \left[ -\frac{4}{3} \left( \frac{8\pi^2 m}{h^2} \right)^{\frac{1}{2}} \frac{\phi^{3/2}}{eF} \right]$$

where  $I$  is in amps/cm<sup>2</sup>

$F$  in volts/cm

$E_{F(0)}$  and  $\phi$  in eV.

The Fowler-Nordheim equation makes it clear that no heat energy is required. This has been verified by several workers (34), who have demonstrated field emission at liquid helium temperatures.

The wave mechanical theory agrees with observations that show the emitted current increases exponentially as a function of the applied electrostatic field. A 1 per cent change in the field produced roughly a 10 per cent change in the emitted current. Hence, this non-linear

relationship could be used to produce amplification.

Field emission will be extremely sensitive to small variations in the work function of the surface, since this occurs in the exponential factor. Hence, the various crystal planes of a material have quite different field emission characteristics.

The Fowler-Nordheim theory predicted huge current densities - of the order of  $10^8$  amps/cm<sup>2</sup>. This amazing prediction was confirmed in 1940 by Haefler (35) who measured a current density of  $10^6$  amps/cm<sup>2</sup>.

The wave-mechanical theory of field emission developed by Fowler and Nordheim in 1928 still appears to be essentially correct. Although the theory has been in agreement with most of the observed data, it fails to account for the nature of field emission at large current densities. It is observed that the density of the emitted electron beam does not increase as a function of the applied field as rapidly as the Fowler-Nordheim theory predicted. This discrepancy has been explained in a modified wave mechanical theory (36) which introduces the hypothesis of the electron space charge and the effect this has on the electrostatic field.

### 2.3 The Influence of Adsorbed Layers.

The phenomenon of adsorption was discovered in 1773 by Scheel, who observed the condensation of gases (e.g. oxygen) on the surface of active charcoal.

Clean surfaces, being extremely reactive combine spontaneously with most gases (that is, the activation energies for the reactions are almost zero, (37, 38)), but the nature of the binding forces can vary

to a considerable extent.

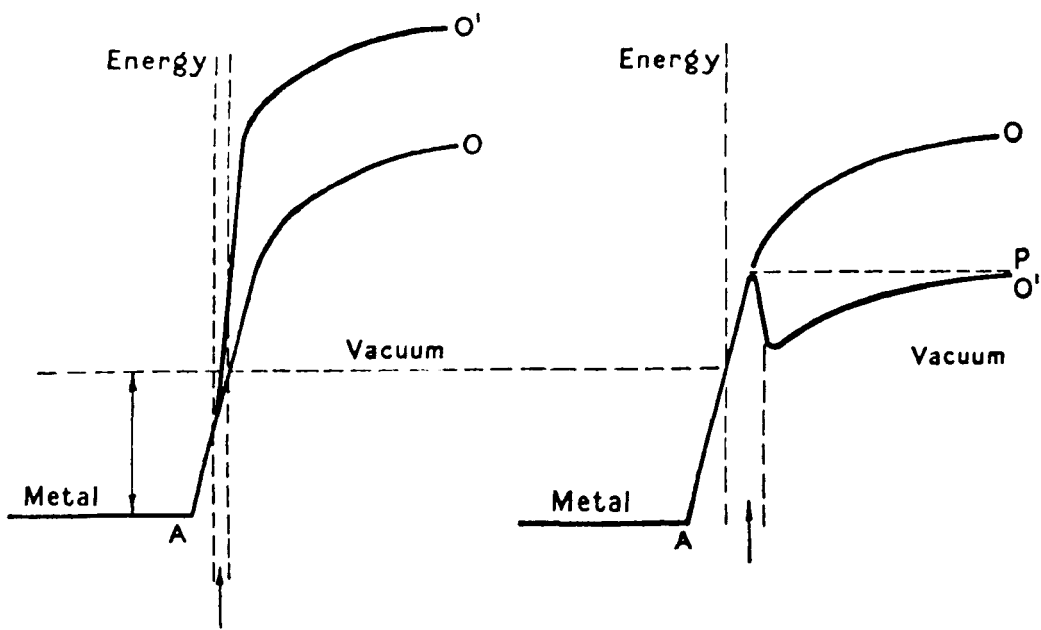
Two main types of interaction can be distinguished. If the bond between the adsorbent and surface is strong, the phenomenon is called chemical adsorption or chemisorption; if it is weak it is called physical adsorption.

The main differences between chemisorption and physical adsorption can be summarized as follows:-

- (a) In physical adsorption the binding is mainly due to van der Waals forces, while in chemisorption valence forces are responsible.
- (b) The binding energy is much stronger in chemisorption than in physical adsorption (approximately  $10^5$  cal/mole and  $10^3$  cal/mole respectively).
- (c) Chemisorption, unlike physical adsorption, is specific.
- (d) Physical adsorption, unlike chemisorption, is generally reversible (i.e. on decreasing the pressure the adsorbed gas is desorbed).

The centre of charge density of the electrons in non polar atoms is coincident with that of their positive charges, but when adsorbed on surfaces they become polarized. Hence, adsorbed films consist of a layer of dipoles. In extreme cases the electrostatic field at the surface is strong enough to ionize the adsorbed film, producing an adsorbed layer of ions.

These adsorbed dipole layers modify the surface barrier and thus the work function. Consider an electron of charge  $e$  near to a plane of charge density  $\sigma$ . The force on it will be  $2\pi\sigma e$ , and the force between



(a) Adsorbed layer-negative outwards. (b) Adsorbed layer-positive outwards.

Effect of adsorbed layers on the potential near a metal surface.

Figure 19.

two such plane sheets of equal and opposite charge density is  $4\pi\sigma'e$ . The difference in potential between the two planes is  $4\pi\sigma'd$ , where  $d$  is the distance of separation. A dipole layer with  $n$  dipoles/cm<sup>2</sup> can be considered to be made up from two such charge planes. Hence, as the dipole moment  $M$  of each is equal to the product  $ed$ , and since  $\sigma = ne$ , the potential difference is  $4\pi nM$ . The work function of a surface will be increased by  $4\pi neM$  if the dipoles have their negative charges outwards, and decreased by the same amount if the dipoles have their positive charges away from the surface.

These two cases are illustrated in Figure (19). It can be seen that the adsorbed layers change the potential barrier at the surface from 0 to  $0^1$ .

From the kinetic theory of gases the period of time,  $t_m$ , that is required for an initially clean surface to be contaminated with a monolayer is given by the equation

$$t_m = \frac{Nm}{\beta V}$$

where  $\beta$  is the sticking coefficient, i.e., the fraction of the molecules bombarding the surface which are adsorbed,  $V$  is the number of molecules bombarding a square centimeter of the surface per second, and  $Nm$  is the number of sites per monolayer.

At a pressure of  $10^{-7}$  torr and assuming a sticking coefficient of unity a clean surface will adsorb a monolayer in seconds. Most sticking coefficients are found to be fairly high, of the order of 0.1 - 0.5, and vary with coverage and temperature (39).

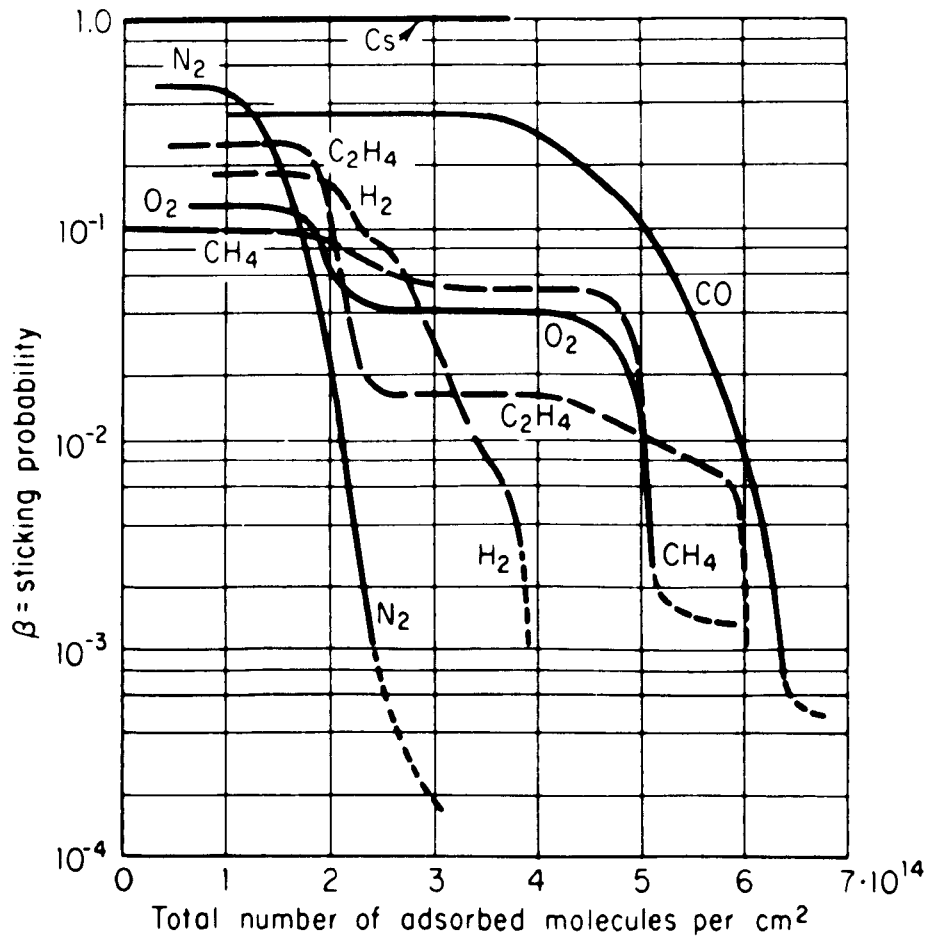


**Figure 20.**

Bloomer and Haine (40) investigated the adsorption of oxygen on a clean tungsten surface and found the time required to produce a monolayer to be given by

$$t_m = \frac{2.4 \times 10^{-6}}{P} \text{ seconds}$$

where P is the pressure in torr.

Hence, in an investigation of clean surfaces, it is imperative to have a residual gas pressure that is maintained at or below  $10^{-9}$  torr.

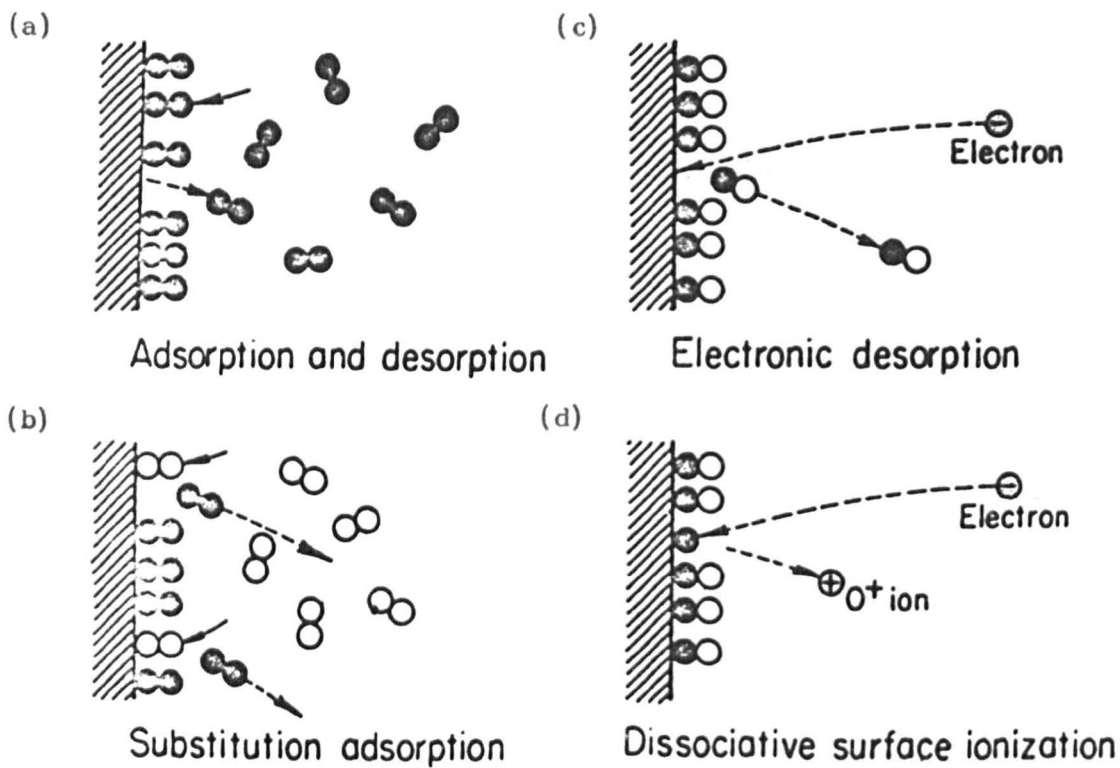
Flash filament techniques have been used by many workers to investigate how the sticking coefficients vary as a function of coverage. Figure (20) illustrates the change in sticking coefficients for various gases on the 411 plane of tungsten at room temperature.

Gas surface interactions can be divided into four main groups (41).

Firstly, the phenomenon of adsorption and desorption acting concurrently and in equilibrium (see Figure (2ia)).

Secondly, the phenomenon of substitutional adsorption (Figure (20b)). The binding energy between a surface and an adsorbent will be different from the one between the same surface and another adsorbent. Hence, it is possible for some atoms or molecules to adsorb on a surface by displacing previously adsorbed layers. This process becomes important when gases are introduced into systems with previously contaminated surfaces.

Thirdly, there is the possibility of ionic or electronic desorption (42). An electron or ion, if it has sufficient energy, can



Schematic representation of significant gas-surface reactions.

Figure 21.

desorb weakly adsorbed particles.

Finally, there is the possibility of dissociative surface ionization (Figure (21d)). An incident beam of particles may dissociate the adsorbed molecules producing the desorption of ions (43).

## 2.4 The Influence of Temperature on Work Function Values

In the course of this work it has been assumed that work functions are independent of the temperature. In fact, most work functions increase in a non-linear manner as a function of the temperature. This variation is usually stated in one of two ways:- either the work function coefficient is quoted at a definite temperature, or the change in work function is described in the form of a virial equation.

According to Herring and Nichols (44) three factors contribute to the temperature coefficient:-

- (1) The surface potential barrier will be modified by the thermal expansion of the lattice.
- (2) The increase in the vibrational amplitude of the atoms due to thermal excitation will cause the charge distribution near the surface to change.
- (3) The Fermi-Dirac energy distribution of the electrons will be slightly altered with increasing temperature. Hence, the value of the Fermi energy will change and the work function will be altered.

With these three premises Herring and Nichols presented a theory which describes the temperature variation of work functions that agrees with the measured results (45) to within 25%.

Metal	Temp. °K for $10^{-7}$ torr vapour pressure	Richardson Constants		Usable emission amps/cm <sup>2</sup>
		A amps/cm <sup>2</sup> degree <sup>2</sup>	$\phi$ eV	
Cs	273	160	1.81	$4 \times 10^{-27}$
Ba	580	60	2.11	$1 \times 10^{-11}$
Ni	1270	60	4.1	$5 \times 10^{-9}$
Pt	1650	170	5.40	$2 \times 10^{-8}$
Mo	1970	55	4.15	$5 \times 10^{-8}$
C	2030	48	4.35	$2 \times 10^{-8}$
Ta	2370	60	4.10	$6 \times 10^{-1}$
W	2520	80	4.54	$4 \times 10^{-1}$

Figure 22.

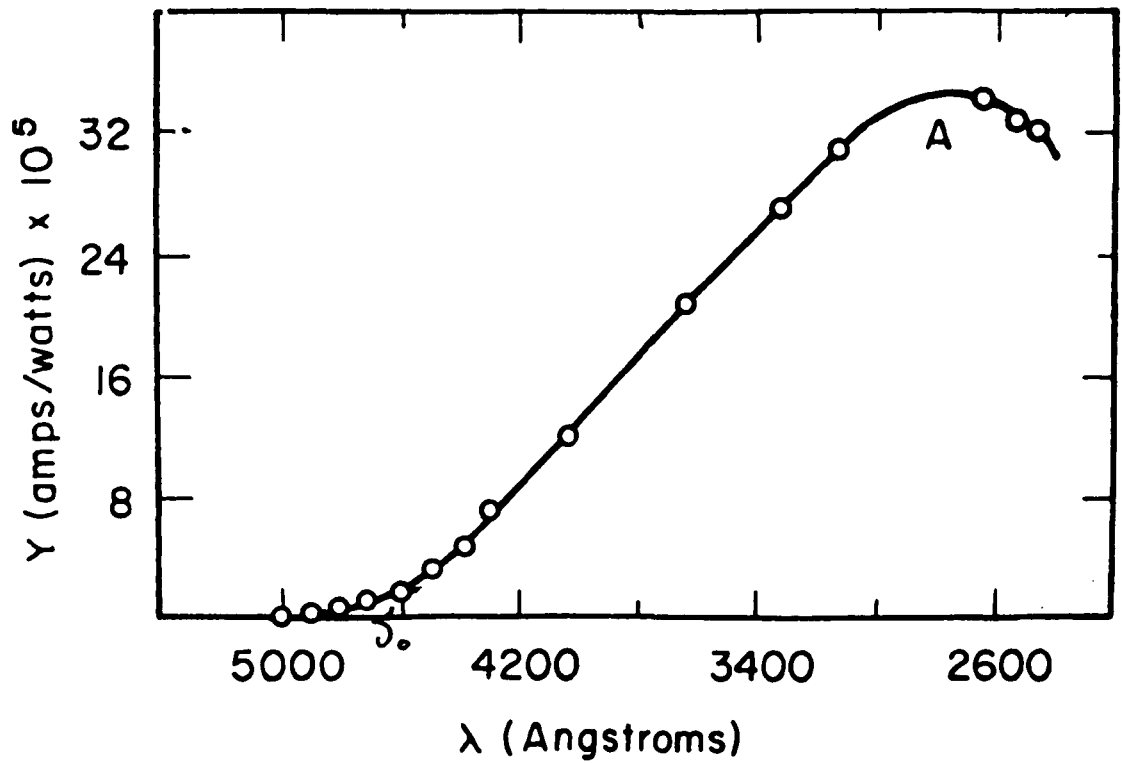
## 2.5 Experimental Methods used to measure Work Functions

### 2.5.1 The Thermionic Work Function

The Richardson-Dushman equation (2-5) suggests that  $\log \frac{I}{T^2}$  plotted as a function of  $\frac{1}{T}$  should result in a straight line. Thus it could be concluded that from the gradient a value for the work function could be determined. However, because of complicating factors, Richardson plots are not linear, and hence Richardson work functions differ from the true work function (46). The electron reflection coefficients (i.e., the proportion of free electrons which do not escape but are reflected by the surface back in to the metal) vary as a function of temperature and therefore the pre-exponential factor is not constant. A negative space charge is produced above the surface potential barrier, thus changing the value of the apparent work function. The space charge can be reduced by increasing the strength of the electrostatic field between the emitter and collector, but this increased field affects the nature of the surface potential barrier.

Thermionic work function determinations in addition to these theoretical limitations are restricted in their application,

Thermionic emission techniques are limited to temperatures where the surface will emit measurable currents without the excessive evaporation of the emitter itself. In practice, the vapour pressure of the material must not exceed  $10^{-7}$  torr. It can be seen from Figure (22) that this factor limits the application of thermionic emission studies to a few refractory materials.



The spectral distribution curve of a typical metal.

Figure 23.

Thermionic emission only becomes measurable at relatively high temperatures, usually in the order of  $1,000^{\circ}\text{C}$ , and therefore its use in the investigation of work function changes as a function of the adsorption of impurity layers is limited.

### 2.5.2 The Photoelectric Work Function

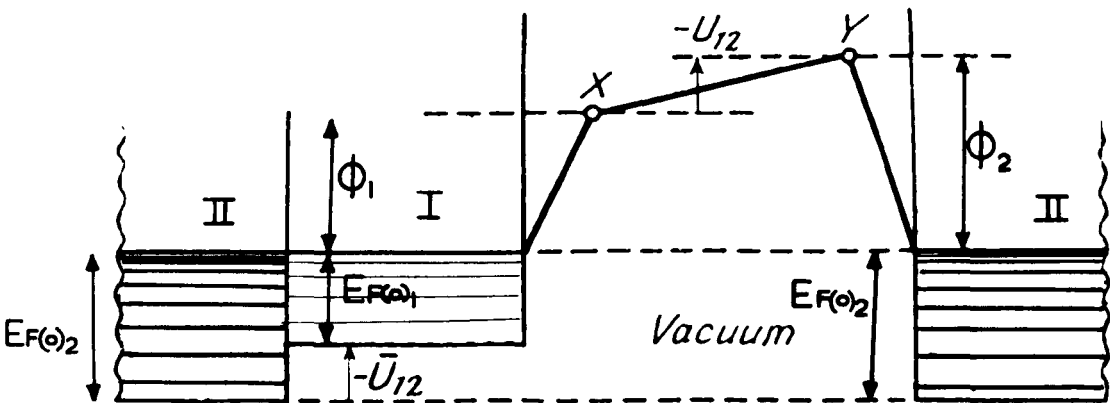
Einstein's equation concerning the photoelectric emission of electrons,  $E = h\nu - \phi$ , suggests that the work function  $\phi$  of a material may be determined by measuring the maximum kinetic energy  $E$  of the photo electrons, and the frequency  $\nu$  of the incident electromagnetic radiation.

However, at temperatures above  $0^{\circ}\text{K}$  the threshold frequency is not well defined but tails off (see Figure (23)).

The small photoemission observed for frequencies slightly below the threshold frequency at  $0^{\circ}\text{K}$ ,  $\nu_0$ , corresponds to the electron energies in the tail of the Fermi-Dirac distribution at higher temperatures. It is therefore difficult to measure accurately the threshold frequencies at temperatures above absolute zero. This restriction limits the application of the method to work function determinations

The photo electrons will be emitted from the areas with the lowest work function. This need not necessarily be typical of the surface as a whole, but may correspond to regions of contamination.

Another disadvantage of the photoelectric method is that in gaseous environments it is difficult to avoid the production of ions



Potential variation between two directly connected metal electrodes.

Figure 24.

which, when adsorbed on the surface, will change the surface potential and hence the measured work function.

For the above reasons, photo electric investigations are usually limited to clean surfaces under ultra high vacuum conditions at relatively low temperatures.

### 2.5.3 The Contact Potential Difference Work Function

The variation in potential between two metals I and II separated by a vacuum is shown schematically in Figure (24). If the two metals are connected by an external circuit, equilibrium will be realized when the two Fermi levels  $E_F(0)_1$  and  $E_F(0)_2$  have the same height, which implies that a potential difference  $U_{12} = E_F(0)_2 - E_F(0)_1$  exists at the junction between the two metals. This potential difference is called the Volta effect, or contact potential difference. Its magnitude is, as can be seen in the figure, equal to the difference in work functions:-

$$U_{12} = \phi_1 - \phi_2 \quad (2-19)$$

The validity of equation (2-19) rests on the assumption that the two conductors are in equilibrium at the same temperature. Thus, from this relationship it can be seen that if the work function of one of the surfaces is known it is possible to determine the other if the value of  $U_{12}$  is known.

The Kelvin method of measuring contact potential differences consists of observing the displacement current which is generated when the capacity of a capacitance constructed from the two surfaces to be

compared is varied. The voltage required for compensation is equal and opposite to the contact potential difference. A low frequency amplifier and a cathode ray tube are usually employed to determine the balance point.

It can be shown (47) that the voltage  $\delta V$  induced across the external circuit is given by:

$$\delta V = \frac{RU_{12}A\alpha P}{4\pi d} \frac{\cos Pt}{(1 + \alpha \sin Pt)^2} \frac{1}{9 \times 10^{11}} \text{ volts} \quad (2-20)$$

where  $R$  is the resistance of the external circuit.

$U_{12}$  is the contact potential difference.

$A$  represents the area of the surfaces.

$\frac{P}{2\pi}$  is the frequency of vibrations.

$d$  corresponds to the normal separation.

$\alpha$  is the amplitude of vibration.

Since measurements are made at the null-point, an accurate knowledge of the geometry is not required.

This method of determining work functions has the added advantage of not introducing surface disturbances through:- heating; irradiation; or electron bombardment. It is also possible to investigate surfaces in gaseous environments, since it does not cause charge build up.

The only disadvantage of this method is that it gives the arithmetic mean work function of the material under investigation. In other words it does not indicate how the work function changes from one position to another.

The Kelvin method of determining contact potential differences has been found to agree with electron beam methods to within experimental limits (48).

## 2.6 Conclusion

In this chapter the relevant details of electron emission and work function measurements have been reviewed. The importance of work function determinations as a classical method of studying surface phenomena has been emphasized. These techniques have proved to be particularly useful in probing the nature of the electronic interaction between chemisorbed atoms and the adsorbent surface.

To appreciate the need for the present investigations it is first necessary to consider the previous work in this field which will be given in Chapter III.

## CHAPTER III

### REVIEW OF PREVIOUS EXPERIMENTAL DETERMINATIONS

#### 3.1 Introduction

An immense amount of work has been carried out during the last fifty years on work function investigations.

Many of the early experimental determinations were impeded by limitations in the techniques involved. Early attempts at measuring work functions were affected by contaminating layers produced by impurity gases resulting from insufficient out-gassing of the components and inadequate vacuum conditions. Despite the inevitable doubt as to the absolute values obtained from these inquiries, many valuable trends were observed.

In this review of the previous experimental determinations the factors which influence electron emission and work function values are considered separately, keeping all other variables as constant as possible.

#### 3.2 The Dependence of Work Function Values on the Method of Measurement

There are three main techniques employed in determining the electron work functions of the elements:- thermionic, photoelectric and contact potential difference methods. When applied to comparable surfaces the three methods yield values that differ by as much as a few tenths of a volt. This spread is greater than the experimental errors of the measuring techniques and represents the difference between different kinds of phenomena. To illustrate this effect the work functions of polycrystalline tungsten obtained by the three main methods will be reviewed.

Measurements have recently been obtained by Nichols (49) of the average thermionic constants, using Richardson plots over a temperature range 1,300 to 2,200°K. Polished polycrystalline tungsten had a work function of 4.464 volts and unpolished, a value of 4.45 volts. These results emphasize the fact that the average thermionic work functions from polycrystalline emitters are dependent upon the effects of polishing and the types and relative amounts of the various exposed crystal faces.

Because they involve electron emission, thermionic determinations will be very close to that of the lowest work function patch on the surface.

An investigation of the photoelectric work function of aged polycrystalline tungsten has been carried out by Apker, Taft and Dickey (50). Three different photoelectric methods were used:-

- 1) An analysis of the spectral distribution by Fowler's method.
- 2) By extrapolating  $(\text{current})^{\frac{1}{2}}$  - voltage curves to the saturation line.
- 3) Du Bridge's method (143, 144).

The values obtained from the three methods differed by only a few hundredths of a volt, the average being 4.49 volts. In 1964 Hopkins and Ross (51) carried out experimental determinations of the work function of tungsten employing contact potential difference techniques. Using the Kelvin method they obtained a value of 4.54 volts for well aged polycrystalline tungsten. This value has been confirmed by Hopkins and Riviere (52, 53).

It can be seen that the thermionic and photoelectric work functions, 4.45 and 4.49 volts respectively (the unpolished thermionic sample being considered) are lower than the value obtained from contact potential investigations. The contact potential difference method, because it does not involve the emission of electrons, gives an average value for the work function. Hence, it is not surprising that the value obtained by this method is higher than those obtained using other techniques involving electron emission.

Comparisons between thermionic and other work function methods are further complicated by the wide difference between the temperatures at which they are observed (54).

Unfortunately, the exact crystal orientation of the surface of thermally well-aged tungsten foil is not known. Recent work has shown that it is not completely random, but that the process of rolling tungsten often orients the surface crystallites in the [100] direction (55). The different work function values may therefore be caused by different degrees of annealing. The thermionic samples, because of their high temperature, are probably almost completely strain free.

### 3.3 The Effect of Surface Structure

#### 3.3.1 The Variation of Work Function as a Function of Crystal Plane

Surfaces, when emitting electrons, become polarized. Schottky (56) suggested that the force between the polarized surface and the emitted electron can be considered as attraction between the electron and its mirror image. If the distance between the surface and electron

is  $x$ , this force is  $\frac{e^2}{4\pi\epsilon_0(2x)^2}$ , where  $\epsilon_0$  is the dielectric constant for a vacuum.

The energy  $\phi$  required to remove the electron from a very small distance from the surface  $r_0$ , to infinity is obtained by integrating between these limits, and is  $\frac{e^2}{16\pi\epsilon_0 r_0}$ .

Schottky argued that for distances less than  $r_0$ , where the surface cannot be considered to be a smooth plane, the field produced by the individual atoms should be considered constant and equal to  $\frac{e}{16\pi\epsilon_0 r_0^2}$  from 0 to  $r_0$ .

The difference in potential energy is therefore:

$$\frac{e^2 r_0}{16\pi\epsilon_0 r_0^2} = \frac{e^2}{16\pi\epsilon_0 r_0}$$

The sum of these two factors is the work function.

Hence,

$$\phi = \frac{e^2}{16\pi\epsilon_0 r_0} + \frac{e^2}{16\pi\epsilon_0 r_0} = \frac{e^2}{8\pi\epsilon_0 r_0}$$

Substituting  $r_0$  in angstroms and  $\phi$  in electron volts, the relationship becomes

$$\phi = \frac{7.2}{r_0}$$

This indicates that, for any given material, the more closely packed planes will have the highest work function.

The fact that the electron emission from surface is dependent on the orientation of the surface to the crystal lattice was first observed when the electron emission of polycrystalline metal surfaces

ORIENTATION	FIELD EMISSION	THERMIONIC		C. P. D.
	MULLER (59)	SMITH (60)	NICHOL (61)	LOVE (62) & DYER.
311				4.18
116	4.30	4.29		
013	4.31			
012	4.34			
122	4.35			
111	4.39	4.39	4.39	
110			4.68	
112	4.65 - 4.88	4.65	4.69	
011	570 - 5.99	5.26 estimated		
001			4.56	

Figure 25.

was examined by means of the electron microscope. The conclusion that the work function has different values for areas of different orientation has been confirmed by direct measurement.

The most reliable determinations of the variation of work function as a function of the different crystal planes have been made with tungsten.

It can be seen from Figure (25) that there is good agreement between workers concerning the strongly emitting planes - that is, the ones with the lowest work functions. However, though tungsten may be outgassed thoroughly, the values obtained for the weakly emitting planes vary considerably from one worker to another. This discrepancy almost certainly represents differences in the degree of past annealing.

The measured work functions of tungsten lie between a lowest value of 4.30eV for the (116) plane and a highest value of approximately 5.8eV for the (011) plane. Tungsten is not unique in having work function values that differ by a 1.5eV margin from one crystal plane to another. Mrowka (57) and Smoluchowski (58) have presented theoretical explanations of the influence of the crystal orientation on work functions, but agreement between their calculated values and the measured ones has been inconclusive.

### 3.3.2 The Influence of Surface Irregularities

Except for completely clean single crystals real surfaces are composed of numerous regions of differing composition. The image potential of an electron outside a smooth surface will be different from

that for an irregular surface, and hence there will be a significant variation in work function values as a function of the surface structure.

Farnsworth and Chung Fu Ying (63) working in the United States have compared the work functions of bulk metals and condensed films. They have found that both silver and gold when condensed from the vapour phase on to substrates at room temperature have work functions that are about 0.3 volts lower than those of the bulk metal. When these condensed films were annealed at a temperature of about 350<sup>o</sup>C the work functions changed to those of the bulk metals. Farnsworth and Chung Fu Ying believed that these effects were due to the presence of large densities of lattice flaws which were frozen into the films on condensation and that they were removed by annealing.

A technique has recently been developed which utilizes an electron beam scanning process to investigate work function variations (64). The information, which is usually displayed on a television screen can be resolved to within a few microns. It is possible with this scanning system to monitor continuously changes in the surface patchiness due to thermally induced atomic migrations.

Because of the practical limitations of controlling the surface conditions it is extremely difficult to obtain reproducible work function values.

### 3.3.3 The Variation of Work Function Values as a Function of Film Thickness

Most of the physical properties of metal films change from the bulk characteristics as their thickness is reduced, and therefore a variation in the work function as a function of film thickness is to

be expected. Recent work on the influence of the film thickness on work function values is somewhat contradictory.

Using thermionic techniques, Rauh and Thorn (65) obtained data which indicated that the work function of a uranium film increases with increasing depth of deposit up to 15 atomic layers, when it reaches a limiting value of 3.47 volts. This observation that uranium films which are thicker than 15 atomic layers have a work function that is independent of depth - i.e., constant at 3.47 volts - is in fair agreement with previous determinations of the bulk work function of uranium (66,- 67).

The dependence of the photoelectric work function on depth has been investigated by Garron (68). Results obtained from aluminium, gold and silver films up to a thickness of 800 Å confirm Rauh and Thorns' reported variation in work function with increasing film thickness.

The results mentioned above are not in agreement with the observations of Bryla and Feldman (69) who, using a contact potential difference method, failed to observe any variation in the work function of gold, platinum and silver films as a function of film thickness.

The lack of agreement between different workers in this field may be because of irregularities and impurities in the materials masking any variation in the work functions produced by different film depths.

### 3.3.4 The Influence of Underlying Structure

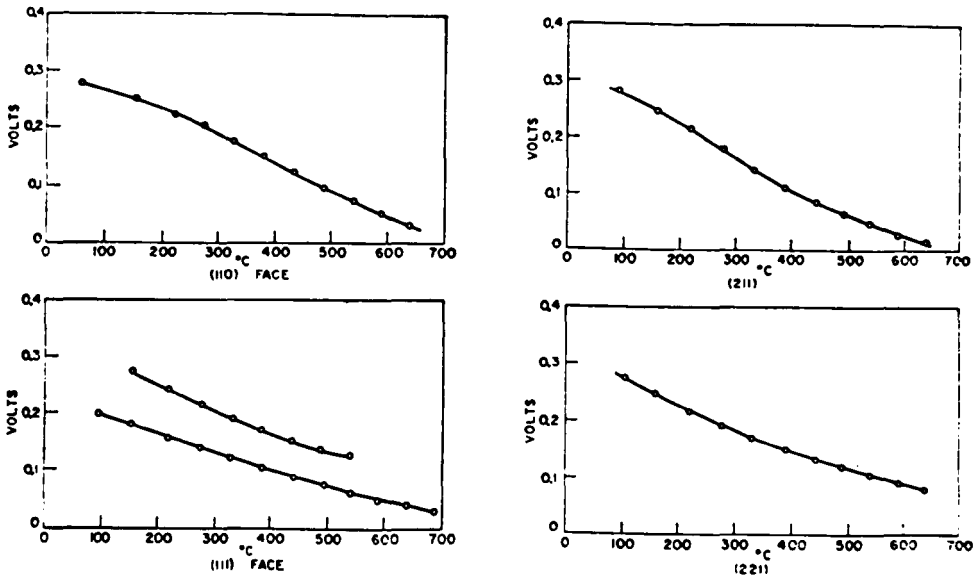
Low energy electron diffraction experiments carried out by experimenters (70, 71) indicated that films which are deposited by evaporation at a slow rate have an orientation which is related to the microstructure of the underlying substrate. Hence, since the work function of a crystal is dependent on the crystal face which forms the surface, it is to be expected that the work function of a metal will be influenced by the characteristics of the substrate.

Blackmer and Farnsworth (72), using photoelectric methods have measured the electron emission properties of silver films as a function of substrate structure. They found that silver films deposited on quartz and molybdenum substrates had a work function of 4.41eV, compared with a value of 4.50eV when deposited on bulk silver. Electron diffraction patterns from the evaporated silver films on fused quartz indicate a micro-crystalline structure, hence the low values are almost certainly associated with the minute size of the crystal.

It is therefore extremely important when investigating the properties of thin films to take into account the rate of deposition and the orientation, temperature and contamination of the substrate.

### 3.4 The Temperature Dependence of Work Function Values

Most of the early experimental determinations of the temperature dependence of the work function were hampered by limitations in the techniques involved. These investigations are liable to suspicion for one or more of the following reasons: the temperature range was limited;



Temperature dependence of the (110), (111), (211), and (221) faces of copper.

TABLE I. The temperature coefficient of the work function of single-crystal faces of copper.

Orientation	$d\phi/dT$ at 600°K
(100)	$-13.8 \times 10^{-4} \text{ V/}^\circ\text{K}$
(211)	-6.5
(110)	-5.2
(221)	-4.0
(111)	-3.4

Figure 26.

the vacuum techniques were inadequate; and polycrystalline samples were used. Against this background the measurements performed by such workers as Shelton (73) and Hutson (74) are suspect. In order to overcome some of these limitations Blevis and Crowell (75) measured in a continuous fashion, variations in the work function of single crystal surfaces over a wide temperature range (0 to 700°C). Using the diode retarding-field method determinations were made on [100], [110], [111], [211] and [221] faces of single copper crystals. Although the method is not suitable for determining absolute work functions it is extremely sensitive to small changes in the work function.

Measurements obtained from copper samples of [110], [211], [111] and [221] orientations are illustrated in Figure (26). It can be seen that the work functions decrease with increasing temperature. The results of the determinations are summarized at the bottom of Figure (26) where  $\frac{d\phi}{dT}$  at 600°K is listed.

Underwood's (76) absolute work function values of 5.64 and 4.98 volts for the [100] and [111] faces at room temperature, when combined with the sensitive changes in work function obtained by Blevis and Crowell, yields the absolute variation in work function as a function of temperature (illustrated in Figure (27)). Also shown in the figure is Bolshov's (77) thermionic determination of the work function of copper at its melting point.

It was observed by Bolshov that the work function varies continuously as the temperature is increased through the melting point.

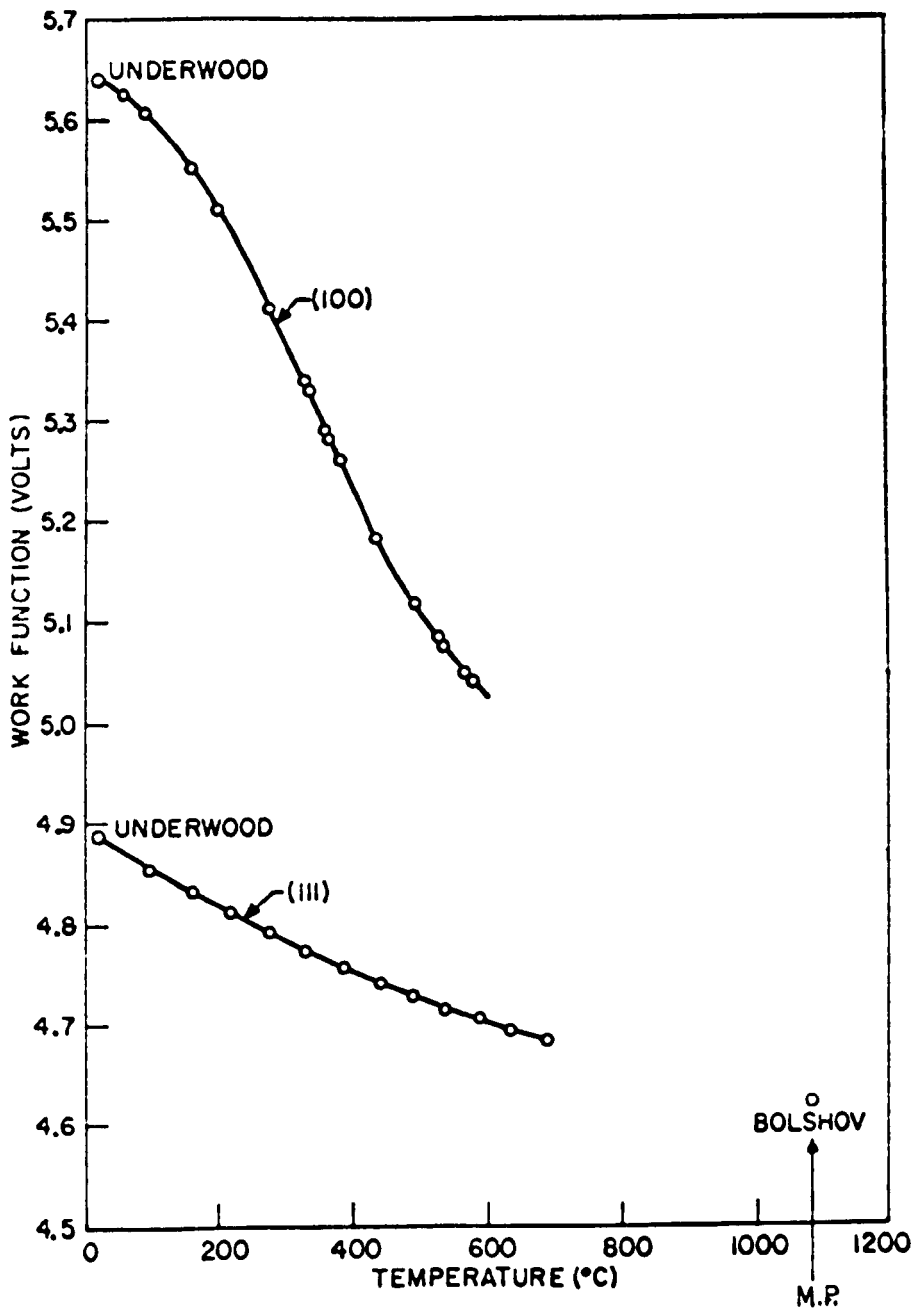


Figure 27.

It is therefore probable that the work functions of all the crystal faces approach a common value near the melting point. Considering that Bolshov used thermionic techniques at the melting point of copper (at a temperature of  $1083^{\circ}\text{C}$  the vapour pressure of copper is approximately  $5 \times 10^{-3}$  torr(145)) these investigations are liable to suspicion.

Other workers (78 ,79) investigating the temperature dependence of the work function of tungsten, confirm that the work functions of the [112], [116] and [111] faces tend to converge near the melting point.

### 3.5 The Influence of Adsorbed Films

The adsorption of gases on solids is spontaneous, so there is a drop in the free energy of the system. Considering that, prior to adsorption, the adsorbent molecules move freely in three dimensions, the adsorption of gases is therefore accompanied by a large decrease in entropy. Since the change in enthalpy,  $\Delta H$ , of the system is given by  $\Delta H = \Delta F + T\Delta S$ , it follows that  $\Delta H$  must always be negative - i.e., all adsorption processes are exothermic.

The work function changes observed when surfaces adsorb gases have been used in the interpretation of the electronic processes taking place near the surface. Many systems have been investigated by work function techniques, but there is still considerable disagreement over important features. Much of the divergence of opinion is almost certainly due to poor gas phase analysis.

Since Langmuir (80), many authors have discussed the interaction of hydrogen with clean tungsten surfaces. In most of the investigations a tungsten surface was bathed in an atmosphere of hydrogen; changes in the total pressure were attributed entirely to hydrogen.

Moore and Unterwald (81) have investigated surface and gas phase residues using flash filament and mass spectroscopic analysis. Carbon monoxide was found to be so persistent that they believed that most of the published work with hydrogen was performed unintentionally in an atmosphere of carbon monoxide. The carbon monoxide was probably produced from carbon and oxygen atoms dissolved in the tungsten, which diffuse to the surface and then combine.

The stability of glass at high temperatures and in gas discharges has recently been investigated by Bills and Evett (82). Measurements performed on pyrex borosilicate type glasses indicate that large quantities of decomposition products can be evolved from glass either by heating above about 350°C in a vacuum (122) or by a chemical sputtering process initiated by bombarding the glass with low energy ions.

Thus, in attempting to outgass glass vacuum systems by baking, many workers may have unwittingly contaminated the surfaces of the system. This of course throws suspicion on all gas and surface phase work carried out in glass high vacuum systems.

### 3.5.1 Influence of Temperature on Adsorbed Layers

Ehrlich (83) using work function and flash filament techniques, has investigated the variation in sticking coefficient for nitrogen on tungsten. There was an observed decrease in the sticking coefficient as the temperature was increased. The heats of adsorption also varied as a function of temperature. At low temperatures, i.e., below 115°K, nitrogen adsorbs as molecules with a binding energy of 9kcal/mole. Above a temperature of 115°K the binding energy increases to 20kcal/mole.

Ehrlich proposed that at low temperatures nitrogen molecules are physisorbed on tungsten surfaces and at higher temperatures the nature of the bonding changes into a chemisorbed state. It is probable that many gaseous molecules or atoms may first adsorb on surfaces by a physical process which acts as a reservoir for the subsequent adsorption into a more strongly bound chemisorbed state.

### 3.5.2 The Dependence of Work Function Values on Adsorbate Coverage

The influence of adsorbate coverage on work function values is usually explained by assuming that molecules (which may possess permanent or induced dipole moments) when adsorbed on surfaces, produce electrical double layers.

The change in the work function,  $\Delta\phi$ , can be related to the fractional coverage,  $\theta$ , by

$$\Delta\phi = \pm 4\pi N_s \mu\theta \quad (3-1)$$

where  $N_s$  is the number of adsorption sites per  $\text{cm}^2$  and  $\mu$  is the dipole moment associated with each adsorbed molecule.

It should be possible to determine  $\mu$  from plots of  $\Delta\phi$  as a function of  $\theta$ . Baker and Rideal (84) investigated the adsorption of CO, C<sub>2</sub>H<sub>4</sub> and H<sub>2</sub> on evaporated films of Co, Fe, Ni and Ta. They observed a linear change in the photoelectric work function as a function of adsorbate coverage, when  $\theta < 0.6$ .

Considering that evaporated metal films are extremely porous, the agreement between equation (3-1) and Barker and Rideal's work is almost certainly fortuitous.

Eisinger (85, 86), attempting to make significant comparisons with equation (3-1) considered the adsorption of nitrogen on an array of identical sites, in this case the (113) face of a tungsten crystal. Flash filament techniques were used to determine the amount of adsorbed gas, and photoelectric methods were employed to measure the work functions.

A plot of  $\Delta\phi$  as a function of the coverage,  $\theta$ , was found to be linear until the number of adsorbed nitrogen atoms was double the number of surface tungsten atoms, and at this point there was an increase in the gradient.  $\Delta\phi$  still continued to increase linearly with coverage.

The two gradients obtained from the plot, when substituted into equation (3-1), indicate that for a coverage of  $\theta = 0.5$  there is a change in the dipole moment from  $1.6 \times 10^{-17}$  to  $7.3 \times 10^{-17}$  e.s.u.

The magnitude of the dipole is in itself an indication of the bond type; large  $\mu$  values (i.e.,  $> 10^{-16}$  e.s.u.) indicate predominantly ionic bonds, while small  $\mu$  values suggest covalent bonds.

It can thus be seen that it is possible to make detailed interpretations of adsorption mechanisms from work function changes as a function of adsorbent coverage.

### 3.5.3 The Influence of Crystal Orientation on Adsorption

Mac Rae (87), working at the Bell Telephone Laboratories, has investigated the influence of crystal orientation on adsorption characteristics. Low energy electron diffraction techniques were used to study the adsorption of oxygen on the [111], [001] and [110] surfaces of nickel. The three surfaces, when covered with a monolayer of oxygen were found to have extremely ordered three-dimensional structures, composed of both oxygen and nickel atoms. The structures were different from each other, and peculiar to the different crystal planes. In many respects the ordered structures had more in common with three-dimensional compounds than the two-dimensional structures usually assumed for adsorbed films.

The mechanism of adsorption was observed to be dependent on the orientation of the surfaces. This is illustrated by the work function increases due to the adsorption of oxygen. The difference in work functions between the clean surfaces and the surfaces having adsorbed layers were:- 1.2, 0.6 and 0.25 volts for the [111], [110] and ]001] planes, respectively.

Field emission studies have been used by Holscher (88) to examine the chemisorption of nitrogen on individual crystal faces of tungsten. The work function changes for the different planes were

Surface potentials of nitrogen on individual crystal faces of tungsten, after 10 min exposure to  $p = 10^{-6}$  Torr at  $300^{\circ}\text{K}$ .

Crystal face	Work functions (V)		Surface potential (V)
	$\phi_W$	$\phi_{W-N}$	$\phi_W - \phi_{W-N}$
(311)	4.50	4.76	-0.26
(611)	4.30	4.59	-0.29
( $n$ 11) <sup>a</sup>	4.40	4.27	+0.13
(100)	5.2	4.3	+0.9
(310)	4.35	4.74	-0.39
(111)	4.40	4.70	-0.30
Total surface	4.50	4.32	+0.18

<sup>a</sup> This notation indicates that the face in question was in the [110] zone with the image located just outside the dark spot of the (100) face.

Figure 28.

measured by means of Fowler-Nordheim plots. The results (see Figure (28)), which are in agreement with previous findings, confirm that the work function changes of individual crystal faces are considerably different from the changes of overall work functions of polycrystalline samples.

#### 3.5.4 Reference Surfaces in Gases

By the very nature of the Kelvin method of determining contact potential differences, it is imperative to have a reference surface whose work function is known. Therefore, when investigating the adsorption of gases, it is of the utmost importance to have a standard electrode whose work function will not be altered by the admission of the gas.

Bomke (89), using photoelectric measurements, observed that the work functions of cadmium and zinc remain constant at their ultra-high vacuum values when nitrogen and the noble gases are introduced at room temperature. De Voe (90), using similar techniques, verified these observations.

Gold, because of its relative chemical inertness, is an excellent reference surface. Hopkins, Mee and Parker (91) have recently investigated the influence of oxygen on the work function of gold. They concluded that the surface potential of vacuum deposited gold films is unaltered by the presence of oxygen at low pressures (up to 1 torr). Trapnell (92), observed that at room temperature and low pressures, gold chemisorbs neither nitrogen nor hydrogen.

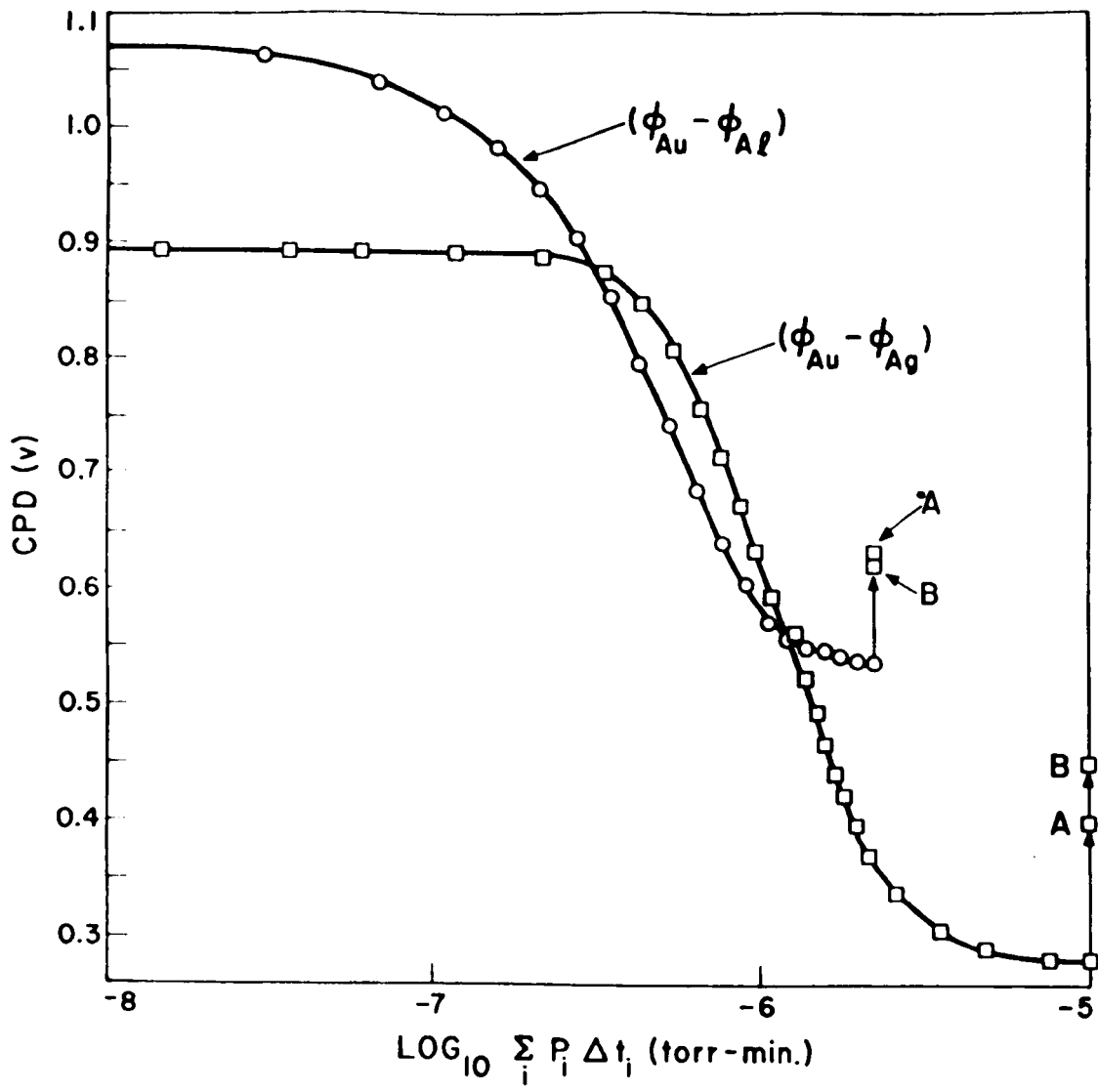


Figure 29.

These measurements clearly indicate the remarkable stability of gold surfaces in low pressure atmospheres of oxygen, nitrogen and hydrogen.

The absolute work function of an evaporated gold film has been determined by Anderson (93), employing the Kelvin method. Using a barium reference electrode he gives a value of 4.83eV. These measurements are subject to criticism, owing to the extreme reactivity of the standard surface. Rivière (94) quotes a value of 4.70eV, when measured with respect to well-aged polycrystalline tungsten.

These determinations of the work function of evaporated gold films are liable to suspicion, since they have been made in experimental tubes which have been pumped and baked on mercury systems prior to sealing off.

In 1966 Huber, (95), using a mercury-free vacuum system, investigated the effect of mercury vapour contamination on the work function of gold. He demonstrated that mercury is extremely reactive towards gold, lowering its work function by approximately half a volt (see Figure (29)). The measured work function of mercury-free gold surfaces was  $5.22 \pm 0.05\text{eV}$ .

Rivière (96) using similar mercury-free vacuum techniques, has recently confirmed Huber's observations. It would therefore appear that the measurements of the work function of gold which were determined in the past were in fact measurements of the characteristics of mercury contaminated surfaces.

### 3.6 Previous Determinations of the Work Function of Mercury

The phenomenon of electron emission from mercury surfaces is employed extensively in modern industry. The range of uses is very wide, embracing mercury vapour lamps and mercury switching devices. Considering the importance of rectification and inversions in the electrical supply industry, it is surprising that only a few determinations have been carried out of the work functions of mercury surfaces.

It will be recalled that the usable thermionic emission from a surface is restricted by the maximum temperature at which it can be operated without excessive evaporation of the material itself. The practical limit is a vapour pressure of about  $10^{-7}$  torr. The vapour pressure of mercury is only less than  $10^{-7}$  torr at temperatures below  $-40^{\circ}\text{C}$ . Therefore it would appear impracticable to use thermionic techniques to determine the work function of mercury.

In 1958 Gomer (97), and in 1963 Parker, Anderson and Hardy (98) carried out field-emission experiments with mercury whiskers. (The whiskers were produced from mercury vapour condensing on a tungsten substrate cooled to between  $-60^{\circ}\text{C}$  and  $-80^{\circ}\text{C}$ ). The field-emission patterns obtained from single 110 oriented mercury whiskers were used to investigate the growth kinetics of the samples. Unfortunately, they did not construct any Fowler-Nordheim plots to obtain a work function value. Although a considerable amount of work has been carried out on field emission from mercury samples, there has not been a published value for the field-emission work function to date.

Photoelectric determinations of the work function of mercury have been made by Kazda (99), Hales (100) and Roller, Jordan and Woodward (101). Extreme care was taken to obtain pure mercury. The samples were outgassed by vacuum distillation.

Kazda and Hales used a continuous flow system to produce clean liquid mercury surfaces. Both workers measured to within narrow limits a threshold wavelength of  $2,735\text{\AA}$  for mercury at room temperature, which corresponds to a work function of  $4.52\text{eV}$ .

Roller, Jordan and Woodward measured the threshold wavelength for solid mercury surfaces at liquid air temperature. They observed that, with increasing thickness as the film condensed, the work function first decreased to a minimum, and then increased with increasing film thickness to the final constant value of the bulk material.

The final value for a thick layer of mercury was  $4.52\text{eV}$ .

Klein and Lange (102), in 1938, reviewed the then known work function values obtained by contact potential difference techniques. They plotted the following: the first and second ionization potentials, the standard electrode potentials, and the work functions of the elements, as a function of ascending atomic number. Because all the ionization and electrode potentials were known, they were able to estimate the work functions that had not been determined. They quoted a value of  $4.50\text{eV}$  for the work function of mercury.

This figure is liable to suspicion since the work functions they quote in the determination of the work function of mercury are

considerably lower than recent measurements using sophisticated techniques. They quote work functions of 4.32eV, 4.46eV, 4.38eV and 4.46eV for nickel, copper, tungsten and gold respectively; these are considerably lower than the modern accepted values of 4.74eV, 4.50eV, 4.56eV and 5.22eV (94, 146, 95). Hence, the value of 4.50eV which they quote for the work function of mercury is most probably an underestimate.

### 3.7 Conclusion and Statement of Problem

In the course of this chapter the most important factors that influence the characteristics of surfaces have been summarized. It has been established that the various measuring techniques yield different work function values.

It is apparent that appreciable discrepancies exist between the various workers in this field, and that very little work has been carried out on mercury surfaces. In fact, the only consistent determinations were made nearly forty years ago, with rather unsophisticated photoelectric equipment. Indeed, no attempt has been made to determine the work function of clean mercury surfaces by means of the refined techniques now available.

The present work is aimed at determining the work functions of solid and liquid mercury, using contact potential difference methods. It is also intended to investigate a new technique of measuring the characteristics of surfaces which have an appreciable vapour pressure.

## CHAPTER IV

### DESCRIPTION OF APPARATUS AND EXPERIMENTAL PROCEDURE

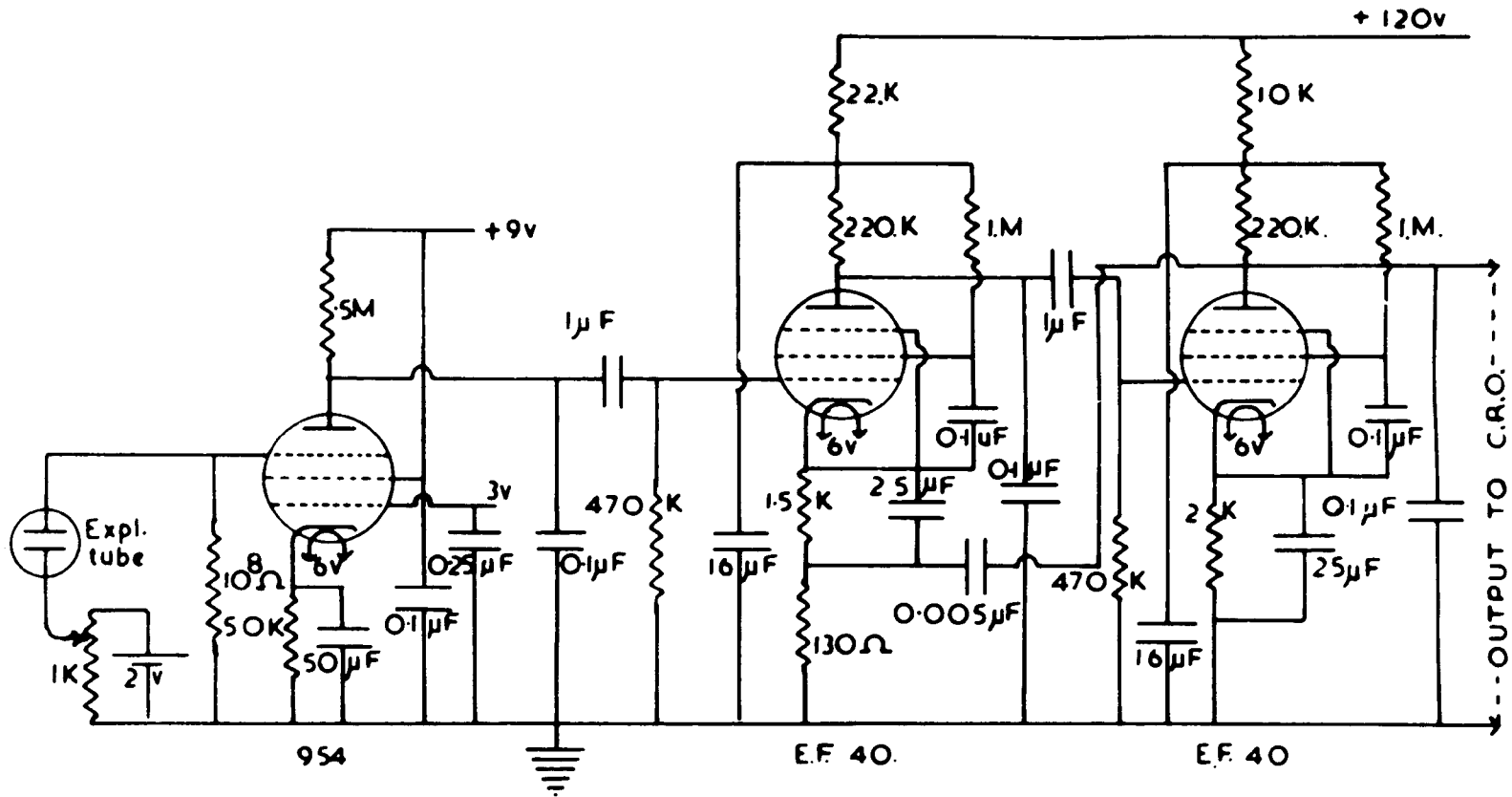
#### 4.1 Introduction

Electron emission techniques for determining work functions are unsuitable for this work. It is difficult to obtain sharp threshold frequencies with photoelectric methods and such methods cannot be used to investigate adsorption phenomena since it is difficult to avoid the production of ions which, when adsorbed on the surface will change the nature of the surface potential. Thermionic emission techniques are impracticable when used to investigate metals with low melting points.

The only practicable methods are those that entail contact potential difference methods.

Zisman's (103) modification of Kelvin's method of determining the Volta potential was used in this work. In this a vibrating capacitor is constructed from the surface under investigation and a reference surface of known work function. The induced contact potential difference between the two surfaces is equal to the difference of their work functions. Hence, the work function of the reference surface must be known before the other can be calculated.

There is neither electron emission nor an incident beam of photons, so that the use of the method does not change the characteristics of the surfaces. The main disadvantage of this system is that it gives an average work function for the whole surface, and it is unsuitable in any investigation of surface irregularities and patchiness etc.



CONTACT POTENTIAL DIFFERENCE CIRCUIT AND LOW FREQUENCY AMPLIFIER

## 4.2 Method and Technique of Work Function Measurement

It is customary in the theoretical treatment of the Kelvin method to assume that the vibrating capacitor system is completely isolated. In practice, the vibrating system is one of several capacitors which includes the capacitor between the vibrating surface and the electrostatic shield. Therefore, there will be several contact potential differences, and no single applied potential will exactly compensate the potential between the two surfaces.

In this work, extraneous fields were minimized by making the distance between the surfaces under investigation very small relative to the distances between the vibrating system and other metal components.

The contact potential differences were measured using the standard procedure - i.e., backing off the signal from the vibrating capacitor system, by applying a measured potential in series with the plates.

The first stage of the amplifying system consisted of a type 954 electrometer valve, from which the output was fed into a two stage feedback amplifier employing two E.F.40 valves (see Figure (30)).

Because the input signal was of a low frequency, large coupling capacitors were used. The decoupling capacitors were also large, so as to filter out as much 50c/s interference as possible. This decreased the amplifications, but increased the signal to noise ratio. Noise was further reduced by using accumulators and dry batteries for the power supplies.

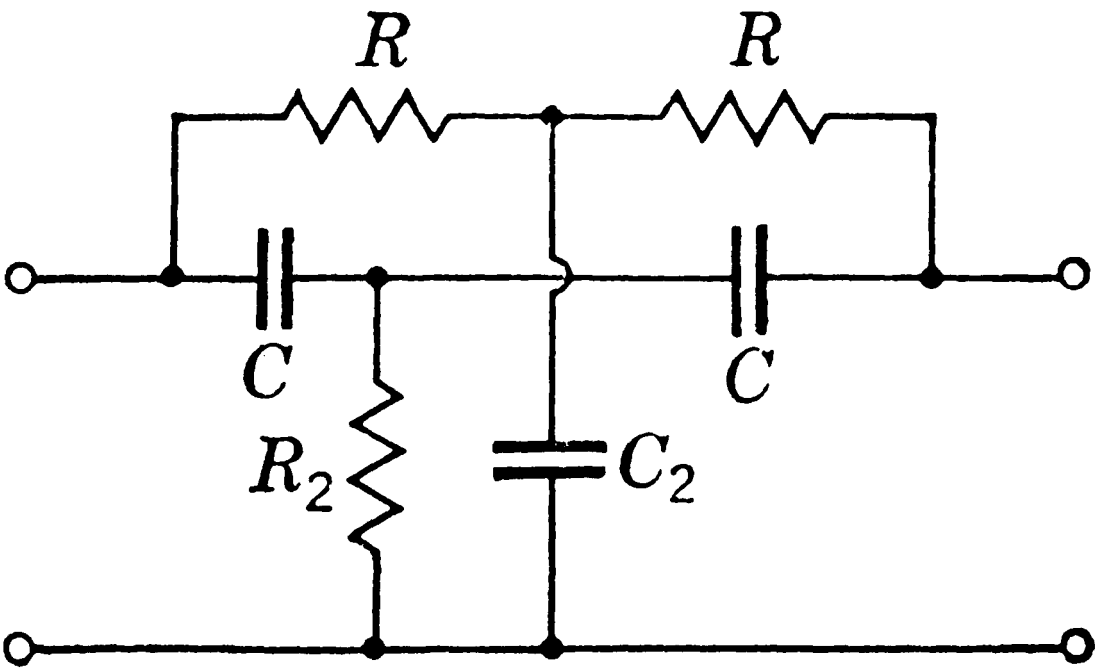


Figure 31.

The signal, amplified by a factor of about 10,000, was fed into a 50c/s twin parallel T filter (see Figure (31)), to reduce the mains interference. The output was displayed on a Telequipment type S.32 oscilloscope, fitted with a type P.A. 3 pre-amplifier.

The reversible backing-off potential was supplied from an accumulator placed across a 1000 ohm linear potentiometer, and was measured on a calibrated multi-range Crompton meter (see appendix II).

Under the most favourable conditions the contact potential differences could be measured to within a millivolt, an error which is small compared with the measured potentials.

All components of the amplifying and potentiometer systems were placed in metal electrostatic screening boxes, which were connected by earthed coaxial leads (75 ohm). Care was taken to ensure that all coupling loops were reduced to a minimum.

Vibrational instabilities were reduced by mounting the measuring equipment on a firm base disconnected from the pumping frame.

#### 4.3 The Experimental Apparatus

The investigations were carried out in two separate vacuum systems, one constructed from borosilicate glass, the other from stainless steel.

Glass was used in the construction of approximately half of the experimental apparatus, but because of its inherently low impact strength and chemical instability, it was decided to continue the work in a demountable stainless steel vacuum system. The operation of the two vacuum systems involve quite different techniques, so it is appropriate to discuss them separately.

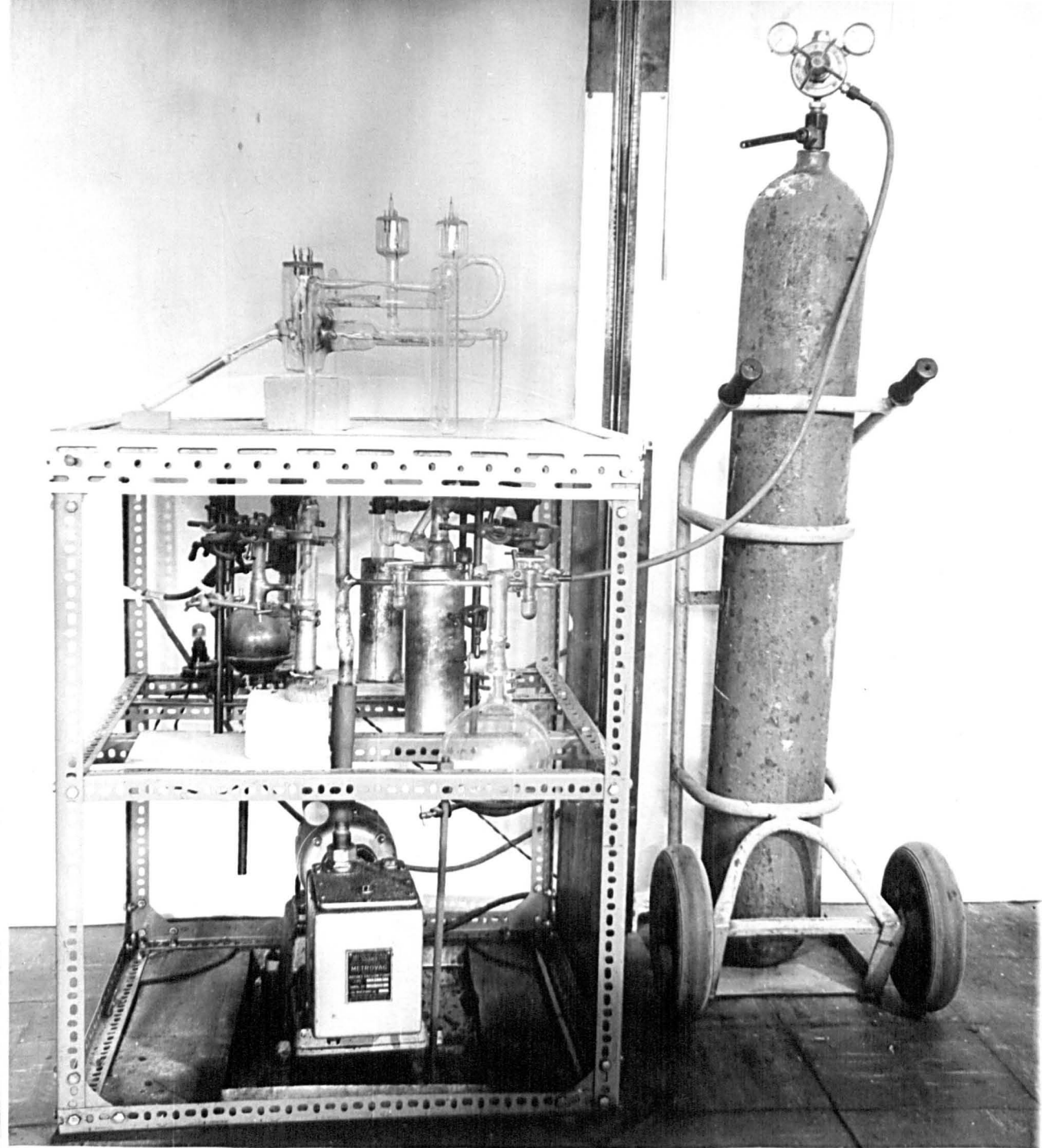


Figure 32.

#### 4.4 The Glass Vacuum System

This part of the experimental equipment was designed to attain the lowest possible pressure, so that any clean surfaces produced in the apparatus would not be contaminated too quickly by gas phase residues (i.e., to extend the time available for experimental observation).

A photograph of the vacuum system and manifold is shown in Figure (32). A schematic representation of the apparatus is shown in Figure (33).

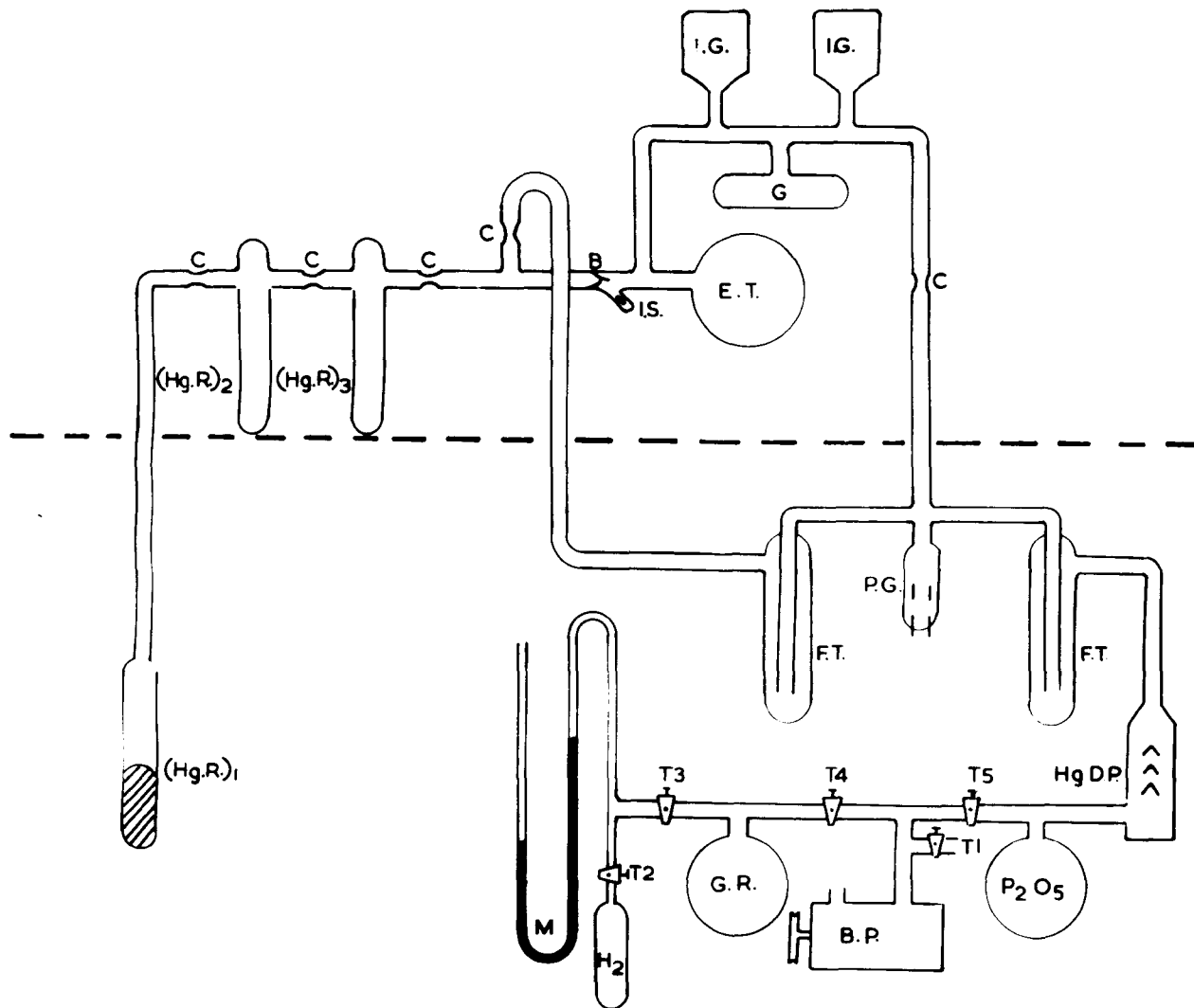
The initial stages of the system, which produced a pressure of  $5 \times 10^{-7}$  torr, consisted of a three stage mercury diffusion pump, which was backed by a Metrovac high speed rotary pump.

To reduce water vapour contamination and the diffusion of oil from the backing pump, a phosphorus pentoxide trap was inserted between the backing and mercury diffusion pumps. For ease of manipulations grease taps were used below the diffusion pump, but because they cannot be thoroughly outgassed, and would therefore have acted as a source of impurity, they were not employed above this stage.

The mercury used in the diffusion pump was purified by acid treatment and vacuum distillation. Mercury vapour was prevented from diffusing into the high vacuum system by two liquid nitrogen traps connected in series.

A Penning gauge, mounted between the oven base and the liquid nitrogen traps, was used to measure the ultimate pressure of the system while the manifold was being outgassed. The Penning gauge consisted of

- G.R. GAS RESERVOIR
- P.G. PENNING GAUGE
- C. CONSTRICTION
- B. BREAKER
- I.S. IRON SLUG
- G. GETTER
- E.T. EXPERIMENTAL TUBE
- D.P. DIFFUSION PUMP
- B.P. BACKING PUMP
- H<sub>2</sub> HYDROGEN CYLINDER.
- (Hg.R.)<sub>1-3</sub> MERCURY RESERVOIRS.
- T1-T5. GREASED TAPS.
- F, T, FREEZING TRAPS.
- M. MANOMETER.
- OVEN BASE.



a ring-shaped anode positioned equidistant between two circular cathodes, 1 cm apart. A magnetic field of about 600 gauss was produced normal to the plates by a strong permanent magnet. A potential of 2,000 volts was applied between the electrodes to induce a discharge. The resulting electrons described helical trajectories, thus giving an appreciable current amplification. When monitoring pressures below  $10^{-5}$  torr, it was necessary to initiate breakdown with a high frequency leak detector. A multi-range micro-ammeter was used to determine the breakdown current which, with the aid of a calibration curve (Appendix 1), provided a measure of the pressure. The lower limit of the instrument was found to be about  $10^{-7}$  torr, where the discharge terminated.

The vacuum system was designed to allow hydrogen to be introduced into the apparatus so that the contaminating metal oxides could all be reduced. The hydrogen, which was supplied from a high pressure cylinder, was introduced through the greased tap, T<sub>2</sub>, into the gas reservoir, G.R. The hydrogen pressure was measured on the manometer, and was always maintained below 50 torr, so as to reduce the risk of an accidental explosion.

#### 4.4.1 The Glass Ultra-High Vacuum System

At a pressure of  $5 \times 10^{-7}$  torr a clean surface will be contaminated by a monolayer in a few seconds. Thus, in any investigation of clean surfaces, it is essential to obtain pressures considerably lower than those produced by the initial stages of the vacuum system.

The conventional vacuum system was linked to the ultra-high vacuum system by means of a system of glass "pig's-tails" breakers and

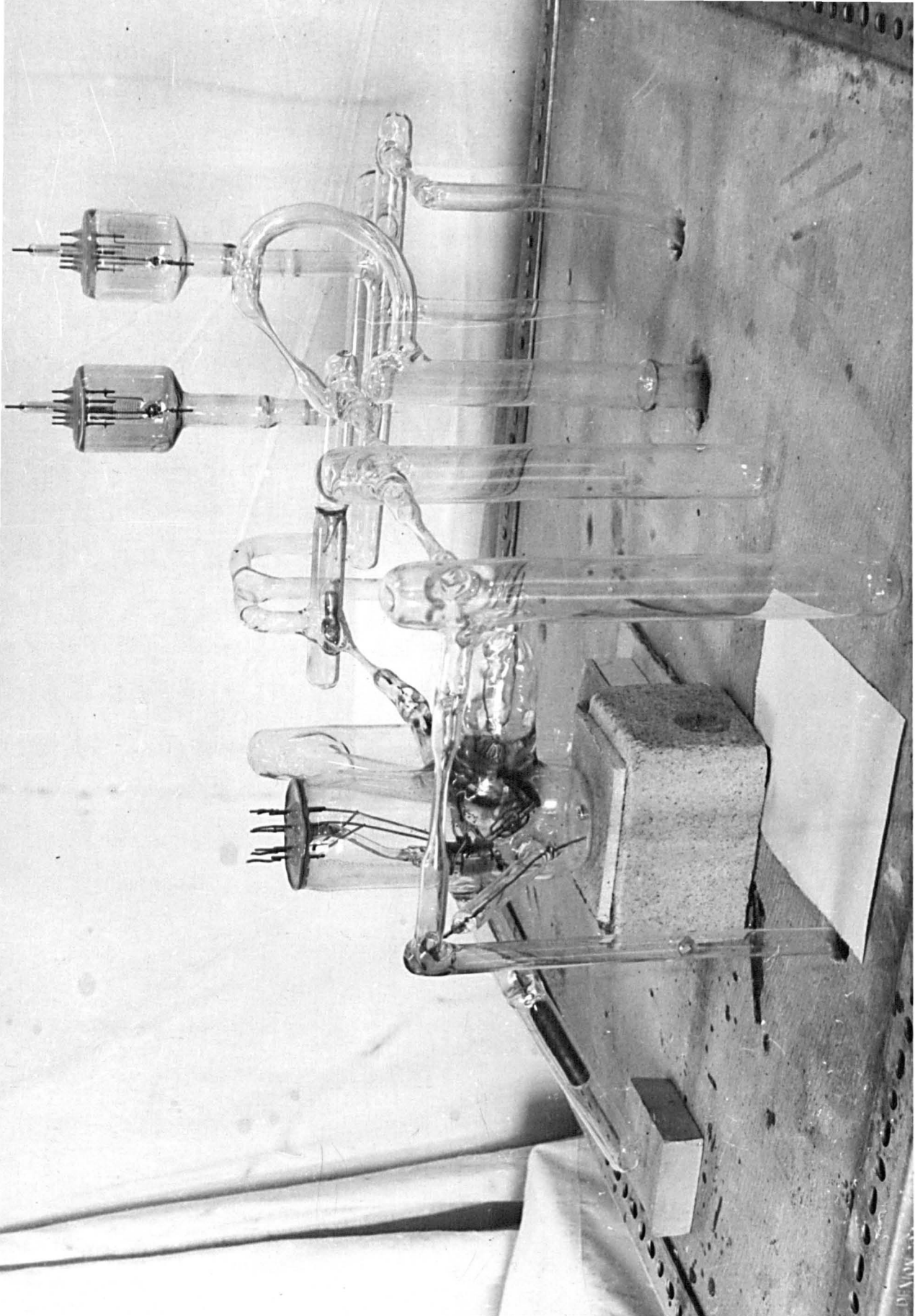


Figure 34.

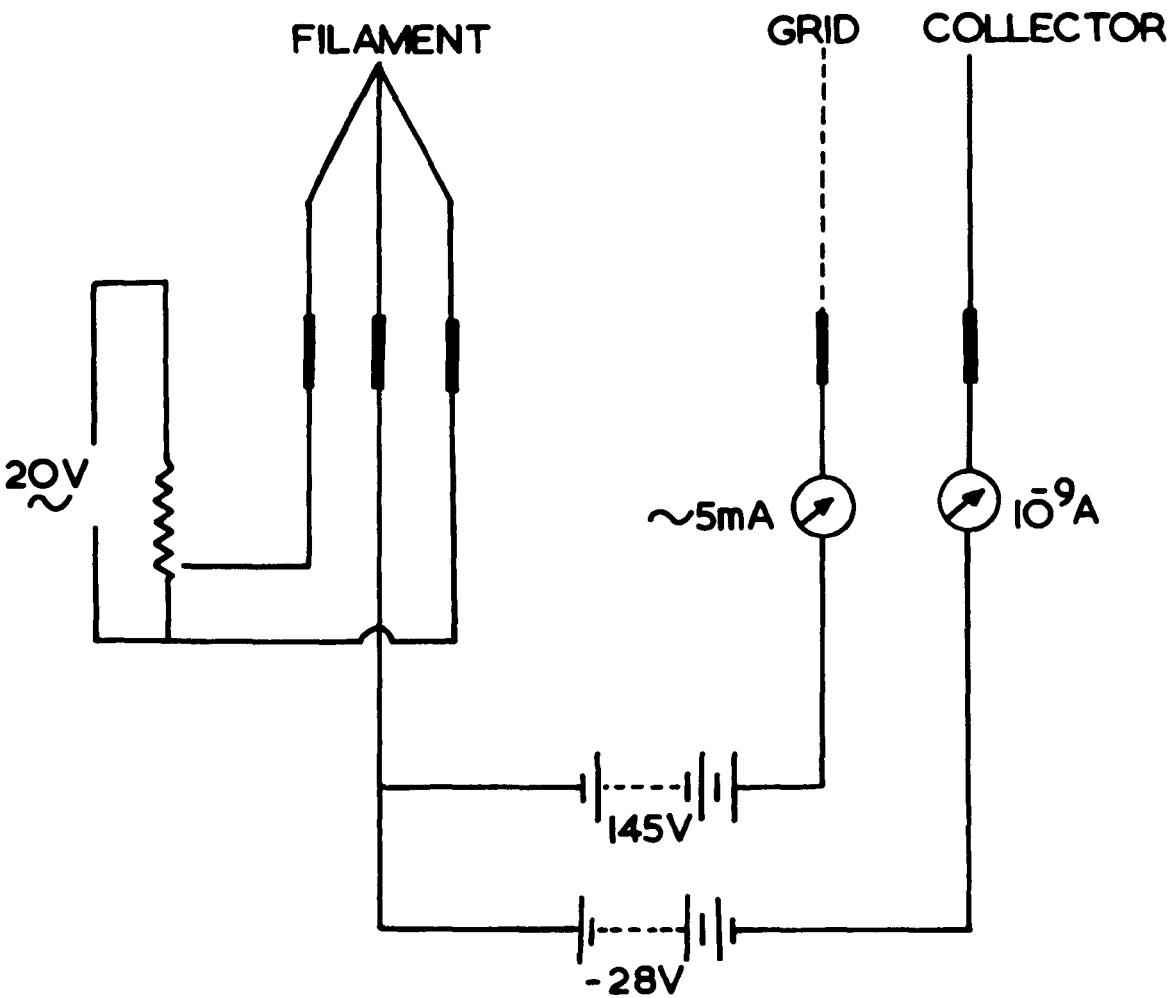
constrictions, and hence the use of grease taps above the diffusion pump was eliminated. The breakers were opened magnetically by means of a soft iron slug enclosed in a glass envelope to prevent outgassing into the equipment. The manifold was isolated from the conventional vacuum system by carefully heating the constriction C until the glass fused.

The ultra-high vacuum system consisted of a getter tube, two Alpert ionization pumps, a mercury purification system and the experimental tubes. A photograph of this part of the apparatus is shown in Figure (34).

The getters were commercially produced barium evaporators and 12 of these were spot welded onto a nickel wire lattice. The structure was placed in a side-arm so that the sublimed metal would not contaminate the experimental tubes. A radio-frequency eddy current supply was used, both to outgass and to fire the getters. When flashed the getters lowered the gas pressure by an order of magnitude.

After the getters had been fired, the pressure was further lowered by means of a commercially produced Alpert type inverted ionization pump and gauge (Mullard I.C.G. 12 gauges).

The ionization gauge head consisted of a tungsten filament placed about a centimeter away from the helical molybdenum grid, along the axis of which was a tungsten wire collector. The whole assembly was placed inside a glass envelope, the inner surface of which was coated with a conducting screen, which was usually maintained at the



CIRCUIT FOR ALPERT PUMP

Figure 35.

same potential as the collector, thus increasing the pumping speed. The thermionic electrons which were emitted when the filament was heated were accelerated towards the positively charged grid. The energetic electrons ionized the gas molecules to produce positive ions, which were accelerated towards the screen and collector, where they were subsequently trapped (104).

A schematic representation of the geometry and potentials in the gauge is shown in Figure (35).

A milliammeter and a microammeter were used to measure the thermionic electron current and the positive ion currents respectively. If the electron current was maintained at a constant value the positive ion current was proportional to the gas pressure. The approximate pressure (to the nearest order of magnitude) in the high vacuum system was obtained from the calibration relationship:-

$$P = \frac{1}{S} \frac{I_p}{I_e}$$

where  $P$  represents the gas pressure in torr,  $I_p$  is the positive ion current, and  $I_e$  is the thermionic electron current. The relative sensitivity,  $S$ , of ionization gauges for various gases have been investigated by Lafferty (105). The sensitivities do not vary by more than an order of magnitude from one type of gas to another.  $S$ , for carbon monoxide, nitrogen and oxygen in this type of gauge is of the order of 12 and, because the pressure measurements were only needed to the nearest order of magnitude, the above sensitivity was used.

By using two Alpert gauges in series it was possible to obtain pressures of about  $10^{-10}$  torr. At these low pressures several hours are required to produce a monolayer of adsorbed gas, and hence the apparatus was capable of maintaining clean surfaces.

#### 4.4.2 Glass Vacuum Techniques

All the glass components in the vacuum system, which were constructed from borosilicate pyrex glass, were cleaned by washing in nitric acid, distilled water, methylated spirits and finally acetone. The experimental tubes were connected to the pumping system by wide bore tubes to obtain the maximum pumping speed.

The vacuum system was initially evacuated, by means of the rotary backing pump, down to a pressure of  $10^{-3}$  torr. At this pressure most of the large leaks could be detected with a high frequency spark coil. The location of the leaks was indicated by a bright discharge, or by the discharge changing colour when an organic volatile liquid (usually carbon tetrachloride) was applied near to the leak.

The pressure in the system was reduced to  $10^{-7}$  torr by means of the three-stage mercury diffusion pump. The ultra-high vacuum system was outgassed by baking at a temperature of  $250^{\circ}\text{C}$  for several days. The pressure increased to about  $10^{-3}$  torr and then, as the outgassing rate decreased, the pressure fell again to  $10^{-7}$  torr. At this stage the vacuum system was flushed with a low pressure stream of hydrogen for several hours at the baking temperature.

The metal components were further reduced by heating to a dull red temperature, either by passing a current through them, or by means

of an eddy-current heater. At the end of this period the hydrogen was evacuated from the system, and the baking resumed for three days, until the Penning gauge ceased to function (i.e., the pressure was below  $10^{-7}$  torr).

When the glassware had been thoroughly outgassed the baking oven was removed to facilitate the outgassing of the metal components.

The Alpert gauges were outgassed by heating the filaments to white heat and maintaining them at a potential of minus 550 volts relative to the grids and collectors. The resulting thermionic currents desorbed contaminants adsorbed on the surface of the grids and collectors.

The metal samples were outgassed by heating them to a temperature at which the evaporation rate was beginning to become significant, so that the more volatile impurities would be sublimed off leaving the clean samples behind. The standard procedure of metal outgassing followed by baking was continued until the Alpert gauges recorded no appreciable gas evolution.

During the whole of the outgassing process the freezing traps were continuously immersed in liquid nitrogen to stop mercury vapour diffusing into the manifold.

After the initial evacuation had been accomplished, the manifold was isolated from the vacuum system by melting the constriction (see Figure (33)). The pressure was then reduced by two orders of magnitude by firing several of the getter strips and leaving the active films for

several hours to adsorb the gas phase residues. The flashing routine, followed by several hours adsorption, was repeated three or four times until there was no further pressure drop.

To complete the evacuation, the Alpert gauge was switched on for several days. The pumping speed of Alpert pumps is proportional to the pressure and hence an exponential decrease in pressure is observed. If the system did not contain any leaks the pressure subsequently fell to about  $5 \times 10^{-10}$  torr.

#### 4.4.3 Construction of the Glass Experimental Tubes

Six experimental tubes were constructed to investigate particular phenomena, and their design varied considerably. The tubes (which will be described individually in the next chapter) were all constructed to determine work function values, so they contained many common characteristics.

Since bulk metal components are difficult to outgas, glass was used as the material of construction, as far as possible.

The tubes contained two electrodes, the Kelvin electrode (which was usually the reference surface) being vibrated normally to the surface under investigation. The Kelvin electrodes were mounted on a spring system constructed out of two crossed tungsten strips. The sensitivity of the system was increased by placing the plates as close together as possible, care being taken to avoid contact during operation. The sensitivity was further increased by adjusting the spring system, so that the Kelvin assembly had a high frequency of

oscillation. (A frequency of between 20 and 40c/s seemed to be the optimum).

Most of the clean surfaces were prepared by evaporating a thin film of the metal under investigation onto a pyrex substrate. The glass discs were formed in carbon moulds at a temperature of about 800°C, by gently pressing soft globules of pyrex into shape. To make electrical contact with the far side of the substrates, tungsten rods were carefully eased through the molten glass. After being slowly annealed the discs were ground flat by means of carborundum powder, and then flame polished to produce microscopically smooth faces. The flame polishing process oxidised the tungsten rods producing high resistance oxide layers, which were subsequently removed by washing with a sodium hydroxide solution. As an added precaution, small spots of aquadag were placed on the ends of the tungsten rods, to guarantee good electrical contact.

To increase the accuracy of the system, the areas of the surfaces were made as large as possible, but the diameter was limited to about 3cms, because of field effects between the electrodes and the glass envelope. The weight of large electrodes was also prohibitive since it was very difficult to devise a suitable vibrating system.

The clean films were evaporated from small beads mounted on tungsten helical supports. A length of 30 s.w.g. wire of the metal to be evaporated was coiled around a helix of 25 s.w.g. tungsten wire and melted in an atmosphere of hydrogen, to reduce dissolved oxygen

and any oxide present. The reduced filaments were supported on 18 s.w.g. nickel leads, which were spot welded to the tungsten rods in the envelope pinch. The hydrogen adsorbed by the beads during the reduction process was expelled during the subsequent outgassing processes. To restrict the beams of evaporated metal the filaments were enclosed in cylindrical nickel shields. The completed evaporation assemblies were then carefully positioned near and normal to the corresponding glass substrates.

The Kelvin electrodes were mounted on hinges; this enabled the reference surfaces to be moved from a position opposite the evaporation beads to the experimental region. A glass covered iron slug was used to magnetically deflect the Kelvin assembly from one stable position to the other. The moveable Kelvin electrodes were electrically connected to the pinch leads by means of ductile nickel tapes, care being taken to shield the vulnerable regions against short circuiting induced by the evaporated metal. After being cleaned in nitric acid and distilled water the envelopes were drop sealed onto the pinches, after which they were slowly annealed, and then coupled to the vacuum system.

#### 4.5 The Stainless Steel Ultra-High Vacuum System

Materials used in the construction of ultra-high vacuum systems must satisfy several fundamental criteria. These include a low vapour pressure at outgassing temperatures, chemical inertness, ease of fabrication, and impermeability to gases.

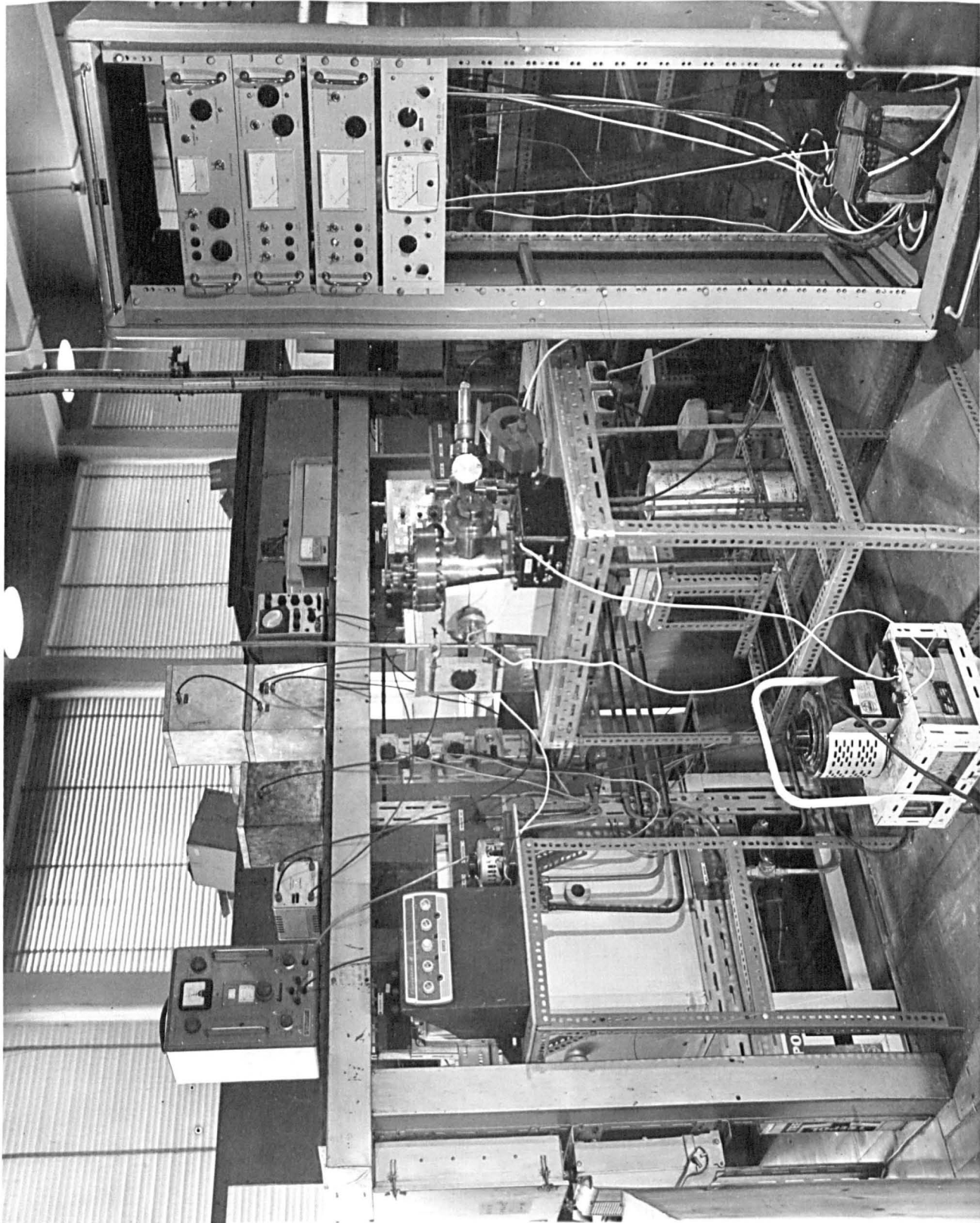


Figure 36.

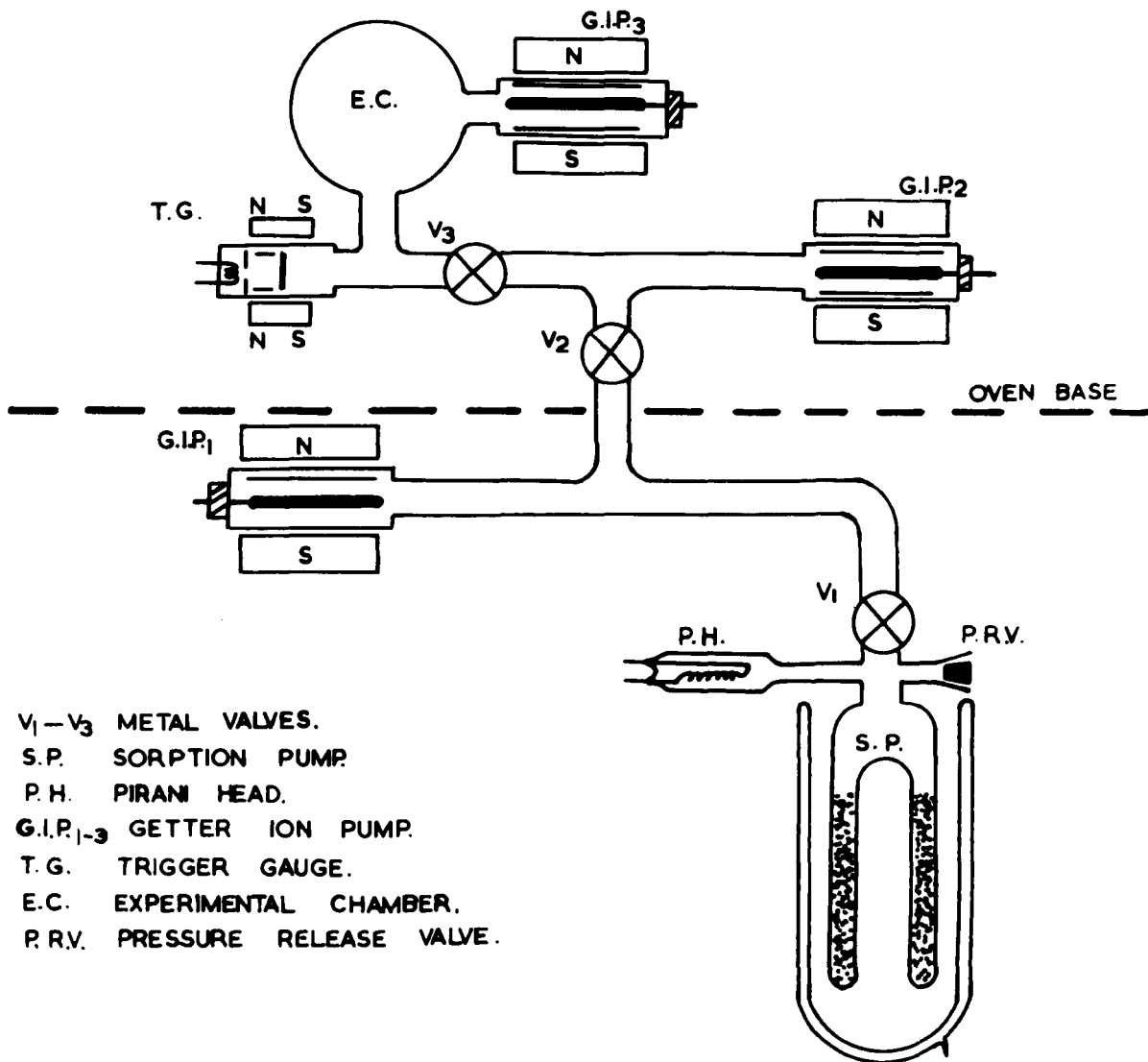


Figure 37.

Stainless steel systems not only satisfy these requirements, but also have the added advantage of being demountable and free of moving parts. Stainless steel systems, unlike the conventional glass ones, are completely free of mercury and contaminating organic vapours.

A photograph of the stainless steel vacuum system and measuring equipment can be seen in Figure (36). A schematic representation of the system is shown in Figure (37).

The pressure in the system was reduced from atmospheric to about  $10^{-3}$  torr using a sorption pump containing molecular sieve (aluminium calcium silicate).

At this stage a Pirani gauge head (Edwards Type M.6.A.), located just above the sorption pump, measured the pressure in the system.

Before being immersed in liquid nitrogen the sorption pump was outgassed by heating to a temperature of about  $250^{\circ}\text{C}$  for several hours. When the molecular fore pump had produced a pressure in the micron range, the first bakeable valve  $V_1$  was closed, and the first getter ion pump G.I.P. was turned on.

The getter ion pumps consisted of a titanium anode of honeycomb structure positioned equidistant between two titanium cathodes. A strong axial magnetic field was maintained between the electrodes by means of a permanent magnet.

The pumping speed of a getter ion pump varies with the nature of the gas being pumped, and it is therefore possible using hydrogen (for which the pumping rate is three times that of air) to use the pumps as leak detectors.

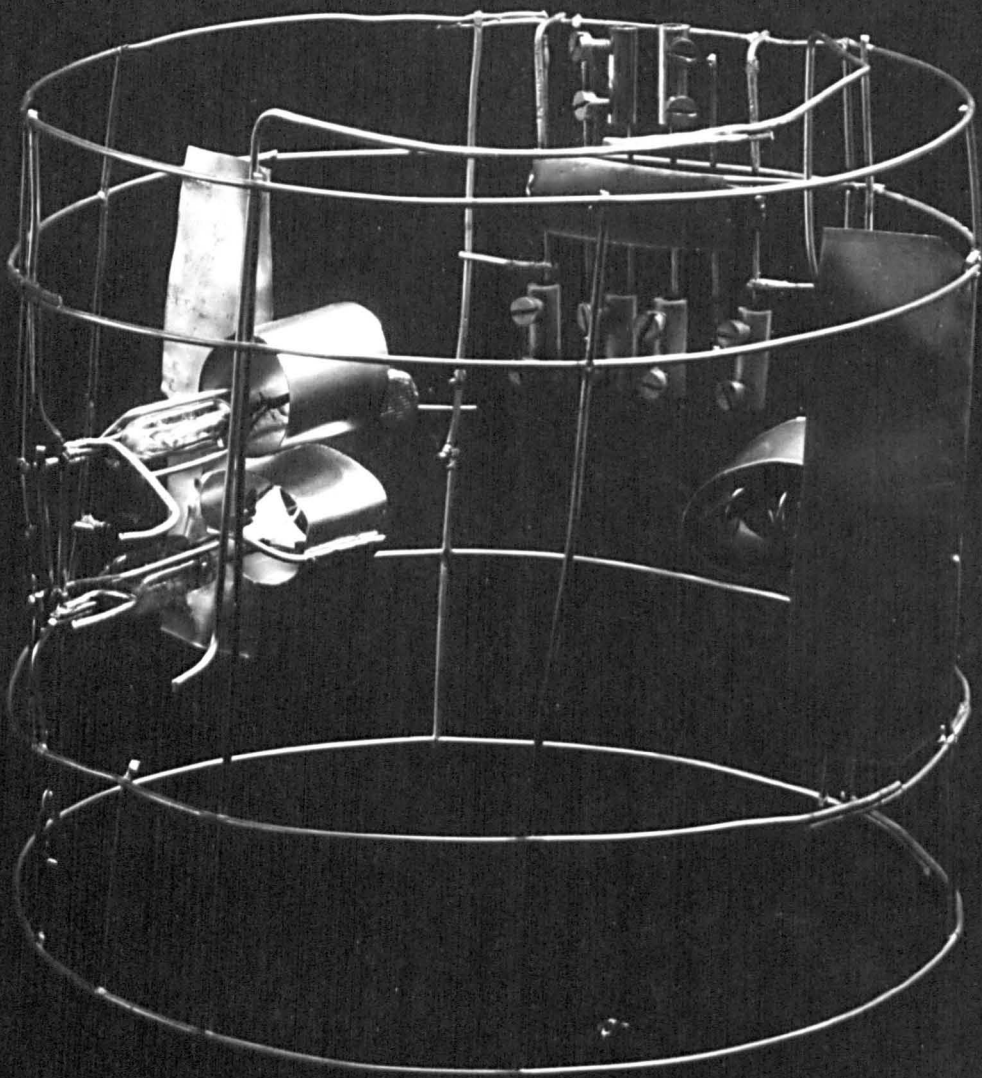


Figure 38.

When the first getter ion pump had reached equilibrium with the outgassing rate of the unbaked system (usually at a pressure of approximately  $5 \times 10^{-7}$  torr) the gaskets and welded joints were carefully exposed to a narrow stream of hydrogen. Any leaks in the system were indicated by a pressure rise of about an order of magnitude.

If these leak detecting tests proved negative, the system was then outgassed at a temperature of about  $230^{\circ}\text{C}$  for a couple of days. The outgassing was discontinued when the first getter ion pump G.I.P.<sub>1</sub> (pumping speed 8 litres/sec below  $10^{-4}$  torr) recorded a pressure lower than  $10^{-8}$  torr. At this stage the second getter ion pump G.I.P.<sub>2</sub> was switched on, and, after it had outgassed itself, the second bakeable valve  $V_2$  was closed. When the pressure had fallen to below  $10^{-9}$  torr the last getter ion pump G.I.P.<sub>3</sub> was turned on to pump the experimental chamber E.C. (the rest of the system was isolated from the experimental chamber by closing the third valve  $V_3$ ). With this cascade pumping technique it was possible to attain pressures below  $10^{-10}$  torr. A trigger discharge gauge, T.G., (General Electric Type 22.G.T.210) was employed to measure pressures below  $10^{-8}$  torr.

The demountable stainless steel components were connected by means of Conseal flanges used in conjunction with oxygen-free, high-conductivity plastic deforming copper gaskets.

For ease of manipulation the metal evaporators and shields were mounted on a nickel wire cage (see Figure (38)), which, when assembled was gently inserted into the cylindrical experimental chamber.

- 1. KELVIN ELECTRODE.
- 2. GOLD FILMS.
- 3-4. GOLD EVAPORATORS.

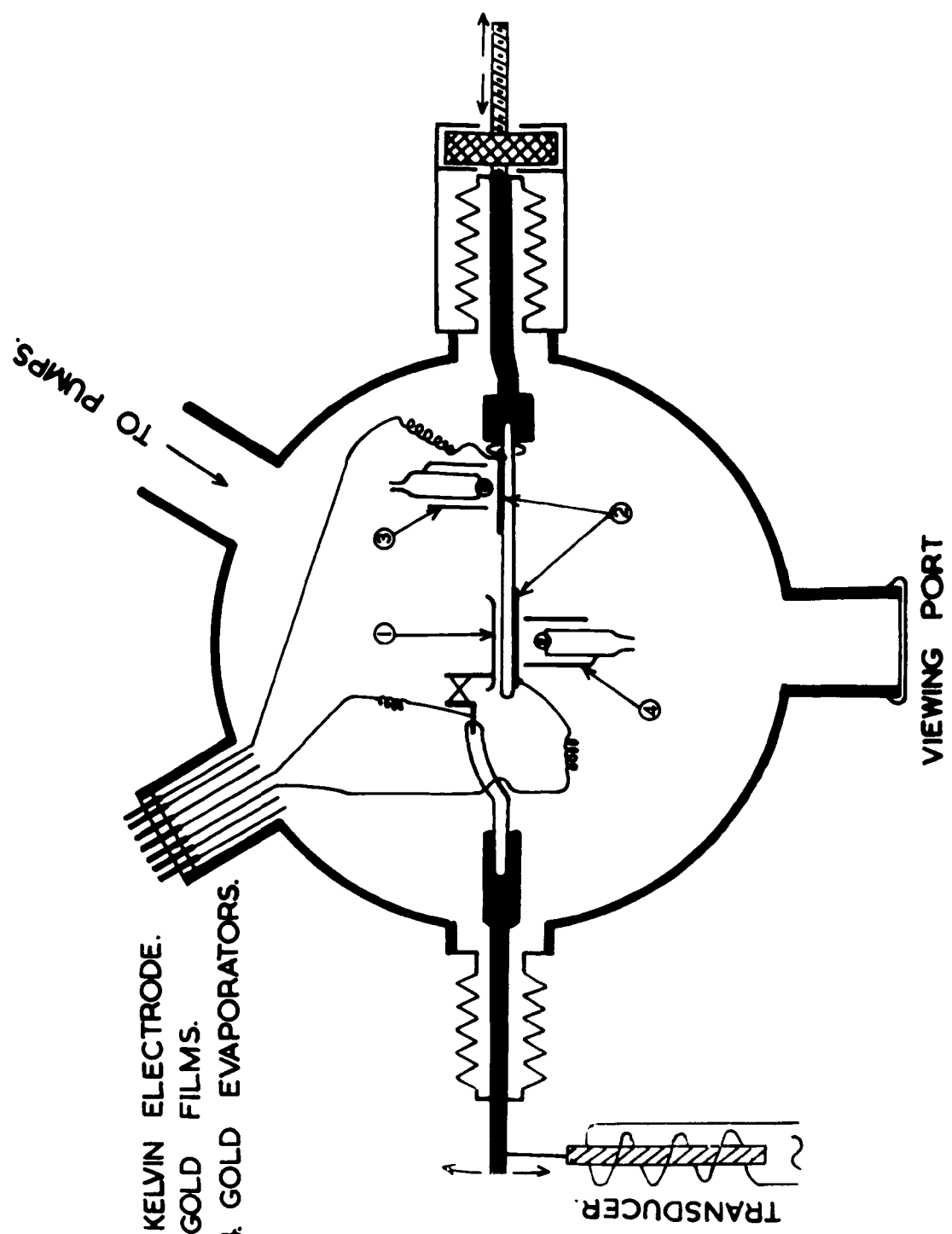
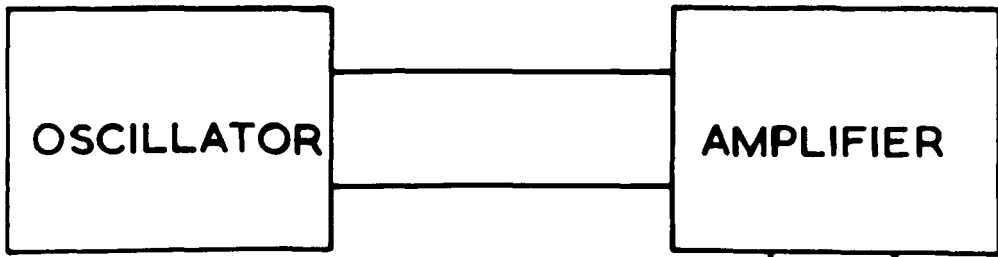


Figure 39.



K.E. KELVIN ELECTRODE.  
 T.A. TRANSMISSION ARM.  
 B. BELLOWS

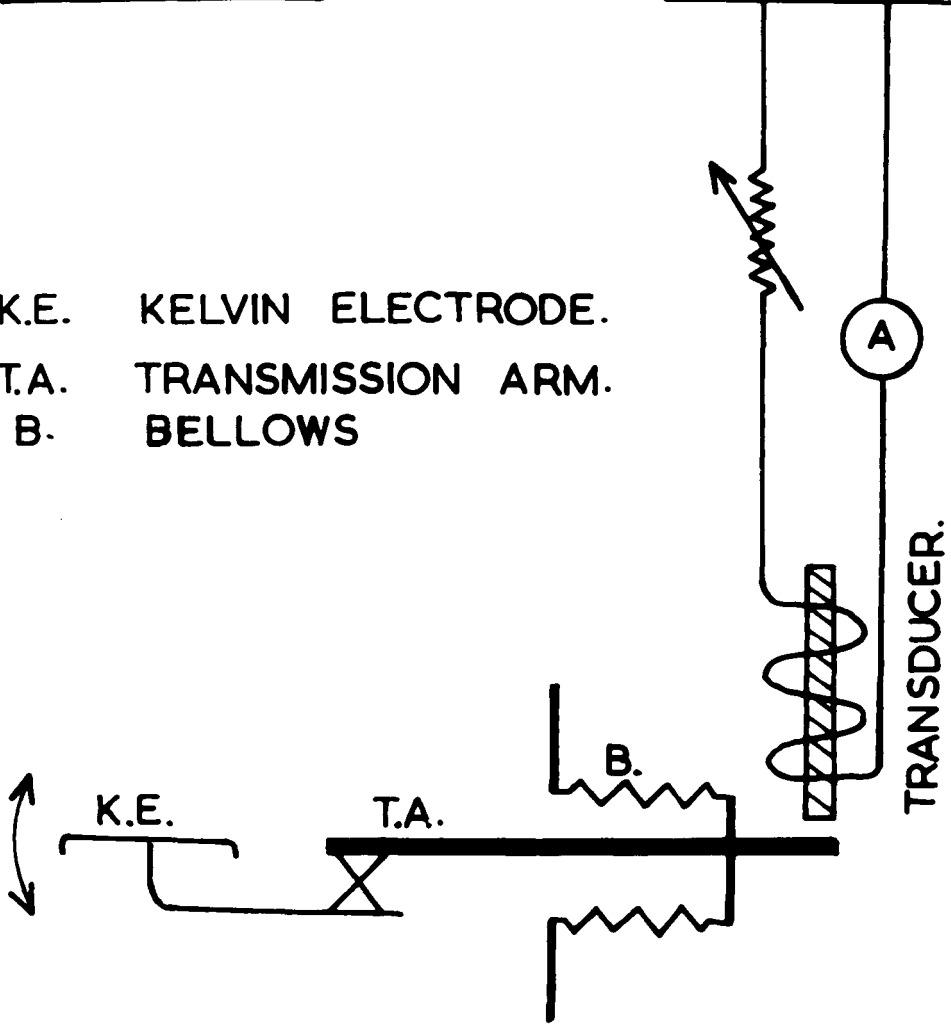


Figure 40.

Electrical contact between the evaporators and the external power supply was made by means of metal to ceramic "feed throughs".

Figure (39) shows a schematic representation of the experimental chamber.

A linear motion drive enabled the clean surfaces under investigation to be moved transversely relative to the Kelvin electrode. To assist the delicate internal operations a  $1\frac{1}{2}$ " Pyrex viewing port was fitted to the chamber.

#### 4.6 The Kelvin Electrode Vibrating System

In the glass experimental tubes the Kelvin electrodes were induced to vibrate by gently tapping the glass envelopes. The system, though adequate, suffered from the following defects:-

- 1) The vibration decayed to zero as a function of time due to internal damping and hence it was difficult to utilize the maximum sensitivity of the equipment.
- 2) The lack of control over the amplitude made it difficult to avoid collisions between the Kelvin electrode and the other surface. As the resulting contact between the plates could change the surface characteristics (e.g., by charge-transfer phenomena) it was decided to investigate other vibrating systems.

A block diagram of the vibrating system used in the stainless steel apparatus can be seen in Figure (40).

The Kelvin electrodes, K.E., were mounted on crossed spring assemblies which had resonant frequencies in the 20-50c/s range. The system was induced to oscillate by vibrating the transmission

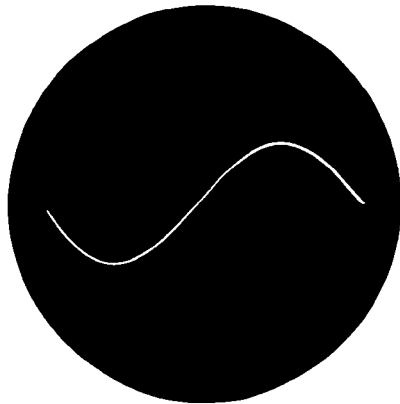
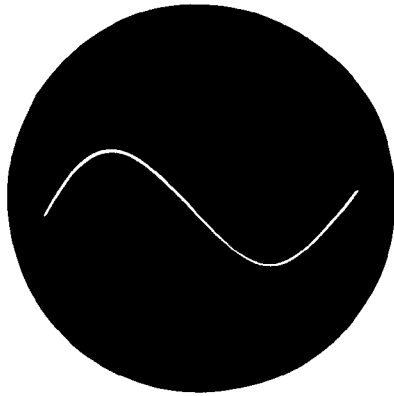


Figure 41.

arm, T.A., at the Kelvin electrodes resonant frequency, a transducer was used to maintain the vibrations.

The transmission arm was connected to the stainless steel chamber by an elastic bellows-type membrane. The flexible coupling caused the vibrating electrode to shift when the pressure in the system was reduced, and therefore, to compensate for any movement, a system of adjusting screws was provided.

It was observed that the resonant frequency slowly fluctuated as a function of time; this was possibly due to the elasticity of the springs changing because of the bakout and outgassing processes. Any change in the resonant frequency was compensated for by adjusting the characteristics of the electronic oscillator. The amplitude was controlled by the variable resistance in the circuit.

The induced contact potential difference between the vibrating plates was measured by the classical Kelvin technique. Photographs of typical oscilloscope displays are shown in Figure (41). The middle oscillograph represents the null point, while the other two signals show equal and opposite off balance points of +0.005 and -0.005 volts respectively. As can be seen in the photographs, when the balance point is passed the phase of the signal changes by  $\pi$  radians, and hence the determination of the null point is considerably simplified.

#### 4.7 Purification of Mercury

The initial charge of mercury, which was carefully poured into the first mercury reservoir (Hg.R)<sub>1</sub> (see Figure (33)) had a purity not less than 99.8%. The first mercury reservoir was located below the

oven base where the temperature did not rise above 30°C and hence the vapour pressure of mercury in the glassware was maintained below 10<sup>-3</sup> torr. After the manifold had been evacuated and baked, the mercury was outgassed by slow refluxing under a pressure of 10<sup>-7</sup> torr, for several days. The impurities outgassed from the mercury would have contaminated the rest of the system, and so at this stage the rest of the manifold was given a second bakeout by heating with a gas flame.

After the system had been thoroughly outgassed, the mercury was slowly distilled from the first to the second reservoir (Hg.R)<sub>2</sub>. To ensure that the less volatile impurities remained in the first distillation tube, a low distillation temperature and hence a slow rate of distillation was maintained. A 100 watt heating tape was coiled round the whole length of the first distillation tube to achieve this. The first distillation was discontinued when three quarters of the original mercury had been distilled (this usually took several days). The first reservoir was then isolated by closing the constriction.

Similar slow distillation techniques were used in the second stage of the mercury purification. The rate of evaporation was controlled by coupling the heating tape to a Variac transformer. When three quarters of the mercury had been distilled into the third reservoir (Hg.R)<sub>3</sub>, the second constriction was sealed. During the two distillation processes the mercury must have further outgassed

and therefore the surfaces of the last reservoir must have been contaminated.

The adsorbed impurities were removed by heating the glass-ware to a temperature of about 300°C with a gas flame.

The final stage of the purification consisted of distilling the mercury from the reservoir (Hg.R.)<sub>3</sub> into the tube connecting the experimental tube to the last distillation reservoir. When the required amount of mercury had been condensed in the tube the two constrictions linking the small tube were closed - leaving the pure outgassed metal in the sealed side arm. The mercury was then admitted into the experimental region by magnetically breaking the isolating seal.

Before the breaker was opened, the pressure inside the experimental tube and the connecting arm were about  $10^{-10}$  torr and  $10^{-7}$  torr respectively. Hence, considering that the volume of the high vacuum system was approximately two orders of magnitude greater than the tube containing the mercury, the partial pressure of the impurities in the experimental tube when the mercury was admitted was unlikely to have been higher than  $10^{-9}$  torr.

#### 4.8 Summary

In the course of this chapter, the experimental apparatus and techniques have been reviewed. In the preparation of the clean films an attempt has been made to obtain materials with a maximum impurity content of one part in  $10^7$ .

## CHAPTER V

### CONTACT POTENTIAL DIFFERENCE MEASUREMENTS ON LIQUID AND SOLID MERCURY SURFACES: RESULTS AND DISCUSSION.

#### 5.1 Introduction

The contact potential difference method of determining work functions is possible only if the work function of one of the surfaces is accurately known at the time of measurement.

At room temperature mercury has a vapour pressure of approximately  $10^{-3}$  torr (see appendix III), which under normal conditions would contaminate a clean reference surface in about a millisecond. Therefore the problem with using the Kelvin method, in conjunction with mercury, is one of keeping the standard surface free from polluting adsorbed layers.

Three different techniques for maintaining this freedom have been investigated and these in chronological order, were:-

- a) The reference surface was heated to a high temperature (in the order of  $500^{\circ}\text{C}$ ), in an attempt to desorb adsorbed mercury molecules.
- b) The mercury was cooled to the temperature of liquid nitrogen, where its vapour pressure is less than  $10^{-15}$  torr, thus effectively eliminating the source of contamination.
- c) The reference electrode was separated from the mercury vapour by a thin insulating glass partition.

The first two methods which were investigated, entailed similar experimental techniques and will therefore be discussed in this chapter.

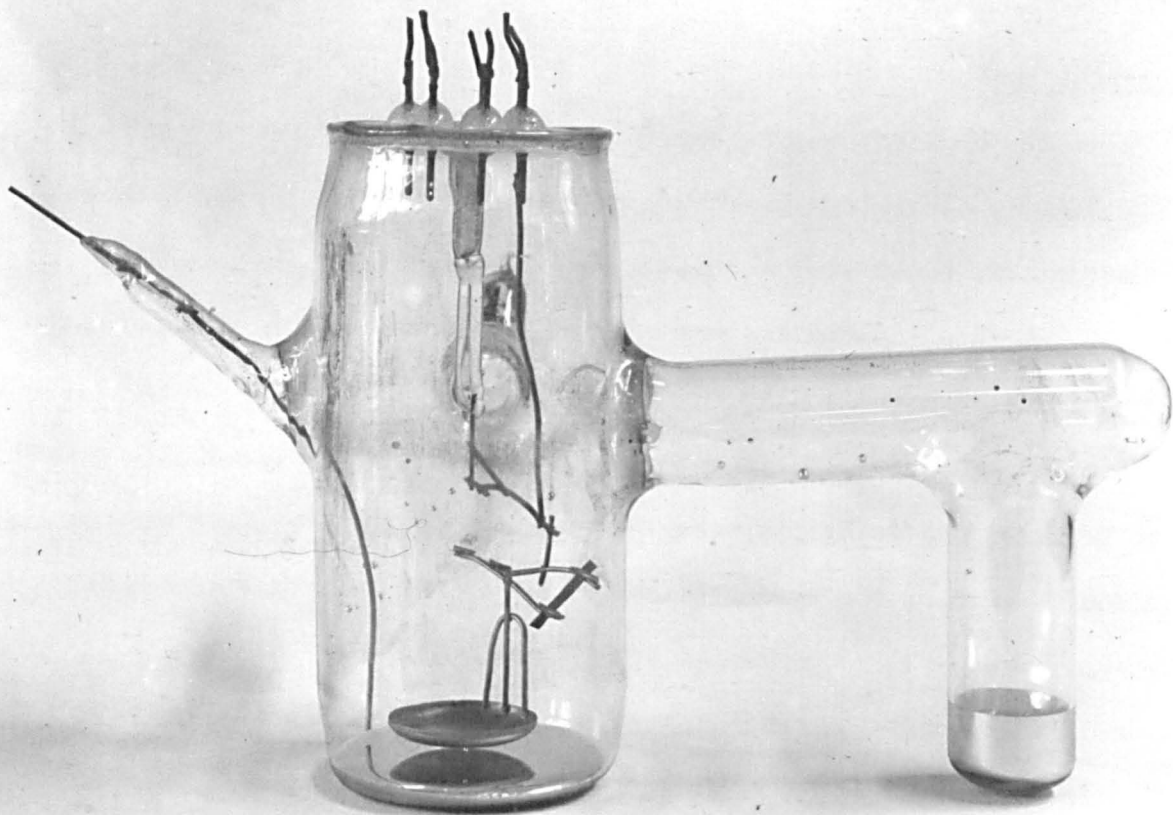


Figure 42.

The other method (i.e., using thin insulating partitions), employed quite a different experimental procedure and will be reviewed in a later chapter.

The results discussed in this chapter were obtained from five experimental tubes. While measurements were being taken, except where otherwise stated, the residual gas pressures were less than  $10^{-9}$  torr. The first two experimental tubes were used to investigate contact potential difference changes between liquid mercury surfaces and hot molybdenum Kelvin electrodes. The remaining three tubes were designed to investigate the surface characteristics of solid mercury films.

## 5.2 Contact Potential Difference Measurements on Liquid Mercury Surfaces

### 5.2.1 Tube 1

The first experimental tube (a photograph of which is shown in Figure (42)) was designed to determine the work function of liquid mercury. The mercury electrode consisted of a pool of the liquid metal positioned at the bottom of the experimental tube. In order to restrict the weight of the mercury the lower end of the tube was flattened.

The distance between the Kelvin electrode and the mercury surface could be adjusted by pouring the required amount of metal into or out of the mercury reservoir side-arm.

Several workers (107, 141) have produced clean surfaces by heating materials to high temperatures. It was therefore decided to investigate the possibility of producing clean mercury-free reference

surfaces by heating molybdenum electrodes to dull-red heat.

Molybdenum was selected because it does not form an amalgam with mercury (108) and its solubility in mercury is below  $2 \times 10^{-5}$  per cent (109). Molybdenum lends itself to this method since its vapour pressure at  $900^{\circ}\text{C}$  is below  $10^{-14}$  torr (138) and the work function of well-aged polycrystalline molybdenum is accurately known (111).

The molybdenum electrode was initially cleaned by slowly etching away the heavily contaminated outer layers with a dilute solution of chromic acid. After the acid treatment the electrode was washed in distilled water, acetone and finally carbon tetrachloride. At this stage the molybdenum was outgassed by eddy-current heating to a temperature of about  $1,000^{\circ}\text{C}$  for several minutes. To reduce any oxide layers the outgassed electrode was employed as the cathode in a low pressure (about 1 torr) hydrogen discharge. After about two days the discharge was terminated and the purification process was completed by subjecting the reduced electrode to a second outgassing process.

At the final seal-off from the manifold the system consisted of the experimental tube containing the required amount of mercury and an Alpert pump. The Alpert gauge and experimental tube were connected by a collapsible constriction.

The partial pressures of the residue gases were further reduced by switching on the Alpert pump, after the mercury had been cooled to liquid nitrogen temperatures (thus effectively eliminating

contaminating mercury vapour from the Alpert gauge). The final constriction was sealed after pumping for about two days, when the partial pressure of the residual gases was approximately  $10^{-10}$  torr. In an effort to desorb adsorbed mercury molecules the molybdenum reference electrode was heated to a dull-red heat by means of an eddy-current heater, which was carefully positioned around the base of the experimental tube. While the Kelvin electrode was being heated the mercury was poured out of the main experimental tube into the reservoir, thus maintaining the mercury at room temperature.

When the molybdenum reference surface had been heated to its maximum temperature (about  $900^{\circ}\text{C}$ ) the eddy-current heater was removed and the correct quantity of mercury was gently poured back into the experimental tube.

During the manipulation of the mercury great care was taken to avoid contact between the liquid metal and the hot Kelvin electrode.

The two surfaces under investigation were electrically connected to the external electronic equipment by means of nickel leads and tungsten seals.

After the experimental tube had been processed using standard high vacuum techniques, contact potential difference measurements were made by the conventional Kelvin method. The molybdenum reference electrode was induced to vibrate by gently tapping the experimental tube.

FIRST TUBE  
CHANGE IN C.P.D. WITH TIME.

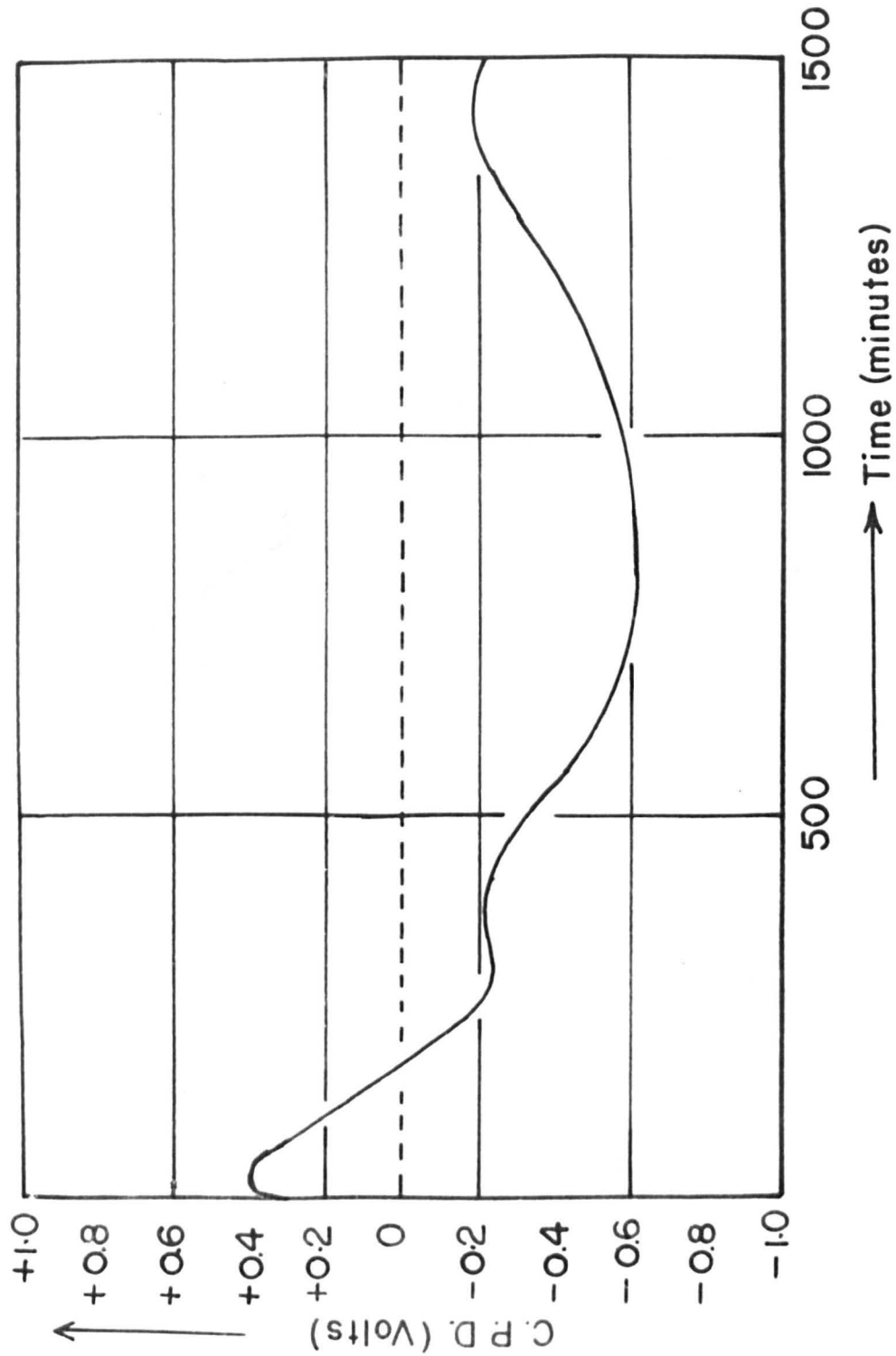


Figure 43.

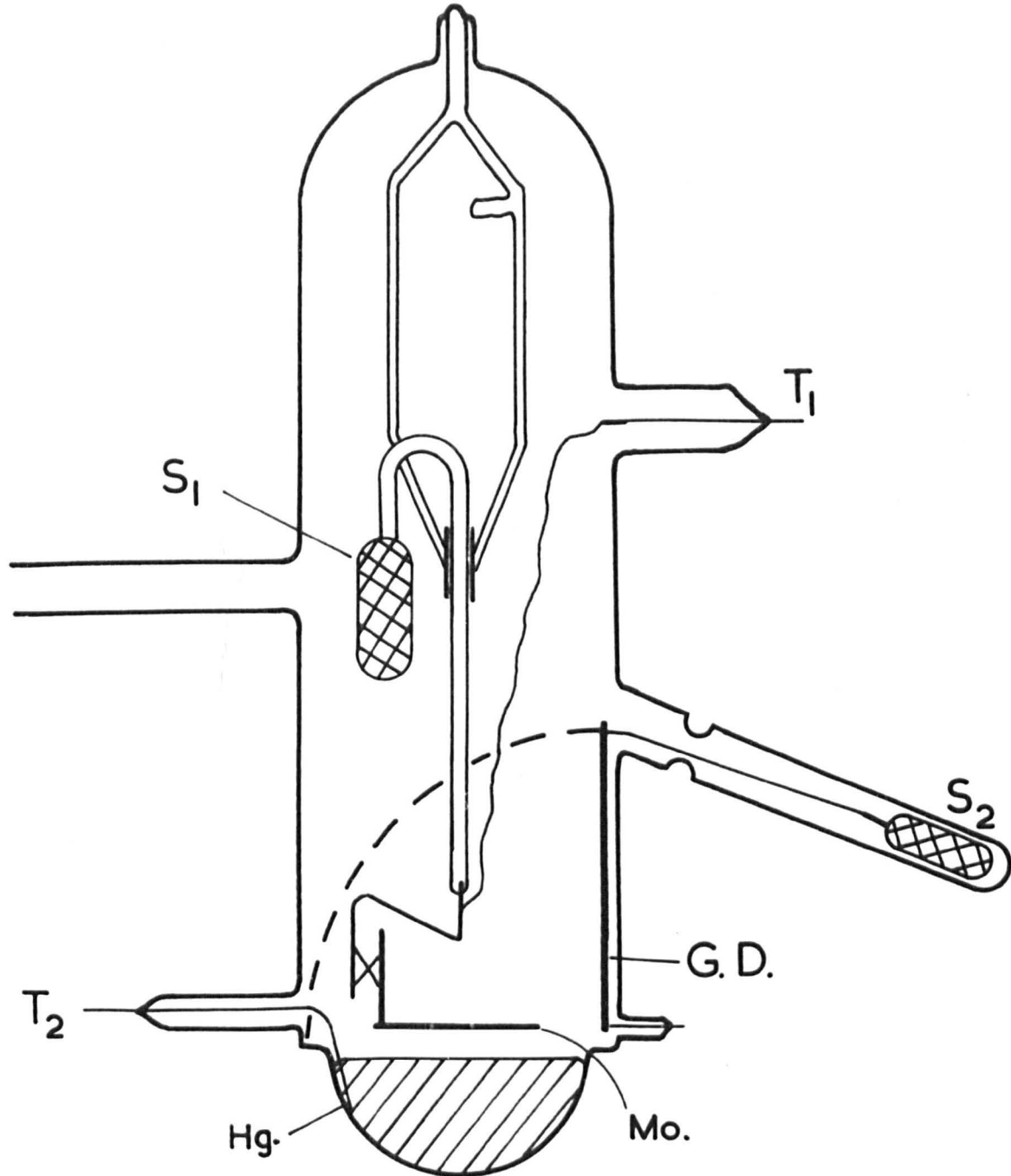
### Results obtained from the First Experimental Tube

The results obtained from this simple tube, which are illustrated in Figure (43), show a completely random fluctuation in C.P.D. measurements as a function of time.

During the series of C.P.D. determinations the temperature of the molybdenum electrode was continuously maintained above a temperature of  $300^{\circ}\text{C}$ . When the eddy-current heater was switched on (usually about every two minutes) to boost the temperature of the reference surface up to a dull-red heat, no discontinuity or sudden change in the C.P.D. measurements were observed. It was therefore concluded that the random variation in C.P.D. measurements probably represented a change in the surface nature of the mercury electrode, rather than a variation in the characteristics of the molybdenum surface.

After repeated C.P.D. runs the glass surfaces inside the experimental tube, in the region of the molybdenum disc, became coated with a thin layer of contamination (this could be observed as a pale-blue bloom). The impurity layer almost certainly originated from the molybdenum electrode, since it was not present before the molybdenum surface was heated and it gradually became thicker with repeated outgassing processes of the Kelvin electrode.

It must therefore be concluded that the impurities outgassed from the molybdenum were contaminating the surface of the liquid mercury. With this simple experimental tube, it was not possible to



- Mo. MOLYBDENUM ELECTRODE.
- Hg. MERCURY ELECTRODE.
- G.D. GLASS DIAPHRAGM.
- S<sub>1</sub>-S<sub>2</sub>. IRON SLUGS.
- T<sub>1</sub>-T<sub>2</sub>. TUNGSTEN SEALS.

Figure 44.

prevent the outgassed residues contaminating the mercury surface. It was therefore decided to construct a new experimental tube, which would incorporate in its design a method of preventing the contamination of the mercury.

### 5.2.2 Tube 2

The second experimental tube was designed to follow C.P.D. changes between a polycrystalline molybdenum reference electrode and a liquid mercury surface, under more carefully controlled purity conditions than the first experimental tube.

A movable glass diaphragm, G.D., (see Figure (44)) was used as a shield to protect the clean mercury surface, Hg, from the contaminating residues, outgassed from the molybdenum disc, Mo, during its heat treatment.

The molybdenum disc was reduced and cleaned by employing the techniques used to condition the electrode in the first experimental tube.

The first stage of the mercury-desorbing heat treatment involved raising the molybdenum electrode by magnetically manipulating the iron slug,  $S_1$ , from its position just above the mercury surface (as shown in the schematic diagram), to a higher level. This enabled the circular glass diaphragm to be carefully placed in a horizontal position, just above the mercury electrode. The diaphragm was then moved from the vertical plane to a horizontal position (as shown in the photograph, Figure (45)), by means of the second magnetic slug,  $S_2$ .

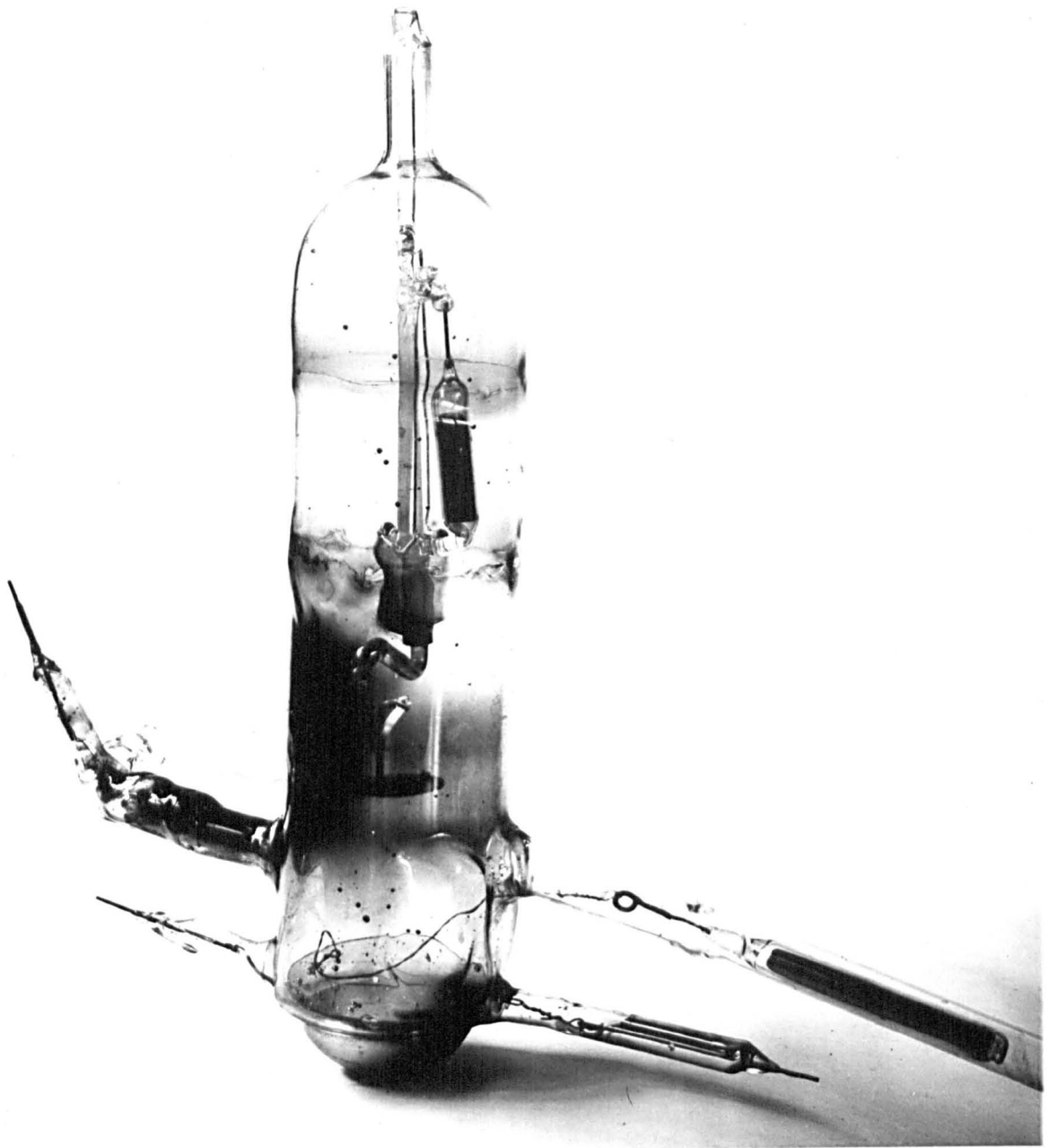


Figure 45.

When the Kelvin electrode was in its raised position (as shown in the photograph) it was eddy-current heated to a dull-red heat. It was hoped to restrict in this way the outgassed contaminants to the section of the experimental tube above the shielding glass diaphragm.

After the diaphragm had been removed to its vertical position, the hot reference surface was then gently lowered to its measuring position, - i.e., just above the mercury surface.

It can be seen from the photograph (Figure (45)) that the blooming produced on the inside of the experimental tube by the outgassed residues was successfully confined to the region of the tube, above the diaphragm. The pool of mercury and the Kelvin electrode were electrically connected to the external electronic equipment by means of the tungsten seals,  $T_1 - T_2$ .

The inter-electrode distance could be finely controlled by pouring small amounts of mercury out of the hemispherical base into the side-arm containing the second iron slug,  $S_2$ .

The C.P.D. measurements were determined by the conventional Kelvin method of tapping the experimental tube to induce the reference electrode to vibrate relative to the surface under investigation.

#### Results obtained from the Second Experimental Tube

Although the glass diaphragm successfully excluded the outgassed contaminants from the mercury pool, the results obtained from this more sophisticated tube displayed the same random fluctuations as

were obtained from the first tube. In common with the previous tube the large variation in C.P.D., as a function of time, appeared to be independent of the temperature of the electrode. The lack of reproducibility almost certainly represents the influence of impurity films on the surface of the mercury.

The possibility that the mercury was reacting with the glass equipment can not be dismissed. Borosilicate-type glasses are known to react with a wide range of metals (110). Hence, the mercury was probably leaching impurities out of the glass tube, which because of the high specific gravity of mercury (i.e. 13.6) would form a thin contaminating layer on top of the metal.

Because of the apparent inertness of boro-silicate type glasses, it is often considered to have no effect on the experiments carried out within. However, glass is known to act as a source of contamination (147, 148). It was therefore concluded that glass is an unsuitable constructional material for investigating the surface characteristics of liquid mercury.

It was therefore decided to abandon the liquid mercury in glass equipment determinations and concentrate on the surface nature of solid mercury films.

It was hoped that by employing liquid nitrogen temperature techniques to "freeze" the impurity layers and subsequently submerge them below condensed films of evaporated mercury.

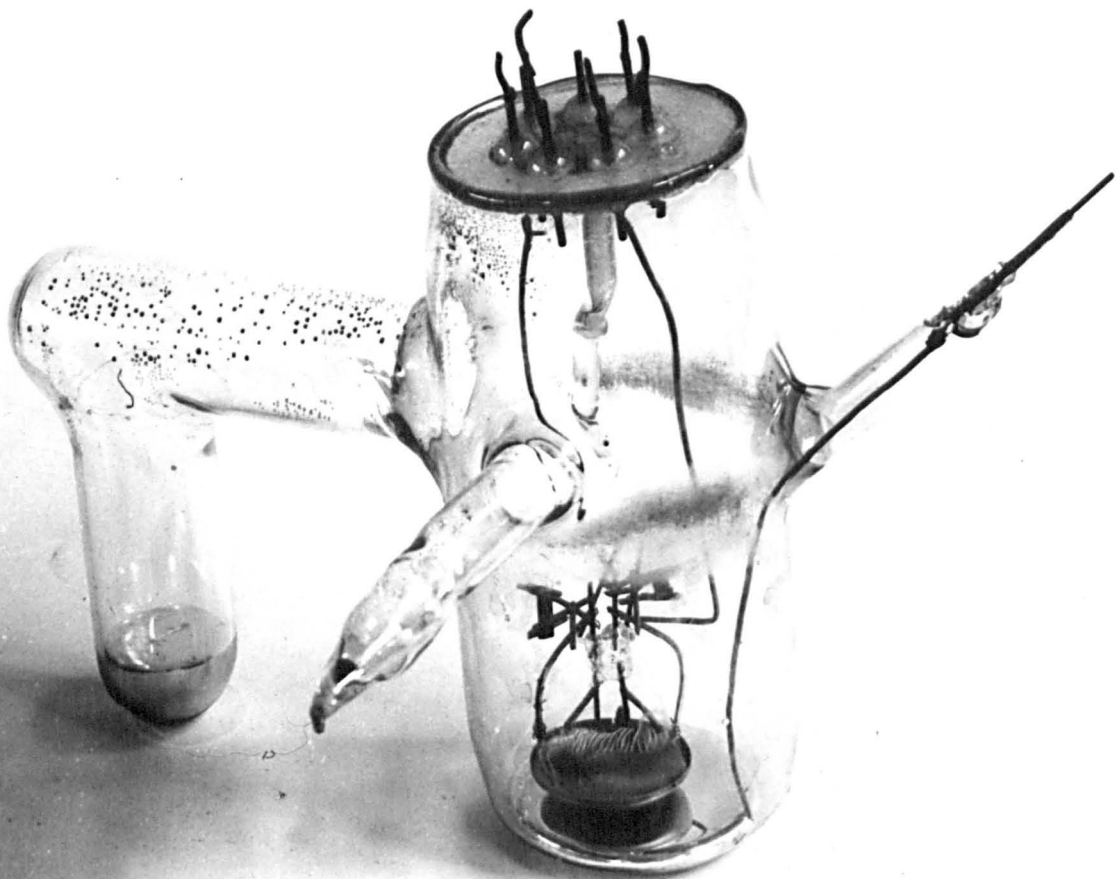


Figure 46.

### 5.3 Contact Potential Difference Measurements on Solid Mercury Surfaces

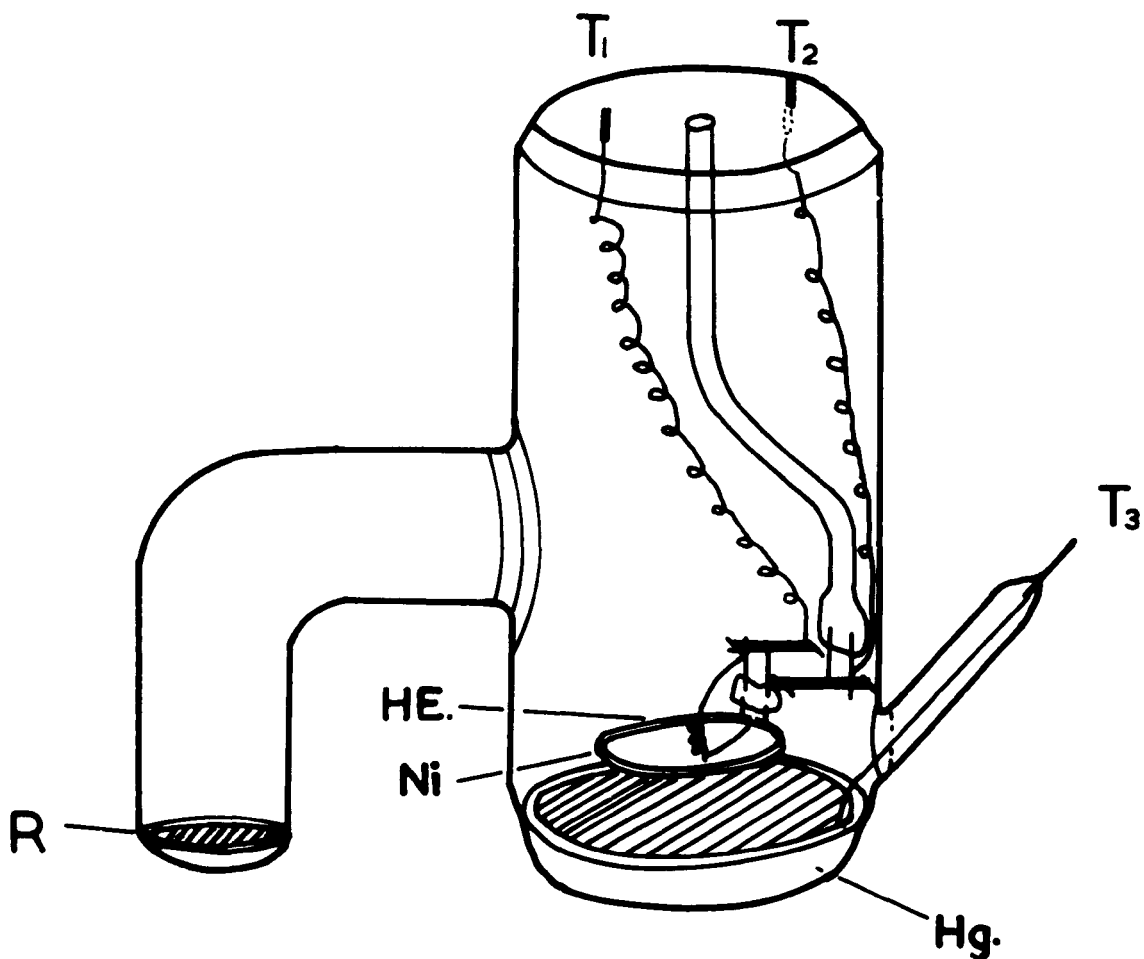
At the boiling point of nitrogen ( $-196^{\circ}\text{C}$  at atmospheric pressure) the vapour pressure of mercury is below  $10^{-15}$  torr (see appendix III). Hence, considering that the duration of the C.P.D. measurement periods rarely exceeded one day, the effect of the vapour on the surfaces under investigation could be ignored.

The investigation of the surface characteristics of solid mercury developed in three stages. The first consisted of investigating the variation in C.P.D. between a solid mercury surface and a hot nickel Kelvin electrode. The second phase of the enquiry measured the C.P.D. between a hot nickel reference electrode and a clean mercury film, evaporated onto a solid mercury substrate (cooled to liquid nitrogen temperatures). The final phase determined the work function of evaporated mercury films deposited at liquid nitrogen temperatures, using freshly evaporated nickel films as the reference surfaces.

Nickel was selected as the reference surface because its effective evaporating temperature is considerably lower than that of molybdenum (112).

#### 5.3.1 Tube 3

The third experimental tube was designed and constructed for the investigation of C.P.D. changes between a polycrystalline nickel reference electrode and solid mercury surfaces. The dimensions of the tube were approximately the same as those for the preceding tubes,



Ni. NICKEL ELECTRODE.  
 Hg. MERCURY ELECTRODE.  
 R. RESERVOIR.  
 HE. HEATING ELEMENT.  
 $T_1-T_3$  TUNGSTEN SEALS.

Figure 47.

being about 15cm long and having a diameter of 6cms (a photograph of the tube is shown in Figure (46)).

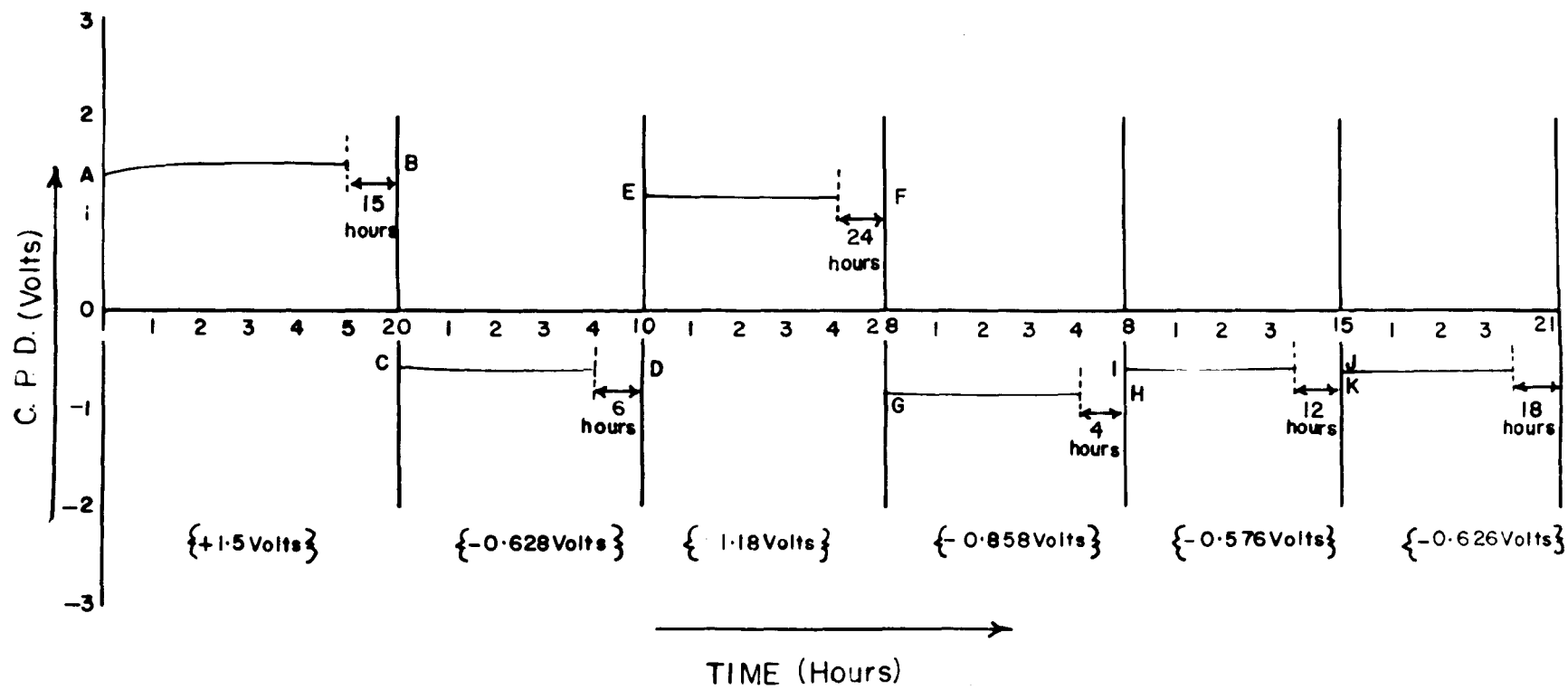
A small permanent magnet was used to deflect the Kelvin electrode from its equilibrium position. The magnetic method of inducing the reference electrode to vibrate (unlike the conventional tapping process) had the advantage of not disturbing the rest of the experimental tube.

The nickel electrode, Ni, (see the line diagram, Figure 47)) was maintained at a temperature of approximately 300°C by means of a small heating element, HE, which was mounted behind the Kelvin electrode. The tungsten mounting springs and seals, T<sub>1</sub> - T<sub>2</sub>, were employed to conduct the electric current through the helical filament. With this design it was hoped that the mercury vapour would preferentially condense on the mercury electrode, Hg, which was cooled to the temperature of liquid nitrogen. In common with the preceding tubes the inter-electrode distance was regulated by pouring mercury into a side-arm reservoir, R.

The nickel electrode was initially cleaned in a dilute solution of nitric acid to etch off the contaminated outer layers. Before assembly the Kelvin electrode was washed in distilled water, acetone and finally ether. To remove adsorbed oxygen and oxide films, the nickel surface was reduced by flushing the experimental tube with hydrogen followed by eddy-current heating to a dull-red heat.

To reduce the partial pressure of the mercury vapour, the mercury end of the experimental tube and the side-arm reservoir, were immersed

Figure 48.



in liquid nitrogen for several days, so that all the mercury vapour condensed on to the solid mercury surfaces. The process was assisted by warming the remainder of the tube with electric heating tapes.

Great difficulties were encountered as the mercury was cooled below its melting point. The solid mercury was found to adhere strongly to the inner walls of the glass envelope (several workers (114, 115) have reported that pure mercury wets degassed glass).

The adhesion of the solid mercury to the glass in conjunction with its high coefficient of expansion ( $41 \times 10^{-6}$  compared with about  $6 \times 10^{-6}$  for borosilicate type glasses) caused the experimental tubes to crack. The cracking was eliminated by the following procedure:-

- a) Making the mercury electrodes much thinner and therefore physically weaker than the glass envelopes.
- b) Removing existing strains in the glassware by thorough annealing.
- c) Gradually warming and cooling the mercury through the phase changes and therefore reducing the magnitude of the strains.

#### Results from the Third Experimental Tube

The C.P.D. readings obtained from this experimental tube are shown in Figure (48), plotted as a function of time after solidification. It can be seen that once the mercury in the tube had been frozen, the C.P.D. was static to within narrow limits, for periods as long as 50 hours, but when the mercury was allowed to liquify and was then resolidified the C.P.D. always changed to a new value (which itself remained constant as a function of time).

Consider the C.P.D. reading of A (see the Figure); over a period of 20 hours it varied by only a small amount, remaining at +1.5 volts. At B the mercury was melted and resolidified; the new C.P.D. reading at C was -0.63 volts - i.e., it had even changed polarity from B to C. From over 30 of these complete cycles three effects were observed:-

- 1) The C.P.D. readings were static (to within a few millivolts) as long as the mercury remained solid.
- 2) The C.P.D. always changed if the mercury was allowed to melt and was resolidified.
- 3) The C.P.D. readings had values between +2 and -2 volts (i.e., a variation of 4 volts).

The C.P.D. changes observed when the mercury was resolidified could be explained by either a variation in the surface characteristics of the standard electrode, or a change in the mercury surface.

The possibility that the standard electrode was changing by adsorbing mercury vapour was eliminated by keeping the mercury electrode solid, while the mercury in the reservoir, R, was melted for a few minutes. There was no change in the measured C.P.D., and so it could be concluded that for the short periods of time that the mercury electrode was melted (approximately five minutes), the surface of the standard electrode did not change.

These results indicate that it was the surface of the mercury electrode which was changing. This could be because:



Figure 49.

A) The phase changes caused the internal structure of the mercury to change and therefore the characteristics of the surfaces (crystal orientation, roughness coefficients etc) varied.

B) The surface was changed by impurities floating on the mercury.

The work function values of metals do not differ from one crystal plane to another by more than a 2 volt margin (59, 60, 61, 62). Hence, considering that the measured C.P.D. readings had a variation of 4 volts, it seems likely that impurity layers were responsible for the observed effects.

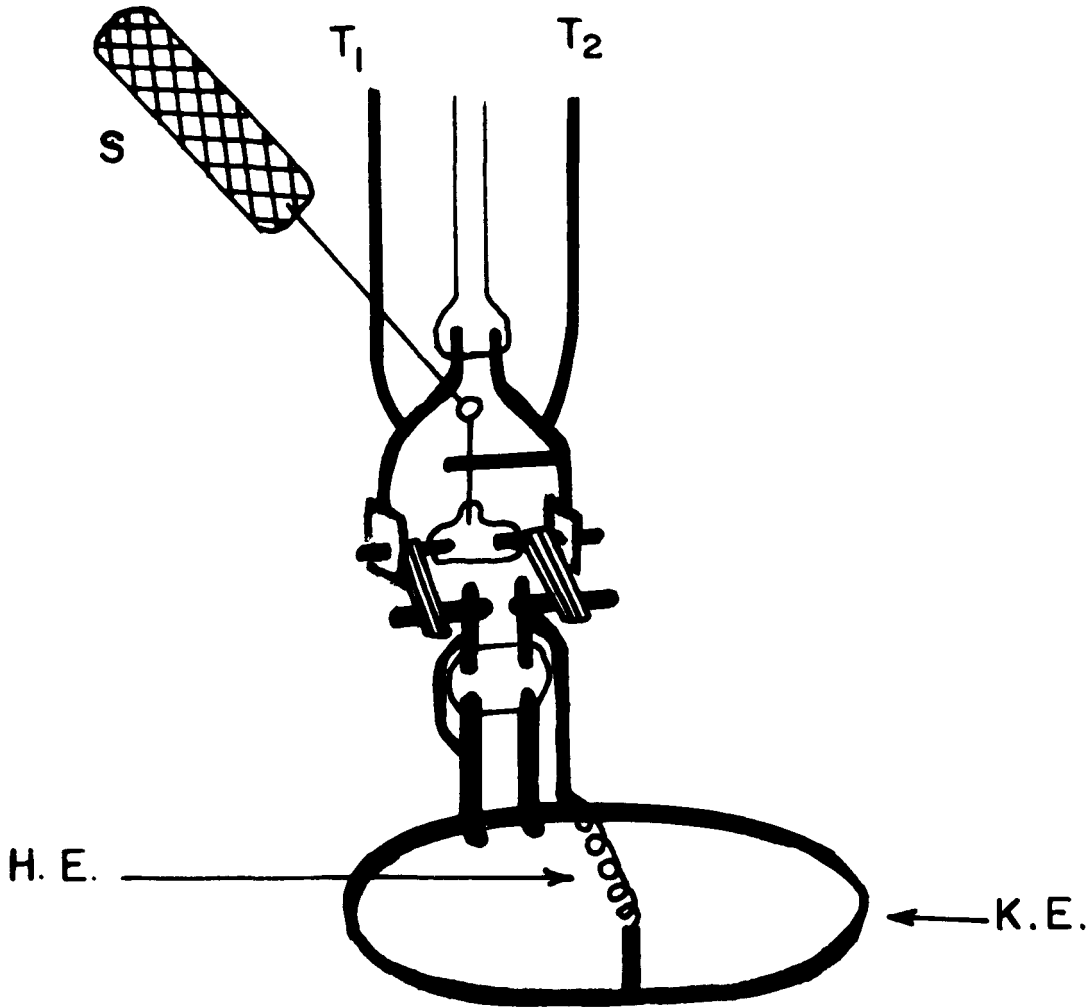
The impurity layers would not be capable of movement once the mercury had been solidified, and hence the C.P.D. measurements would be static.

The impurity-film hypothesis will account for the C.P.D. fluctuations obtained from tubes 1 and 2. The thin contaminating films were almost certainly moving around on the surface of the liquid mercury.

It was decided at this stage to investigate the characteristics of clean evaporated mercury surfaces, using solid mercury films, at liquid nitrogen temperatures, as the substrates. It was thus hoped that the mercury condensed on the solid mercury electrodes would bury the frozen impurity layers.

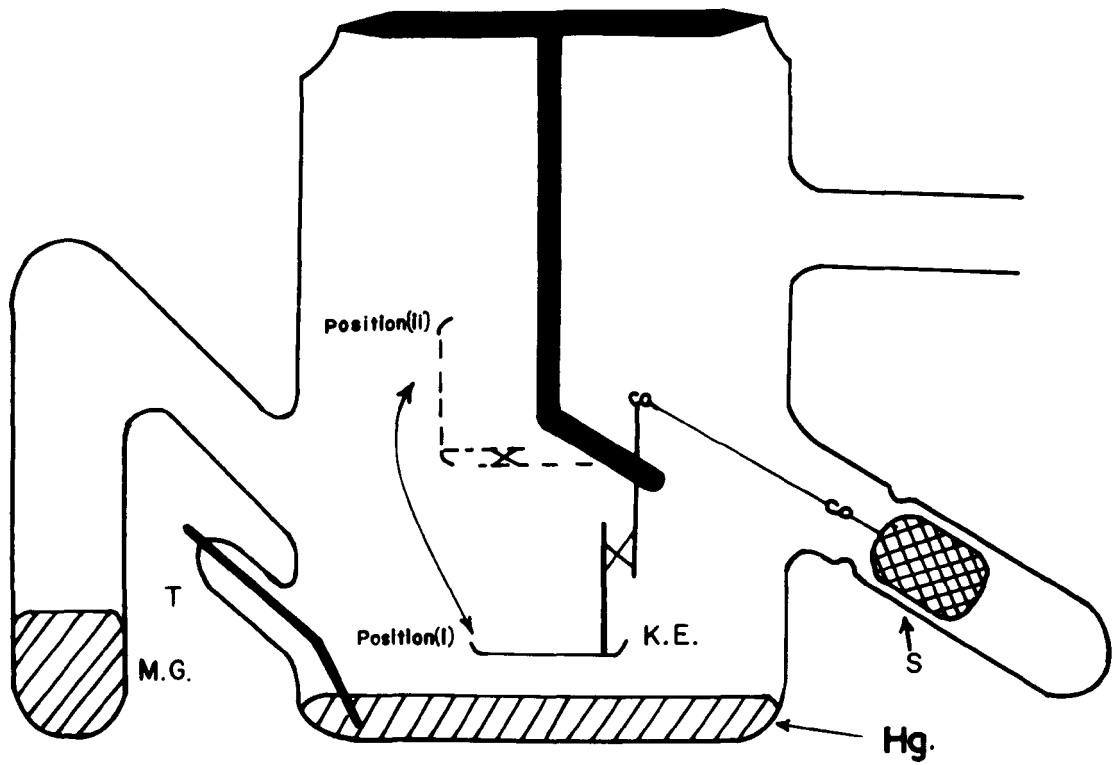
#### 5.3.2 Tube 4

The fourth experimental tube (a photograph of which is shown in Figure (49)) was developed for the investigation of the surface



K.E.    KELVIN    ELECTRODE.  
 H.E.    HEATING    ELEMENT.  
 S.      IRON      SLUG.  
 $T_1-T_2$     TUNGSTEN    LEADS.

Figure 50.



K.E. KELVIN ELECTRODE.  
 Hg. MERCURY ELECTRODE.  
 M.G. MERCURY GUN.  
 S. IRON SLUG.  
 T. TUNGSTEN SEAL.

Figure 51.

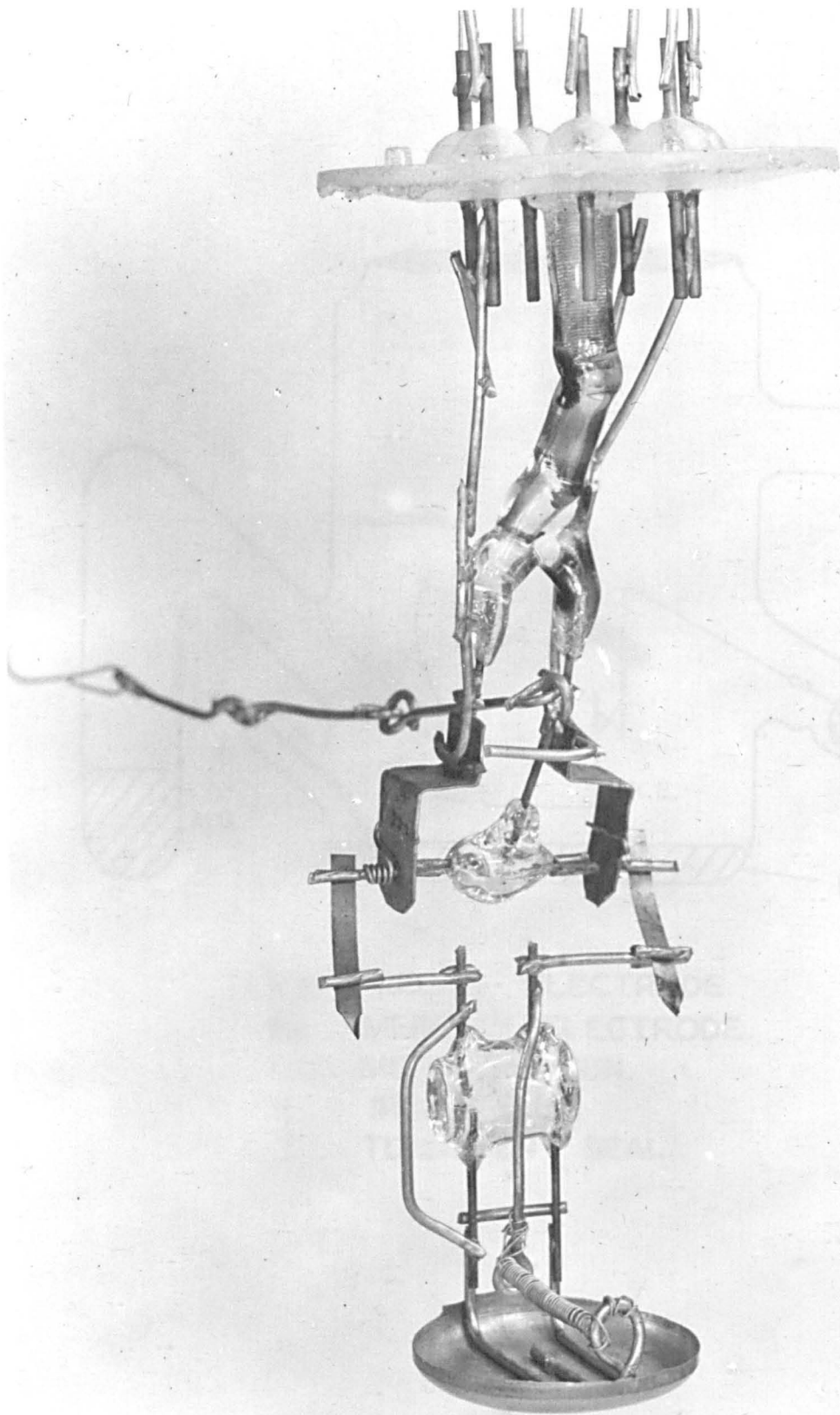


Figure 52.

characteristics of evaporated mercury films deposited at the temperature of liquid nitrogen onto solid mercury substrates.

In common with the previous tube the Kelvin electrode was constructed out of 0.007" polycrystalline nickel sheet, fitted with a helical heating element H.E. (see the schematic representation of the Kelvin assembly, figure (50)).

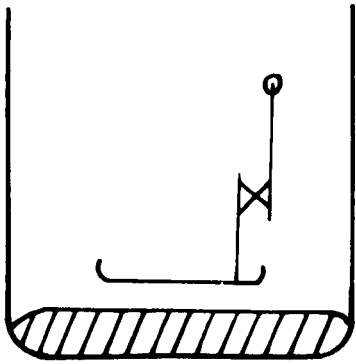
The Kelvin electrode, K.E. (see Figure (51)) could be lifted from position (i) to position (ii) by means of the magnetic slug, S, thus leaving the mercury electrode unobstructed.

It can be seen from the photograph of the Kelvin assembly, Figure (52), that the two current carrying leads feeding the heating element were separated throughout the pivoted vibrating system by glass insulators: this was difficult to construct but proved to be effective.

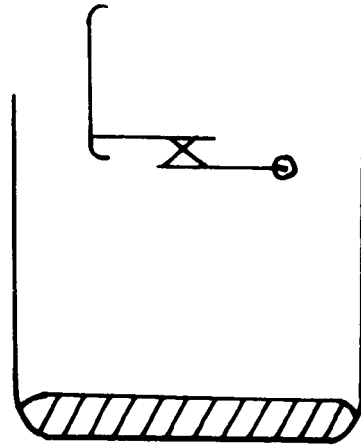
The heating element was continuously maintained at a dull-red heat, except for the short periods during which the C.P.D. measurements were taken (approximately one minute). The procedure was necessary because the large electrostatic and magnetic fields, produced by the heating current, completely distorted the signals.

#### Results from the Fourth Experimental Tube

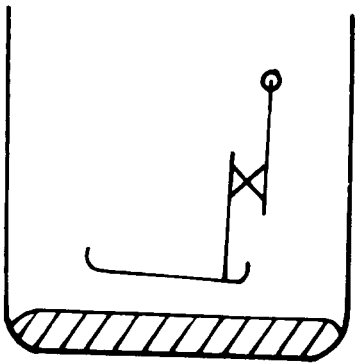
The experimental tube was used initially to confirm the findings obtained from the previous tube (tube 3) - i.e., the work function of solid mercury changes when it undergoes a cycle of phase changes.



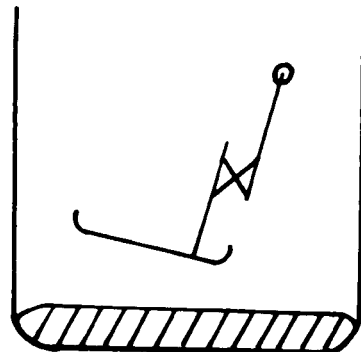
Position (i)



Position (ii)



Position(iii)



Position (iv)

Figure 53.

The C.P.D. readings obtained from this tube when the mercury electrode was melted and resolidified displayed the same general characteristics as illustrated in Figure (48).

With this more sophisticated tube it was possible to investigate the variation in work function as the Kelvin electrode was moved along the frozen mercury surface. At this stage the mercury gun, M.G.<sub>1</sub>, was maintained at the temperature of liquid nitrogen: thus exposing the floating impurity layers.

As long as the Kelvin electrode was kept vibrating around a fixed mean position, e.g., position (i), (see Figure (53)) the C.P.D. measurements were constant as a function of time. However, it was noticed that when the Kelvin assembly was moved by means of the magnetic slug to a new centre of vibration, e.g., position (iii), the C.P.D. changed. The only change in the system was in the position of the Kelvin electrode relative to the mercury surface. Hence, it can be concluded that the solid mercury electrode had a work function which varied as a function of distance along its surface.

No detectable trend was observed when the C.P.D. readings were plotted as a function of position, e.g., a typical set of measurements were:

Position (i) - 0.7 volts

Position (iv) - 2.1 volts

Position (iii) - 1.2 volts

These C.P.D. readings add further weight to the contaminating impurity-layer hypothesis.

CHANGE IN C.P.D. WITH TIME.

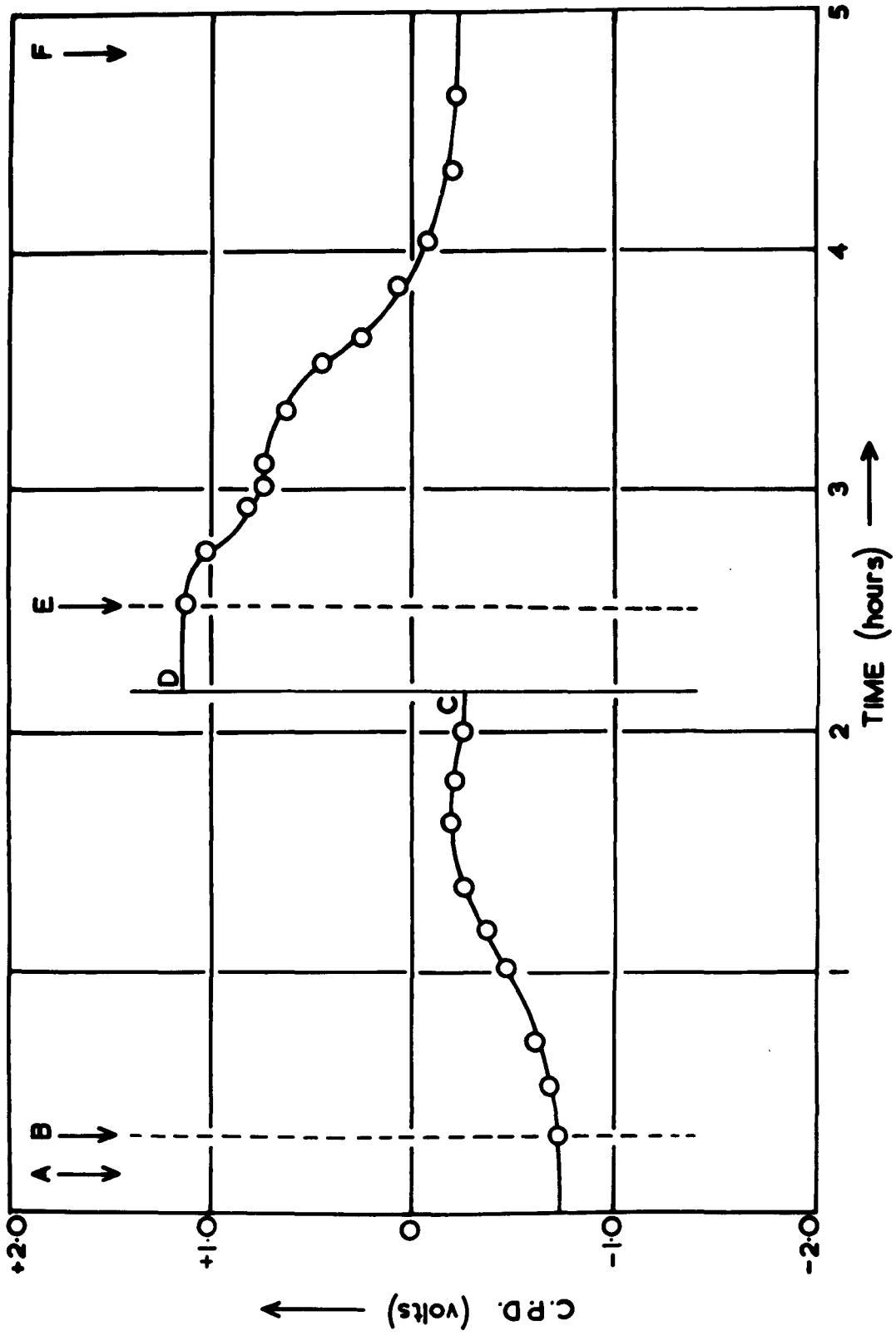


Figure 54.

To prepare reproducible clean mercury surfaces, it was decided to condense an evaporated beam of mercury vapour on top of the frozen contaminating films. This was achieved by lifting the Kelvin assembly from its measuring position (position (i)), by means of the magnetic slug, to a higher position (i.e., position (ii)) so as to leave the mercury substrate unobstructed.

When the Kelvin electrode was clear of the solid mercury surface, the mercury in the mercury gun, M.G., was allowed to melt and reach room temperature. At room temperature the vapour pressure of mercury is approximately  $10^{-3}$  torr and so over a period of several hours the surface of the frozen mercury electrode was covered with a thick layer of evaporated mercury. The thickness of the condensed film could be estimated by observing the opaque layer of condensed mercury deposited onto the walls of the experimental tube in the vicinity of the solid electrode. The films of evaporated mercury, because of their random nature were reproducible.

The change in C.P.D. plotted as a function of time as the solid mercury electrodes were covered with condensed films of mercury can be seen in the graph (Figure (54)).

The initial C.P.D. between the contaminated mercury electrode and the Kelvin surface was constant as a function of time at  $-0.72$  volts (region A). At the point B the Kelvin assembly was magnetically removed from the measuring position and the mercury in the mercury gun was allowed to melt. It can be seen that as the condensed mercury film

increased in thickness the C.P.D. approached a value of -0.26 volts (region C), which changed neither as a function of film thickness nor position along the surface of the condensed film. It was also observed that the C.P.D. between the Kelvin electrode and the condensed film did not change significantly as a function of time.

When the condensed film and frozen substrate were melted and resolidified the C.P.D. changed by +1.4 volts, i.e., to +1.14 volts (point D). While the mercury in the main experimental tube underwent the phase change cycle, the mercury gun was cooled to  $-196^{\circ}\text{C}$ . Hence, the solid mercury substrate was not covered by a clean evaporated mercury film. The reading at D (+1.14 volts) represents the C.P.D. between the polycrystalline nickel reference electrode and the mercury surface contaminated with impurity layers.

At the point E the Kelvin electrode was raised from its measuring position and the mercury gun was slowly warmed to room temperature. It can be seen from the graph that as the mercury vapour condensed onto the mercury substrate the C.P.D. approached a value of -0.23 volts (region F).

The results obtained from over 20 of these phase changes followed by mercury evaporation may be summarized thus:

- 1) The C.P.D. measurements obtained from the contaminated mercury substrates displayed the erratic behaviour as was observed in the previous tube (tube 3).

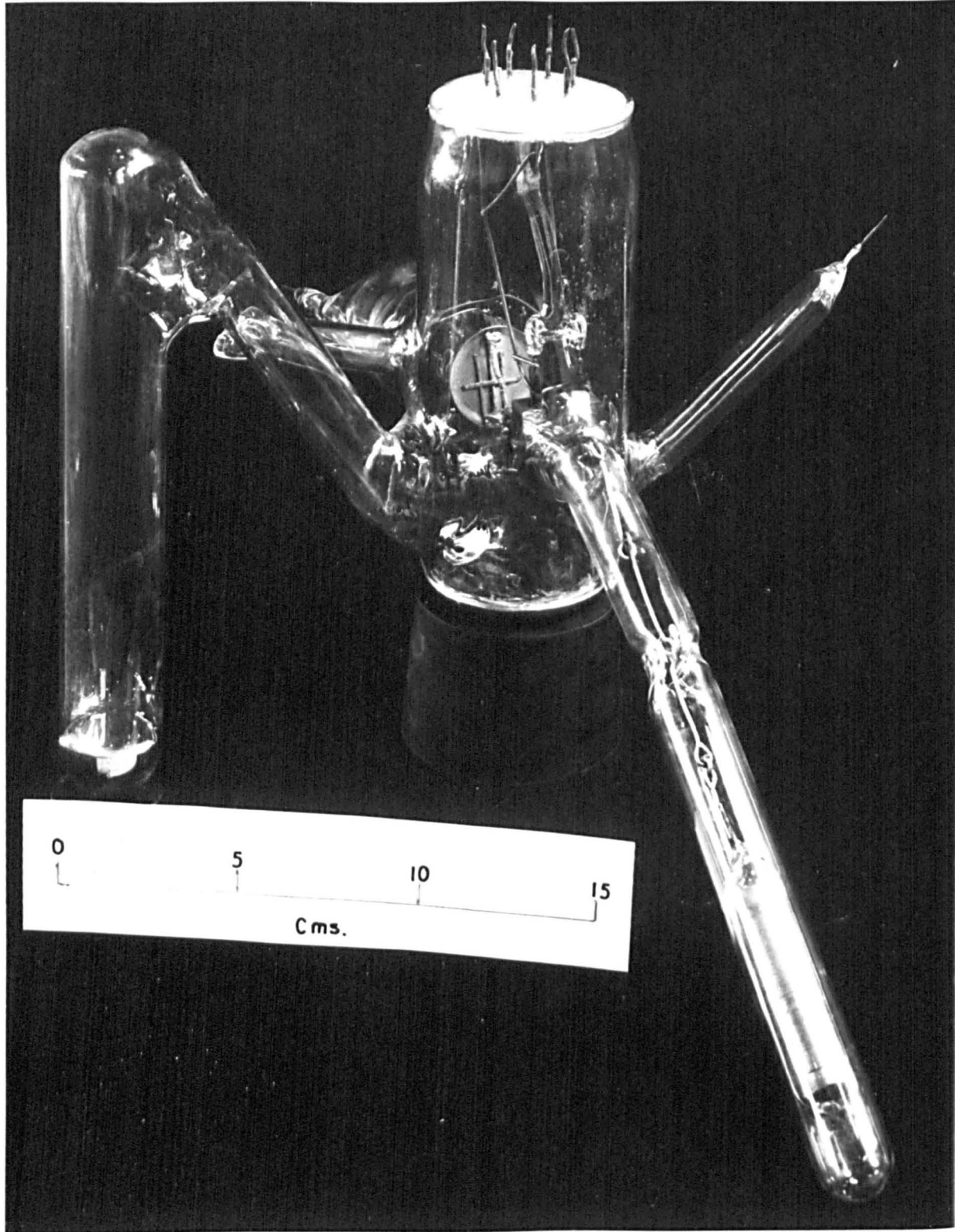


Figure 55.

2) Whenever a clean mercury film was deposited on top of the contaminated substrates, the C.P.D. readings always approached a value of  $-0.24 \pm 0.03$  volts.

It would appear, therefore, that a means had been devised for determining accurately the C.P.D. between mercury films and a reference surface.

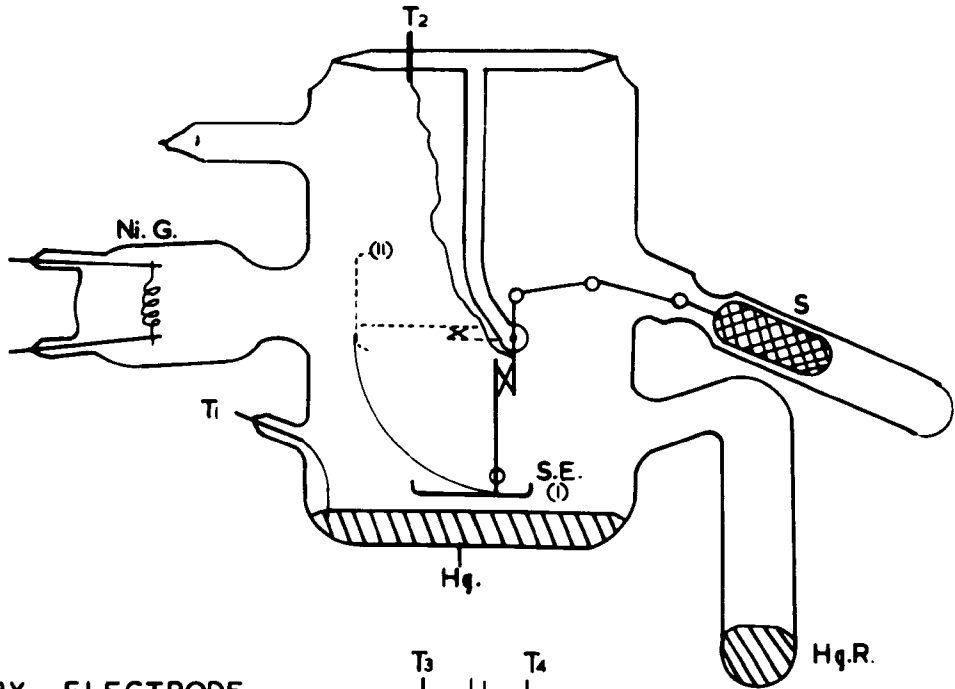
In this tube the reference electrode was constructed out of polycrystalline nickel sheet, the work function of which was unfortunately not known. It was therefore decided to construct a new experimental tube, which would have incorporated in its design a method of producing reference surfaces of known work function.

5.3.3

### Tube 5

A photograph of the fifth and final glass experimental tube constructed to investigate mercury-vacuum interfaces is shown in Figure (55). The tube was developed to measure the C.P.D. between evaporated nickel reference surfaces and condensed mercury films (deposited at the temperature of liquid nitrogen). Therefore, considering that the work function of evaporated nickel films is known accurately (94) the experimental tube enabled the work function of solid mercury to be determined.

In common with the previous tube an electrically heated pivoted standard electrode, S.E., (see the schematic representation, Figure (56)) was mounted just above the mercury electrode, Hg.



- |                                 |          |           |
|---------------------------------|----------|-----------|
| Hg.                             | MERCURY  | ELECTRODE |
| S.E.                            | STANDARD | ELECTRODE |
| Ni.G.                           | NICKEL   | GUN       |
| Hg.R.                           | MERCURY  | RESERVOIR |
| S.                              | MAGNETIC | SLUG      |
| H.E.                            | HEATING  | ELEMENT   |
| T <sub>1</sub> - T <sub>4</sub> | TUNGSTEN | SEALS     |

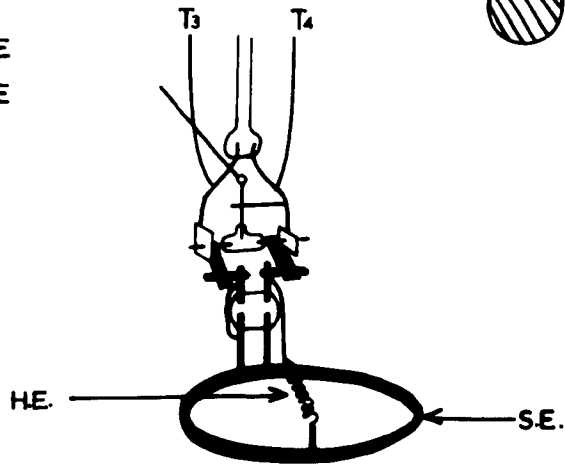


Figure 56.

The Kelvin assembly (see the perspective inset) would be magnetically moved, from the measuring position (position (i)) to a point opposite the nickel gun, Ni.G. (i.e., position (ii)).

For ease of manipulation, as many of the components of the tube as possible were placed in side-arms, e.g., the magnetic slug, S. This system had the added advantage of permitting faulty components to be replaced without dismantling the rest of the experimental tube.

The first stage in the preparation of the clean mercury films consisted of cooling the mercury electrode, Hg, and the mercury reservoir, Hg.R., to the temperature of liquid nitrogen (by immersing the bottom parts of the experimental tube in a Dewar flask containing liquid nitrogen). This effectively reduced the vapour pressure of the mercury to zero.

When all the mercury had condensed, either onto the mercury electrode, or the reservoir (this usually took several days), the Kelvin assembly was magnetically raised from position (i) to position (ii). Hence, the surface of the mercury substrate was unobstructed and ready to receive the evaporated mercury beam.

At this stage the mercury side-arm reservoir was slowly warmed to room temperatures thus evaporating a thick layer of condensed mercury onto the solid mercury substrate.

After a clean mercury surface had been deposited, the reservoir was re-cooled to the temperature of liquid nitrogen and so the vapour pressure of mercury in the experimental tube was again at an extremely low level.

CHANGE IN C.P.D. WITH TIME.

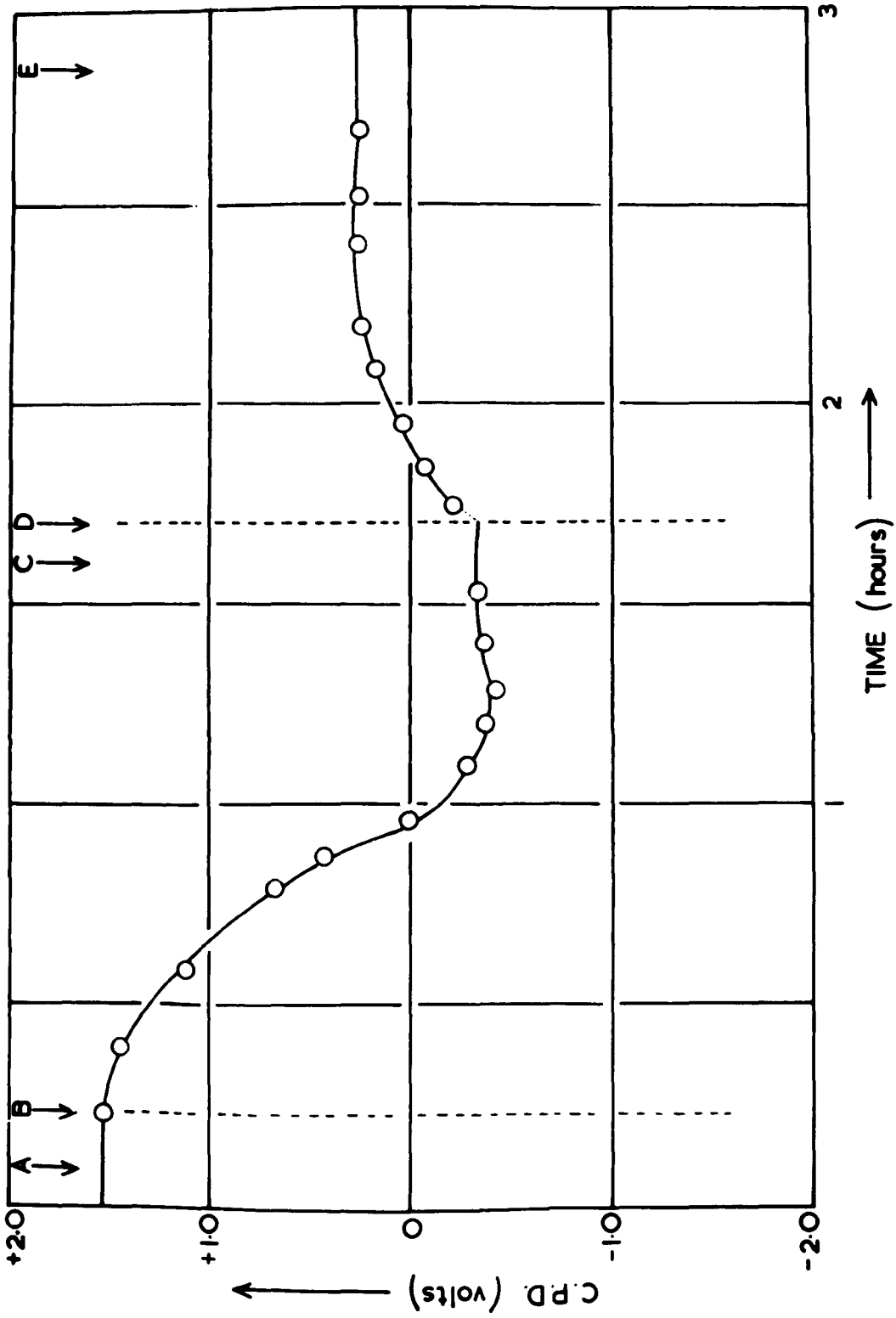


Figure 57.

The clean reference surface was produced by condensing a beam of evaporated nickel (from the nickel gun, Ni.G.) onto the polycrystalline nickel substrate. At a high temperature (i.e., approximately 1,400°C) nickel and tungsten combine to form an alloy. However, if the proportion by weight of nickel to tungsten on a filament of the latter is kept below 30%, the nickel will evaporate at its melting point in preference to alloying (142). The construction of nickel evaporators in the form of coiled coils on 27 s.w.g. tungsten wire fulfilled this condition.

The final stage of the experimental procedure used to determine the work function of solid mercury consisted of lowering the Kelvin assembly from the evaporation position to its measuring position (i.e., position (i)).

#### Results from the Fifth Experimental Tube

Before being employed in the determination of the work function of mercury, this tube was used to investigate the surface nature of contaminated solid mercury (i.e., without a freshly evaporated layer of mercury). In common with the two previous experimental tubes, the work function of frozen mercury films was found to change:-

- A) After a cycle of phase changes.
- B) As a function of position on the surface.

A typical set of C.P.D. readings, plotted as a function of time, obtained from this experimental tube, are shown in Figure (57).

The initial reading of +1.54 volts - i.e., region A, represented the C.P.D. between the Kelvin electrode (of unknown work function) and the contaminated mercury,

At B the Kelvin assembly was magnetically raised to position (ii) - leaving the mercury electrode unobstructed. The mercury in the reservoir was then melted and warmed to room temperature, thus enabling the mercury substrate to be covered with a condensed film of mercury. It can be seen that, over a period of 1 $\frac{1}{4}$  hours, the C.P.D. changed from + 1.54 volts and approached a steady value of - 0.34 volts (region C). At this stage the mercury in the side-arm was resolidified and cooled to -196°C.

The readings measured in region C represented the C.P.D. between the reference surface and the clean condensed mercury film, deposited at - 196°C, onto the contaminated mercury substrate.

At D the Kelvin assembly was moved from its measuring position to position (ii) - i.e., opposite the nickel gun. At this stage a beam of evaporated nickel was condensed onto the reference electrode. It can be seen, from the graph, that as the thickness of the condensed film increased, the C.P.D. approached a value of + 0.29  $\pm$  0.05 volts (region E).

The figure of + 0.29  $\pm$  0.05 volts represented the C.P.D. between an evaporated mercury film (condensed at - 196°C, onto a mercury substrate) and an evaporated nickel film (deposited onto a polycrystalline nickel substrate).

The  $\pm 0.05$  volts error represents the total deviation for ten different experiments, each of which involved many repeated evaporations to determine the degree of consistency as a function of thickness.

Assuming Riviere's (94) value of 4.74eV for the work function of nickel, the work function of evaporated mercury at a temperature of  $-196^{\circ}\text{C}$  is therefore 4.45eV.

The most outstanding feature of the C.P.D. readings, obtained from any one experiment was the constancy as a function of time. It was difficult (owing to the nature of the method) to reduce the interval between the end of evaporation and the first reading to less than a minute. After the first measurement the potentiometer setting did not have to be readjusted for several days.

This extremely low level of contamination can probably be ascribed to the getter-action of the mercury beams condensed at the temperature of liquid nitrogen (many sticking coefficients increase with decreasing temperature (139, 140)).

#### 5.4 Conclusions

All the experiments described in this chapter have been directed towards determining the work function of mercury.

The presence of thin impurity layers floating on the liquid mercury (i.e., in the first two experimental tubes) prohibited the measurement of the work function of mercury at room temperature.

Using evaporation techniques at the temperature of liquid nitrogen (i.e., in the last two tubes) the contaminating films were

successfully frozen and submerged beneath films of mercury.

The work function value, obtained from the fifth experimental tube is slightly lower than the determinations reported by other workers (99, 100, 101).

This difference may represent a difference in the surface characteristics of the reference electrode. Rivière condensed the nickel films onto glass substrates, while in this investigation the substrates were constructed out of polycrystalline nickel. The difference may also be due to the notorious difficulty in outgassing nickel completely.

Several workers (113) have reported that annealing can change the work function of a surface by as much as a tenth of a volt. Therefore, considering that the mercury films were deposited at liquid nitrogen temperatures, it seems likely that they would have contained many imperfections and had high roughness factors. It would therefore seem probable that the slight disagreement represents the degree of annealing of the mercury films.

The solid mercury techniques can only be used to measure work functions at the temperature of liquid nitrogen. To extend the study to liquid mercury it was considered necessary to examine the thin partition method mentioned earlier.

## CHAPTER VI

### THE GLASS PARTITION METHOD:

#### RESULTS AND DISCUSSION

##### 6.1 Introduction

Although the low temperature techniques, which were reviewed in the previous chapter, proved successful in the determination of the work function of solid mercury, it still remained necessary to measure the work function of liquid mercury.

Mercury at room temperature has a vapour pressure of approximately  $10^{-3}$  torr, which would contaminate a clean surface in about a millisecond. At this stage in the investigation it was decided to place the liquid mercury in a separate sealed glass container thus maintaining the Kelvin electrode free of mercury contamination.

It was hoped that the insulating glass partition (i.e., which separated the reference surface from the mercury vapour) would not change the C.P.D. between the two metal electrodes by a significant amount.

The assumption that the C.P.D. between two surfaces is equal to the difference of their work functions is only realized when the two Fermi levels are the same in equilibrium.

The amorphous structure of glass and the localized nature of its electrons renders it difficult to discuss the energy band scheme of the material. The physical meaning of Fermi levels in glass is therefore somewhat more abstract than that in the case of metals.

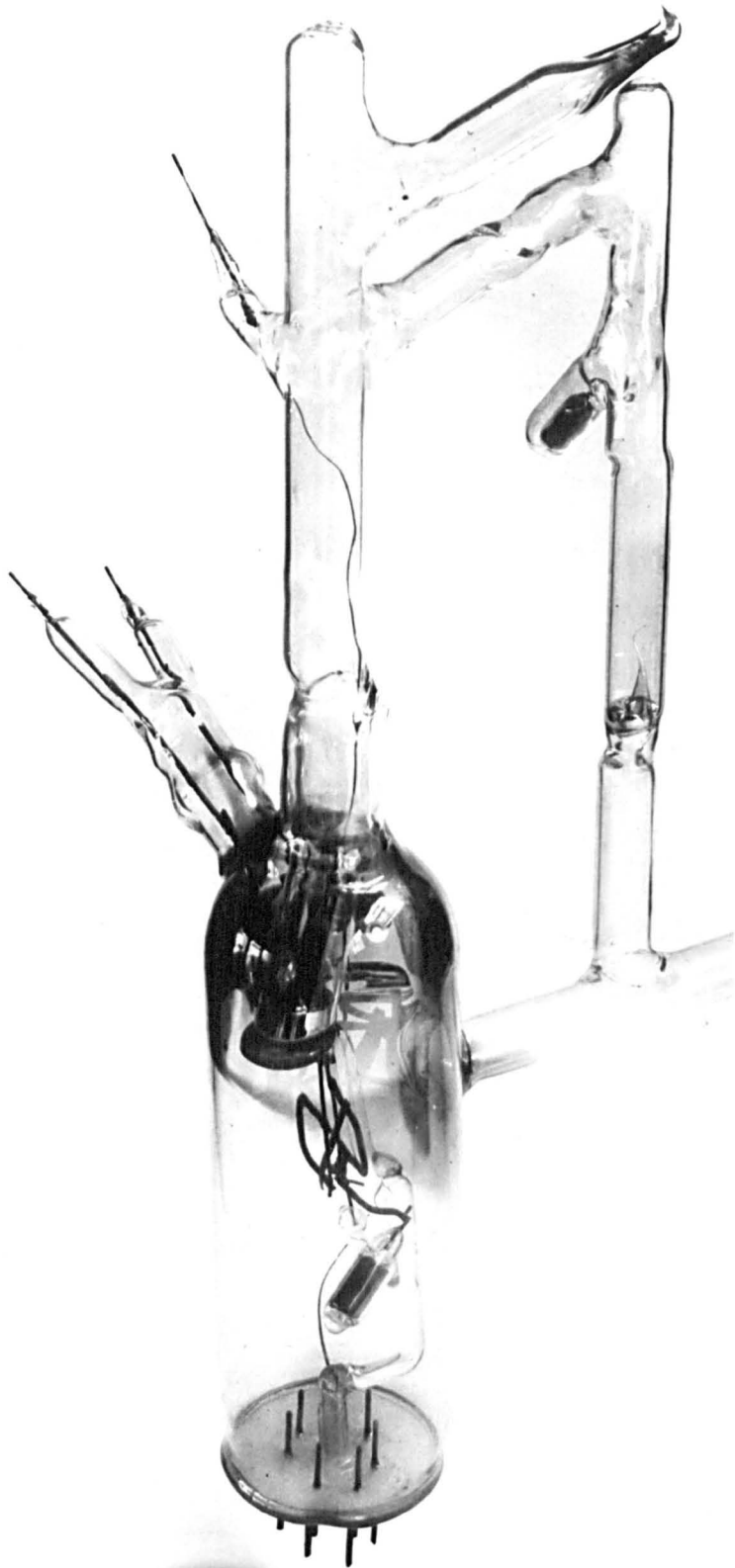


Figure 58.

It was therefore hoped that an insulating glass partition when placed between two metals would not deform their Fermi levels. The partitions were constructed out of 1 m.m. thick borosilicate glass sheets. Before assembly the partitions were rigorously cleaned by soaking in chromic acid and washing with distilled water, ethyl alcohol and acetone.

With the glass partition method it was possible to investigate the lower surfaces of the liquid mercury electrodes. Hence, the impurity layers (encountered in the earlier experimental tubes) floating on the top mercury surface, were clear of the mercury-glass interface.

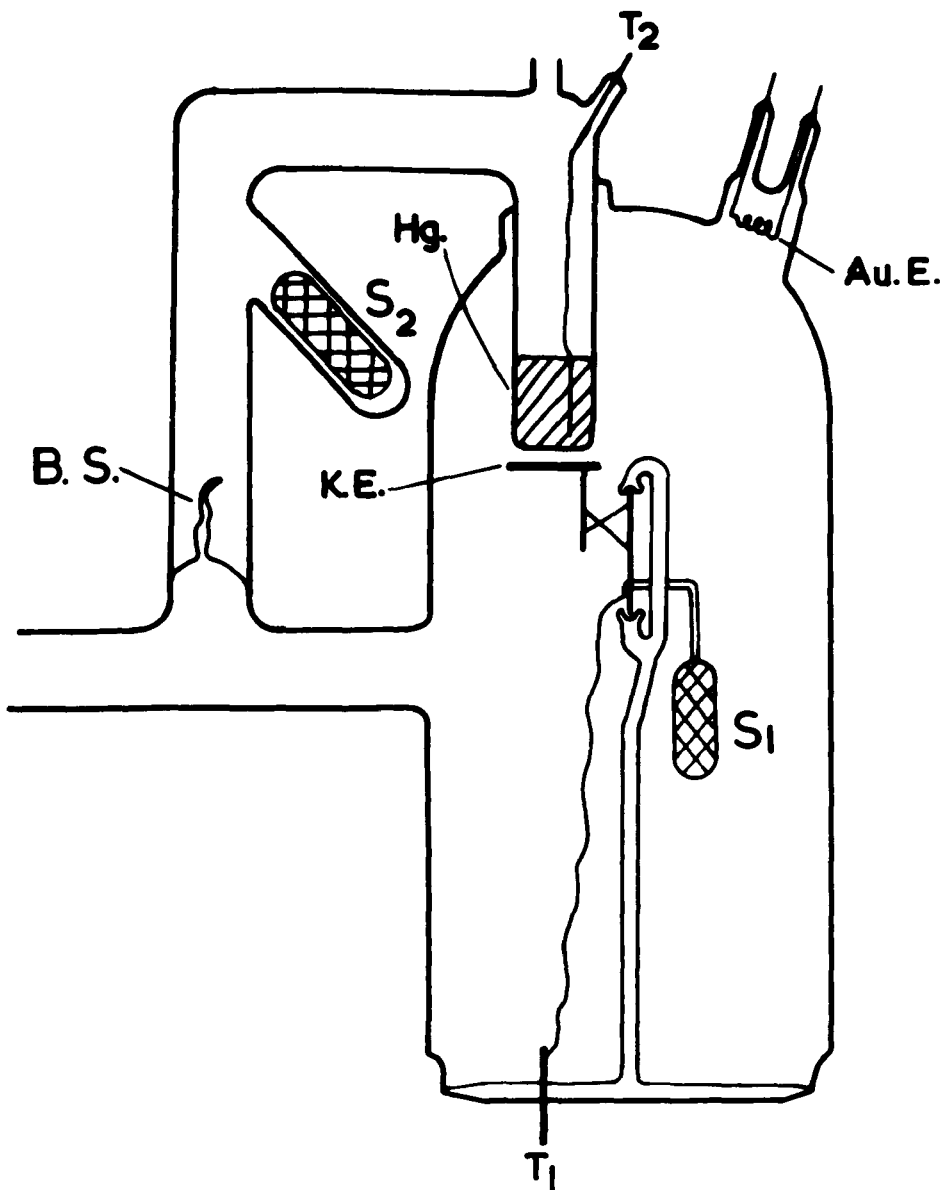
## 6.2 Preliminary Glass Partition Tube

The results obtained from this experimental tube are of interest only in so much as they provided information which resulted in the improvement of the experimental techniques, which were incorporated in subsequent apparatus.

The experimental tube (a photograph of which is shown in Figure (58) was designed to investigate the following phenomena:-

- (A) The effect of thin glass partitions on C.P.D. measurements.
- (B) The influence of mercury vapour on the reference surface.

The apparatus was essentially two separate vacuum systems with a 1m.m. thick glass partition between the two electrodes (see the line diagram, Figure (59)). The section of the experimental tube containing the Kelvin electrode, K.E., was maintained free of mercury vapour by means of liquid nitrogen traps.



K.E. KELVIN ELECTRODE.  
 Hg. MERCURY ELECTRODE.  
 Au.E. GOLD EVAPORATOR.  
 B.S. BREAKABLE SEAL.  
 S<sub>1</sub>-S<sub>2</sub> IRON SLUGS.  
 T<sub>1</sub>-T<sub>2</sub> TUNGSTEN SEALS.

Figure 59.

Considering that the reference surface was free of mercury vapour ( and hence of known work function), it was hoped that the C.P.D. between the mercury electrode, Hg, and the Kelvin electrode would enable the work function of liquid mercury to be calculated.

The Kelvin electrode consisted of a glass disc on to which a thin film of gold was condensed from the gold evaporator, Au.E. The Kelvin assembly was magnetically moved (by means of the iron slug, S<sub>1</sub>) to its measuring position - i.e., under the glass container, after a clean gold surface had been deposited onto the glass substrate.

The second iron slug, S<sub>2</sub>, was placed in a side-arm, so that it could be magnetically induced to smash the internal breakable seal, B.S. Hence, mercury vapour would diffuse from the mercury electrode into the mercury-free region of the experimental tube. It was thus hoped to observe the effect of mercury vapour on the work function of gold.

The C.P.D. produced when the reference surface was vibrated was fed from the electrodes to the external measuring equipment by means of the tungsten seals T<sub>1</sub> and T<sub>2</sub>.

### Results

The results obtained from this tube may be summarized thus:-

- (1) The C.P.D. readings were nearly always large - typically greater than 6 volts.
- (2) If any contact occurred between the glass partition and the vibrating electrode a change in the C.P.D. measurements was observed.

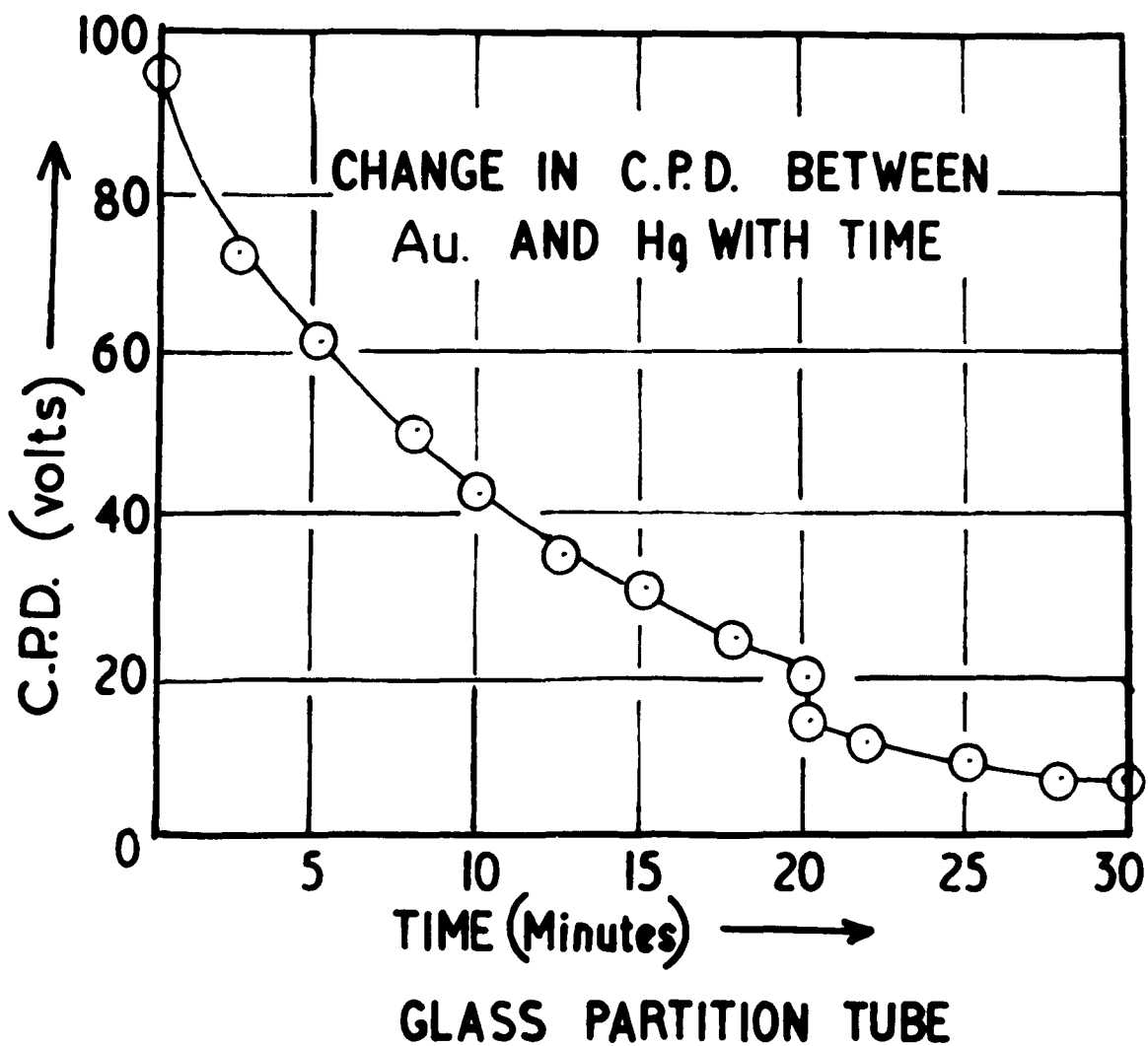


Figure 60.

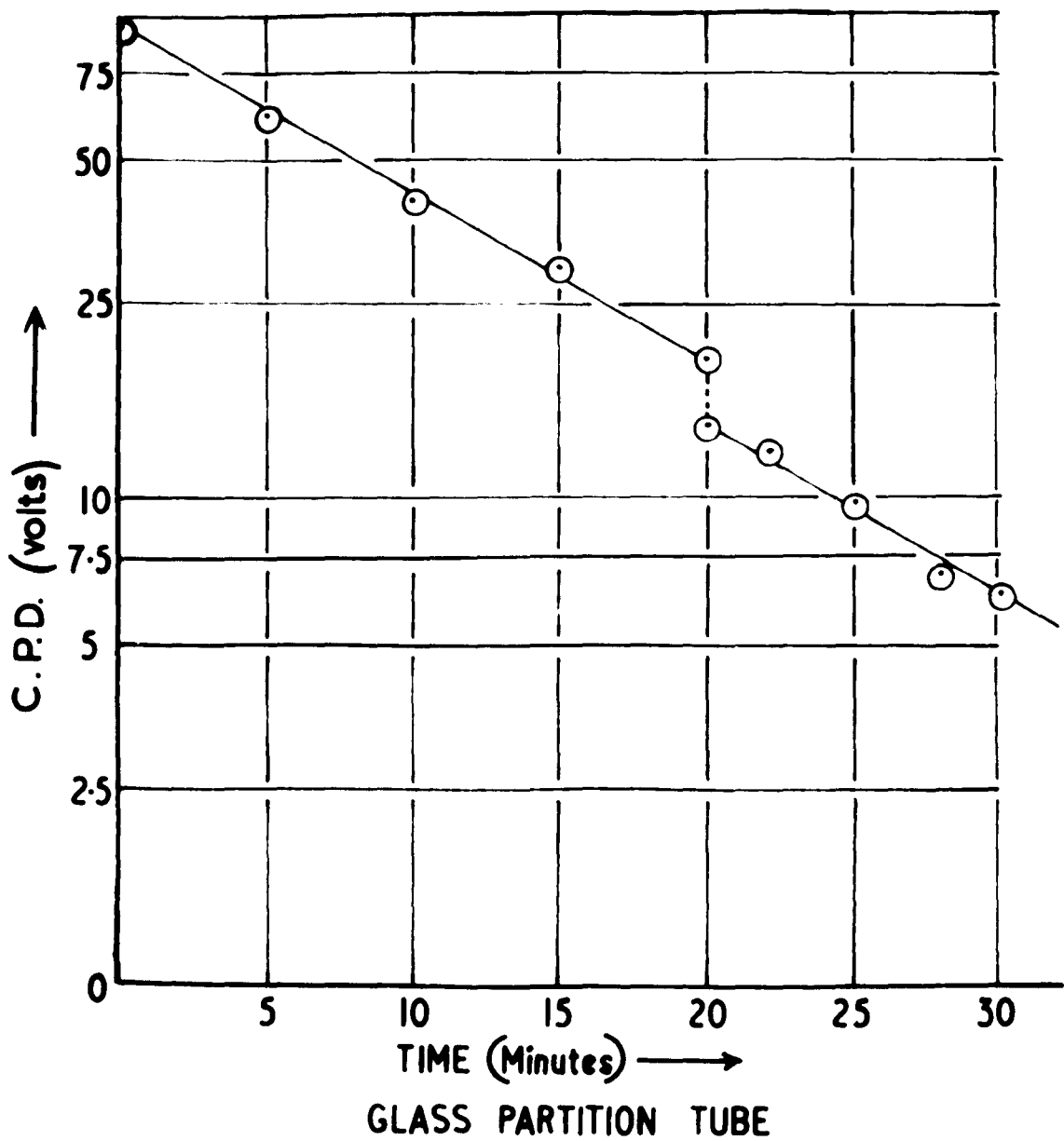


Figure 61.

- (3) After such a C.P.D. change the readings fell approximately exponentially as a function of time (as can be seen on the graph, Figure (60)).
- (4) If any further contact occurred during these decays, a sudden change in the C.P.D. resulted, as can be seen on the graph, after a period of 20 minutes.

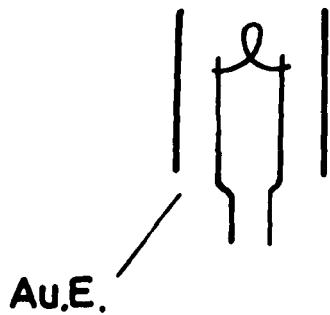
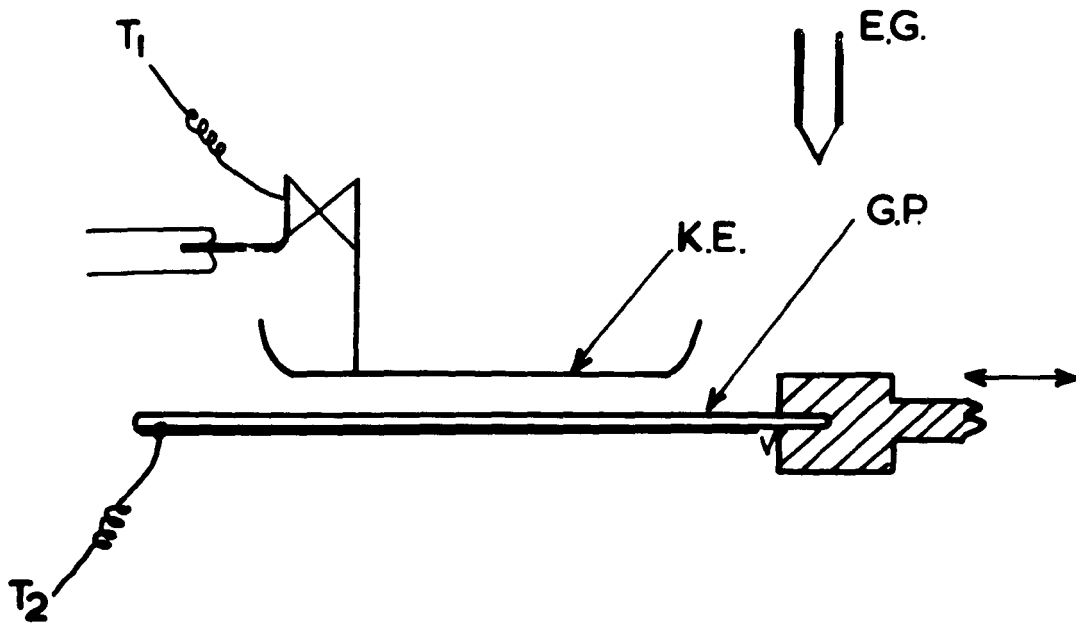
These effects are most probably caused by a charge build up on the insulating partition.

Many investigators (116, 117) have measured the contact charging of borosilicate glasses when they are moved over metal surfaces. It therefore seems likely that the results represent a charge build up, induced by the friction of the collisions between the vibrating electrode and glass partition.

The exponential decay in C.P.D. readings (made clearer in the logarithmic plot, Figure (61)) probably reflects a migration of charge to earth potential.

Because of the nature of the vibrating system (the reference electrode was caused to vibrate by gently tapping the experimental tube) it proved impossible to prevent the vibrating electrode accidentally touching the glass surface. Hence, the C.P.D. readings between the mercury electrode and the gold film were masked by the charge phenomena.

At this juncture it was decided to investigate the glass partition method with more sophisticated techniques, which employed the transducerised vibrational system mentioned earlier (i.e., Chapter IV, page 85.).



- K.E. KELVIN ELECTRODE.
- G.P. GLASS PARTITION.
- $T_1$ - $T_2$ . TUNGSTEN LEADS.
- Au.E. GOLD EVAPORATOR.
- E.G. ELECTRON GUN.

Figure 62.

### 6.3 Investigation of the Charge Transfer Hypothesis; Using the Stainless Steel Equipment

At this point in the enquiry it was considered necessary to verify that the effects obtained from the preliminary glass tube were caused by charge-transfer phenomena.

It was decided to use a demountable stainless steel system fitted with the electronic system of vibration. With this method the amplitude of the vibrating electrode could be controlled; and hence it was hoped to avoid the large C.P.D.s, produced by the inter-electrode collisions.

The basic arrangement of the apparatus within the stainless steel chamber is shown in the schematic representation, Figure (62). The glass partition, G.P., consisted of a rectangular 8 x 5cm. borosilicate glass sheet, of thickness 1m.m.

A gold evaporator, Au.E., was used to deposit a thin film of gold on the far side of the partition (i.e., on the side furthest away from the Kelvin electrode). The gold layer was electrically joined to the measuring equipment by means of a tungsten lead, T<sub>2</sub>, which was fused into the glass sheet. To avoid electrical contact between the evaporated gold film and the stainless steel mount, a small shield (represented as a "V" on the line diagram) was placed near the mount; thus producing a break in the condensed film.

To reduce the weight of the vibrating electrode a metal disc was chosen in preference to a glass substrate. This considerably

CHANGE IN C.P.D. WITH TIME.  
CHARGE INDUCED BY COLLISION.

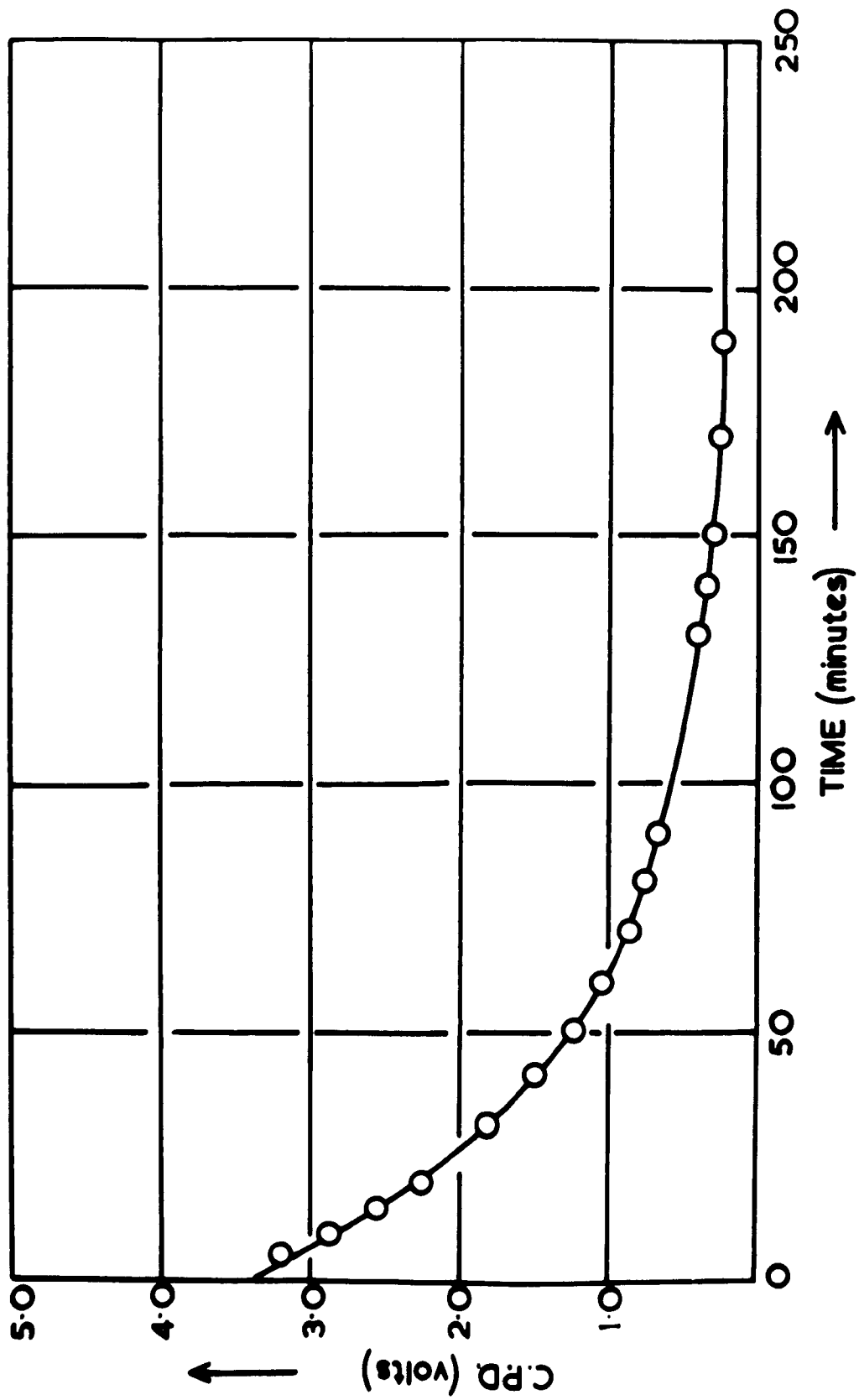


Figure 63.

CHANGE IN C.P.D. WITH TIME.  
(log plot.)

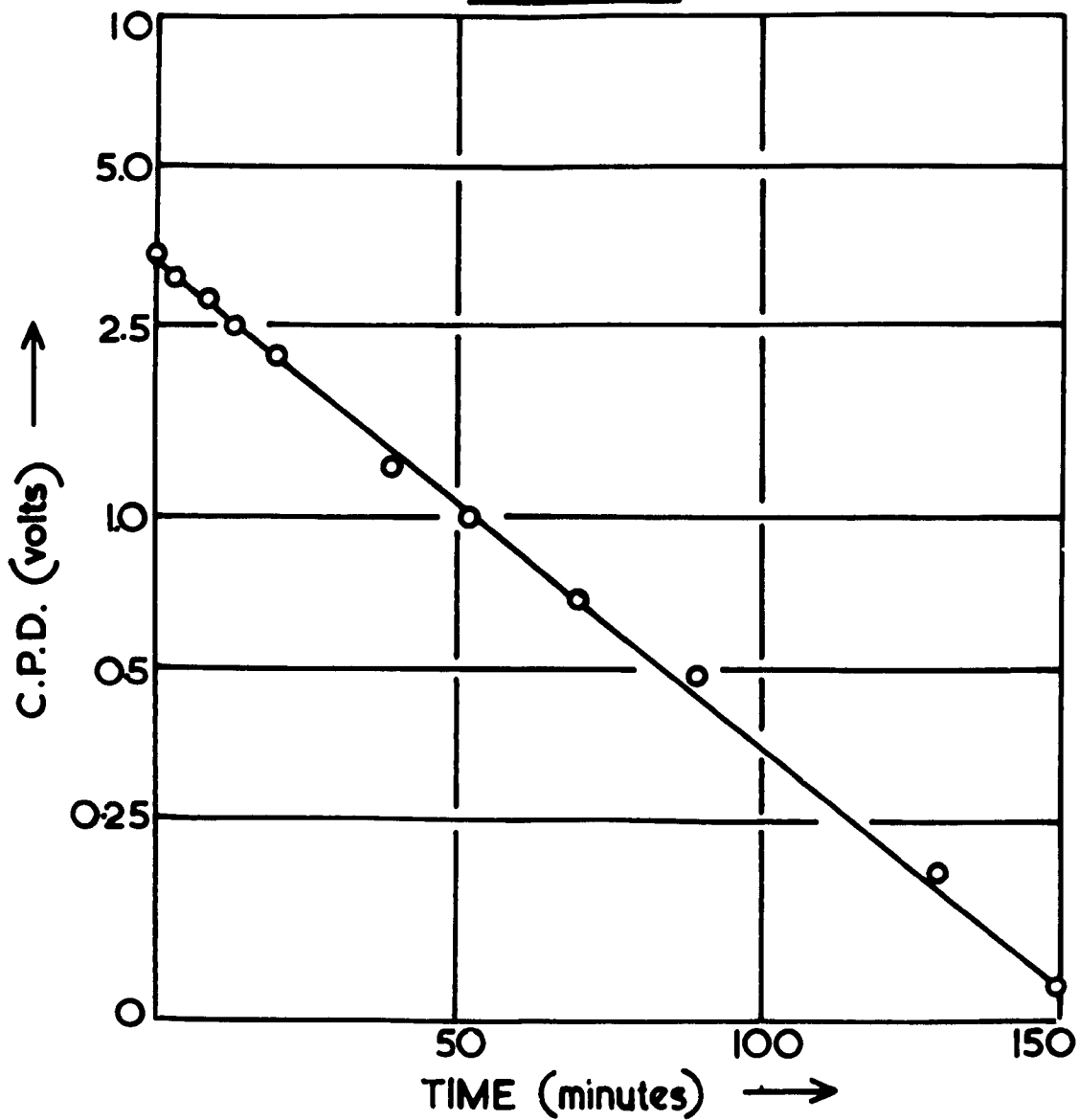


Figure 64.

reduced the weight of the Kelvin electrode; and hence, the frequency of vibration was increased, which therefore produced greater sensitivity. Physical contact between the reference surface and the glass partition was avoided, since the vibrating electrodes amplitude could be accurately controlled.

### Results

To confirm that the large C.P.D.s observed in the glass tube were induced by inter-electrode collisions, the electronically controlled electrode was set vibrating so that it never touched the glass sheet.

The C.P.D. between the gold film on the far side of the glass partition and the nickel reference electrode was +0.23 volts. This reading remained to within narrow limits ( $\pm 0.02$  volts) constant as a function of time.

Large changes in the C.P.D. were observed whenever the Kelvin electrode was forced to strike the partition. A typical run is shown in the graph, Figure (63). It can be seen that in common with the results obtained from the glass experimental tube, the C.P.D. decayed as a function of time. A logarithmic plot (Figure (64)) demonstrates the exponential nature of the decay.

Although the effects had been associated with the inter-electrode collisions, it remained necessary to confirm that charge-transfer phenomena were involved.

To verify that the C.P.D. effects which were produced after the inter-electrode collisions, were caused by a charge-transfer phenomena,

# CHANGE IN C.P.D. WITH TIME.

CHARGE INDUCED BY ELECTRON BOMBARDMENT.

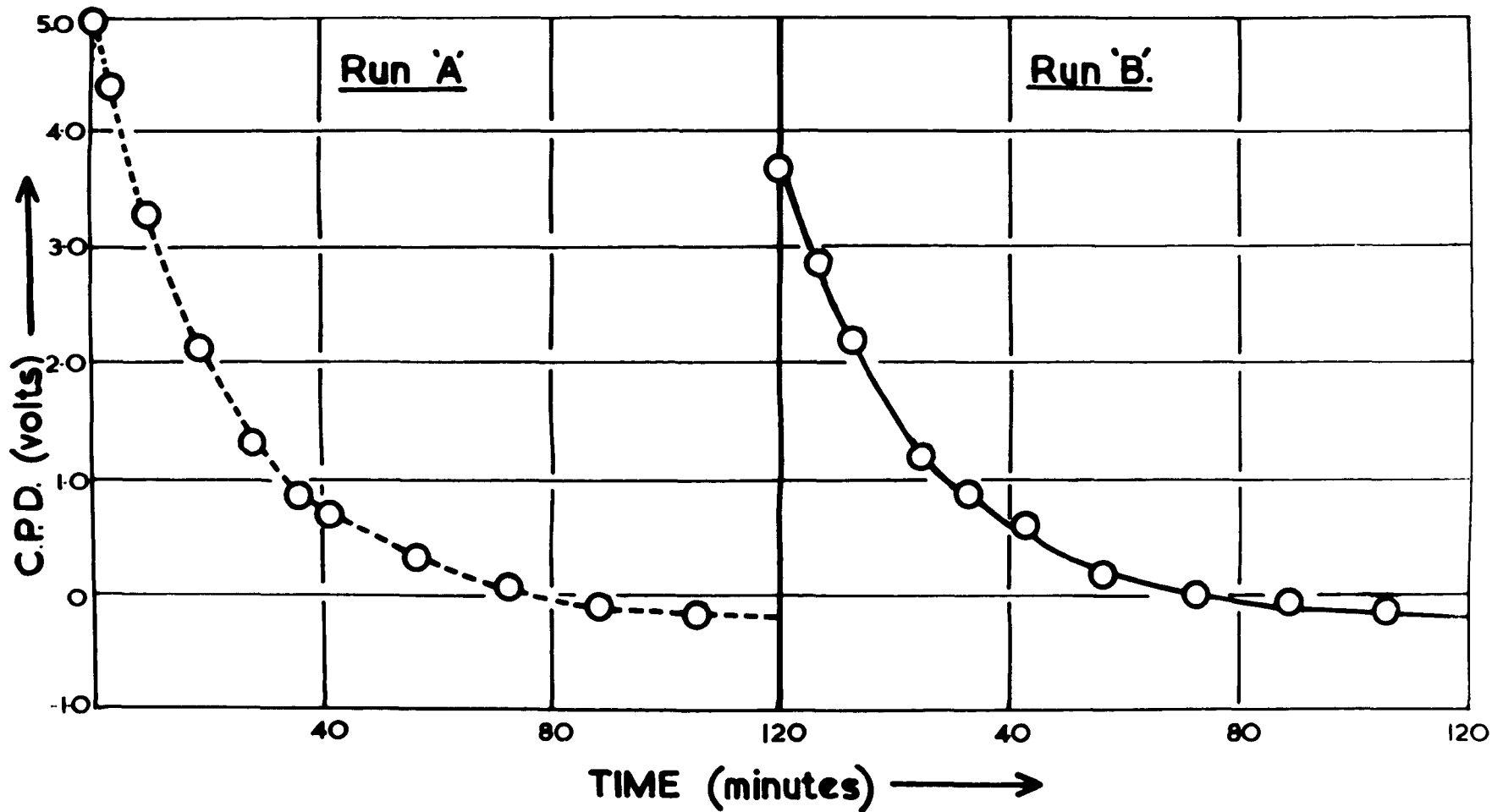


Figure 65.

CHANGE IN C.P.D. WITH TIME.  
(log. plot.)

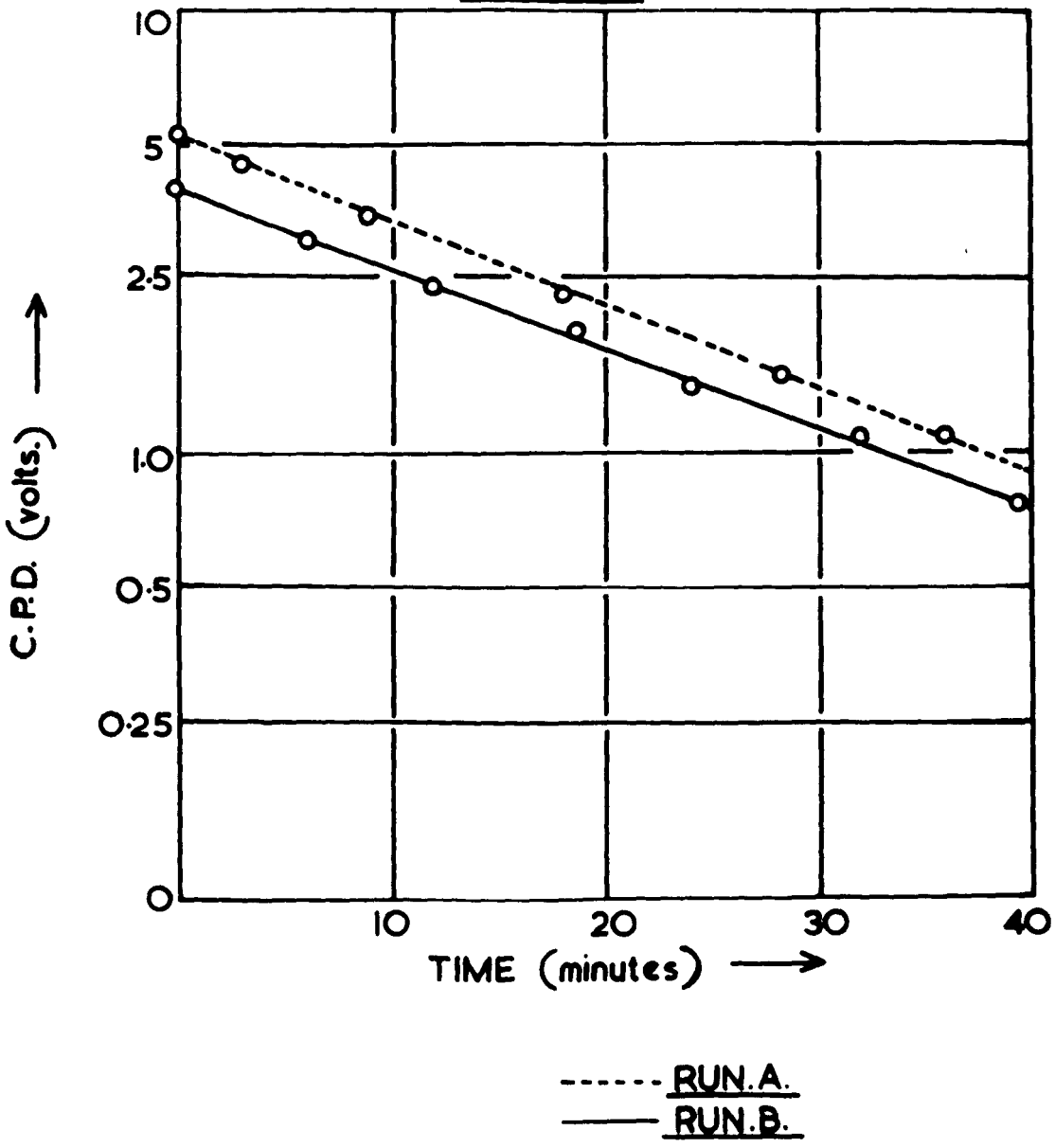


Figure 66.

it was decided to bombard the glass partition with a beam of thermionic electrons. Hence, if charge effects were responsible, similar results would be produced by the electron bombardment treatment,

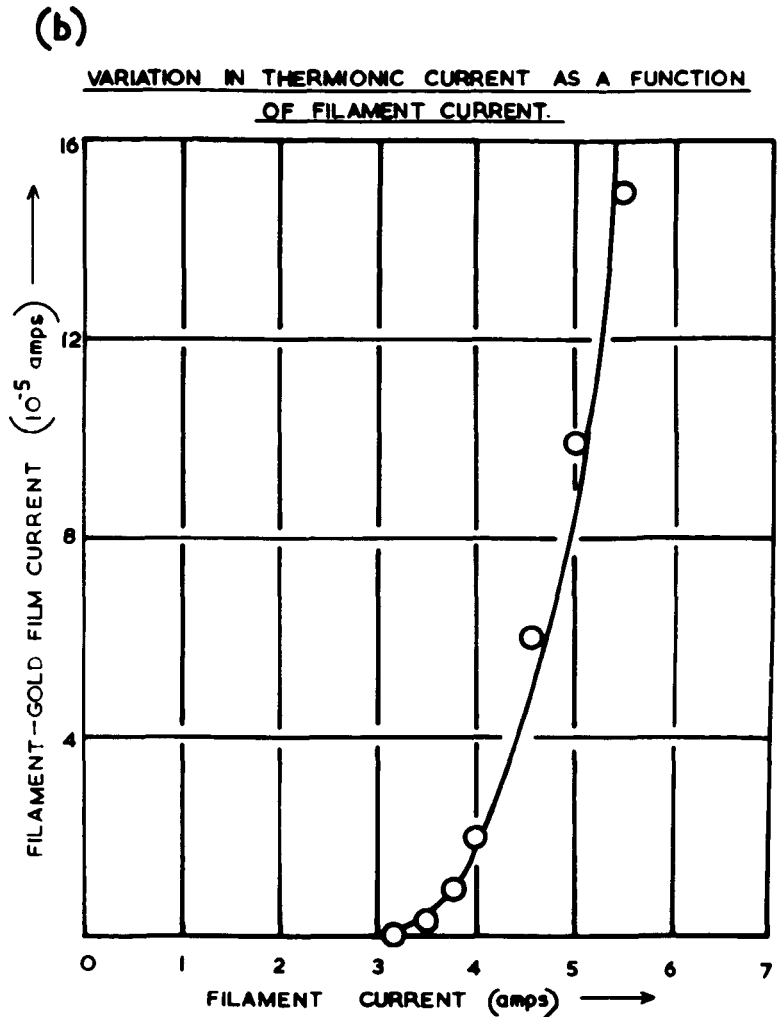
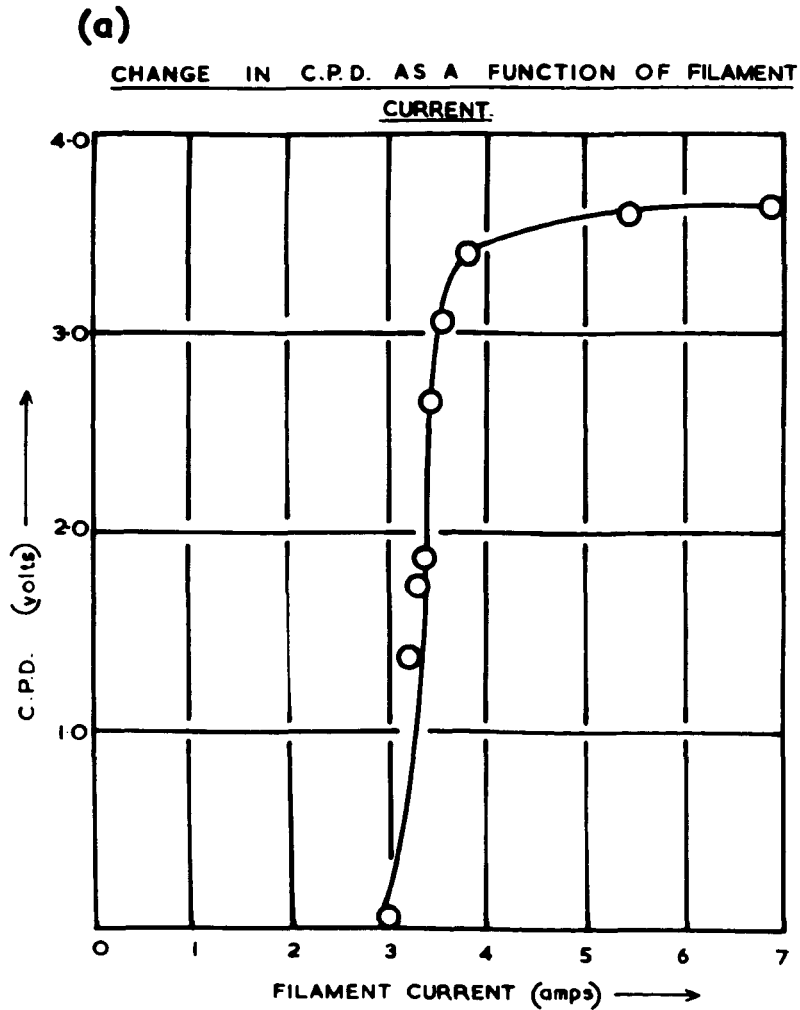
#### Electron Bombardment Effects

The electron gun, E.G. consisted of a tungsten filament mounted in front of the partition (see Figure (62)). To receive the beam of thermionic electrons the glass partition was moved from its measuring position to a position opposite the electron gun. After the filament had been electrically heated to a high temperature (about 2,500°C) for several seconds, the glass partition was quickly returned to its measuring position; and then C.P.D. readings were plotted as a function of time.

It can be seen from the graph (Figure (65)) that the beam of electrons produced large changes in the C.P.D. which subsequently decayed exponentially as a function of time. These exponential changes in C.P.D. are represented by the straight plots in the logarithmic graphs (Figure (66)).

The possibility that photons (originating from the hot filament) were producing the C.P.D. changes was eliminated by biasing the gold film, with a potential of - 50 volts relative to the electron gun. There was no change in the C.P.D. when the biased filament was heated and so it could be concluded that charge-transfer phenomena were responsible for the C.P.D. changes.

Figure 67.



Further evidence that charge effects were involved was provided by a comparison of the C.P.D. changes and the thermionic current characteristics.

It can be seen from the graphs - i.e., Figure (67), that the C.P.D. readings did not alter until the thermionic current became significant (i.e., when a current of about 3 amperes passed through the filament).

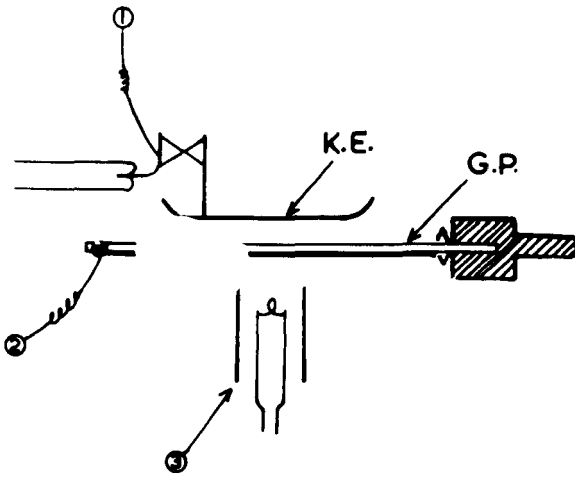
The C.P.D.s were observed to approach a constant value of + 3.6 volts as a function of the filament current (Figure(67)). This plateau probably represents the biasing effect of the electrons trapped on the surface of the glass partition.

The results obtained from the charge-transfer investigations may be summarized thus:-

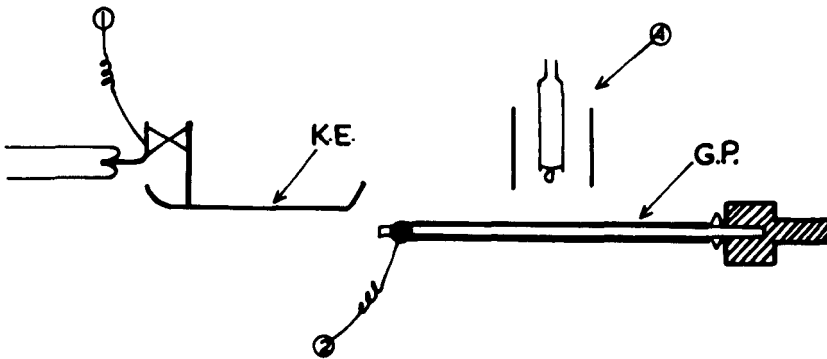
- (1) If any contact occurred between the vibrating electrode and the glass partition a positive change in the C.P.D. measurements was observed - i.e., the glass became negatively charged relative to the reference electrode.
- (2) Whenever the glass partition was bombarded with a beam of electrons the C.P.D. readings increased.
- (3) After the electron bombardment and collision-induced C.P.D. changes, the readings fell approximately exponentially at similar rates.

It therefore seems certain that the large collision-induced C.P.D. changes were produced by a transfer of electrons from the vibrating electrode to the glass partition - caused by the friction of contact.

Position (i)



Position (ii)



- G.P. GLASS PARTITION.
- K.E. KELVIN ELECTRODE.
- 1-2. ELECTRICAL LEADS.
- 3. GOLD EVAPORATOR. (Far Side)
- 4. GOLD EVAPORATOR. (Near Side)

Figure 68.

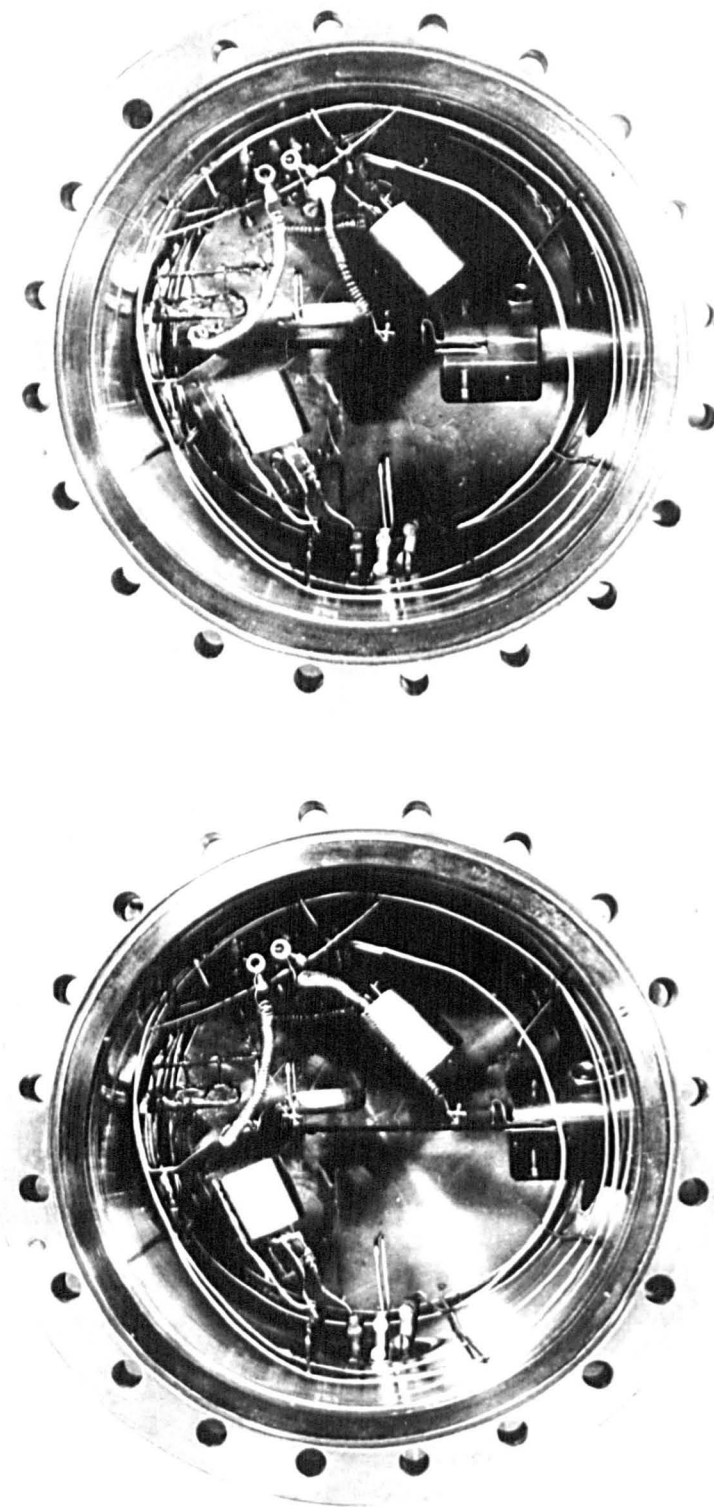


Figure 69.

At this juncture the nature of the collision-induced effects had been explained and avoided by employing the electronic vibrating system. It was therefore decided to investigate the influence of glass partitions on C.P.D. determinations.

#### 6.4 The Influence of Glass Partitions on C.P.D. Determinations

A line diagram of the apparatus used to investigate the influence of glass partitions on C.P.D. measurements is shown in Figure (68). As can be seen the glass partition could be moved (by means of a stainless steel linear feedthrough) from a site opposite the Kelvin electrode - i.e., position (i), to a position clear of the vibrating electrode - i.e., position (ii). A photograph of the equipment is shown in Figure (69). The equipment was designed to measure the change in C.P.D. when a glass sheet was placed between two metal films of known work function.

##### 6.4.1 Contact Potential Difference Measurements Between Gold Surfaces.

To reduce the number of variable factors, it was decided to evaporate the same metal (gold) on the far side of the glass partition as on the Kelvin electrode. Hence, if the metal evaporator contained impurities, both surfaces would be equally contaminated. It was hoped in this way to detect any change in the C.P.D. induced by the glass sheet.

The two surfaces were different in an important respect; with the reference surface, the characteristics of the last few layers to be deposited were measured, while with the film on the far side of

CHANGE IN C.P.D. WITH TIME.

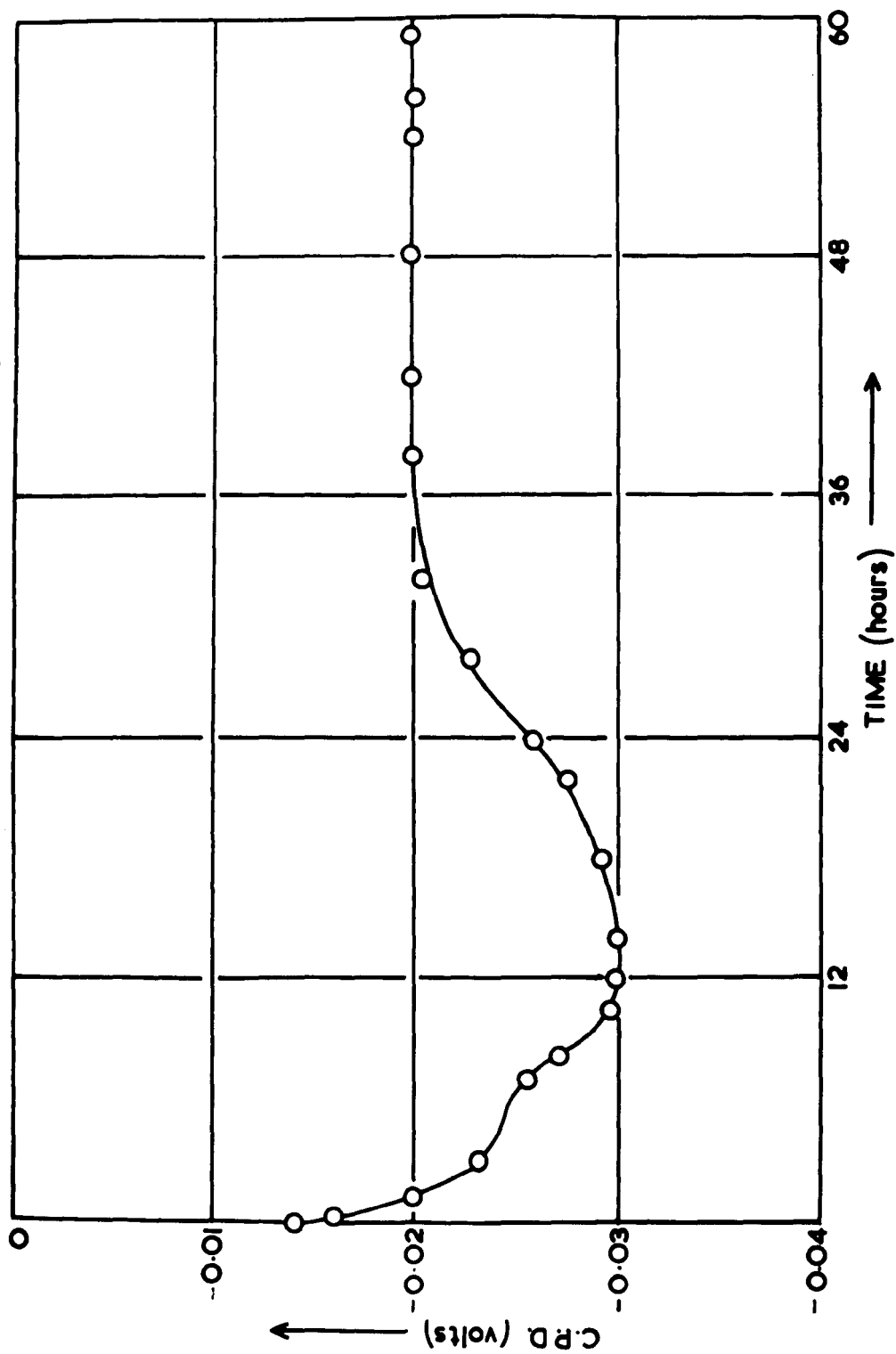


Figure 70.

the glass partition the first few layers to be condensed were investigated. In an effort to bury the outgassed impurities it was therefore decided to deposit the first film onto the Kelvin electrode, while a clean surface was being evaporated onto the vibrating electrode a system of screens shielded the glass partition.

After a thick layer of gold had been deposited onto the reference surface, the glass partition was carefully moved to a position opposite the metal evaporator (position (i)) to receive a gold film on its far side (i.e., the side furthest away from the Kelvin electrode).

### Results

The results obtained from this experiment are illustrated in the graph (Figure 7C), plotted as a function of time after film deposition.

Over a period of several hours the C.P.D. measurements decreased from the initial reading of - 0.014 volts to a minimum value of - 0.03 volts. This decrease in the readings was followed by an increase to a steady value of - 0.02 volts.

With residual gas pressures in the order of  $10^{-9}$  torr adsorbed monolayers will be produced in times not longer than about one hour (118). Since pressures lower than this were not attained initially it must be concluded that adsorption phenomena may have contributed to the changes.

Although adsorption processes can not be excluded it seems likely that annealing effects were mainly responsible for the C.P.D. changes, for the following reasons:-

(a) With the residual gas pressures in the vacuum system ( $5 \times 10^{-9}$  torr at the time of film deposition) adsorbed films would have been produced much more quickly than the observed C.P.D. changes.

(B) Many investigators (91, 92) have reported that gold films do not chemisorb gas phase residues at pressures lower than  $10^{-3}$  torr.

Hence, it seems likely that the final value of -0.02 volts represents the difference in C.P.D. between an annealed gold-glass interface and an annealed gold film, condensed on to the nickel substrate.

The twenty millivolt difference between the measured and theoretical value of 0 volts, was probably caused by one of the following factors:-

- (1) Because of epitaxial growth, the orientation of the substrates would have influenced the structure of the films.
- (2) The roughness coefficient of the gold-vacuum interface almost certainly differed from that of the gold-glass interface.
- (3) The glass partition placed between two surfaces may have produced the C.P.D. difference.

To differentiate between the three factors, it was decided to condense a gold film on to the near side of the glass partition. The C.P.D. readings would still be influenced by the first factor, but not the last two. Hence, the effect of the glass partition on C.P.D. measurements could be ascertained.

CHANGE IN C.P.D. WITH TIME.

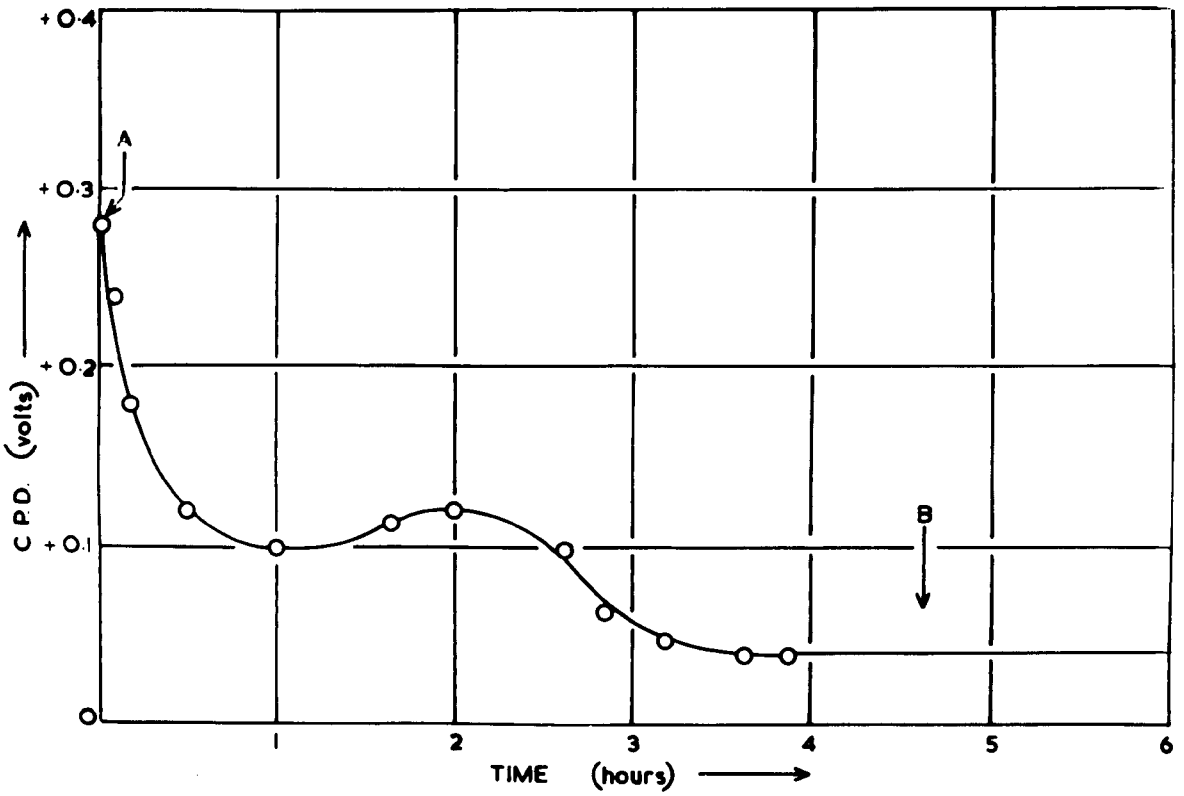


Figure 71.

The C.P.D. readings obtained when a gold film was deposited on to the near side of the glass partition are plotted in Figure (71), as a function of time. After the gold surface had been condensed on to the glass substrate the measurements decreased from the initial value of + 0.28 volts (point A) to a steady reading of + 0.04 volts (i.e., region B). This change in C.P.D. over a period of 4 hours most probably represents the effect of annealing processes since gold is known to be extremely resistant to adsorption phenomena at low residual gas pressures.

Hence, the different substrates (glass and polycrystalline nickel) changed the C.P.D. by a factor of 40 millivolts. It therefore seems reasonable to assume that the readings obtained from the preceding experiment (Figure 70) reflected the different surface conditions of the films. At this juncture, it was decided to determine the influence of glass partitions on C.P.D. readings, between metals of different but known work functions.

#### 6.4.2. Contact Potential Difference Measurements Between Gold and Tungsten Surfaces

With the exception of the metal evaporators, the apparatus employed in this phase of the inquiry was identical to that illustrated in Figure (68).

In order to measure the C.P.D. between a gold reference surface and a tungsten film, deposited on the far side of the glass partition,

CHANGE IN C.R.D. WITH TIME.

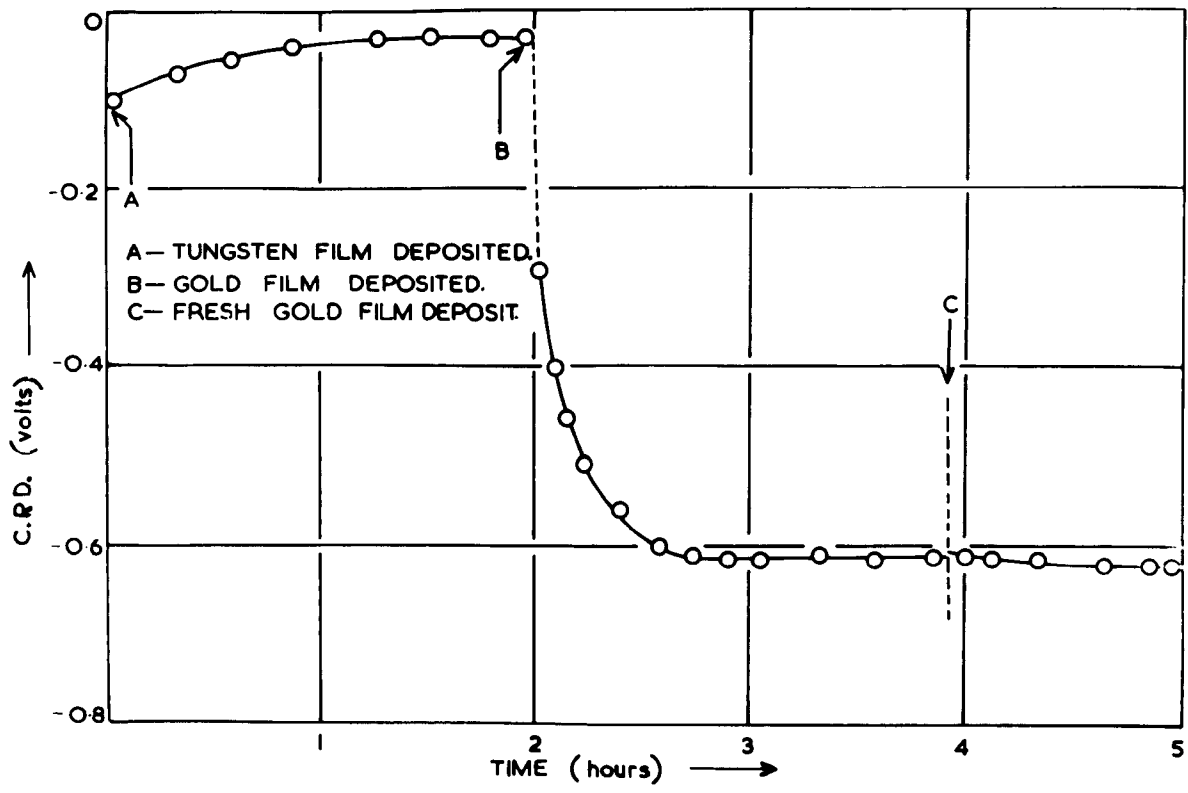


Figure 72.

it was imperative that the impurities dissolved in the tungsten filament did not condense on the glass sheet. Hence, the initial beam of evaporated tungsten (i.e., the most contaminated) was condensed on to the Kelvin electrode.

After a thin film had been deposited on to the vibrating electrode the glass partition was slowly moved to a position opposite the evaporator, where it received a film of evaporated tungsten.

It can be seen from the graph (Figure (72)) that as the film of tungsten increased in thickness the C.P.D. changed from - 0.095 volts (point A) to a steady value of - 0.030 volts. This reading of - 0.030 volts almost certainly represented the different surface characteristics (roughness, orientation etc) of tungsten-vacuum and tungsten-glass interfaces.

When a gold film was condensed on the Kelvin electrode (point B) the C.P.D. changed by a factor of - 0.585 volts to a constant value of - 0.615 volts. A second gold film deposited on top of the first one changed the C.P.D. by a further 8 millivolts.

Combining Rivière's (94) value of 4.565eV for the work function of polycrystalline tungsten with these C.P.D. results, gives the work function of gold to be  $5.18 \pm 0.05\text{eV}$ , which is in fair agreement with Huber's (95) value of  $5.22 \pm 0.05\text{eV}$ . The slight discrepancy between the two determinations most probably reflects the nature of the underlying layers. Huber prepared his reference surface by depositing tungsten films on to borosilicate glass substrates, while in this work the tungsten films were condensed onto polycrystalline nickel substrates.

CHANGE IN C.P.D. WITH TIME.

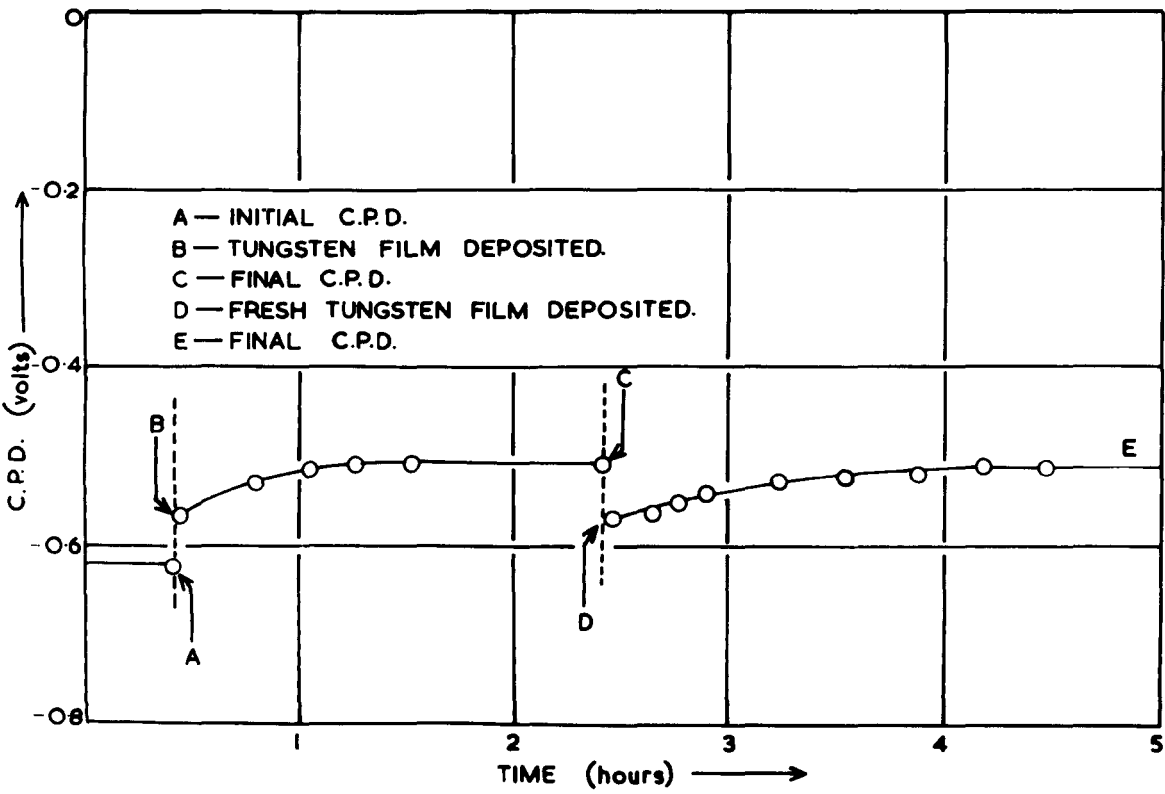


Figure 73.

To corroborate the results, a clean tungsten surface was deposited on the near side of the glass sheet - i.e., the partition was used as a substrate. The resulting changes in the C.P.D. are plotted in Figure (73) as a function of time.

The first set of readings (region A) represented the C.P.D. between the gold Kelvin electrode and a tungsten film on the far side of the glass partition (i.e., the last set of measurements in the preceding graph). It can be seen that, when a tungsten surface was deposited on the near side of the glass sheet, the readings changed to - 0.57 volts, which over a period of an hour approached a constant value of - 0.51 volts (region C).

A second tungsten deposition (point D) gave rise to a similar set of readings. Since tungsten is known to adsorb a wide range of gases (129, 130, 131) it is most probable that adsorption affects contributed to the C.P.D. changes. Therefore in order to determine the work function of gold, it is essential to consider the C.P.D. immediately after the depositions (points B and D) - i.e., before the tungsten surfaces were contaminated.

Combining the readings obtained from the clean gold and tungsten films (- 0.57 volts) with Rivière's value of 4.565 volts for the work function of tungsten, yields a value of 5.14 volts for the work function of gold. Hence, the two techniques employed in this investigation to determine the work function of gold (the glass partition and the conventional Kelvin method) produced values that differed by less than one per cent.

CHANGE IN C.P.D. WITH TIME.

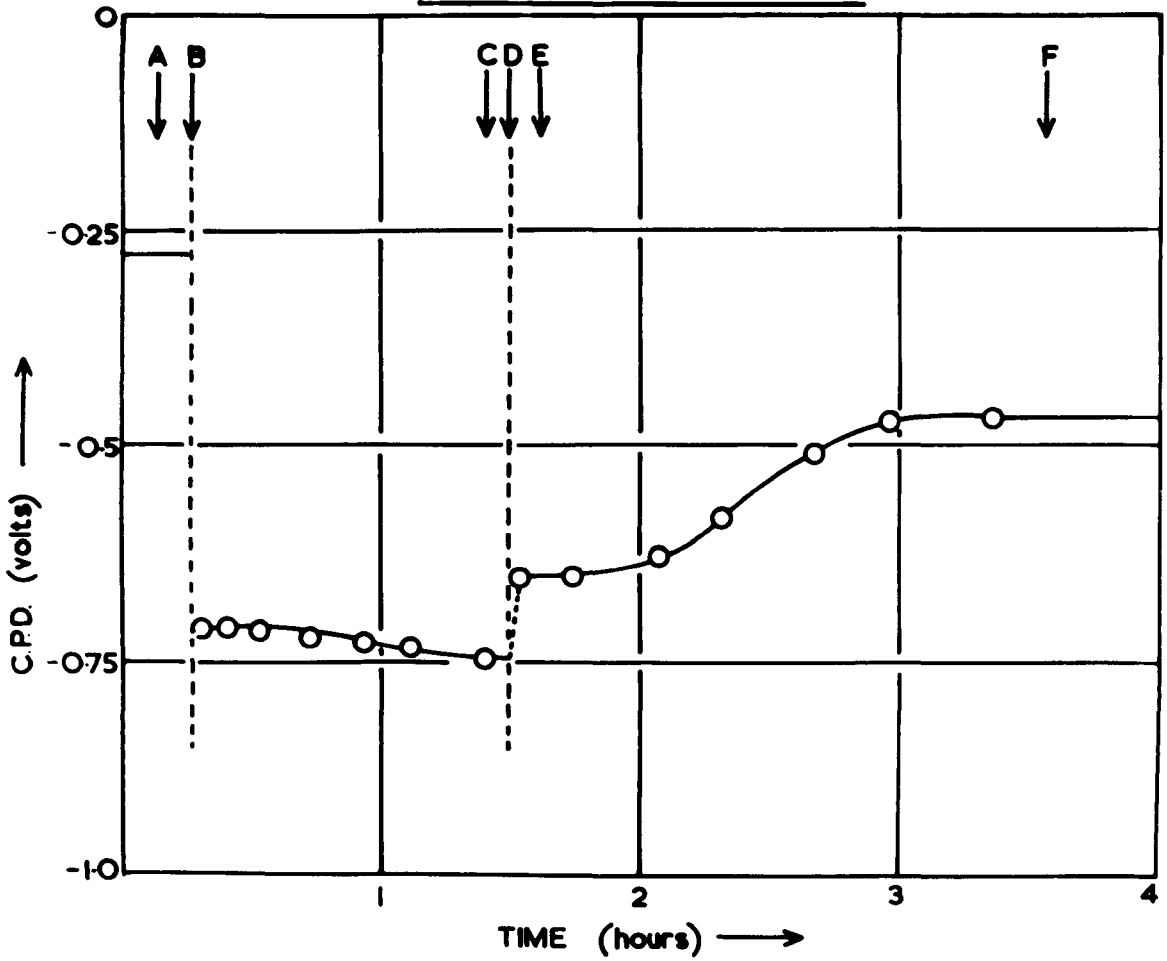


Figure 74.

### 6.4.3 Contact Potential Difference Measurements Between Gold and Silver Surfaces

In order to verify that insulating partitions have only a slight effect on C.P.D. determinations, it was decided to use the partition method to measure the work function of silver.

The changes in C.P.D. with time are plotted in Figure (74). The first set of readings (i.e., region A), corresponds to the C.P.D. between a clean silver film, deposited on the far side of the partition and a contaminated reference surface (of unknown work function).

At point B the Kelvin electrode was standardized with a clean film of condensed gold. After the gold deposition the C.P.D. decreased to - 0.71 volts, and then over a period of one hour decreased further to a constant value of - 0.74 volts (region C). This small final change almost certainly reflects the influence of annealing phenomena; since gold does not chemisorb gases at low pressures ( $10^{-9}$  torr in the experimental chamber), and the silver-glass interface was not in a position to receive contaminants. Thus, the C.P.D. between clean gold and silver surfaces is - 0.71 volts.

Combining these results with the work function of gold obtained from the previous glass partition experiment (i.e.  $5.18 \pm 0.05\text{eV}$ ) produces a work function of  $4.47 \pm 0.05\text{eV}$  for the silver-glass interface, which although a little higher than Rivière's (94) value of 4.31eV is in excellent agreement with Anderson's (119) determination.

At point D (see the graph) a clean silver film was condensed on the near side of the partition, which produced a + 0.095 volts change in the readings to - 0.65 volts (region E). Hence, assuming the work function of gold to be  $5.18 \pm 0.05\text{eV}$ , the work function of the silver-vacuum interface was  $5.53 \pm 0.05\text{eV}$ .

After the final silver condensation the C.P.D. changed from its initial value of - 0.65 volts (region E) to a constant reading of - 0.47 volts (region F). Since silver is known to adsorb a wide range of materials (132, 133) the shift in the measurements over a period of two hours almost certainly represents the adsorption of gas phase residues (of unknown composition) on the silver film.

It can be seen from a comparison of the results, that the silver-vacuum and silver-glass interfaces had work functions that differed by less than two per cent.

#### 6.4.4 Summary of Results

The results obtained from the experiments carried out to determine the influence of glass partitions on C.P.D. measurements may be summarized thus:-

- (1) The metal-glass interfaces and metal-vacuum interfaces had work functions that did not differ by more than two per cent.
- (2) The work functions of the metal-vacuum interfaces were always slightly higher (usually about 50 millivolts) than the metal-glass work functions.

(3) After the annealing processes the metal-glass work functions were extremely stable as a function of time (rarely changing by more than 5 millivolts..

The second effect was almost certainly caused by the different surface conditions. Metal-glass interfaces most probably have rougher surfaces than the metal-vacuum films.

The last effect, besides reflecting the inaccessibility of the metal glass interfaces to contamination, suggests that the surface nature of the near side of the glass partition (i.e., facing the Kelvin electrode) did not change.

It was therefore decided to investigate the stability of the glass-vacuum surface.

## 6.5 The Stability of the Glass Partition

The experiments carried out during this stage of the investigation were intended to determine the reproducibility of the glass-vacuum interfaces as a function of the gas phase pressure and of the distance along the surface of the glass sheets.

### 6.5.1 Effects of Increased Residual Gas Pressure

The residual gas pressure was increased by flashing tungsten filaments (to desorb adsorbed contaminants). Although the total gas pressure was accurately measured by means of a triggered ion gauge the partial pressure of the different gas phase residues was unknown. However, the contaminants were doubtless typical of stainless steel vacuum systems, and hence the observed results were relevant.

# CHANGE IN CPD WITH TIME.

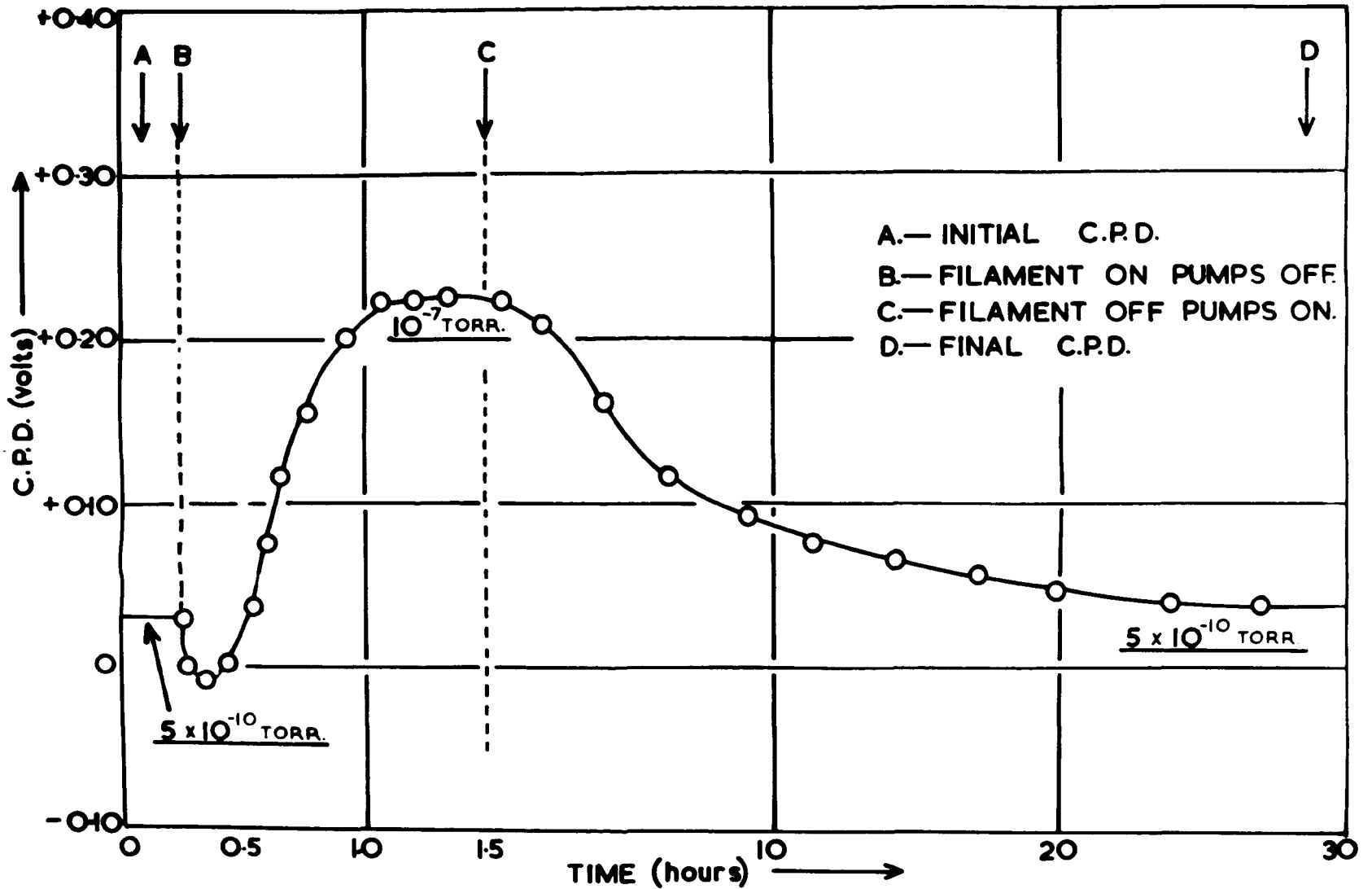


Figure 75.

In order to eliminate charge build up effects, the filament was operated at relatively low temperatures (i.e. about 1,000°C) where the thermionic emission of electrons was negligible (assuming  $A$  and  $\phi$  to be 41 amp.cm<sup>-2</sup>deg.<sup>-2</sup> and 4.45 eV respectively, (134), the thermionic current from the filament would have been approximately 10<sup>-19</sup> amps at 1,300°K).

The results obtained are plotted in Figure (75) as a function of time. The first set of measurements (i.e., region A) represent the C.P.D. between a gold-glass interface and a gold reference surface, with a residual gas pressure of 5 x 10<sup>-10</sup> torr.

When the getter ion pumps were switched off and the tungsten filament flashed (point B), the readings increased by 0.195 volts to a setting of + 0.225 volts, which was constant as a function of time; at this stage in the C.P.D. run the pressure was constant at 10<sup>-7</sup> torr.

At point C the pumps were reintroduced and the filament allowed to cool to ambient temperature. As the pressure fell from 10<sup>-7</sup> torr to its original value of 5 x 10<sup>-10</sup> torr, the C.P.D. readings decreased (over a period of 30 hours) from the maximum to a value of + 0.038 volts).

The two principle features of the curve may be summarized thus:

- (1) After a cycle of pressure changes, the measurements had altered by less than 10 millivolts.

(2) The rise in C.P.D. readings was considerably steeper than the gradual drop (an hour compared with over a day).

Todd (120, 121), working in the U.S.A., has demonstrated that under vacuum conditions the diffusion of water vapour from borosilicate glasses is a reversible process. Hence, these effects were most probably caused by ions or molecules being reversibly adsorbed on the glass-vacuum interface.

The salient feature of the above results, is that at low pressures (i.e. below  $10^{-9}$  torr) the surface nature of the partition was not influenced to any marked extent by its history.

#### 6.5.2 Change in the Surface Conditions of The Glass Partition as a Function of Distance

In order to determine the stability of the glass-vacuum interfaces, as a function of distance, it was decided to measure the C.P.D. between a movable gold reference surface (i.e. it could be moved in a parallel direction above the glass surface) and a gold film deposited on the far side of the partition.

The spatial resolution of the measurements was increased by fitting the Kelvin assembly with a 1.0cm. diameter reference electrode (i.e., instead of the usual 4 cm. electrodes). The decrease in the Kelvin electrodes area was approximately compensated for by the lighter electrodes higher frequency of vibration. Hence, there was only a small drop in the sensitivity of the system.

CHANGE IN C.P.D. WITH DISTANCE.

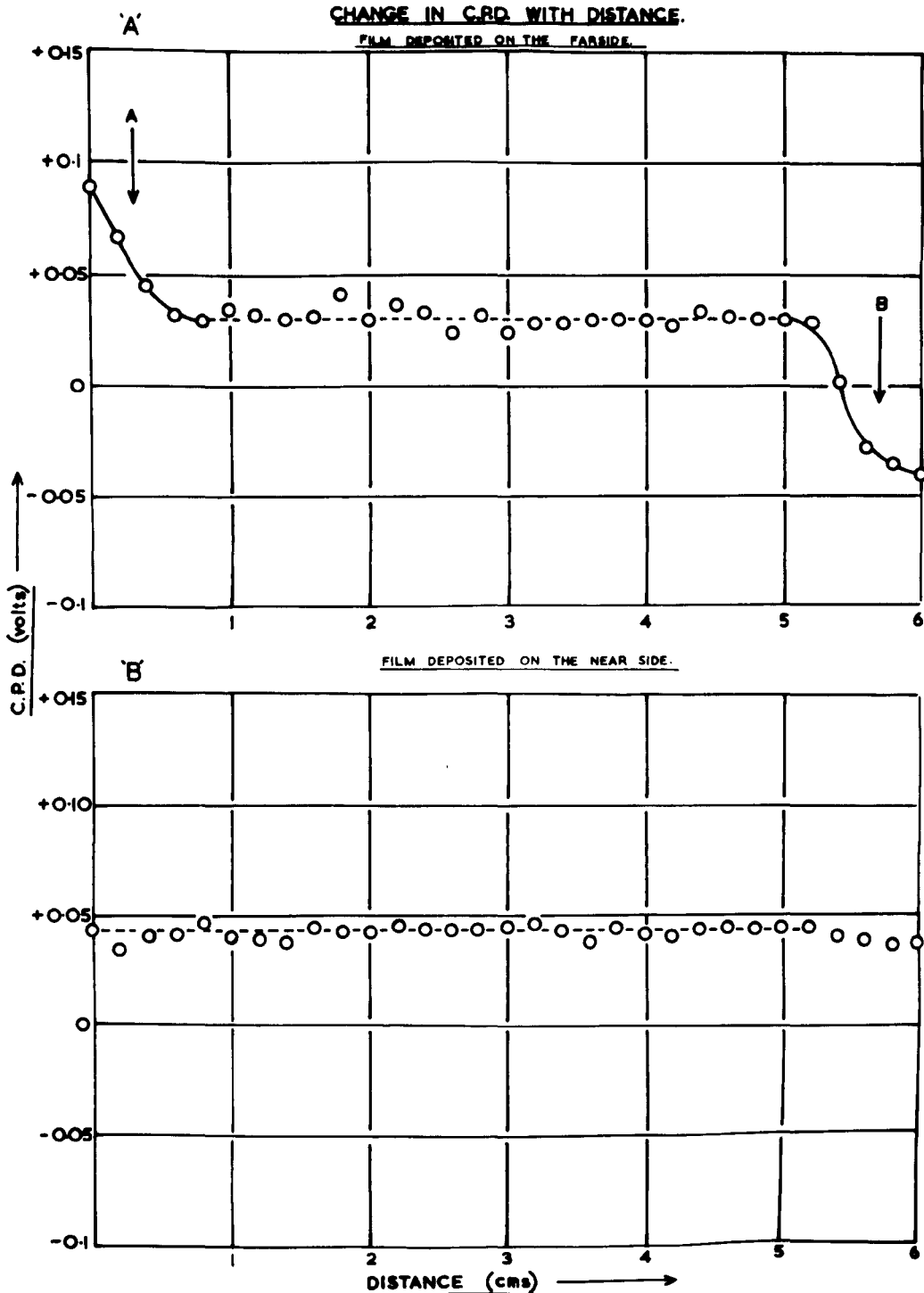


Figure 76.

A threaded counter fitted to the linear motion feedthrough accurately measured the movement of the glass sheet.

The graph (Figure (76'A')) illustrates the variation in C.P.D. as the reference electrode was moved linearly above the surface of the glass partition (with a gold film condensed on the far side).

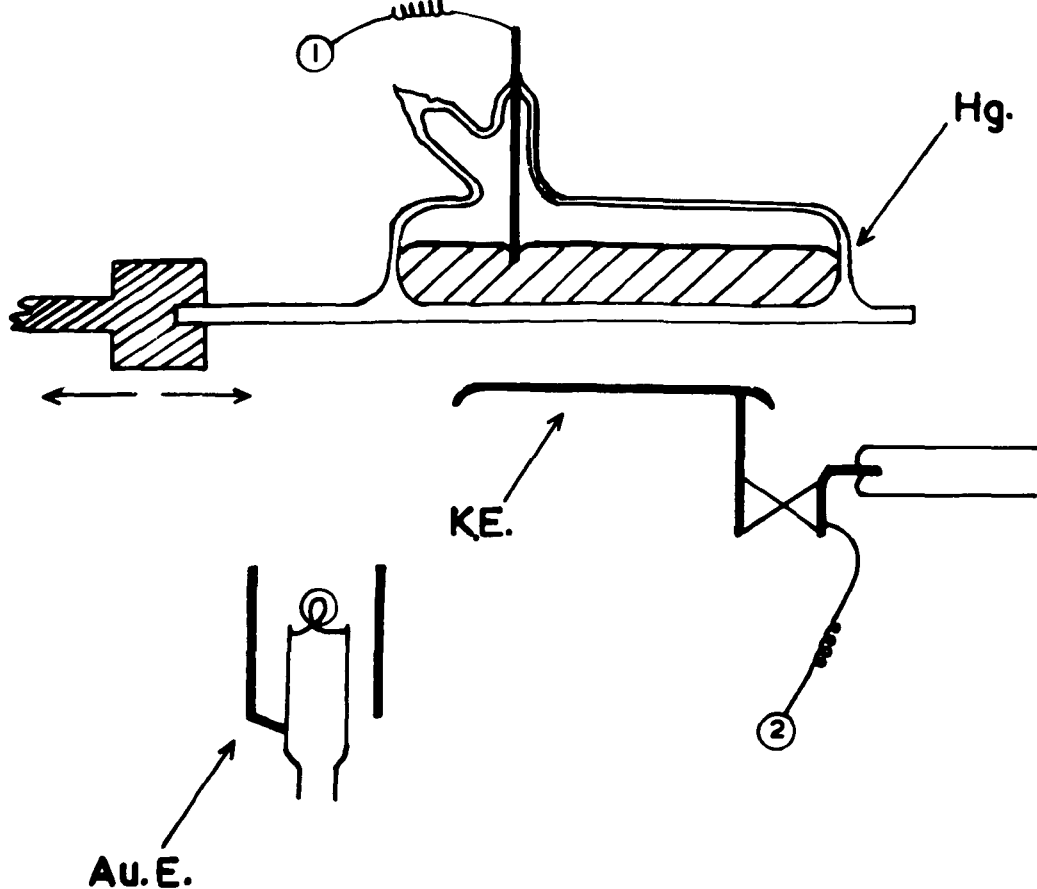
It can be seen that over the central region, the readings were to within 15 millivolts, constant as a function of position. Region A almost certainly corresponds to the influence of the aquadag deposit, used to electrically connect the gold film to the measuring equipment. In a similar manner, region B represents the effect of the stainless steel mount.

Hence, excluding the end regions, the C.P.D. measurements were to within narrow limits independent of position.

When applied to a gold film deposited on the near side of the partition, the linear probing techniques produced the results shown in the bottom graph (i.e., Figure (76'B')). Since the condensed gold covered both the stainless steel mount and the aquadag layer, the C.P.D. readings were virtually constant as a function of distance.

### 6.5.3 Conclusions

From the above considerations it is apparent that the only process likely to cause a significant change in the C.P.D. readings is the physical adsorption of ions or molecules. This effect was eliminated by operating at sufficiently low gas pressures.



1 cm.

- K.E. KELVIN ELECTRODE.
- Hg. MERCURY.
- Au.E. GOLD EVAPORATOR.
- 1-2. ELECTRICAL LEADS.

Figure 77.



Figure 78.

## 6.6 Determination of the Work Function of Liquid Mercury

A line diagram of the apparatus employed to determine the C.P.D. between a gold reference surface and a mercury-glass interface is shown in Figure (77).

The mercury electrode, Hg, consisted of a pool of liquid mercury enclosed in a sealed glass container; fitted with a thin (1m.m.) plane glass wall. Except for the electrical feedthrough, the mercury container was constructed out of borosilicate glass (a photograph of this component is illustrated in Figure (78)).

After being soaked in chromic acid for a week, the container was washed in distilled water and fitted to the glass high vacuum system (see Figure (33)), to be processed.

The inner surfaces of the glassware were outgassed by being baked at 250°C, under high vacuum conditions for several days. When the residual gas pressure was below  $5 \times 10^{-9}$  torr a small amount of mercury was triple distilled into the container. After receiving the required quantity of mercury the glass vessel was separated from the manifold by means of a collapsible seal.

At this stage the mercury electrode assembly was placed in the stainless steel vacuum chamber a short distance (a few millimeters) above the Kelvin electrode (see the schematic representation). Extraneous fields were minimized by making the reference surface smaller than the mercury electrode (diameters of 2.5 cms. and 3.5 cm. respectively).

CHANGE IN C.P.D. WITH TIME.

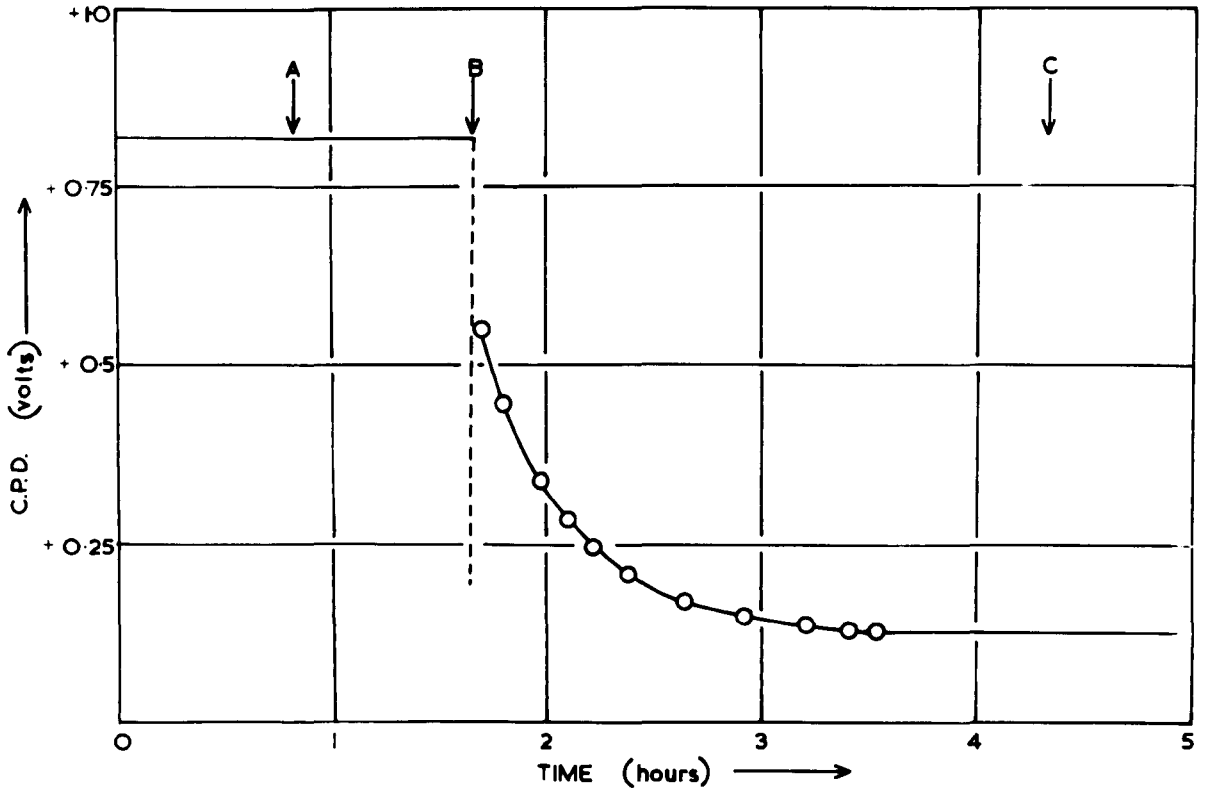


Figure 79.

The stainless steel apparatus and the outer walls of the glass container were outgassed by being heated to a temperature of  $220^{\circ}\text{C}$ , under high vacuum conditions, for several days. In order to restrict the vapour pressure of the mercury to about 50 torr the outgassing temperature was maintained below  $230^{\circ}\text{C}$ .

An important feature of the experimental configuration was that the mercury container was positioned above the vibrating surface i.e., the lower surface of the mercury electrode was investigated. Hence, any insoluble impurities (e.g., particles from thermal decomposition of the glass (122)) would have floated away from the mercury-glass interface.

The first stage of the experimental procedure consisted of measuring the C.P.D. between the Kelvin electrode (of unknown work function) and the mercury-glass interface. At this juncture the mercury electrode was moved to a position opposite the gold evaporator, Au.E. (by means of the linear feedthrough) where it received a condensed film of gold. The C.P.D. between the gold film (of known work function) and the Kelvin electrode standardized the reference surface. Hence, the difference of the two C.P.D. determinations when combined with the work function of gold yielded the work function of liquid mercury,

### Results

The results of the C.P.D. measurements made with the liquid mercury equipment, are shown in Figure (79), plotted as a function of time.

The initial reading of + 0.82 volts (region A) corresponds to the C.P.D. between the liquid mercury-glass interface and the Kelvin electrode (of unknown work function). When a clean gold film was deposited on the near side of the glass partition (point B) the readings decayed exponentially from a value of + 0.55 volts to a steady reading of + 0.13 volts. The exponential decay almost certainly reflects the influence of the thermionic electrons emitted from the hot metal evaporator being trapped on the surface of the glass partition, and subsequently leaking away to earth potential.

The constant reading of + 0.13 volts (region C) represents the C.P.D. between the gold film, which was condensed on the near side of the glass surface, and the vibrating electrode. Combining this reading with the work function of gold, 5.18eV (which was determined at an earlier stage in the investigation - i.e., page 124) produces a value of 5.31eV for the work function of the reference surface. Hence, from the original C.P.D. (+ 0.82 volts) and the work function of the standardized Kelvin electrode, the work function of the liquid mercury glass interface was 4.49eV.

It will be recalled that in section 6.4 the work functions of metal-vacuum interfaces were usually about 50 millivolts higher than those of the metal-glass interfaces. It therefore seems likely that the work function of a liquid mercury-vacuum interface will be greater than the measured value of 4.49eV, by a factor of about 50 millivolts.

Thus, the work function of mercury, at room temperature, is  $4.54 \pm 0.02\text{eV}$ . The  $\pm 0.02\text{eV}$  error represents the total deviation from the experiments carried out in section 6.4.

## 6.7 Conclusions

The work described in this chapter developed in two stages. The first, and by far the longest, investigated the effect of glass partitions on C.P.D. determinations.

The second phase of the enquiry was the use of the techniques already developed to measure the work function of mercury at room temperature.

It has been established that the large C.P.D. changes encountered with the preliminary experimental tube, were caused by collisions between the electrodes. These effects were completely eliminated by introducing a transducerized system of vibration.

## CHAPTER VII

### CONCLUSIONS AND SUGGESTIONS FOR FURTHER WORK

The experiments described in the preceding two chapters have been directed towards the determinations of the work function of mercury. Three different techniques of maintaining the reference surface free of contaminating mercury vapour were investigated.

Although the first method (which employed hot molybdenum reference electrodes) failed to yield reproducible results, it successfully demonstrated the contaminating action of borosilicate glasses on mercury surfaces.

The solid mercury and glass partition techniques produced values of 4.45eV and 4.54eV respectively for the work function of mercury.

The ninety millivolt difference between the two determinations was most probably caused by one or more of the following factors:-

- (1) Work functions are known to change as a function of temperature; it is therefore certain that the difference in temperature between the samples contributed to the difference in values.
- (2) It is possible that at the phase change (i.e., the melting point at  $-39^{\circ}\text{C}$ ) there is a discontinuity in the work function of mercury.
- (3) Liquid and solid mercury most certainly have different roughness factors.

The change in temperature of about  $220^{\circ}\text{C}$  would have changed the work function, but this change would probably not have amounted to

more than 0.02eV (temperature coefficients are of the order of  $10^{-4}$ eV/°C (135)). Hence, the first factor fails to account for the observed difference of 0.09eV. Borshov (123) using thermionic emission techniques observed that the work function of copper varies continuously as the temperature is raised through the melting point. It would therefore seem unlikely that there is a discontinuity in the work function of mercury at the phase change.

The 90 millivolt difference between the work function of liquid and solid mercury is most probably mainly due to dissimilar roughness factors.

Many workers (124) have reported that thin condensed films exist in the form of islands which flow together as the film thickness is increased. This mechanism of formation most certainly introduces discontinuities into evaporated surfaces. At liquid nitrogen temperatures the mobility of the condensed mercury atoms will be extremely low; and hence it can be assumed that the lattice imperfections would not have been annealed.

The liquid mercury-glass interfaces most probably had low roughness factors since polished borosilicate glass surfaces usually have roughness factors of about 2.5 (125). It therefore seems likely that the solid mercury films had rougher surfaces than the liquid mercury-glass interfaces.

Rough surfaces are known to have lower work functions than smooth ones (136, 137); it would therefore seem certain that the

difference between the results represents the degree of annealing of the solid and liquid films.

In the course of this work a new measuring technique was developed, which extends the scope of C.P.D. determinations. The glass partition modification of the Kelvin method has the advantage of enabling the work functions of volatile liquids and solids to be measured.

Good agreement was also observed between the present determination of the work function of gold and those of Huber (95) and Rivière (96). These investigations have demonstrated that gold films, when prepared in mercury-free ultra high vacuum systems, have work functions which are higher than those reported by earlier workers (using mercury contaminated systems).

#### Suggestions for Further work

This work has emphasized the importance of ultra-high vacuum techniques in work function investigations.

The results obtained from liquid mercury surfaces (Chapter V) suggest that a programme of investigations under more controlled conditions of preparation (e.g., substituting inert containers for the contaminating glass envelopes) might be of considerable value.

Eventually, efforts must be made to observe the change in the work function of mercury as a function of temperature.

The glass partition method could be employed to cover the range of temperatures from  $-196^{\circ}\text{C}$  to about  $200^{\circ}\text{C}$  (i.e., where the vapour pressure of mercury acting on the glass containers becomes appreciable). Such an

investigation is also necessary in order to confirm Bolshov's (123) observation that phase changes are not accompanied by a discontinuity in the work function.

It has been postulated in this work that thin impurity layers floating on top of the liquid mercury surfaces were responsible for the random C.P.D. fluctuations reported in Chapter V. This hypothesis could be confirmed by using the glass partition method to compare work function values obtained from the top and bottom horizontal faces of mercury samples.

The variation in work function of metal films as a function of thickness should be re-examined. These investigations are usually complicated by two extraneous factors:-

- (1) When a series of films is condensed it is possible to produce a sandwich type structure (i.e. alternate metal and adsorbed layers).
- (2) Changes in the surface characteristics due to the lack of epitaxy.

The first factor is usually minimized by using extremely low residual gas pressures.

The second effect could be eliminated by using the glass partition method to investigate the change in work function of a metal-glass interface as the thickness of the metal film is increased, by condensing more metal onto the far side of the sample (i.e. although the metal film would increase in thickness the structure of the metal-glass interface would remain the same).

Using a mercury reference surface it would be useful to investigate the effect of mercury vapour on the work functions of clean metallic surfaces.

The surface characteristics of the mercury electrode would not be changed by the mercury vapour and hence it could be assumed that any variation in the C.P.D. readings would correspond to a change in the work function of the other surface.

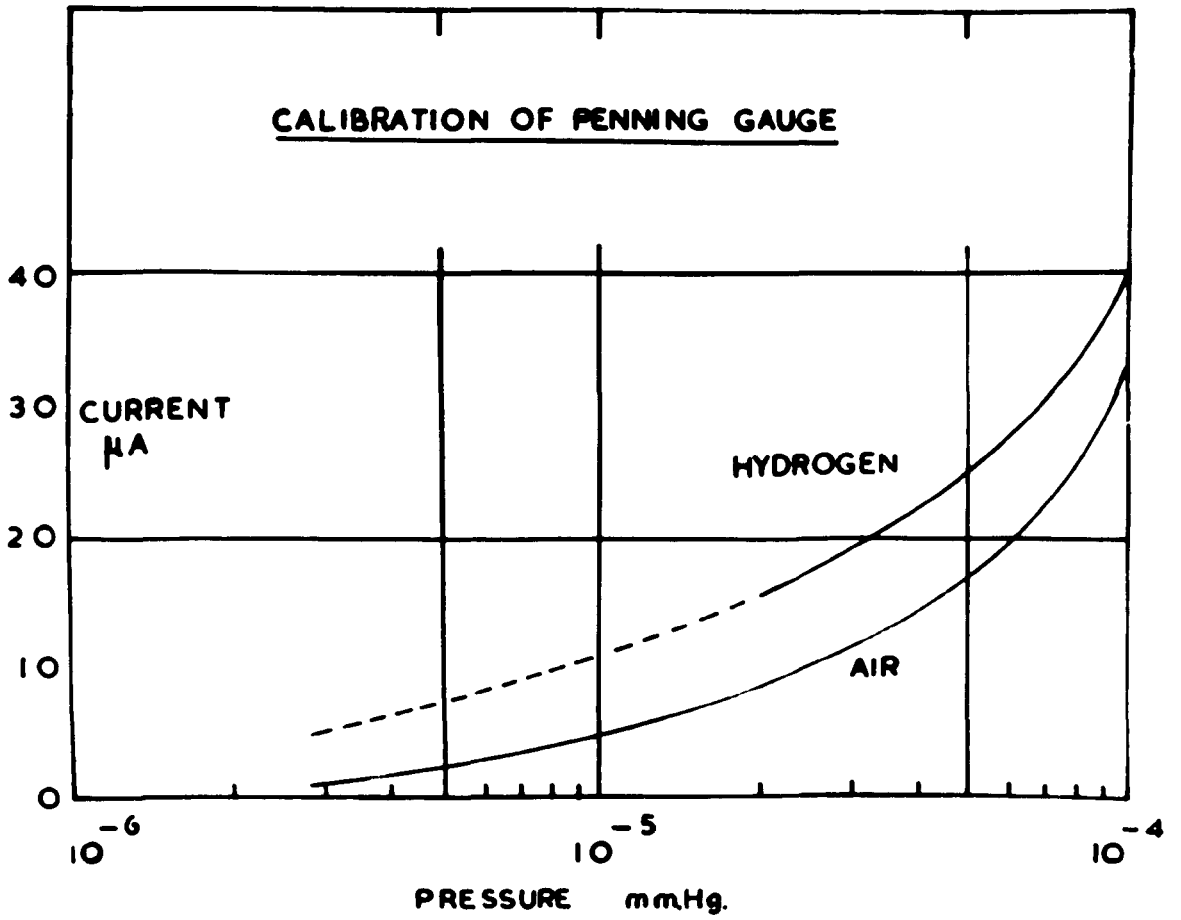
The Kelvin C.P.D. method of determining work functions has been utilized throughout the present study and could be used satisfactorily in further work. The technique could be improved, however, by replacing the customary vibrating motion by rotary motion. Koim (126), employing this technique made rapid inter-comparison measurements among several electrodes with a sensitivity of  $\pm 1$  millivolt.

The scope of C.P.D. determinations could be extended by the introduction of automatic recording systems. Several workers (127, 128), who have applied these techniques to adsorption studies, have reported a response of 0.1 volt/sec coupled with a sensitivity of 0.5 millivolts.

APPENDIX I

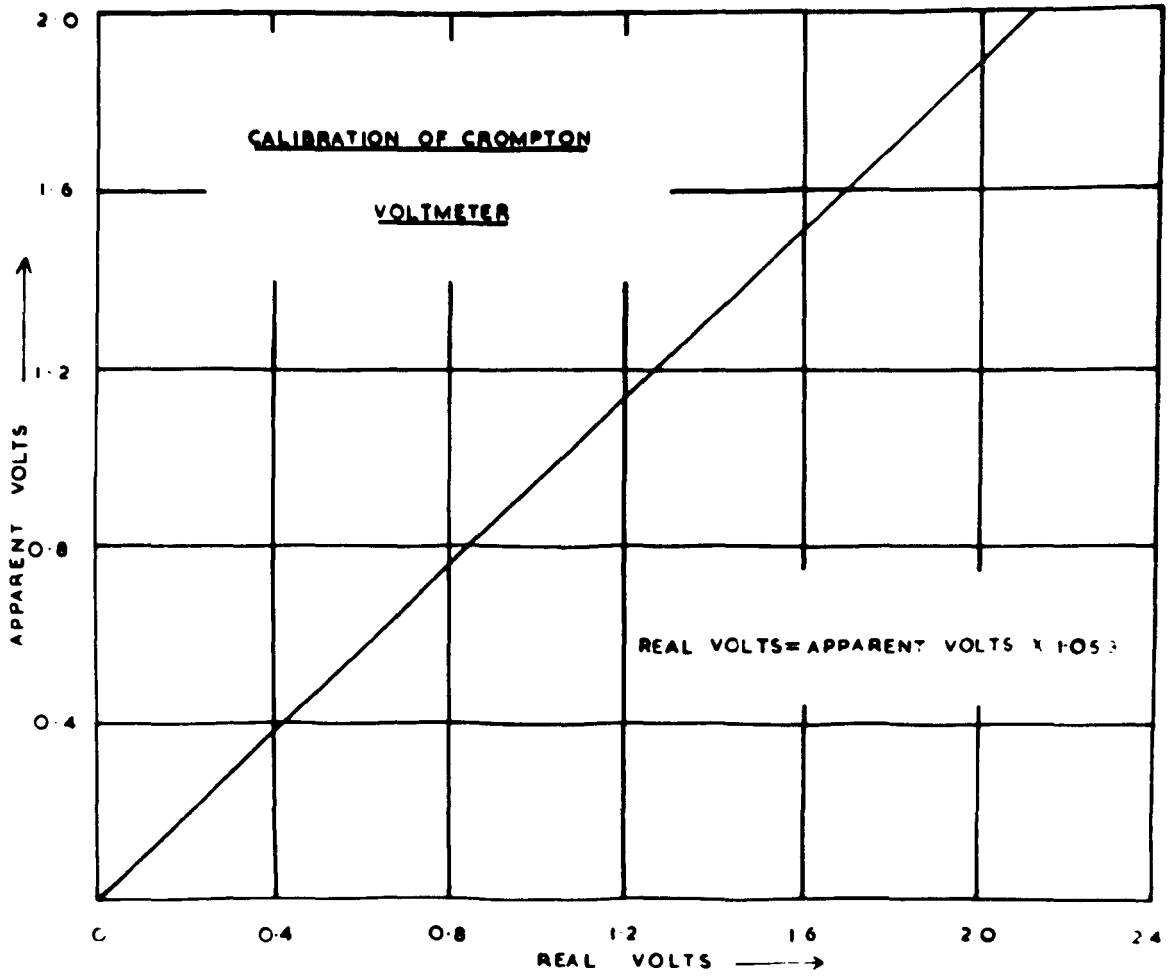
Penning Gauge Calibration Curve

CALIBRATION OF PENNING GAUGE



APPENDIX II

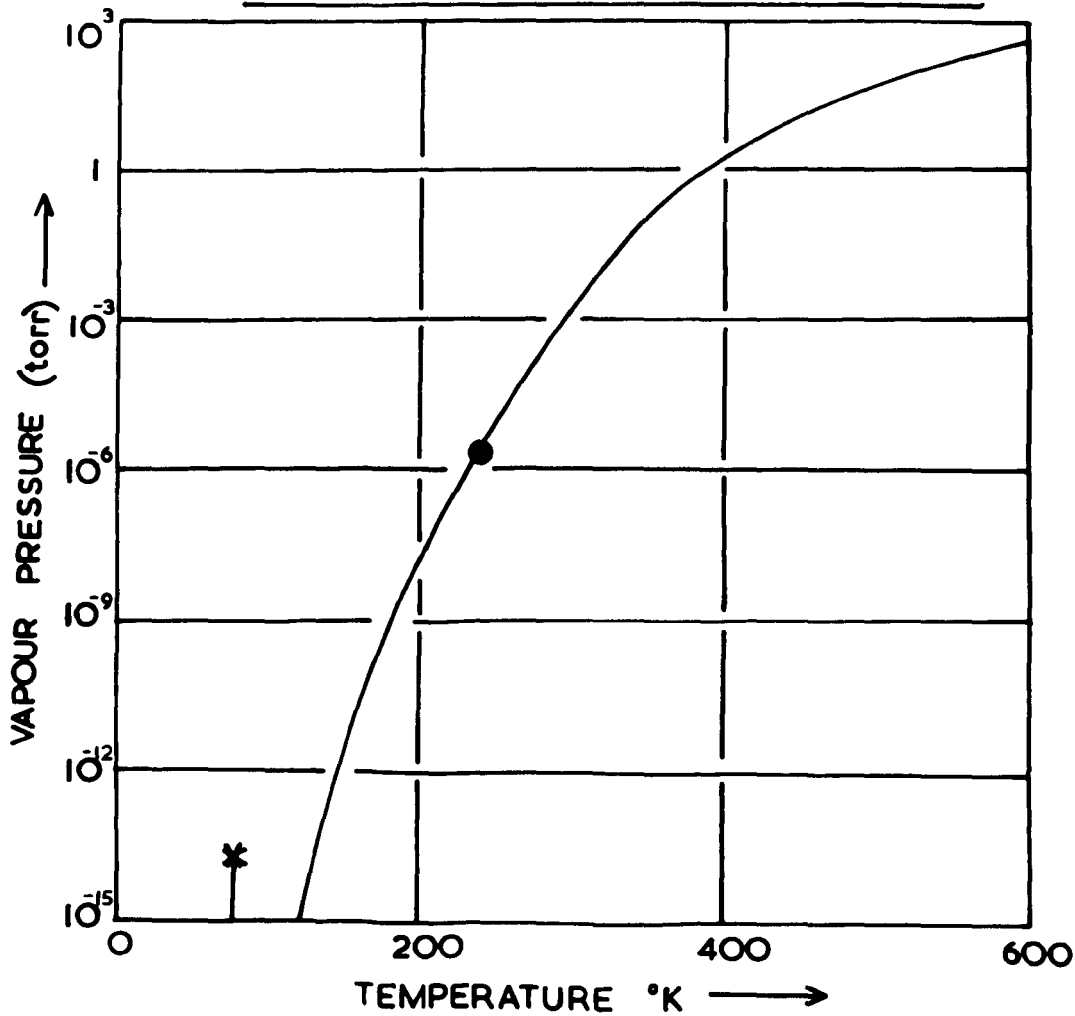
Calibration of Crompton Voltmeter



APPENDIX III

Vapour Pressure of Mercury

# THE VAPOUR PRESSURE OF MERCURY.



● MELTING POINT OF Hg.  
\* BOILING POINT OF  $N_2$ .

Physical Constants of the Metals Investigated

Element	Ionization potential (volts)	Electro-negativity	Type of crystal structure	Lattice spacing (Å)	Density (gm/cc)	Work function (eV)
Ag	7.54	1.9	F.C.C.	4.085	10.49	4.31 (R)
Au	9.18	2.4	F.C.C.	4.078	18.88	5.22 (H)
N	8.1	2.0	B.C.C.	3.165	19.3	4.56 (R)
Ni	7.61	1.9	F.C.C.	3.523	8.902	4.74 (R)
Hg	10.39	2.7	R.	3.005	13.546	4.53 (K)
Mo	7.35	1.8	B.C.C.	3.147	10.22	4.22 (R)

F.C.C. - Face Centred Cubic

R - Rhombohedral

B.C.C. - Body Centred Cubic

(R) - Rivière

(H) - Huber

(K) - Kagda

## LIST OF SYMBOLS

A	Richardson emission constant
$\text{\AA}$	Angstrom = $10^{-8}$ cm.
C	Capacity
C.P.D.	Contact potential difference
d	Inter electrode distance
e	Electronic charge
eV	Electron volt
$E_F(0)$	Fermi level
F	Free energy
H	Enthalpy
h	Planck's constant
I	Current
$I_e$	Thermionic electron current
$I_p$	Positive ion current
k	Boltzman's constant
K	Absolute temperature
m	Electron mass
M	Dipole moment
$N_s$	Number of adsorption sites per $\text{cm}^2$ .
P	Electron momentum
P	Pressure in torr.
R	Universal gas constant

$S$	Relative sensitivity of ionization gauge
$T_F$	Fermi temperature
$U_F$	Electron velocity at the Fermi level
$V$	Voltage; potential
$\alpha$	Amplitude of vibration
$\beta$	Sticking coefficient
$\delta$	Secondary emission coefficient
$\epsilon$	Dielectric constant
$\theta$	Fractional coverage
$\lambda$	Wavelength of radiation
$\mu$	Dipole moment
$\nu$	Frequency of radiation
$\nu_0$	Photoelectric threshold frequency
$\rho$	Charge density
$\phi$	Work function
$\chi$	Height of the potential barrier
$\psi$	Time dependent electron wave function

## LIST OF FIGURES

1. Distribution Functions
2. Fermi Level Values
3. Effects of Lattice Structure
4. Extended-Zone Scheme of Copper and Lead
5. Plot of Energy against Wave-Number
6. Wave-Number Spaces
7. Band Theory of Solids
8. Comparison of Internal and Surface Crystal Environments
9. Chemical Behaviour of Different Planes
10. Schematic Diagram of Field-Emission Microscope
11. Surface of Tungsten Photographed in the Field-Emission Microscope
12. Sections of a Face-Centred Cubic Structure
13. Adsorption of Oxygen in Nickel Surfaces
14. Energy Levels on a Metal and the Potential Energy of an Electron  
near the Metal Surface
15. Energy Distribution of Secondary Electrons
16. The Secondary Electron Yield along the Primary Path
17. The Effect of a Strong Electrostatic Field on the Potential  
Barrier
18. Simplified Triangular Model of the Surface Barrier
19. Effect of Adsorbed Layers on the Potential near a Metal Surface

20. Sticking Coefficients for a number of Gases on Tungsten
21. Schematic Representation of Significant Gas-Surface Reactions
22. Thermionic Emission Data
23. The Spectral Distribution Curve of a Typical Metal
24. Potential Variation between Two Directly Connected Metal Electrodes
25. Variation in Work Function as a Function of Crystal Orientation
26. Temperature Coefficient of the Work Function of Single-Crystal  
Faces of Copper
27. Work Function Values near the Melting Point of Copper
28. Surface Potentials of Nitrogen on Individual Crystal Faces of  
Tungsten
29. Change in C.P.D. as a Function of Mercury Contamination
30. Contact Potential Difference circuit and Low Frequency Amplifier
31. Twin Parallel T Filter
32. Photograph of Pumping Frame and Measuring Equipment
33. Line Diagrams of Glass Vacuum System
34. Photograph of Manifold and Experimental Tube
35. Circuit for Alpert Pump
36. Photograph of Stainless Steel Vacuum System
37. Schematic Representation of Stainless Steel Vacuum System
38. Photograph of Wire Cage
39. Line Diagram of Stainless Steel Experimental Chamber
40. The Kelvin Electrode Vibrating System

41. Photograph of Oscilloscope Displays
42. Photograph of the First Experimental Tube
43. Change in C.P.D. with Time
44. Schematic Representation of the Second Experimental Tube
45. Photograph of the Second Experimental Tube
46. Photograph of Tube 3
47. Line Diagram of the Third Experimental Tube
48. Change in C.P.D. with Time
49. Photograph of the Fourth Experimental Tube
50. Schematic Representation of Tube 4
51. Line Diagram of Kelvin Assembly
52. Photograph of Kelvin Assembly
53. Variation in Position of the Kelvin Electrode
54. Change in C.P.D. with Time
55. Photograph of the Fifth Tube
56. Schematic Representation of Tube 5
57. Change in C.P.D. with Time
58. Photograph of the Preliminary Glass Partition Tube
59. Line Diagram of Glass Experimental Tube
60. Change in C.P.D. with Time
61. Logarithmic Plot of C.P.D.
62. Schematic Representation of Apparatus
63. Change in C.P.D. with Time

64. Change in C.P.D. with Time (log plot)
65. Electron Bombardment Induced C.P.D. Changes
66. Logarithmic Plot of C.P.D.
67. Comparison of C.P.D. and Thermionic Current Changes
68. Line Diagram of Apparatus
69. Photograph of Apparatus
70. Change in C.P.D. with Time
71. Change in C.P.D. with Time
72. C.P.D. between Gold and Tungsten Films
73. C.P.D. Changes between Tungsten and Gold Surfaces
74. Change in C.P.D. with Time
75. Change in C.P.D. as a Function of Adsorption
76. Change in C.P.D. with Distance
77. Schematic Representation of Apparatus
78. Photograph of Apparatus
79. C.P.D. Changes between Gold and Mercury Surfaces

## REFERENCES

- |     |   |                        |     |      |        |
|-----|---|------------------------|-----|------|--------|
| 1.  | Herring, C;<br>Galt, J.K.                 | Phys. Rev.             | 85  | 1060 | (1952) |
| 2.  | Holloway, D.G.                            | Cont. Phys.            | 1   | 230  | (1960) |
| 3.  | Drude, P.                                 | Ann. Physik.           | 3   | 1566 | (1900) |
| 4.  | Bohm, D;<br>Pines, D.                     | Phys. Rev.             | 98  | 414  | (1955) |
| 5.  | Oguri, T.                                 | J. Phys. Soc. Japan    | 19  | 83   | (1964) |
| 6.  | Ehrlich, G;<br>Hudda, F.G.                | J. Chem. Phys.         | 36  | 3233 | (1962) |
| 7.  | Menzel-Kopp;<br>Menzel, E.                | Z. Phys.               | 144 | 538  | (1956) |
| 8.  | MacRae, A.E.;<br>Germer, L.H.             | Phys. Rev. Letters     | 8   | 489  | (1962) |
| 9.  | Flinn, P.A.;<br>Ruby, S.L.;<br>Kehl, W.L. | Science                | 143 | 1434 | (1964) |
| 10. | Brandon, D.G.                             | Brit. J. App. Phys.    | 14  | 474  | (1963) |
| 11. | Kridhof, E.W.;<br>Moret, H.               | J. Sci. Instrum.       | 39  | 132  | (1962) |
| 12. | Moore, G.E.                               | J. Appl. Phys.         | 30  | 1086 | (1959) |
| 13. | Moore, G.E.                               | J. Appl. Phys.         | 32  | 1241 | (1961) |
| 14. | Lichtmann, D.                             | J. Vacuum Sci. Technol | 2   | 70   | (1965) |
| 15. | Bruger, R.M.                              | J. Appl. Phys.         | 29  | 1150 | (1958) |
| 16. | Cooper, E.G.<br>Muller, E.W.              | Rev. Sci. Inst.        | 29  | 309  | (1958) |
| 17. | Brandon, D.G.                             | Surface Science        | 3   | 1    | (1965) |

- |     |   |   |     |      |        |
|-----|---|---|-----|------|--------|
| 18. | Suhrmann, R.;<br>Wedler, G.;<br>Schumick, G.S.; | Trans. Inter. Conf.<br>on Structure and<br>properties of thin films |     |      |        |
| 19. | Geus, J.W.                                      | Surface Science   | 2   | 48   | (1964) |
| 20. | Jourdain, P.;<br>Thureau, P.                    | C.R. Acad. Sci.   | 257 | 2015 | (1963) |
| 21. | Palatnik, L.S.;<br>It'inskii                    | Dokl. Akad. Nauk.<br>S.S.S.R.                                       | 154 | 155  | (1964) |
| 22. | Wedler, G.;<br>Fouad, M.                        | Z. Phys. Chem.  | 40  | 12   | (1964) |
| 23. | Cutler, P.H.;<br>Davis, J.C.                    | Surface Science   | 1   | 194  | (1964) |
| 24. | Dushman, S.                                     | Phys. Rev.  | 21  | 623  | (1923) |
| 25. | Nordheim, L.                                    | Z. Phys.  | 46  | 833  | (1927) |
| 26. | Nordheim, L.                                    | Proc. Roy. Soc.   | 121 | 626  | (1928) |
| 27. | Nordheim, L.                                    | Phys. Z.  | 30  | 177  | (1929) |
| 28. | Hertz, H.                                       | Ann. Phys. Lpz.   | 31  | 983  | (1887) |
| 29. | Austin, L.;<br>Starke, H.                       | Ann. Physic   | 9   | 271  | (1902) |
| 30. | Rudberg, E.                                     | Proc. Roy. Soc.   | 127 | 111  | (1930) |
| 31. | Rudberg, E.                                     | Phys. Rev.  | 45  | 764  | (1934) |
| 32. | Parker, J.H.                                    | Phys. Rev.  | 93  | 1148 | (1954) |
| 33. | Fowler, R.H.;<br>Nordheim, L.                   | Proc. Roy. Soc.   | 119 | 173  | (1928) |
| 34. | Harpern, B.;<br>Gomer, R.                       | J. Chem. Phys.  | 43  | 1069 | (1965) |
| 35. | Haefner, R.H.                                   | Z. Phys.  | 116 | 604  | (1940) |
| 36. | Cutler, R.H.;<br>Wagy, D.                       | Surface Science   | 3   | 71   | (1965) |

37.	Roberts, J.I.	Proc. Roy. Soc.	161	141	(1937)
38.	Gomer, R.; Hulme, J.K.	J. Chem. Phys.	27	1363	(1957)
39.	Ehrlich, G.	J. Phys. Chem.	60	1388	(1956)
40.	Bloomer, R.N.; Haine, M.E.	Vacuum	3	128	(1954)
41.	Alpert, D.	Physics Today	16	22	(1963)
42.	Hartman, T.E.	Rev. Sci. Instr.	34	1190	(1963)
43.	Moore, G.E.	J. Appl. Phys.	32	1241	(1961)
44.	Herring, C.; Nichols, M.H.	Rev. Mod. Phys.	21	185	(1949)
45.	Crowell, G.R.; Armstrong, R.A.	Phys. Rev.	114	1500	(1959)
46.	Hensley, E.B.	J. Appl. Phys.	32	301	(1961)
47.	Myers, H.P.	Proc. Phys. Soc.	66	493	(1953)
48.	Anderson, P.A.	Phys. Rev.	88	655	(1952)
49.	Nichols, N.H.	Phys. Rev.	78	158	(1950)
50.	Apker, L.; Taft, E.; Dikkey, J.	Phys. Rev.	73	46	(1948)
51.	Hopkins, B.J.; Ross, K. . . .	Brit. J. Appl. Phys.	15	89	(1964)
52.	Hopkins, B.J.; Rivière, J.C.	Proc. Phys. Soc.	81	590	(1963)
53.	Hopkins, B.J.; Rivière, J.C.	Brit. J. Appl. Phys.	15	941	(1964)
54.	Herring, C.	Phys. Rev.	59	889	(1941)
55.	Moore, G.E.; Allison, H.W.	J. Chem. Phys.	23	1609	(1955)

56.	Schottky, W.	Phys. Z.	15	526	(1914)
57.	Mrowka, B.	Z. Techn. Physik	18	572	(1937)
58.	Smolochowski, R.	Phys. Rev.	60	661	(1941)
59.	Muller, E.W.	J. Appl. Phys.	26	732	(1955)
60.	Smith, G.F.	Phys. Rev.	94	295	(1954)
61.	Nickols, M.H.	Rev. Mod. Phys.	21	202	(1949)
62.	Love, H.W.; Dyer, G.L.	Can. J. Phys.	40	1837	(1962)
63.	Farnsworth, H.E.; Chung Fu Ying.	Phys. Rev.	85	485	(1952)
64.	Hass, G.A.; Thomas, R.E.	Surface Science	4	64	(1966)
65.	Rauh, E.G.; Thorn, R.J.	J. Chem. Phys.	31	1481	(1959)
66.	Rentschler, D.E.; Henry, D.E.; Smith, K.O.	Rev. Sci. Instr.	3	794	(1932)
67.	Hole, W.L.; Wright, R.W.	Phys. Rev.	56	785	(1939)
68.	Garron, R.	C.R. Acad. Sci. Paris	254	243	(1962)
69.	Bryla, S.M.; Feldman, C.	J. Appl. Phys.	33	774	(1962)
70.	Hopkins, B.J.; Ross, K.J.	Brit. J. Appl. Phys.	16	1319	(1965)
71.	Farnsworth, H.E.	Phys. Rev.	43	904	(1933)
72.	Blackmer, L.L.; Farnsworth, H.E.	Phys. Rev.	77	826	(1950)
73.	Shelton, H.	Phys. Rev.	107	1553	(1957)

74.	Hutson, A.R.	Phys. Rev.	98	889	(1955)
75.	Blevis, E.H.; Crowell, C.R.	Phys. Rev.	133	580	(1964)
76.	Underwood, N.	Phys. Rev.	47	502	(1935)
77.	Bolshov, V.G.	Bull. Acad. of Sci.	20	1128	(1956)
78.	Smith, G.F.	Phys. Rev.	94	295	(1954)
79.	Nichols, M.H.	Phys. Rev.	100	1115	(1955)
80.	Langmuir, I.	Phys. Z.	15	516	(1914)
81.	Moore, G.E.; Underwald, F.C.	J. Chem. Phys.	40	2626	(1964)
82.	Bills, D.G.; Evetts, A.A.	J. Appl. Phys.	20	564	(1959)
83.	Ehrlich, G.	J. Phys. Chem.	59	473	(1955)
84.	Barker, M.; Rideal, E.K.	Nature	174	1185	(1954)
85.	Eisinger, J.	J. Chem. Phys.	27	1206	(1957)
86.	Eisinger, J.	J. Chem. Phys.	28	165	(1958)
87.	Mac Rae, A.U.	Surface Science	1	319	(1964)
88.	Holschor, A.A.	J. Chem. Phys.	41	579	(1964)
89.	Bomke, H.	Ann. Phys. Lpz.	10	579	(1931)
90.	De Voe, C.F.	Phys. Rev.	50	581	(1936)
91.	Hopkins, B.J.; Mee, C.H.B.; Parker, D.	Brit. J. Appl. Phys.	15	865	(1964)
92.	Trapnell, B.M.W.	Proc. Roy. Soc.	218	566	(1953)
93.	Anderson, P.A.	Phys. Rev.	115	553	(1959)

94.	Rivière, J.C.	Proc. Phys. Soc.	70	676	(1957)
95.	Huber, E.E.	Appl. Phys. Letters.	8	169	(1966)
96.	Rivière, J.C.	Appl. Phys. Letters.	8	172	(1966)
97.	Gomer, R.	J. Chem. Phys.	28	457	(1958)
98.	Parker, R.L.; Anderson, P.A.; Hardy, S.C.	Appl. Phys.	3	93	(1963)
99.	Kazda, C.B.	Phys. Rev.	26	643	(1925)
100.	Hales, W.B.	Phys. Rev.	32	950	(1928)
101.	Roller, D.; Jordon, W.H.; Woodward, C.S.	Phys. Rev.	38	396	(1931)
102.	Klein, O.; Lange, E.	Zeits. f. Elektro- chemie	44	542	(1938)
103.	Zisman, W.A.	Rev. Sci. Inst.	3	367	(1932)
104.	Bayard, R.T.; Alpert, D.	Rev. Sci. Inst.	21	571	(1950)
105.	Lafferty, J.M.	J. Appl. Phys.	32	424	(1961)
106.	Olsen, L.O.; Smith, C.S.; Crittenden, E.C.	J. Appl. Phys.	16	425	(1945)
107.	Law, J.T.; Allen, F.G.; Singer, J.H.; Hagstrum, H.D.	J. Appl. Phys.	30	1563	(1959)
108.	Miller, G.L.	Metal. Ind. Lond.	75	411	(1949)
109.	Hansen, M.	Der Aufbau. der Zweist- offlegierungen Julius Springer. Berlin.			(1936)
110.	Mitoff, S.P.	J. Amer. Ceram. Soc.	40	118	(1957)

111.	Wright, R.W.	Phys. Rev.	60	465	(1941)
112.	Holland, L.	Vacuum Deposition of Thin Films. Chapman and Hall			(1956)
113.	Maddison, R.C.	Ph.D. Thesis, University of Keele			(1964)
114.	Briggs, L.J.	J. Appl. Phys.	24	488	(1953)
115.	Briggs, L.J.	J. Appl. Phys.	26	784	(1957)
116.	Peterson, J.W.	A. Appl. Phys.	25	501	(1954)
117.	Peterson, J.W.	J. Appl. Phys.	25	907	(1954)
118.	Bloomer, R.N.; Haine, M.E.	Vacuum	3	128	(1954)
119.	Anderson, P.A.	Phys. Rev.	59	1034	(1941)
120.	Todd, B.J.	J. Appl. Phys.	26	1238	(1955)
121.	Todd, B.J.	J. Appl. Phys.	27	1209	(1956)
122.	Donaldson, E.E.	Vacuum	12	11	(1962)
123.	Bolshov, V.G.	Bull. Acad. of Sci.	20	1128	(1956)
124.	Hayes, R.E.; Alsford, R.W.; Kennedy, D.I.	Conference on Sorption Properties of Vacuum deposited metal films, Liverpool.			(1963)
125.	Kivel, J.; Albers, F.C.; Olsen, D.A.; Johnson, R.E.	J. Phys. Chem.	67	1235	(1963)
126.	Kolm, H.H.	Rev. Sci. Instrum.	27	1046	(1956)
127.	Simon, R.E.	Phys. Rev.	116	613	(1959)
128.	Delchar, T.A.; Ehrlich, G.	J. Chem. Phys.	42	2686	(1965)

129.	Quinn, C.M.; Roberts, M.W.	J. Chem. Phys.	40	237	(1964)
130.	Crowell, A.D.; Norberg, A.L.	J. Chem. Phys.	37	714	(1962)
131.	Ehrlich, G.; Hudda, F.G.	J. Chem. Phys.	35	1421	(1961)
132.	Nadjakov, G; Vasilev, V.	C.R. Acad. Bulg. Sci.	16	353	(1963)
133.	Culver, R.; Pritchard, J.; Tompkins, F.C.	Z. Elektrochem.	63	741	(1959)
134.	Nichols, H.H.	Phys. Rev.	78	158	(1950)
135.	Comsa, G.; Gelberg, A.; Iosifescu, B.; Musa, G.	Stad. Cercetari. Fig. 9		429	(1958)
136.	Clarke, E.N.; Farnsworth, H.E.	Phys. Rev.	85	884	(1952)
137.	Farnsworth, H.E.	Proc. Phys. Soc.	71	703	(1959)
138.	Edwards, J.W.; Johnson, H.L.; Blackburn, P.E.	J. Amer. Chem. Soc.	74	1539	(1952)
139.	Pasternak, R.A.; Wiesendanger, H.U.D.	J. Chem. Phys.	34	2062	(1961)
140.	Hickmott, T.W.	J. Chem. Phys.	32	810	(1960)
141.	Good, R.H.; Muller, E.W.	Handbuch der Physik	21	206	(1956)
142.	Olsen, L.O.; Smith, C.S.; Crittended, E.C.	J. Appl. Phys.	16	425	(1945)
143.	Du Bridge, L.A.	Phys. Rev.	43	727	(1933)

144.	Du Bridge, L.A.; Hergenrother, R.C.	Phys. Rev.	44	861	(1933)
145.	Honig, R.E.	R.C.A. Review	23	567	(1962)
146.	Jain, S.C.; Krishnan, K.S.	Proc. Roy. Soc.	217	451	(1953)
147.	Hickmott, T.W.	J. Appl. Phys.	31	128	(1960)
148.	Redhead, P.A.; Hobson, J.P.; Kornelson, E.V.	Advances in Electronics and Electron Physics	17	323	(1962)